THE UNIVERSITY OF MANITOBA

GRAIN BOUNDARIES AS DISLOCATION SOURCES

by

T. F. Malis

A THESIS

SUBMITTED TO THE FACULTY OF GRADUATE STUDIES

IN PARTIAL FULFILMENT OF THE REQUIREMENTS FOR THE DEGREE

OF DOCTOR OF PHILOSOPHY

DEPARTMENT OF MECHANICAL ENGINEERING

WINNIPEG, MANITOBA

January, 1975.

GRAIN BOUNDARIES AS DISLOCATION SOURCES

by

T. F. MALIS

A dissertation submitted to the Faculty of Graduate Studies of the University of Manitoba in partial fulfillment of the requirements of the degree of

DOCTOR OF PHILOSOPHY

ABSTRACT

GRAIN BOUNDARIES AS DISLOCATION SOURCES

By

T. F. Malis

An investigation was conducted into the role of grain boundaries as sources of lattice dislocations during yielding. An extensive review of the literature was conducted in order to establish a firm base for the study of this relatively new field. This included grain boundary structural models, the defect structure associated with the boundary, previous experimental confirmation of grain boundary source operation, and the proposed models for such sources, including the stress required and the means of enhancing the applied stress to this value.

An electron microscope examination was then conducted on several materials which possessed microstructures conducive to boundary sources and which had been strained to points well below and up to the yield point. Two techniques were developed to aid the thin foil examination. One led to a reduction in thin foil deformation due to foil handling, and the other was a thin foil mapping technique to provide comparative data on the densities and distributions of lattice defects pertinent to the

yield process.

The experimental results indicated that the great majority of boundary sources were nonregenerative in nature, and involved the nucleation and emission of both perfect and partial dislocations from grain boundary ledges. These dislocations were nucleated at low stresses and many were retained at the boundary. Emission occurred preferentially from triple points in the early stages of yielding. The proportion of strain contributed by boundary sources was negligible in high purity Al. In high purity Cu, the most extensively studied material, it was significant in only the first stage of what appeared to be a two-stage yielding process common to all the materials. In the second stage grain interior sources were predominant. In medium purity Ni, boundary sources were present in substantially larger numbers, and in Cu - 1 wt % Sn, they were present in sufficient numbers to control the major portion of the entire yield process. A number of factors, such as stacking fault energy or elastic anisotropy, appeared to influence boundary source characteristics or their operation, but the most important were the initial states of the boundaries and the distribution of solute or impurity atoms within the material.

With the experimental observations in mind, a detailed model of boundary sources was constructed. It

proposes dislocation nucleation from groups of small boundary ledges, with the ledge geometry providing the major portion of the necessary stress concentration for this nucleation. Additional stress concentration is supplied by interaction of the stress fields from the ledges within each group. The variation in the number, size and spacing of ledges within each group, along with the variation in individual ledge geometry, account for the observed non-homogeneous distribution of boundary sources. Several specific aspects of this model are then discussed, as well as its implications for other important facets of mechanical behavior.

ACKNOWLEDGMENTS

I would like to express my gratitude to the Steel Company of Canada Ltd., for their financial assistance. There are many people who rendered assistance during the course of this study, particularly Mr. J. Van Dorp, Dr. M. C. Chaturvedi, and Dr. D. J. Lloyd. I owe a special debt to my supervisor, Dr. K. Tangri. Through his teaching, criticism and encouragement, he has been instrumental in refining my capabilities as a scientist, with regards to both the conduction of research and the art of communicating it to others. Finally, I wish to thank my wife, Margaret, for her endurance of the student's life and the grueling pace often associated with completion of this work.

TABLE OF CONTENTS

Page

Page

LIST OF TABLES

LIST OF MICRO-MAPS

LIST OF FIGURES

Page

Page

Page

Page

1.0 INTRODUCTION

An overwhelming majority of engineering materials are used in the polycrystalline state, hence grain boundaries have always been considered to play an important role in plastic deformation. This role has centered around their ability to act as obstacles to the movement of dislocations. Thus, the classical concept has long been one of yield initiation via dislocation generation in grain interiors and subsequent dislocation pileups against the boundaries causing source activation in the next grain. However, during the past decade, an increasing amount of evidence has established that grain boundaries can also act as dislocation sources, particularly in the early stages of yielding. This region is generally referred to as the premacroyield strain region, and it extends from the first substantial movement of dislocations to the point where massive dislocation movement and multiplication is required to maintain the plastic strain rate imposed by the testing machine. It thus separates the microyield region (plastic strain of zero to around 1×10^{-4}) from the macroyield region (yield point).

The operation of grain boundary sources in the premacroyield region would have a number of consequences:

1) It might affect either the type, character or number per source of dislocations generated,
2) It would affect the work hardening behavior of materials in which cross-slip, and hence tangling, is relatively easy. This behavior would be affected by the changed location of these tangles from

the grain interior to the grain perimeter when boundary sources predominate,

3) The work hardening behavior with respect to solute atoms or particles hindering dislocation movement would be also affected, since solute levels and distribution at the grain boundary can be different from those of the grain interior in many materials.

In addition, the possibility of grain boundaries acting as dislocation sources may have implications for mechanical properties above the yield point, such as creep and fatigue strengths, or the amount of ductility a material possesses.

Although the concept of grain boundary dislocation sources has been formulated for some time, relatively little detailed experimental work has been conducted on their operation or their influence on the yielding process. Therefore this study was directed towards the following objectives:

1) To examine and correlate the many theoretical models for grain boundary structure and grain boundary lattice defects, dislocation nucleation at, and generation from these boundaries, the stresses required for operation of boundary sources and the means of obtaining these stresses,

2) To verify that grain boundary dislocation generation can occur in the premacroyield region of a pure FCC metal (Cu) in which it had not previously been observed, by designing a microstructure conducive to such generation,

3) To develop a method of extracting quantitative data (via electron microscope thin foil examination) concerning boundary source operation,

4) To use this method for measuring relative source densities and distributions in Cu at various strains in the premacroyield region,

5) To study some of the parameters, such as solute content, stacking fault energy, elastic anisotropy and initial boundary defect density, that should influence boundary source operation, by examining selected materials (Cu-1wt%Sn, Ni, Al) in a similar microstructural state to that of the Cu,

6) To examine the characteristics of individual sources in any material, for the purpose of establishing a boundary source model which will account for these characteristics and those determined in 4) and 5).

2 GRAIN BOUNDARY STRUCTURE AND ASSOCIATED CRYSTAL DEFECTS

A grain boundary may be defined as the contact region between two crystals differing only in orientation (1). This definition, although relatively straightforward, sheds little light on the nature of this region, either on the scale of the individual atoms or the larger scale of the various defects present among the arrays of atoms. It is essential to realize that the strength of polycrystals indicates the presence of strong interatomic forces across this region. Thus it is not a "space" between two crystallites (as often represented in drawings) but a transition zone or a special lattice between the two misoriented crystal lattices. It accordingly possesses its own special characteristics, particularly with regard to the interaction of different types of dislocations. The character is also highly variable, and must change as the misorientation changes. This zone is spatially more restricted than our common notion of a lattice, being essentially a two-dimensional film curved so as to surround the grains in three dimensions. This latter point is particularly easy to forget since we are accustomed to observing "ribbons" of grain boundary in transmission electron micrographs.

2.1 GRAIN BOUNDARY PARAMETERS

Before studying the various models which have

been postulated to describe the structure of boundaries, it would be valuable to describe how a boundary is defined with respect to the crystallites it separates. If the crystallites are infinitely large, three angular parameters define their misorientation; one a rotation about an axis normal to the mirror plane separating them (twist component) and two about mutually perpendicular axes within this plane (tilt components). This mirror plane is normally the boundary plane (symmetric boundary), but does not necessarily have to be (e.g. in an asymmetric boundary). For the more normal case of a boundary in a thin foil, two additional parameters describe the orientation of the boundary plane to the foil (2). As shown in figure 1, these are θ, denoting the inclination of the boundary to the foil surface, and ϕ, denoting the angle between the boundary - foil intersection and θ, the misorientation of a common crystallographic direction. This latter parameter encompasses the three angular parameters described above. This normally suffices to accurately reference the boundary, but with the advent of increasingly sophisticated models, Chalmers (3) has recently proposed that an additional three orthogonal inrotational translations are required to describe the relaxation of individual atoms at the boundary. However necessary these may be theoretically, they are as yet of

Figure 1. Geometrical conventions for characterizing a grain boundary (ABCD) in a thin foil of finite thickness, t (after Murr et al, 2).

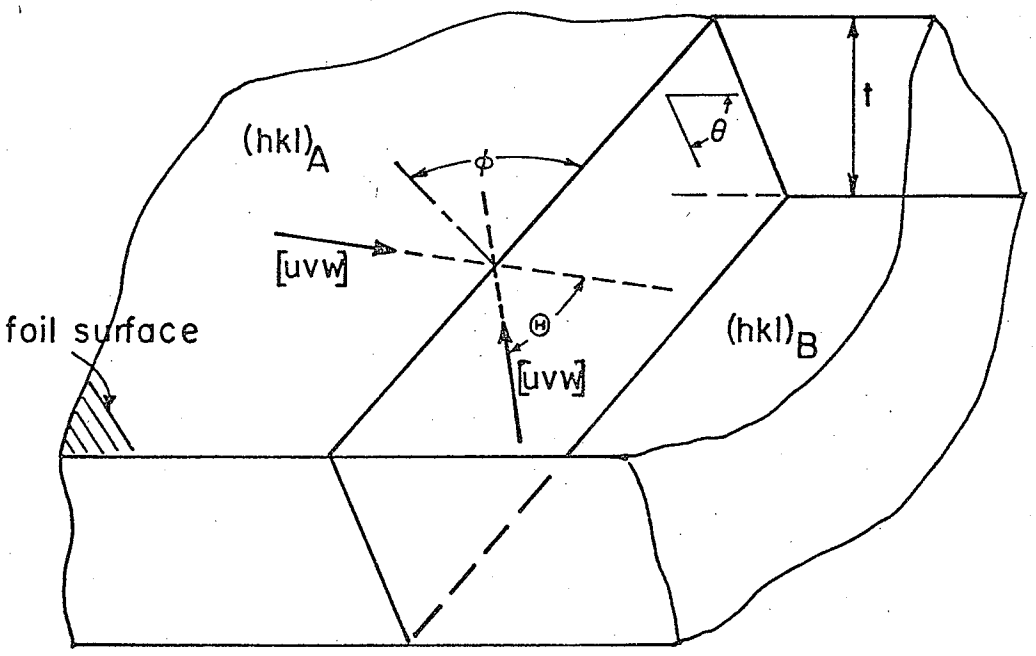
(hkl)A
φ
θ
t
[uvw]
foil surface
Θ
(hkl)B
[uvw]

limited importance experimentally, thus the first five parameters are considered sufficient for most boundary descriptions. It should be pointed out that the above symbols are somewhat confusing in that a great many authors use the lower case theta (θ) to denote the misorientation angle and the lower case alpha (α) to denote the inclination angle of the boundary with the foil surface.

2.2 MODELS OF GRAIN BOUNDARY STRUCTURE

There are two basic approaches to considering models for grain boundaries (4). In one approach the boundary is viewed as a smooth, homogeneous layer purely for thermodynamic purposes. In the other, the basic structure of this layer is described. This study deals with the latter. Gifkin states (4) that a model must satisfy the following criteria to be completely acceptable:

a) it must result in a boundary width of three to four atom diameters to correlate with experimental observations.

b) it must produce a reasonable value of grain boundary energy and the orientation and temperature dependence thereof.

c) it must account for the change in orientation between the two grains while still taking into

account individual atom interactions.

d) it must be able to explain, to at least some degree, a host of properties such as boundary sliding, migration, segregation, corrosion, melting and low temperature mechanical behaviour.

This last requirement is the most difficult to fulfill. The main difficulty to date appears to be that a given model may elegantly account for the behaviour of one or two boundary properties, yet break down completely when the others are considered. For this reason, plus the fact that some models have not yet been evaluated with respect to even the first three criteria, it is impossible to rigorously assess their shortcomings and merits. Thus they will be presented only briefly, with perhaps some indication of current popularity, in order to establish a physical basis for the consideration of dislocation generation from grain boundaries.

One problem endemic to most models is that they were originally constructed to explain the structure of simple "special" boundaries, such as low angle pure tilt or twist boundaries or coincidence boundaries. Ultimately, however, they should be able to give at least an approximate picture of that most common of boundaries in normal materials, the random, high angle (high θ) grain boundary.

2.2.1 AMORPHOUS MODEL

This model, developed by Rosenhain and co-workers (5, 6) was the first real attempt to account for boundary properties. In essence, it considered the boundary as an amorphous, undercooled liquid, i.e. possessing no long range periodic structure. Although this could qualitatively explain such phenomena as grain boundary sliding and brittleness at high and low temperatures, respectively, it has been generally discounted for a number of reasons (1). A calculation of the excess internal energy based on this model leads to calculated values of boundary thickness much larger than observed experimentally. Also, it seems inherently unreasonable that so thin a region would not be influenced at all by the periodic crystal structures on either side of it. Most important, such a model completely fails to account for the variation in many boundary properties with both orientation and/or inclination.

The concept on which the model is based has some value with regard to such matters as calculation of grain boundary energy. Also, as McLean comments (7), the boundary layer bears some similarity to an amorphous layer in that both are regions in which the perfect crystal structure is forbidden, thus tempering somewhat the comparison of this region to a special lattice. Aaron and Bolling (8)

have considered grain boundary energy using somewhat of an amorphous model, that is, the boundary structure with the lowest free volume possesses the lowest energy boundary. They conclude that high angle boundaries are most likely constructed according to a "structureless" model built on the random close-packing of atoms. As we shall soon see, however, there is a good chance that this could correspond to a structured model which allows individual atom relaxation into the lowest energy configuration.

2.2.2 DISLOCATION MODELS

These models consider grain boundaries as planar arrays of dislocations. It is well established that low angle boundaries (9, 10), i.e. low θ values, are composed of arrays of lattice edge dislocations for a pure tilt misorientation, screw dislocations for a pure twist misorientation, or, as is most often the case, dislocations of mixed character for a mixed orientation. This is illustrated in figure 2, with the twist segment on top, the tilt segments on the sides and a mixed segment denoted DCH.

The spacing of these lattice dislocations decreases with increasing misorientation according to $d = \underline{b}/\theta$ (b = Burgers vector, d = spacing), hence the boundary

Figure 2. Illustrating symmetric tilt, twist and mixed low angle grain boundaries for the case of one grain entirely surrounded by another grain, with both sharing a common <001> axis (Bishop and Chalmers, 35).

Figure 3. (a) Dislocation model of a symmetric 53^{o} tilt boundary. (b) Dislocation model of a symmetric 60^{o} tilt boundary (Gleiter, 1).

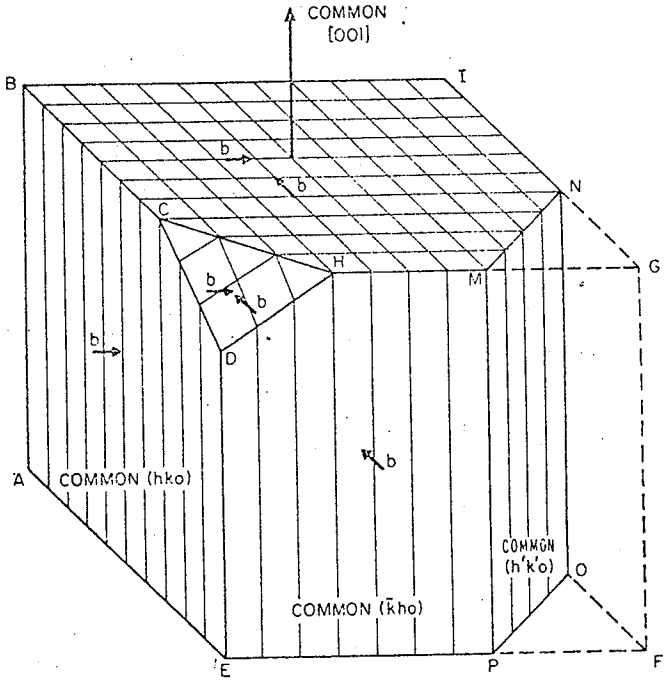
COMMON
[001]
B
T
N
G
C
H
M
D
A
E
P
F
O
b
COMMON (hko)
COMMON (h̄ho)
COMMON
(h'k'o)

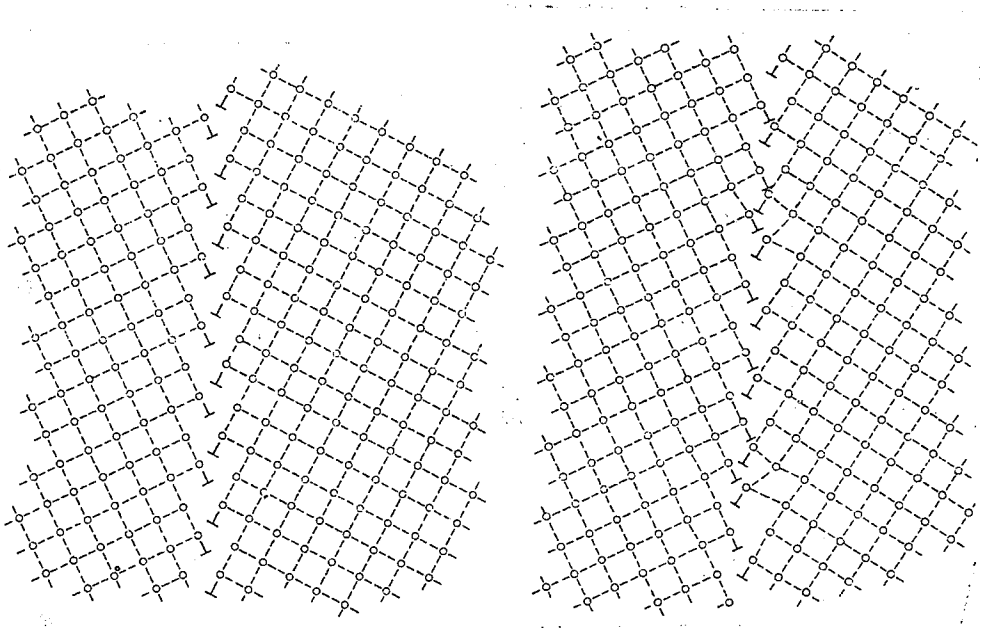

(a) (b)

energy increases with more dislocations per unit length. Up to approximately 15^{o} of misorientation (hence the term low angle boundary), the boundary energy can be accurately calculated from dislocation theory based on linear elasticity. Beyond this point, the dislocation cores become too close to retain their physical identity. The model can be extended on a geometric basis, however (11). This is illustrated in figure 3. The low energy of the 53^{o} tilt boundary of figure 3(a) arises because of the uniform dislocation spacing (one per lattice plane). The higher energy 60^{o} boundary of figure 3(b) may be regarded as a 53^{o} boundary with a 7^{o} low angle boundary superimposed on it. Again, this is only geometrically true, since the two components will interact with regard to the boundary energy. This interaction is almost impossible to calculate because of the physical closeness of the dislocations. More recent models have also discussed boundary structure in terms of dislocations but, because they utilize other concepts as well, they will be presented later.

2.2.3 ISLAND MODEL

This model was first proposed by Mott (12) and later expanded by Gifkins (13) and, as seen in figure 4, it views a grain boundary as consisting of "islands" of

Figure 4. Representation of island model of grain boundaries (with the channels of bad fit shown dashed)
(a) viewed along the boundary plane
(b) viewed normal to the boundary plane (Gifkins, 13).

Figure 5. Coincidence lattice (double circles) resulting from the interpenetration of two crystal lattices (large and small circles). Coincidence lattice unit cell is AOBC and the crystal lattice rotation is shown at right (Fletcher, 29).

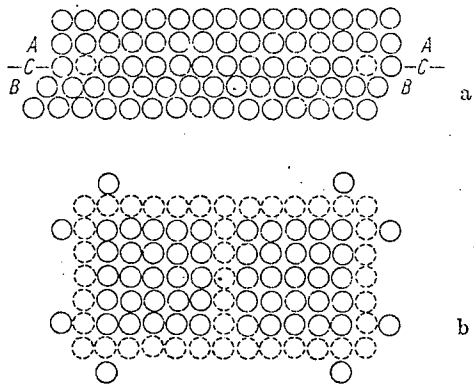
A
C
B
A
C
B
a
b

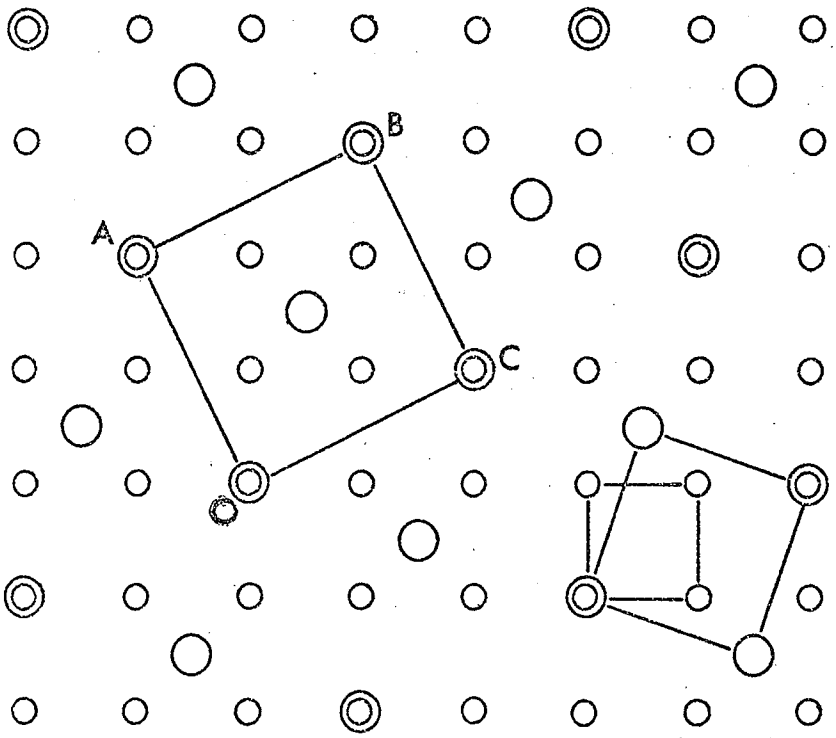
A
B
C

good atomic fit which are surrounded in the plane of the boundary by "channels" of bad fit. These regions have been estimated (13) as varying in size from five to fifty atom diameters (roughly 10 - 100 Å) and thus should be, for the most part, invisible in the electron microscope. They have apparently been seen, in the form of facets, by the field ion microscope (14, 15). Because of the small atomic mismatch across the islands of good fit, short range elastic strains exist which vary in magnitude with the misorientation and account for a minor, but nonetheless significant, portion of the grain boundary energy. Gifkins has stated that these regions of good fit would tend to be oriented so as to permit continuity of slip across them, although this would be very difficult for small island sizes.

The channels of bad fit are essentially relaxed vacancies and can be identified with the ledges on the edges of microfacets, hence the resemblance, as we shall see later, between these regions and grain boundary dislocations associated with ledges. The elastic strains would be much more severe in these channels and despite their smaller area relative to the islands, they are thought to contribute the major portion (roughly 60%) of the total grain boundary energy. The special coincidence boundaries (discussed next) are seen as special cases of this

model where the islands are very large, occupying the entire boundary in the limit of a coherent twin boundary.

Overall, the island model appears to be regarded as a good physical picture of boundary structure, but it has been largely supplanted by more specific models.

2.2.4 COINCIDENCE MODEL

This model hinges on the concept of a coincidence lattice (16, 17), which simply states that when two misoriented crystal lattices are allowed to interpenetrate each other, some of the lattice points will coincide, e.g. O, A, B, C in figure 5. These points form a lattice of larger spacing than either of the original ones, which is called the coincidence lattice for that particular misorientation. The degree of coincidence is denoted by Σ, the reciprocal of the fraction of shared sites, e.g. $\Sigma = 1$ indicates that all sites of the two lattices are shared (coherent twin boundary). For most random orientations about a given axis of rotation, it can be seen that Σ is very large and the concept of coincidence loses much of its utility. For certain orientations, however, the fraction of shared sites becomes very large, and grain boundaries oriented so as to lie along planes of this lattice which possess a high density of shared sites are expected

to have low boundary energies (16). This is due to the absence of long-range elastic strains (much the same as for the "islands" of the previous section. Balluffi and Tan (18) indicate that boundaries with $\Sigma \leq 20$ should fall into this category of a "special" boundary. Although a great deal of experimental work has demonstrated that some amount of energy decrease is achieved for these orientations (roughly 10%), recent work by Dimon and Aust (19) indicates that it can be much larger (30%), while occurring over a very narrow range of orientation. Marked changes in the properties of these boundaries from those of random boundaries was first established by Kronberg and Wilson (20) and has since been well-documented (21). It was further discovered experimentally (22) that deviation of the boundary plane from this low energy plane of the coincidence lattice led to a stepped boundary in order to maximize the amount of boundary lying along the low energy plane. In this fashion, changes in direction of the boundary can be brought about by the proper combination of steps of varying orientations and spacings (figure 6). It should be noted that a similar tendency has recently been demonstrated to occur on a much larger scale, i.e. for large grain boundary facets (23).

For small deviations from the exact coincidence

Figure 6. Grain boundary curvature effected by variation in step orientation and dimensions. TP = boundary triple point, K = boundary kink (Murr et al, 2).

Figure 7. Illustrating the creation of boundary dislocations due to orientation deviation from exact coincidence.
(a) 53^{o} tilt boundary about [001] - low Σ
(b) creation of $\frac{a}{10}$ [310] boundary dislocation due to 3^{o} deviation (Bishop and Chalmers, 35).

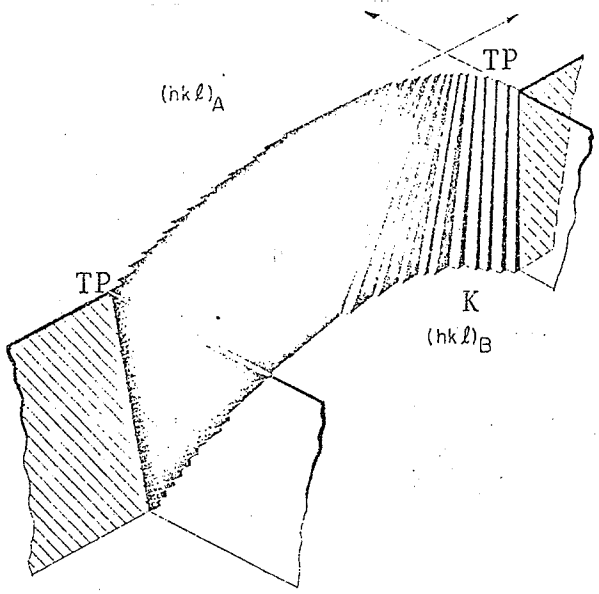
TP
$(hk\ell)_A$
TP
K
$(hk\ell)_B$

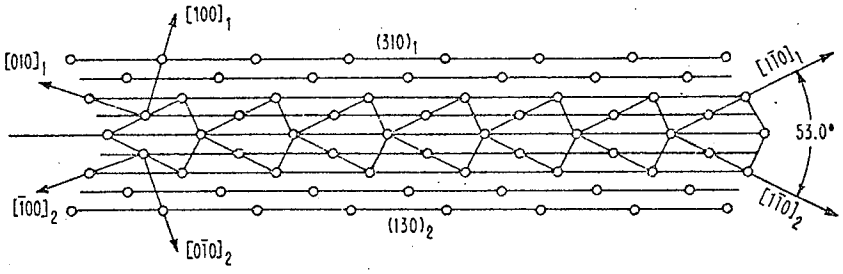
$[100]_1$
$(310)_1$
$[010]_1$
$[1\bar{1}0]_1$
53.0°
$[\bar{1}00]_2$
$[1\bar{1}0]_2$
$(130)_2$
$[0\bar{1}0]_2$

(a)

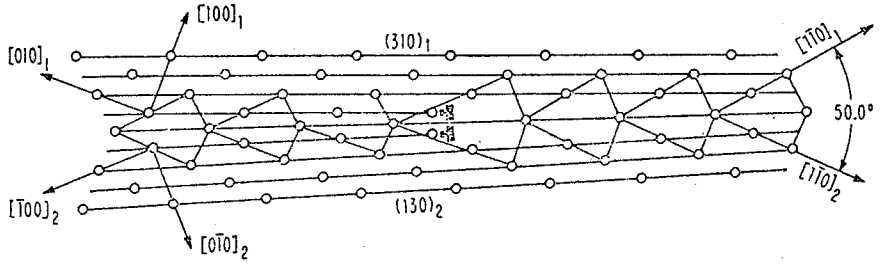
$[100]_1$
$(310)_1$
$[010]_1$
$[1\bar{1}0]_1$
50.0°
$[\bar{1}00]_2$
$[1\bar{1}0]_2$
$(130)_2$
$[0\bar{1}0]_2$

(b)

orientation (a few degrees), the boundary may be returned to the low energy orientation by imposing a dislocation network on the boundary which amounts to a sub-boundary of the coincidence lattice (22, 24). An example of such a dislocation is shown in figure 7 for a simple tilt boundary. The Burgers vectors of these dislocations (as for all boundary dislocations) may be derived from the DSC lattice of Bollmann (17). This lattice consists of all possible translations of one crystal lattice with respect to another. Thus, unlike the coincidence lattice which deals only with shared sites, the DSC lattice deals with all sites. Figure 8 illustrates this for a simple 36.9^{o} tilt boundary about <001>. The two interpenetrating lattices are shown (one open circles, one solid) and a cell of the coincidence lattice, ABCD. The primitive or base vectors of the DSC lattice, $\overline{b}_1$, $\overline{b}_2$, $\overline{b}_3$ indicate that a translation of the solid circles with respect to the open circles by any of these amounts (or multiples thereof) results in an identical configuration. In this sense, $\overline{b}_1$, $\overline{b}_2$ and $\overline{b}_3$ represent the smallest possible Burgers vectors for perfect grain boundary dislocations. The DSC lattice is simply constructed by drawing an orthogonal network through all lattice sites. The base vectors are then the shortest translations between sites in the three orthogonal directions. The DSC lattice is derived, in turn, from

Figure 8. DSC and coincidence lattice for a 36.9° tilt boundary about [001]

(a) viewed parallel to the rotation axis

(b) showing the three base vectors of the DSC lattice (Balluffi et al, 47).

Figure 9. Illustrating the O - lattice, similar to the coincidence lattice (AOBC), but supplemented by additional non - lattice points (such as O') about which the two interpenetrating lattices may be rotated with respect to each other (Fletcher, 29).

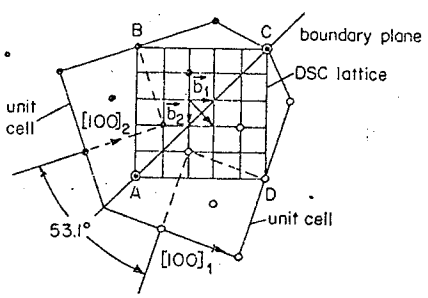
B
C
boundary plane
DSC lattice
unit cell
$[100]_2$
$\vec{b}_1$
$\vec{b}_2$
A
D
unit cell
53.1°
$[100]_1$

(a)

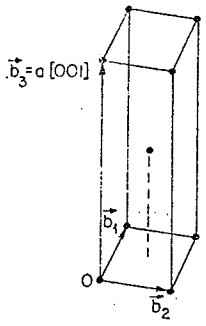
$\vec{b}_3$=a [001]
$\vec{b}_1$
O
$\vec{b}_2$

(b)

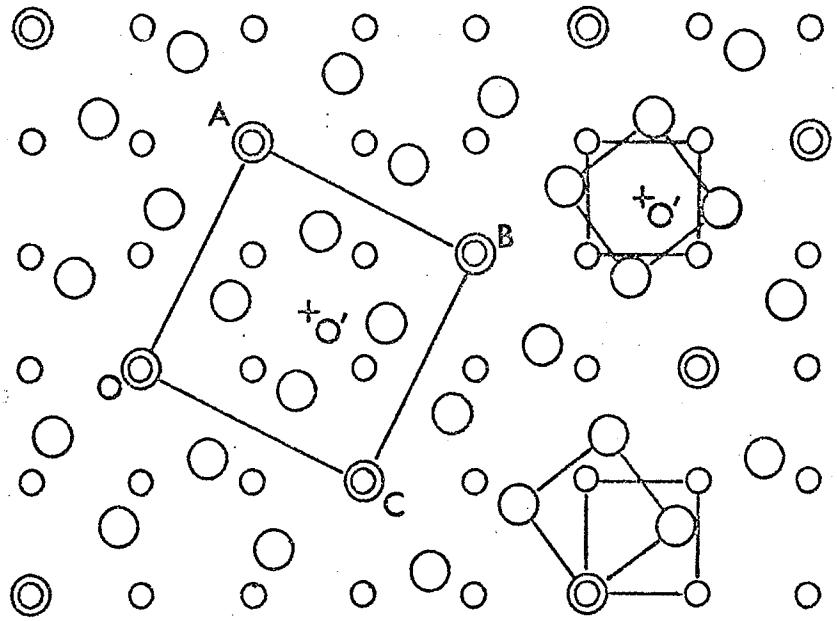
A
B
C
O'
O'

Bollman's generalized O - lattice (figure 9).

Although it somewhat resembles a coincidence lattice, the O - lattice is far more flexible as it permits crystal lattice translations about points in its lattice which are not crystal lattice sites, e.g. O' in figure 9. This occurs when the translation of one crystal lattice with respect to another is by a non - DSC vector (25). This would result in the breakdown of the coincidence model, but, as stated, the O - lattice merely shifts its lattice points off those of the crystal lattice. The significance of this is that virtually any boundary can be geometrically characterized even though its detailed physical structure is unknown.

These boundary dislocations have been experimentally observed (26, 27, 28) but only with difficulty, and for small deviations from coincidence. This is caused by two factors. First, the spacing of the dislocations is very sensitive to deviation from coincidence due to the relatively small values of Burgers vectors. These Burgers vectors decrease with increasing Σ (29), i.e. as the coincidence lattice becomes larger. Thus the dislocations are very close together even for orientations only a degree or so from exact coincidence. Second, the reduced Burgers vector results in poor electron microscope contrast due to the reduced strain field. Thus, Balluffi and Tan (18) have

recently proposed that such networks may be present over the entire misorientation range, only they cannot possibly be resolved. In such a case, it would be difficult to consider them in the normal physical sense of a dislocation network.

One final point of importance is that, while coincidence boundaries can account for a substantial fraction of all possible misorientations (24), there is no particular reason that they have to. That is, grain orientations are set either from nucleation in the melt or recrystallization nuclei, and not from energetic considerations which would only be realized when they begin to meet and form grain boundaries. Thus, Loberg et al (15) found no particular preference for exact coincidence orientations in a review of field ion microscope orientation determinations. One factor that could modify this randomness in the direction of more coincidence boundaries is that of texture, since this will at least orient grains so as to possess a common pole of low crystallographic index, which is essential to high degrees of coincidence. Also, it bears emphasis that, for a given orientation, the grain boundary will tend, through boundary migration and/or annealing twin formation, to lie along the lowest energy plane of the coincidence lattice for that orientation. The difference for different orientations is purely one of degree, since the reduction in

energy will be greatest for the high coincidence orientations.

2.2.5 STRUCTURAL UNIT MODEL AND OTHERS

One of the major weaknesses in the coincidence model is that the geometric requirements of lattice coincidence are quite rigid, i.e. the density of coincident sites drops precipitously when the misorientation moves even slightly away from exact coincidence. On the other hand, the change in properties which is characteristic of these boundaries often persists up to several degrees from exact coincidence (1). This led Bishop and Chalmers (30) to propose their "coincidence - ledge - dislocation" model of boundary structure which has subsequently evolved into the well-known structural unit model (1, 31, 32). The critical difference in this model is that it stresses boundary coincidence, i.e. sharing of atoms along the boundary plane, rather than lattice coincidence. As summarized by figure 10, an exact coincidence boundary (figure 10a) may thus be viewed as constructed of microledges of equal width (figure 10b). It may also be viewed as a "shared atom" configuration (figure 10c) or, alternatively, as a "translated" one (figure 10e). The array formed by the shared atoms of figure 10(c) is shown in figure 10(d), and the variation in the make-up of the structural units with misorientation is shown in figure 10(m).

Figure 10. Coincidence - ledge - dislocation representation of (a)-(f) 28.1° exact coincidence tilt boundary about [001] (g)-(l) 29.4° off - coincidence tilt boundary about [001] (m),(n) structural units for low Σ boundaries (Bishop and Chalmers, 30).

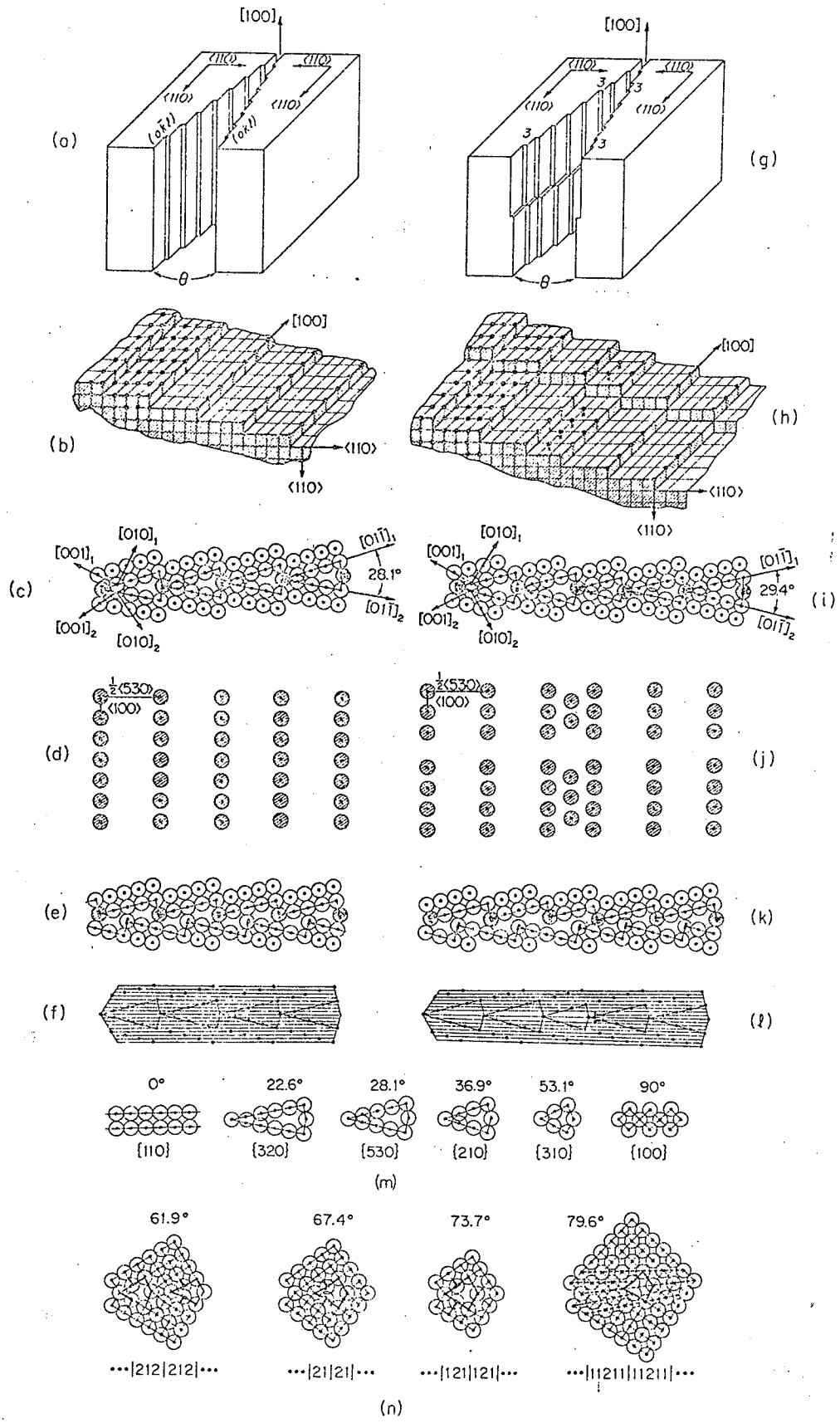
(a)
[100]
⟨110⟩
⟨110⟩
⟨110⟩
⟨110⟩
(0k̄l)
(0kl)
θ
(g)
[100]
⟨110⟩
⟨110⟩
3
3
3
3
⟨110⟩
θ
(b)
[100]
⟨110⟩
⟨110⟩
(h)
[100]
⟨110⟩
⟨110⟩
(c)
[010]₁
[001]₁
[01$\bar{1}$]₁
28.1°
[001]₂
[010]₂
[01$\bar{1}$]₂
(i)
[010]₁
[001]₁
[01$\bar{1}$]₁
29.4°
[001]₂
[010]₂
[01$\bar{1}$]₂
(d)
½⟨530⟩
⟨100⟩
(j)
½⟨530⟩
⟨100⟩
(e)
(k)
(f)
(l)
0°
22.6°
28.1°
36.9°
53.1°
90°
{110}
{320}
{530}
{210}
{310}
{100}
(m)
61.9°
67.4°
73.7°
79.6°
•••|212|212|•••
•••|21|21|•••
•••|121|121|•••
•••|11211|11211|•••
(n)

The units are designated in terms of the ledge lengths expressed as multiples of a/2 <110> (for this case), e.g. "3" for the 36.9° structural unit of figure 10(m). Deviations from exact coincidence are simply achieved by a mixture of the units from the two nearest exact coincidence orientations. Thus, for a 29.4° boundary, shown in figure 10(g-l), this results in four - "4" units followed by one "3" unit, i.e. a straight proportional mixture. For higher misorientations, the boundaries are mixtures of "2" ledges and an increasing number of "1" ledges (which are essentially regions of single crystal). These are shown in figure 10(n). In this fashion the boundary coincidence is high even though the lattice coincidence is low. Extra deviations (tilt or twist) result in additional ledges (figure 10g, h). The concept of the model in terms of dislocations arises from viewing any row of atoms ending at the boundary as the extra half plane of a dislocation, e.g. figure 10(e) or 10(k). It can be seen that the perturbations resulting from off-coincidence orientations (figure 10j) can be regarded in the same light as the coincidence lattice sub-boundary networks. These perturbations (dislocations) have the important effect of creating a long-range stress field at the boundary, with the extent being comparable to the distance between the perturbations (30). There is even a limited resemblance to

the island model in that the minority structural units of an off-coincidence boundary may be regarded as the bad fit regions (high strain) around the regions of good fit (low strain), although the two concepts are dimensionally different, one linear and the other, an area.

In recent years, this model has undergone further development by consideration of the structural units in terms of free energy as well as geometry. Thus Chalmers and co-workers (31, 32) have considered individual atomic displacements through computer calculations. (It should be noted that a similar consideration was undertaken by Baroux and co-workers (33, 34), but only in the geometric sense). The rationale leading to this consideration arises from the strength of grain boundaries. Since substantial numbers of dislocations can pile up against boundaries without penetrating through them, their strength should at least be of the same order as that of the perfect crystal (1), yet the shared fraction of atoms is relatively small, even for unrelaxed models. This localized relaxation results in an overall energy decrease (figure 11 - where $E(a) > E(b) > E(c)$), even though a trade-off is involved because of the addition of long-range elastic distortion. It is essential to realize that such relaxation will destroy all coincidence at the boundary. In this model, asymmetrical boundaries are

Figure 11. (a) 38^{o} tilt boundary - rigid structural unit model
(b) same boundary allowing crystal translation for energy reduction
(c) same boundary allowing individual atom relaxation for energy reduction (Gleiter, 1).

Figure 12. Asymmetrical 29^{o} tilt boundary about [001], composed of symmetrical segments DE, EF and FG (Chalmers and Gleiter, 32).

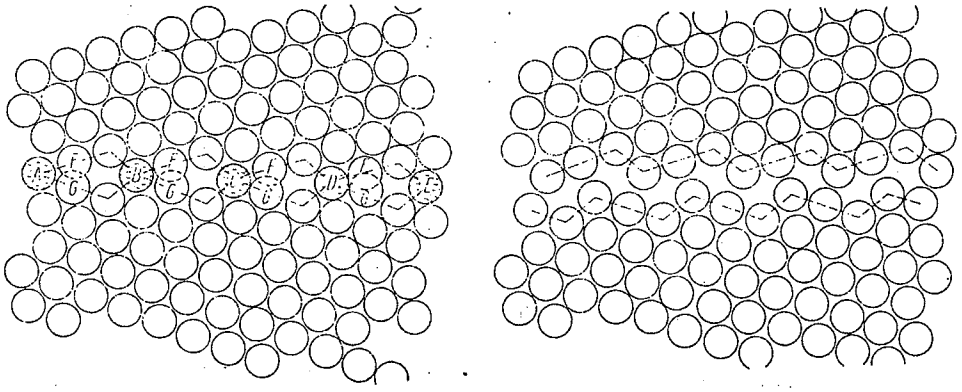

(a) (b)

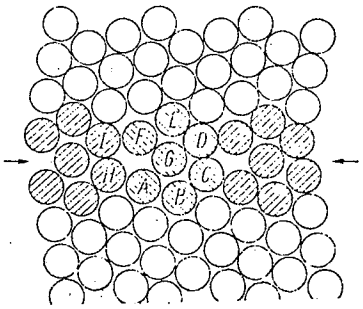

(c)

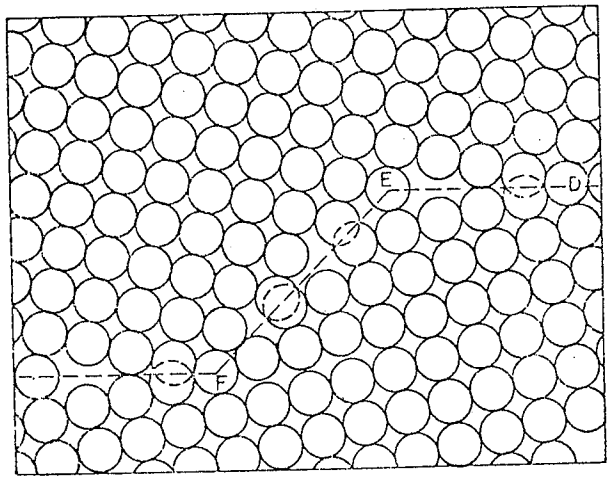

simply constructed by stepped segments of symmetrical boundaries, each with its own mixture (if need be) of structural units (figure 12).

Mention should be made of two very recent grain boundary models which, like the structural unit model, attempt a multi-faceted approach at describing the structure. In the planar matching model (36, 37), the basic premise is that families of atomic planes which meet at the boundary so that their traces are only slightly mismatched, will give rise to boundary dislocations similar to interfacial dislocations between two phases which are partially coherent (37). Another way of viewing these is to consider the slight mismatch of equi-spaced grids as producing a Moiré pattern in which the Moiré lines are lines of relatively bad atomic fit, i.e. dislocations (36). These dislocations would be somewhat different from the off-coincidence networks discussed earlier, especially in the fact that their spacing would be much less sensitive to deviation from a symmetric orientation (where the planes matched perfectly) and that their Burgers vectors would always lie in the boundary plane (37). Although the theory experimentally has been seen to account for some boundaries (38, 39), there is some question whether it can account for all boundaries (40), as a general model should. In addition, the model works best

when the matching planes are of low index, i.e. atomically smooth (37), and it could be questioned whether this is a reasonable assumption for random high angle boundaries.

The other model of Marcinkowski and co-workers is a coincidence-dislocation approach to boundary structure (41). The major premise is that all boundaries can be regarded as being composed of dislocations, said dislocations being regarded as various combinations of crystal lattice dislocations. For exact coincidence orientations, these lattice dislocations are visualized as coming from the primary slip planes of both grains, and the coincidence site lattice (denoted the primary coincidence lattice) is identical to that discussed previously. For off-coincidence orientations, lattice dislocations are visualized to come into the boundary from secondary slip planes also. It is shown that a new, larger coincidence lattice results (denoted the secondary coincidence lattice). The model takes issue with the Bollmann formulation for grain boundaries (17) in stating that boundaries can only be constructed in discrete fashion, i.e. as integral functions of the number of lattice dislocations used and the spacings of the slip planes used, and <u>not</u> in a continuous manner as the 0 - lattice approach allows. Hence the generation of specific coincidence lattices, primary and secondary. The model has been formulated

for both symmetric (42) and asymmetric (43) tilt boundaries, and for twist boundaries (44), in both ordered and disordered simple cubic lattices. In addition it has been extended for the above cases to the body-centered cubic lattice (45) and experimental observations of boundary dislocation networks have been conducted on a FeCo alloy with this structure (46). Much as in the planar matching model, this model thus furnishes a possible explanation for such networks which are very regular and spread over the entire boundary, yet have far too great a spacing to be the aforementioned off-coincidence sub-boundaries. However, as with the earlier, simpler dislocation models, there still remains the fact that, by and large, these boundary dislocations can only be considered geometrically and not physically. Thus, while these recent models are being assessed (and likely refined), the revised structural unit model appears currently to be the most acceptable for generating the best overall picture of the actual structure of the boundary, energetically, geometrically and physically. This picture appears to be moderately clear for relatively simple boundaries and is furnishing at least a dim outline of even the most random boundary. It would be appropriate at this point to consider the crystal defects associated with this basic structure.

Leaf blank to correct numbering

2.3 GRAIN BOUNDARY DEFECTS

2.3.1 TERMINOLOGY

As with any field which experiences a sudden surge of interest and new growth, there has been a proliferation in the terminology pertaining to grain boundaries which reflects the increasing sophistication with which this region has been studied. Unfortunately, the evolution of this terminology has been anything but orderly.

The topography of grain boundaries is moderately clear. Triple points generally refer to the intersections of three grain boundaries (figure 6, p.17) but can be used to describe twin boundary - grain boundary intersections. Large, relatively sharp changes in boundary curvature have been sometimes called kinks (k in figure 6) and are generally a consequence of limited grain growth. Small scale boundary curvature, such as shown in figure 6, is brought about by steps and/or ledges. The ledge is normally considered to be the longer of the two but, as is apparent by now, many authors use the two interchangeably. At the same time, these features are generally larger than the steps/ledges evident on even the most planar portions of boundary, e.g. figure 10 (p23). No real distinction appears to have been made between the two, so henceforth the latter will be termed microsteps or microledges.

The one boundary defect which has a counterpart in the grain interior is the grain boundary dislocation (GBD) and it is here that the terminology has run rampant. Brandon et al (22) referred to off-coincidence boundary dislocations as a dislocation sub-boundary. Schober and Balluffi (26, 27) have referred to them as intrinsic GBD's and McLean (7) has called them structural dislocations. To Bishop and Chalmers (35) they were secondary intrinsic GBD's (primary intrinsic GBD's were those forming exact coincidence boundaries). Brandon (24) discussed step dislocations, i.e. those associated with boundary steps, whereas Ishida et al (48) simply call these grain boundary dislocations, a term which they also apply to those making up the boundary structure and any lattice dislocations which have impinged upon the boundary (49). Similar "blanket" definitions have also been used by Bell and Langdon (50) and Ashby (51). Gleiter et al (52) used GBD only to denote boundary dislocations generated within the boundary. These and any other dislocations superfluous to the boundary structure were referred to by Schober and Balluffi first as extraneous GBD's (53), then as extrinsic GBD's (47). McLean (7) mentions intergrain dislocations in much the same context. Malis et al (54) have subdivided extrinsic dislocations into primary extrinsics (referring to those resulting from lattice dislocation - intrinsic GBD interactions) and secondary extrinsics (referring to those

produced in the boundary).

Marcinkowski (55) has defined the dislocations resulting from lattice dislocations cutting through the boundary as virtual grain boundary dislocations (VGBD's), meaning that they possess a stress field but no definable Burgers vector, although he has since reconsidered this assignation (57). Some authors have regarded boundary dislocations and steps as essentially equivalent (2) but there are important differences. As Ashby notes (51), movement of a true step produces boundary migration without relative displacement of the two grains, whereas GBD movement does. A step is a poor source or sink of vacancies while a GBD can be a good one. Furthermore, a GBD can interact strongly with solute stoms whereas a step generally does not (having a much weaker strain field). Finally, McLean (7) has proposed two overall structures for the grain boundary region - the general structure (that which brings about the misorientation between the two grains) and the defect structure (consisting of everything else associated with the boundary). This is a useful division for, as shall be seen shortly, it is the defect structure which appears to play the major role in dislocation generation from grain boundaries.

The confusion in terminology has been at least

partially cleared up by Hirth and Balluffi (56). They have proposed that any dislocation lying in a boundary be denoted a GBD. The one major exception to this blanket definition is for those dislocations forming the intrinsic structure of the boundary, i.e. those which bring about the misorientation. These are denoted intrinsic GBD's (IGBD's). As shown in figure 13, the Burgers vector of a GBD may be determined from a Frank circuit, the familiar circuit based on a lattice surrounding the defect in question. In the case of a GBD this is the coincidence lattice. Figure 13 illustrates this for a coherent twin boundary in the FCC lattice (for simplicity). Figure 14 illustrates what Hirth and Balluffi call a Read circuit, which can be based either on individual crystal lattices or suitably rotated DSC lattices. The closure failure in either case represents the total IGBD Burgers vector content of that portion of the boundary within the circuit, although this total may be decomposed in different ways, e.g. figure 14a where F_1F_2 can be decomposed in two ways. This may sound confusing, but it must be remembered (as emphasized earlier) that these are geometric equivalents only, hence the flexibility in partitioning the total Burgers vector content. When a GBD is present (figure 14 b or c), the closure failure gives the IGBD content plus the GBD Burgers vector. In such cases the IGBD content of a boundary can only be determined

Figure 13. (a) Coherent twin boundary in the FCC structure
(b) containing a Shockley twinning dislocation
(c) containing a pure ledge
(d) containing a GBD with Burgers vector normal to the boundary.

The Frank circuits are denoted $S_1F_1F_2S_2$ and two cells of the coincidence lattice are shown, as well as the DSC - lattice (Hirth and Balluffi, 56).

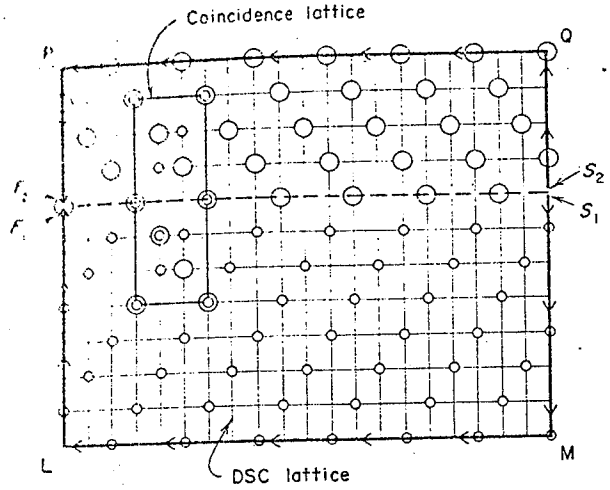
Coincidence lattice
P
Q
S_2
S_1
L
M
DSC lattice

(a)

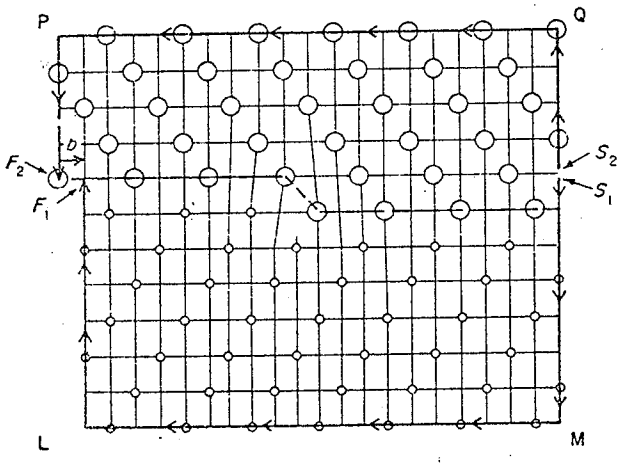
P
Q
b
F_2
F_1
S_2
S_1
L
M

(b)

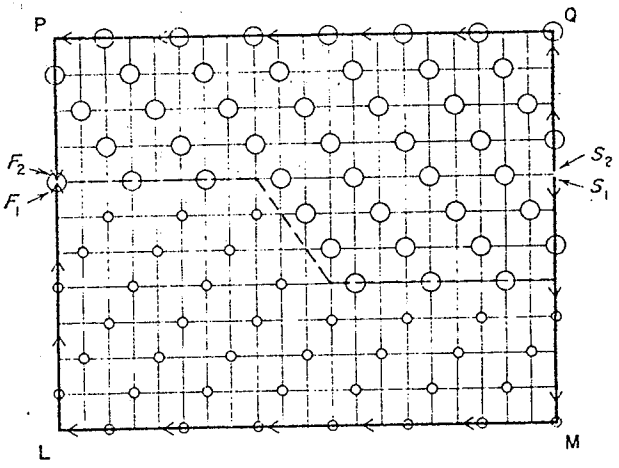
P
Q
F_2
F_1
S_2
S_1
L
M

(c)

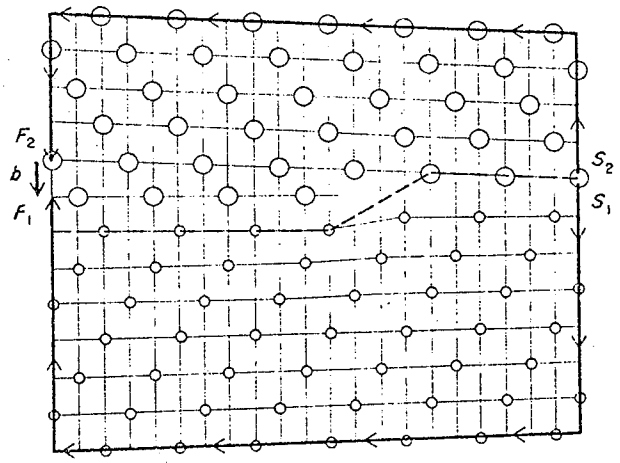
F_2
b
F_1
S_2
S_1

(d)

Figure 14. As figure 13 except that rotated DSC - lattices for each grain are shown, and Read circiuts based on the DSC - lattices (solid lines) and crystal lattices (dashed lines) are also indicated.

(a) Demonstrates how the total Burgers vector content (F_1F_2) may be regarded as four $\frac{a}{3}$ [111] IFBD's (spacings in the common DSC - lattice normal to the boundary) or six $\frac{a}{6}$ [112] IGBD's (spacings along the individual rotated DSC - lattices) (Hirth and Balluffi, 56).

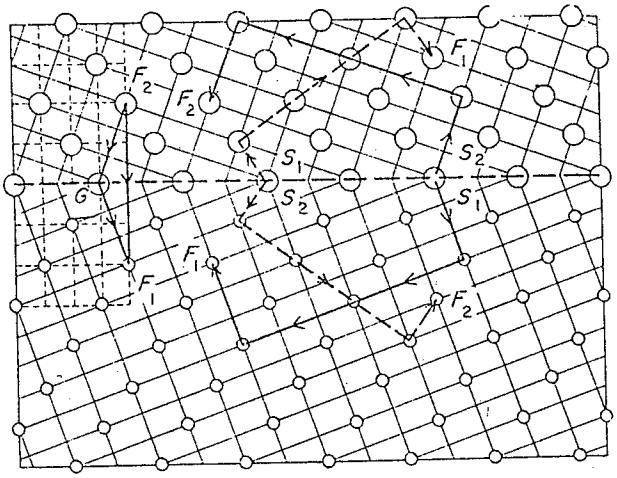

(a)

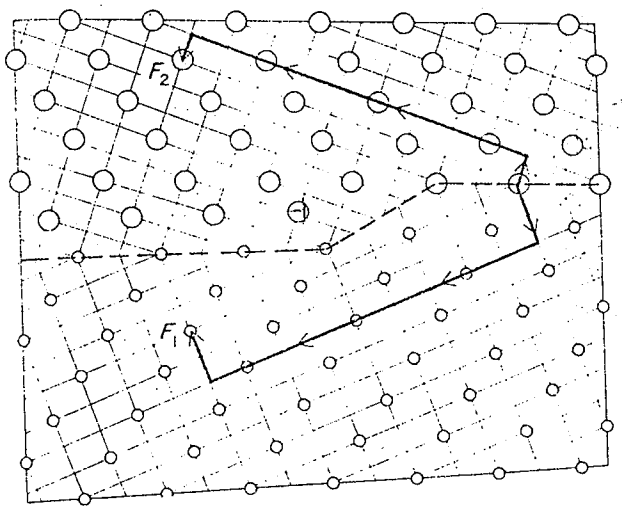

(c)

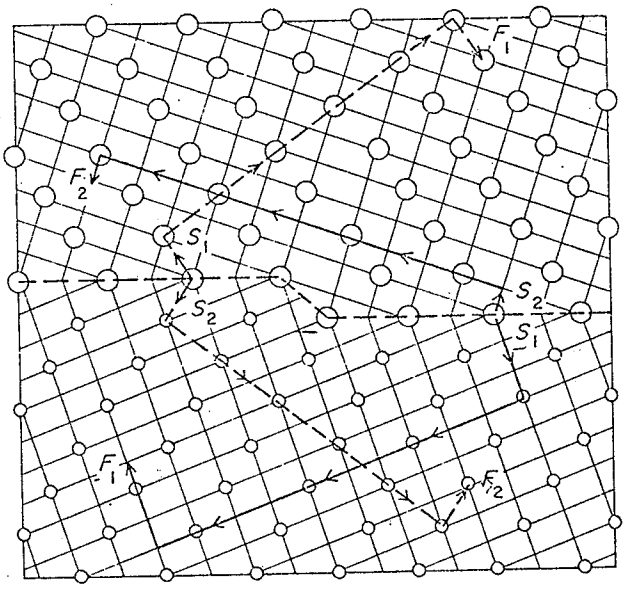

(b)

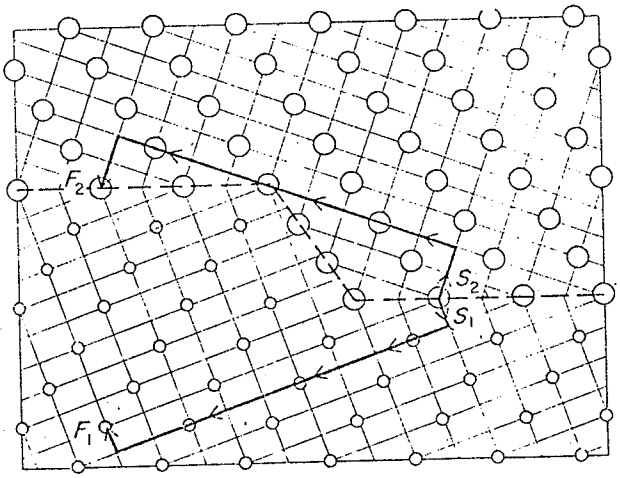

(d)

by constructing both Frank and Read circuits and taking the difference.

The second major classification of Hirth and Balluffi was to denote boundary dislocations as either primary or secondary, where primary refers to lattice Burgers vectors and secondary to any other Burgers vectors of the DSC - lattice. Thus the twin boundary dislocations of figure 13(b) and (d), IGBD's of low angle boundaries and some GBD's resulting from lattice dislocations impinging upon boundaries (53) are classified as primary.

It has become an established experimental fact that boundary steps can have GBD's associated with them (22, 48), e.g. when the step height is not an integral multiple of the coincidence lattice spacing (figure 15). Hirth and Balluffi have extensively categorized this situation. They first define a monatomic climb ledge (C - ledge) associated with a GBD whose Burgers vector is normal to the boundary. As shown in figure 16(c) and (d), the ledge character of the GBD (actually the extra half plane) arises because its climb along the boundary either expands or contracts the volume of the grain it lies upon. Glide ledges (G - ledges), also monatomic, are those associated with GBD's whose Burgers vectors are parallel to the boundary. The glide character arises because of the fact that the ledge movement (figure 16 (e) and (f)) takes place merely by

Figure 15. (a) C - ledge with Burgers vector normal to the boundary

(b) G - ledge with Burgers vector parallel to the boundary

Note that the step height is not an integral multiple of the coincidence lattice unit cell (large squares) (Darinskii and Fedorov, 58).

Figure 16. (a),(b) Construction of a reference bicrystal containing a defect - free grain boundary.

(c),(d) Introduction of a GBD with C - ledge character.

(e),(f) Introduction of either a pure ledge or a GBD with G - ledge character (Hirth and Balluffi,56).

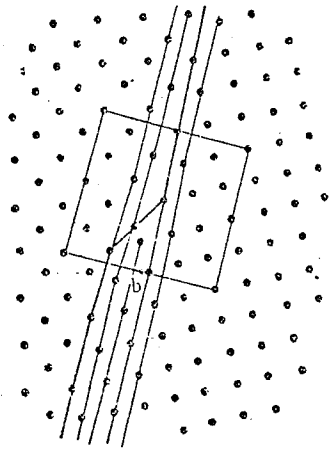

(a)

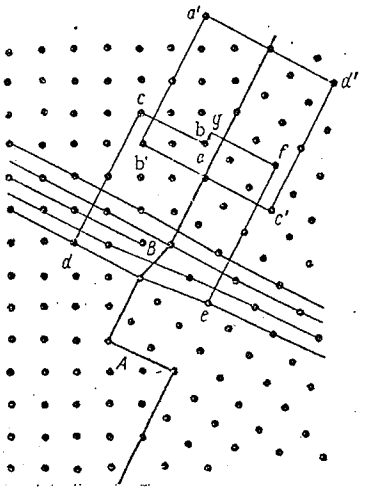

(b)

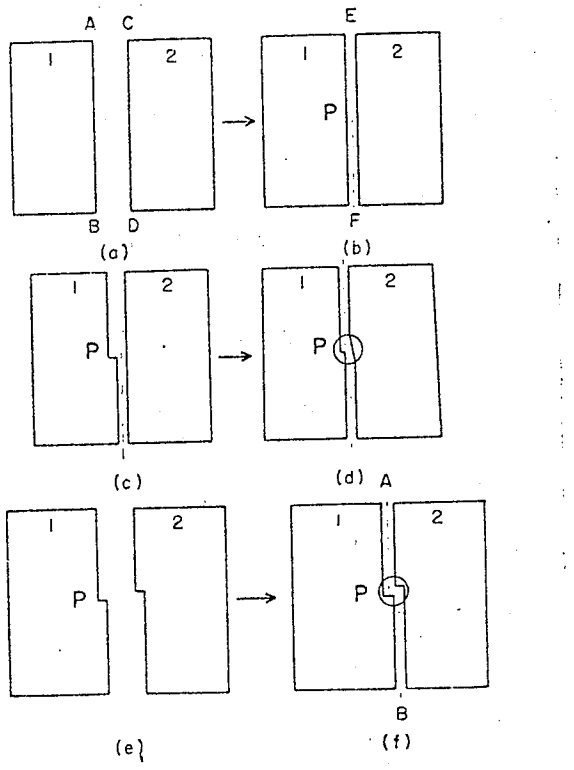

transferance of atoms from one crystal to the other. A pure ledge results (figure 16 f) when no displacement between the matching ledges occurs (no associated Burgers vector). A pure GBD may occur for the case of figure 16(b) when a localized displacement parallel to the boundary occurs that has no accompanying ledge characteristics. Thus figure 15(a) would be a GBD with C-ledge character and figure 15(b) would be a GBD with G-ledge character. A summary of the defects defined by Hirth and Balluffi is given in Table 1.

In addition, we will define a GBD-macroledge as an association of any GBD with a step of greater than monatomic height (such as if the G-ledge of figure 15(b) moved to the step, A). This distinguishment must be made since the GBD-macroledge would be much less mobile than either the C-ledge or G-ledge, even at elevated temperatures.

2.3.2 DIFFRACTION CONTRAST AND OTHER ASPECTS

The diffraction contrast of GBD's is rather complex, since the strain field extends into both grains, and no universally acceptable means of Burgers vector determination has evolved to date. Some contrast effects can be used to distinguish between various boundary defects. Gleiter (59) observed that pure steps showed very weak

TABLE 1

GRAIN BOUNDARY LINE DEFECTS AND CIRCUITS FOR REVEALING THEM (after Hirth and Balluffi,56)

ENTITY	DESCRIPTION
Grain boundary dislocation (GBD)	Any dislocation lying in a grain boundary. Its Burgers vector is a vector of the DSC-lattice.
Climb ledge (C-ledge)	A grain boundary ledge associated with a GBD which requires climb to move in the boundary plane.
Glide ledge (G-ledge)	A ledge associated with a GBD which may glide in the boundary plane.
Pure ledge	A ledge with no associated GBD.
Intrinsic grain boundary dislocation (IGBD)	A GBD which is part of the boundary structure and therefore does not possess a long-range stress field.
Frank circuit	Modified Burgers-type circuit for revealing GBD's
Read circuit	Modified Burgers-type circuit for revealing both GBD's and IGBD's.

Note: It is important to remember that the C- and G- designation refer to the dislocation movement in the boundary plane only. Thus they should not be confused with the dislocation's movement in the grain interior,i.e. a C-ledge will glide into the grain interior,but climb in the boundary plane.

contrast (due to their small strain field), a contrast which did not change noticeably with tilting. GBD's, on the other hand, can be made to disappear quite readily and their contrast can be quite strong, depending on the magnitude of their Burgers vector. Ishida and Henderson-Brown (49) noted that GBD's showed a contrast reversal from black to white when tilted from a strong operating reflection to its negative. They further maintained that this would also apply to dislocations adjacent to the boundary, presumably because their strain field would extend into the adjacent grain. Thus there is likely to be a definite zone around the boundary proper in which lattice dislocations will be indistinguishable from GBD's. With regard to the contrast reversal, McDonald and Ardell (60) have discovered that it does not occur when the strongly diffracting grain is on the lower side of the boundary plane in a thin foil (this would be the left-hand grain in figure 1), thus the above criterion should be used cautiously in separating GBD's from lattice dislocations. McDonald and Ardell also note that an indicator of the strong two beam condition in only one grain is an attenuation in the boundary fringes toward the thick end of the boundary wedge, i.e. if the two beam condition was operating in the left-hand grain of figure 1, the fringes would disappear towards AB. Deviation from such a condition would result in the normal

boundary contrast with fringing at both top and bottom and attenuation in the center. The importance of this lies in the fact that high contrast micrographs of GBD's for studying fine details, are best obtained in the dark field of the strong two beam case, e.g. (46).

IGBD Burgers vectors are generally small and their contrast quite weak (26, 27), but Ishida and McLean (61) have recently suggested that the Burgers vectors of IGBD's in random high angle boundaries should approach lattice Burgers vectors. They calculated the three base vectors of the DSC-lattice (figure 8b, p.19) for various FCC and BCC grain misorientations. They found that, as Σ increased (i.e. tending toward more random orientations), $\underline{b}_1$ and $\underline{b}_2$ decreased while $\underline{b}_3$ approached the interplanar spacing of the planes normal to the misorientation axis. Thus, for symmetrical boundaries, the IGBD Burgers vector would lie in the plane of the boundary, as in the planar matching model. This works quite well for low index misorientation axes, but would not seem to be of much significance for high index ones. Visual confirmation of this hypothesis would be difficult because of the close spacing for IGBD's. Nevertheless it is difficult to believe that these IGBD's would be those seen in "normal polycrystalline specimens", as Ishida and McLean suggest. If that were the case, boundaries even in annealed material would be expected to

show a very high GBD density. There is field ion microscope evidence that IGBD's with lattice Burgers vectors exist, e.g. $\frac{a}{3}$ <111> IGBD's in BCC tungsten (62), but it is to be remembered that boundaries in such specimens are highly textured and are not totally representative of normal polycrystals.

If, in some cases, IGBD's and GBD's can individually show similar contrast, the same would apply to the GBD-macroledge configuration. One therefore has to examine both the shape and density of the defects. Figure 17 shows what this author believes to be reasonably clear examples of these defects (in agreement with the authors of the studies). Thus strong contrast, irregular spacing and curvature indicate the defects of figure 17(a) are likely pure GBD's. The boundary dislocations of figure 17(b) are more regularly spaced, but still relatively far apart. This separation plus the strong contrast and curvature, favor them to be GBD's. The faint network of background defects (fine lines running almost vertically) is almost certainly of IGBD's because of their close and very regular spacing and weak contrast. In figure 17(c) the large fringe shifts, straightness of the defects and semi-regular spacing indicate a pure ledge character, the strong (in part) contrast and spacing variation in different boundary segments rule out IGBD's, hence the conclusion that they are GBD-macroledges.

Figure 17. (a) Pure GBD's in a grain boundary of 0.2C-Nb steel (Buzzichelli and Mascanzoni, 63).
(b) GBD's and IGBD's in an Al bicrystal boundary (Kegg et al, 64).
(c) GBD-macroledges in a grain boundary of Fe-0.75Mn (Ishida et al, 48).
(d) Pure ledges in Fe-0.75Mn (48).

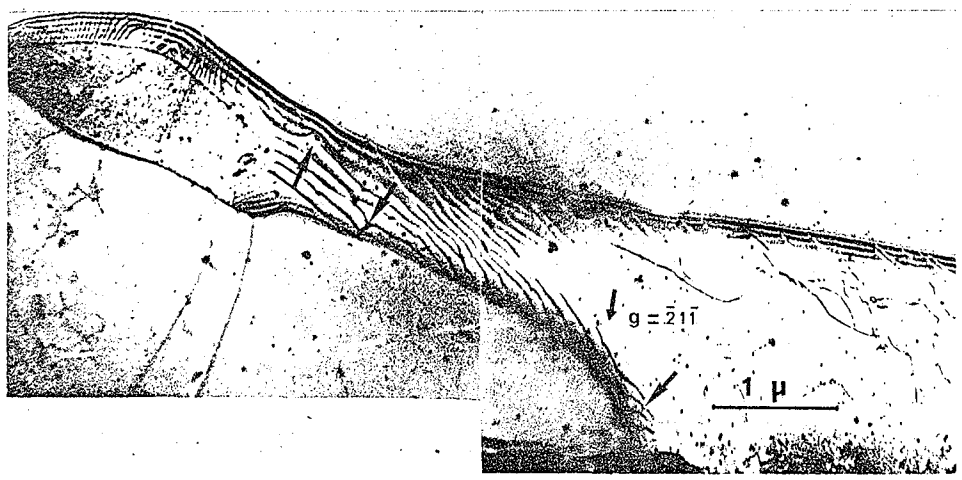

(a)

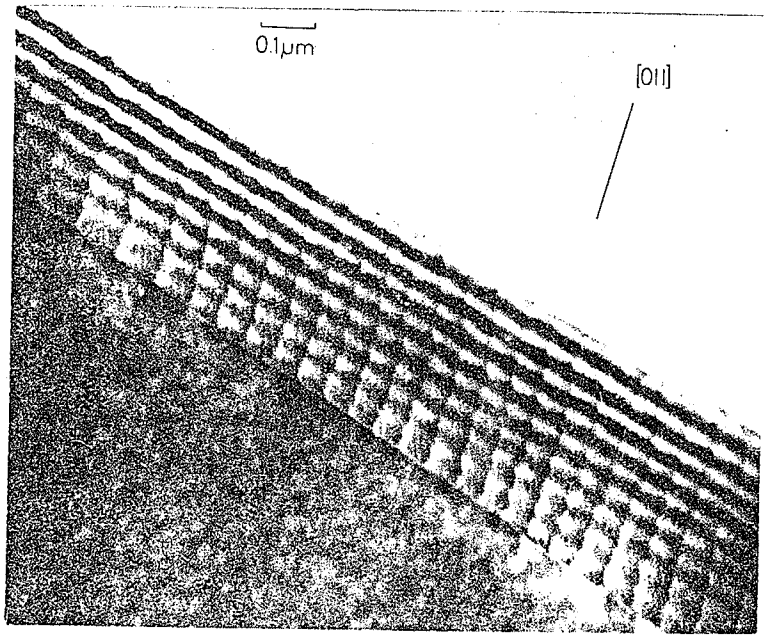

(b)

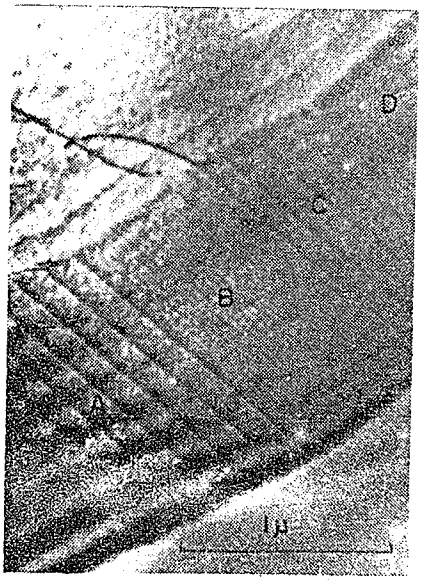

(c)

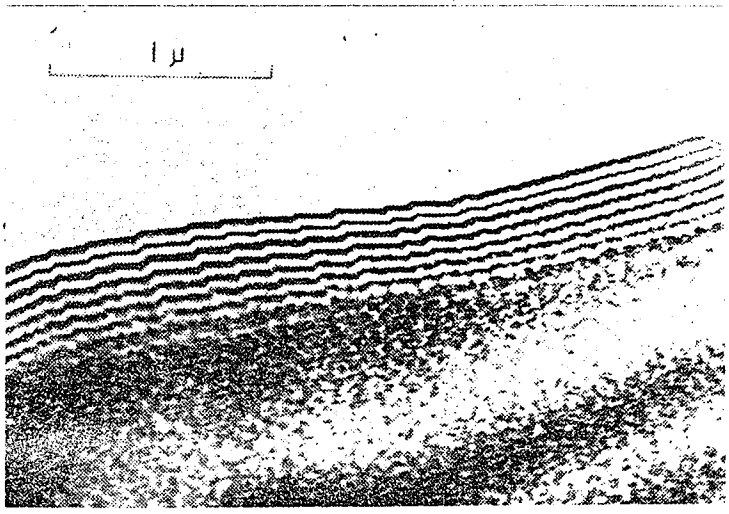

(d)

For figure 17(d), the complete lack of contrast and pronounced fringe shifts easily identify the defects as pure ledges. Unfortunately, cases such as these are the exception rather than the rule and a good deal of thought should generally go into the identification of a boundary defect. For example, the fact that both C-ledges and G-ledges have step characteristics gives rise to the possibility of their creating small fringe displacements (Gleiter has calculated (59) that a 3Å step can, under certain extreme conditions, produce a fringe displacement of over 100 Å). This displacement would be very similar to those from monatomic pure ledges. In addition, the fact that both the C-ledge and the G-ledge have steps of similar dimensions renders them practically identical for pure contrast purposes. We shall later see that this may well have occurred in the literature. A summary of contrast characteristics is given in Table 2.

As with their diffraction contrast, the interactions between boundary defects are being increasingly observed and discussed. Ashby (51) has suggested that supersteps (the equivalent of GBD-macroledges) could form by the combination of several smaller GBD-macroledges, resulting in an energy reduction. In the same way, Ishida and McLean (61) propose that a pure GBD with a Burgers vector

TABLE 2

DIFFRACTION CONTRAST EFFECTS FOR BOUNDARY DEFECTS

DEFECT	CHARACTERISTICS
pure ledge	-small (and occasionally undetectable) to very large boundary fringe displacements -very weak contrast -semi-regular spacing for groups of ledges -generally linear
pure GBD	-no fringe displacement under any conditions -generally strong contrast -generally curvilinear
IGBD	-generally very weak contrast -very small, regular spacing -array covers entire boundary -generally linear
GBD-macroledge	-fringe displacement as pure ledge -contrast as pure GBD -semi-regular spacing for groups -generally linear
C-ledge, G-ledge	-small (and normally undetectable) fringe displacement -varying contrast -generally curvilinear

that is a multiple of the DSC-lattice base vector could be more energetically favorable than a GBD-ledge defect, even though the Burgers vector associated with the latter might be slightly smaller. Both of these thoughts suggest that the majority of GBD-ledge configurations would eventually disappear in a prolonged anneal. There should be no reason why GBD's could not interact with the IGBD network for near-coincidence orientations, as Schober and Balluffi propose (53). However, when the spacing of this network becomes so fine that the IGBD's lose their physical identity, it would seem reasonable to regard any such interaction as unlikely. On the other hand, Pumphrey and Gleiter (65) have observed GBD's "smearing-out" in the boundary plane in the electron microscope and eventually disappearing. One would think that this multiple dissociation would certainly involve the IGBD network. From Pumphrey and Gleiter's observations, it would appear that temperature is the critical factor through its effects on the kinetics of dislocation reactions and possible non-conservative dislocation motion necessary for such reactions. Thus the "smearing-out" phenomenon was a moderately high temperature one.

Finally, Ashby (51) has made some interesting comments on the nature of any boundary dislocations which

stands apart from other boundary defects so as to possess a separate identity. First, outside the dislocation core, they should behave identically to lattice dislocations as far as their long-range elastic strain fields are concerned, i.e. with regard to interactions, line tension, etc. Second, for the core itself, he proposed that it would be elongated in the plane of the boundary and shortened normal to it in order to take advantage of the additional atomic relaxation available therein. As Ashby puts it, this "reflects a balance between the elastic energy stored in the two half-crystals and the misfit or distortion energy associated with the disturbed atom positions in the boundary". He estimated that this would lead to a core energy approximately one-half that of a lattice dislocation, creating, in effect, a binding energy for the GBD to the boundary.

2.4 GRAIN BOUNDARY SEGREGATION

It would be appropriate, at this point, to briefly discuss boundary segregation, i.e. local variation in composition at the boundary, since one solid solution will be studied and even the pure metals to be examined will possess varying numbers of impurity atoms. This will be done with reference to their relation to boundary structure, so that both may later be used to facilitate the understanding

of dislocation generation from boundaries. This area of grain boundary research is somewhat better established than others because of such aspects as grain boundary embrittlement furnishing powerful commercial incentives for its study. In addition, it can be detected, to at least some degree, by relatively simple techniques. Thus several excellent reviews have been written which combine the theoretical models with a substantial amount of experimental data on all aspects of the models. Among these are Gleiter and Chalmer's relatively recent review of equilibrium segregation (21) and Westbrook's reviews on non-equilibrium segregation (66, 67).

2.4.1 EQUILIBRIUM SEGREGATION

At or near grain boundaries, a local variation in composition may exist in equilibrium with the matrix. This is by far the most common segregation encountered, but unfortunately it is rather difficult to quantify or, occasionally, even to detect at all. This may be understood from figure 18(a) which illustrates that the solute concentration at the boundary can be very large, but confined to a region extremely close to the boundary. In the past it has been detected by such means as microhardness, chemical etching, autoradiography and lattice parameter

Figure 18. Schematic representation of the solute profiles at grain boundaries for various bulk solute levels (BSL) for

(a) equilibrium segregation

(b) non-equilibrium segregation due to vacancy migration

(c) non-equilibrium segregation due to boundary migration (boundary movement indicated by arrow).

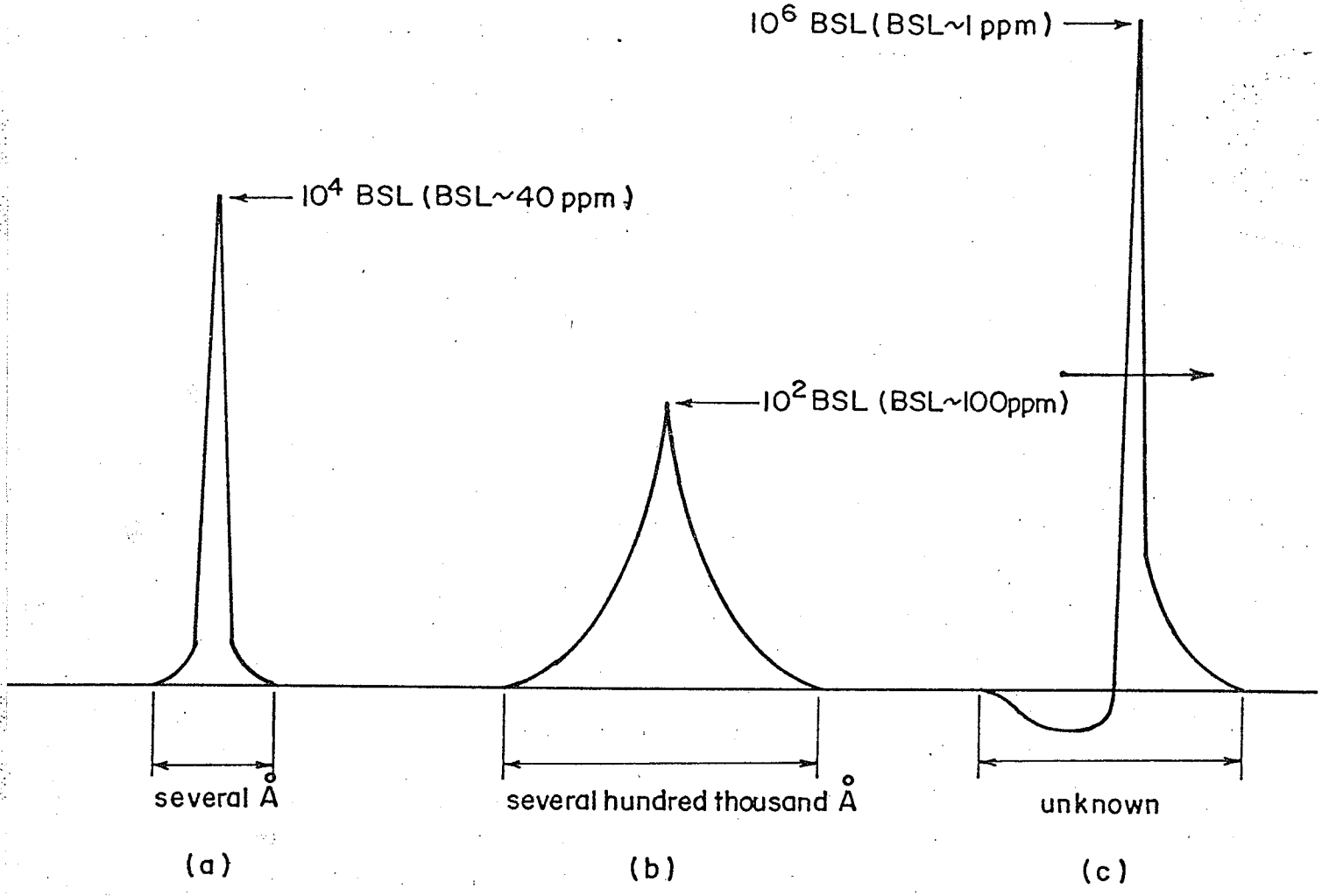
10^6 BSL (BSL~1 ppm)
10^4 BSL (BSL~40 ppm)
10^2 BSL (BSL~100ppm)
several Å
several hundred thousand Å
unknown
(a)
(b)
(c)

variation, but more recent and sophisticated methods such as field ion microscopy and auger electron spectroscopy have been able to quantify it with greater accuracy (21).

The driving force for this segregation may be examined from two different viewpoints. One is that any solute which causes a reduction in the grain boundary energy will tend to segregate to the boundary to lower the energy of the polycrystal as a whole. Such reductions are by no means minor, e.g. Hondros and Seah (68) have shown that as little as 0.5 wt. % Sn reduces the grain boundary energy of Fe by a factor of two.

The second viewpoint, that of elastic interaction, simply states that oversized impurity atoms will migrate to regions of tensile strain (e.g. open spaces) in the grain boundary, while undersized atoms migrate to regions of compressive strain (e.g. overlapping atoms). This approach thus utilizes the structural concept of grain boundaries and the fact that equilibrium segregation of impurity atoms of various sizes exists is verification of the basic physical picture of boundary structure, i.e. a region containing both (+) and (-) strains. Further proof is provided by the fact that non-coincidence (high energy) boundaries show substantially more segregation than coincidence boundaries (21).

In view of the above, it is apparent that, for a given solute, the two critical factors for this segregation are time and temperature, i.e. sufficient time at a high enough temperature will result in an equilibrium amount of the solute being partitioned to the grain boundary. In addition, both theory (21) and experiment (69) show that the equilibrium level increases with decreasing temperature. Thus most quantitative work on this phenomenon involves rapid cooling from the equilibration temperature, because slow cooling would result in levels greater than the equilibrium concentration corresponding to this temperature.

Although equilibrium segregation is normally on a monolayer scale, segregation of a broader nature has been observed in iridium (70) and in Fe - Sn alloys (71) at the higher base solute levels (4 wt. %). In general, the amount of segregation becomes increasingly less sensitive to base solute level at concentrations of these magnitudes. With regard to the degree of enhancement (boundary solute content/bulk solute content), it has been demonstrated both empirically (68) and theoretically (71) that this degree varies as the inverse of the maximum solid solubility of the impurity. Thus, for example, Hondros and Seah (68) obtained enhancements of 3 for Fe-3 wt. % Si (maximum solubility 23 at. %), 460 for Fe-0.2 wt. % Sn (maximum solutility 10 at. %) and 10,000 for Fe-0.0044 at. %S

(maximum solubility 0.1 at. %). This can be useful in predicting the order of enhancement from a given impurity. It is important to note that the effects of multiple impurities are uncertain with regard to any interactions, although Seah and Hondros (71) have found that Sn and S in Fe are non-competitive.

Finally, the pervasiveness of this segregation may be illustrated by the fact that even one part per million (ppm) of certain impurities can, under the right conditions, saturate all the grain boundaries (21). Thus, for all practical purposes, equilibrium segregation is always present to some degree, and its effect on a given property of the grain boundary will depend on the sensitivity of the property to enhanced solute levels.

2.4.2 NON-EQUILIBRIUM SEGREGATION

As implied by the title, these compositional variations are generated by non-equilibrium conditions, such as excess point defect concentrations causing point defect-solute pairs to migrate to the boundaries (which act as sinks for the point defects). Thus, unlike equilibrium segregation, it will ultimately disappear if given enough time. Because of the special driving forces which can cause it, it is much less common than equilibrium

segregation. However, it occurs on a much more detectable scale (figure 18 b), extending as far as 40 microns into the grain interior (72). Thus non-equilibrium segregation is commonly measured by a microhardness increase (up to 35% at the boundary) due to the enhanced solute level. The width of the segregated regions can be so wide that the hardening from opposite boundaries may overlap for smaller grain sizes (72). It should be made clear that the hardness increase due to such segregation is much greater than any microhardness increase attributable to the boundary without solute present, i.e. due to its inherent nature as a highly defected (or strained) region. (The same fact holds for equilibrium segregation). In some cases (73), boundaries also appear to demonstrate a softening effect, likely because of the creation of a vacancy-free zone around them attained when the material is quenched from near the melting point. As with the equilibrium segregation, the enhancement levels are greatest for small amounts of impurities. The illustrative level of figure 18(b) comes from calculations by Anthony (74) based on work in which the base solute level was of the order of 10 - 100 ppm (73, 75).

The most acceptable model of this segregation has been derived primarily by Westbrook and co-workers (73, 75).

It is believed to be caused by the migration of solute - vacancy pairs to the grain boundary during rapid cooling (the effect is markedly reduced by slow cooling (76)). Unlike equilibrium segregation, size misfit does not appear to play the major role, e.g. segregation was found (75) in Zn with Al impurity (atomic radii 1.38 and 1.43 Å, respectively) whereas reverse segregation or boundary softening was found in Pb with Ca impurity (atomic radii 1.75 and 1.97 Å, respectively). It was discovered that the presence of this segregation coincided with a distribution coefficient less than one (ratio of solidus to liquidus concentration at a given temperature), which, in turn, was demonstrated to empirically correlate with a large, positive solute-vacancy binding energy. In addition, it coincided with an activity coefficient (an indicator for the different atomic interactions in a solution) greater than one. This indicates a preference for solute-solute bonds in the system, i.e. good cluster stability. Thus the following picture emerges; a large driving force is obtained upon quenching due to the large number of non-equilibrium vacancies. This, in turn, results in many solute-vacancy pairs (because of the strong binding energy) which migrate towards the most efficient vacancy sinks, the grain boundaries. As these pairs near the

boundary their density increases and collisions take place with increasing frequency, forming di-vacancies and relatively immobile solute clusters. These clusters are thought to give rise to the increased hardness (which, incidentally, is higher than would be expected from the increase of solute in solid solution). Grain boundary softening is also explained by the same model (74, 77) on the basis of the relative mobilities of solute and solvent. Thus, when the solute-vacancy binding energy is of the order of the thermal energy and the solute is quite mobile in the solvent lattice, a net flow of solute away from the boundary can occur because of vacancies using solute atoms as a diffusion path. Since non-equilibrium vacancies are the media for solute transfer, the effect saturates for a solute concentration of a few hundred ppm, which is the order of the maximum non-equilibrium vacancy concentration normally attainable. This also explains the reduction in hardening with a slow cooling rate, since the non-equilibrium vacancy concentration (and, as such, the driving force) is, at a given instant, extremely small. This favors the more mobile single and di-vacancies to migrate to the boundaries instead of the solute-vacancy pairs.

One other theory has been proposed (78), based on the same vacancy-solute mechanism, which predicted maximum

segregation with a slow cooling rate (contrary to the above). This was apparently also confirmed experimentally (79). However, the experimental method used (chemical dissolution of a few microns around the boundary for atomic adsorption spectrophotometry) suffers from the fact that it would have included equilibrium segregation as well, and excluded much of the non-equilibrium segregation. This points out the difficulty in separating the two types of segregation, which, however, must be done in view of the widespread occurrence of equilibrium segregation. A good example of the misinterpretations possible without this dual consideration appears to be provided by a study of binary Cu alloys both quenched and furnace cooled from temperatures ranging from 500 to 1000^{o}C (80). Although the tests were ostensibly a study of equilibrium segregation by means of microhardness tests on the boundary and in the grain interior, the authors stated that "no very great difference" was found in the results for the two cooling rates, contrary to the preceeding discussions for either segregation. Such unexpected results may be explainable via the above dual consideration. Thus, quenching would enhance non-equilibrium segregation, particularly from high temperatures, while slow cooling would enhance equilibrium segregation, particularly from low temperatures, resulting in equivalent

hardness increases even though obtained by different mechanisms. The situation becomes even more complicated when the behaviour of boundary defect densities is also considered. For example, rapid quenching can set up sufficient stresses to cause a very large increase in the density of GBD's and/or GBD-ledges. The multitude of subsequent possible interactions with varying amounts of solute segregation that then arises is very likely the cause of some contradictory stands that have been taken with regard to the influence of these interactions on mechanical behaviour (81, 82).

Mention should be made of one other type of non-equilibrium segregation that applies to super-purity metals and has only recently been detected by Kasen (83). He used high temperature, isochronal anneals to conduct resistivity studies on Al of varying purity (0.5 - 4 ppm). His results indicated that the migrating grain boundaries during the anneals swept up solute as they moved through the lattice. The enhancement that was calculated for this segregation corresponded to equilibrium segregation for a base solute level of 3000 ppm. Since these levels were actually only a few ppm, an additional enhancement above equilibrium levels was obtained (roughly 3000:1). The unusual solute profile associated with such segregation

(figure 18 c) is markedly asymmetrical due to the build-up of solute in front of the moving boundary. It may be pointed out that the profile of figure 18(c) applies at high temperatures, and the room temperature profile will be affected by the cooling rate. Furthermore, the effect practically disappeared at the 4 ppm solute level, thus it should not be significant in metals containing more impurities than this.

In sections 2.2 and 2.3, we have seen that the grain boundary region is far from the simple, unstructured region it was once thought to be. Instead, in most cases, it is a region of both order and disorder, with both its own crystal defects and those from the grain interior present upon it in varying numbers. This variation in the detail of the boundary region may vary, not only from one microstructure to another, but from boundary to boundary within the microstructure, and even from one portion of a boundary to another. Nevertheless, this very complexity can make it possible to postulate <u>detailed</u> interpretations for certain grain boundary phenomena. Such concrete proposals, if proven, will be much more valuable than the general explanations often given, particularly for the role of boundaries in the early stages of yielding.

3 DISLOCATION GENERATION FROM GRAIN BOUNDARIES

Having examined the basic structure of the grain boundary and the crystalline imperfections associated with it, we can now focus our attention on the manner in which this region can produce dislocations at low temperatures and why it does so in preference to the grain interior sources. In view of the relatively recent emergence of this field and the controversies in which it is often embroiled, it would perhaps be appropriate to first examine the previous experimental evidence for such generation.

3.1 EXPERIMENTAL EVIDENCE

As seen in Table 3, the direct visual observation of boundary generation has been quite extensive. The reliability of the evidence was done as objectively as possible, but obviously cannot be considered as final and conclusive. It was felt, though, that this would enable some needed qualitative worth to be placed on the various studies. For example, it was found that numerous cases have occurred in the literature where a reference was made to some other confirmation of boundary generation, even though such generation was only casually mentioned or indirectly inferred. On the other hand, it appears that numerous studies have been conducted in which it was

TABLE 3

EXPERIMENTAL EVIDENCE FOR GENERATION OF DISLOCATIONS FROM GRAIN BOUNDARIES

- all testing at room temperature unless otherwise indicated, all material single phase except where indicated

RELIABILITY A - conclusive proof of generation C - more likely than interior generation
B - high probability of generation D - inconclusive

EP = etch-pitting TEM = transmission electron microscopy

REFERENCE	MATERIAL	EXPERIMENTAL DETAILS	COMMENTS	RELIABILITY
84	Nb	in situ foil heating (TEM)	Very obvious examples of generation.	----
85	Zn	as(84)	Not as obvious as in (84).	----
86	Al	as (84)	No micrographs, but generation mentioned in text.	----
87	18-8 stainless steel	in situ foil straining	Very good pictures of partial and perfect dislocation generation from twin and grain boundaries.	----
88	Fe(99.99)	as (84)	Good sequence of dislocations emanating from supposed Frank-Read source on boundary.	----
89	Al	in situ foil straining (HVEM)	As (86).	----
90	Fe-3Si	20,170 μm gr.diam. near yield point (EP)	Concluded grain interior sources although slip bands against only 1 boundary. Slip initiation stress independent of gr.diam. Higher % of yielded grains in large gr.diam.	B
91	Fe-3Si	30-260 μm gr.diam. near yield point(EP)	Sources generally located on 1 g.b. segment. Most emanation from only 1 side of boundary. Generation into both grains nearly collinear.	A
92	Fe-3Si	90-1600 μm gr.diam. near yield point(EP)	Triple points favored as slip band sites. Interior sources assumed, but slip bands indicated boundary sources, as (90).	A

TABLE 3 (continued)

REFERENCE	MATERIAL	EXPERIMENTAL DETAILS	COMMENTS	RELIABILITY
93	Fe-3Si	premacroyield region (EP)	Enhanced boundary generation in surface grains. Concluded no nucleation involved in boundary generation.	A
94	Fe-3Si	25-800 μm gr.diam. premacroyield region (EP)	Found initiation stress dependant on grain diameter.	B
95	Fe-3Si	10-150 μm gr.diam. (EP)	Only 1 micrograph, which is inconclusive.	D
96	Fe-3Si	1000-5000 μm gr.diam. premacroyield region (EP)	Showed majority of yielded grains to be elastically harder than neighbour grains.	----
97	Fe-3Si	76 μm,pulse loading near yield point(EP)	Conclude boundaries are dislocation sources unless surface scratches are present.	B
98	Fe-3Si	premacroyield region (EP)	Triple points and kinks favored as sources. Higher % of yielded grains in large gr.diam.	A
99	Fe-3Si	(EP)	One micrograph with slip bands emanating from 1 side of 1 boundary.	C
100,101	Fe-3Si	bicrystals near yield point(EP)	Observed primary slip from boundary,interior and crystal surface. Observed secondary slip from boundary.	D
102	β-brass	as (100,101)	Observed secondary slip from boundary.	D
103	Nb(99.85)	30-2300μm gr.diam. near yield point(EP)	Triple points and kinks favored as sources. Observed cases of classical pileup-propagation. Much higher slip band density around boundary than interior at 1.6% strain.	A
104	Cu(99.98)	5000 μm gr.diam.(EP)	Observed primarily interior sources, but some micrographs show slip bands at only 1 boundary.	D
105	MgO	3-100 μm gr.diam. premacroyield region (EP)	Found initiation stress independant of gr. diam. but stress for propagation across grain dependant on same.Observed triple point preferance for slip band location.	A

TABLE 3 (continued)

REFERENCE	MATERIAL	EXPERIMENTAL DETAILS	COMMENTS	RELIABILITY
106	Cu,Ni,Zn Al,Ge	15-110 μm gr.diam. microyield point (slip lines)	Initiation stress dependant on grain diam. Slip began in large grains and spread across grain during premacroyield region.	no figures
107	Pb	bicrystals, 25°-110°C (slip lines)	Observed secondary slip around boundaries, possibly from removal of boundary ledges via dislocation emmission.	C
108	Mg,Al Mg-1Al	large-grained (slip lines)	Observed a zone of secondary slip around the grain boundaries.	C
109	Ti-6Al-4V	quenched from 920°C, aged 4 hr @ 540°C, crept @ 0.9 yield stress for 1000 hr (TEM)	Several figures of likely boundary sources, one clearly showing loops from boundary. Triple points favored. No similar defects seen before straining.	A
110	Ti-5Al-2.5Sn	α-forged,air-cooled from 950°C,3 μm gr. diam.,crept @ 25°C 10,000 hr @ 0.6 yield stress (TEM)	Shows one figure of a grain with clean grain boundaries and extensive dislocation loops bowing out from a triple point.	B
111	Ni-base superalloy	precip.-hardened, crept @ 700°C to 0.2% strain (TEM)	Shows 2 very good micrographs of partial dislocation generation,each of closely adjacent sources. One boundary highly-defected, the other is clean.	A
112	Al	bicrystal (slip lines and TEM)	Concluded sources were in or near the boundary,activated by dislocation pileups.	no figures
113	α-Fe	(TEM)	Shows 1 figure indicating triple point activity. Saw many dislocations near the boundaries.	C
114	Fe(99.6)	55 μm gr.diam., slow-cooled and quenched (TEM)	Observed GBD generation ahead of Luder's front, and some source operation, in slow-cooled material only.	C

TABLE 3 (continued)

REFERENCE	MATERIAL	EXPERIMENTAL DETAILS	COMMENTS	RELIABILITY
115	Armco Fe	(TEM)	Preference for triple points as sources, saw no classical pileups.	B
116	low C steel	strain ageing (EP,TEM)	Observed more boundary sources as fully-aged condition was approached.	EP- B TEM-C
117	austenitic stainless steel	5-10 μm gr.diam., cold-rolled 1-10 % (TEM)	Interior sources assumed, but 1 figure shows bowing away from boundary. Another shows apparent pileups with no matching pileups on opposite boundary. Another shows stacking faults emanating from near a triple point.	B
118	Fe-C	2-phase, cyclic stressing, quenched (TEM)	Boundary generation inferred from precip.-free channels leading into the grain.	D
119	stainless steel	"lightly deformed" (TEM)	Shows 2 figures, each with several adjacent sources of varying clarity.	B
2	304 stainless steel	10-15 μm gr.diam., "lightly cold-rolled" (TEM)	Shows 2 very good figures of dissociated dislocations emanating from boundary ledges. The boundaries are relatively clean.	A
120	as (2)	cold-rolled 1% (TEM)	Shows 2 very good figures with inverse pile-up configurations. Another shows several adjacent sources. Also shows sources in Al.	A
60	as (117)	cold-rolled 2% (TEM)	Shows 1 good figure of what appears to be 2 adjacent sources forming single loops.	A
121	Fe-4P	1000 μm gr.diam. 10 μm subgr.diam. (TEM)	Shows 2 very good figures of dislocation loops emanating from boundaries at 1 and 3% strain.	A
122	Fe-0.9Cu	50μm gr.diam.,0.1% strain (TEM)	Shows 1 good figure of dislocation loops emanating from a boundary.	B
123	Ni_3Fe	ordered (TEM)	Three figures show inverse pileup configurations at boundaries, one at a kink.	B

TABLE 3 (continued)

REFERENCE	MATERIAL	EXPERIMENTAL DETAILS	COMMENTS	RELIABILITY
124	Ni-20Cr	cold-rolled 0.7% (TEM)	One figure shows overlapping stacking faults striking a boundary and causing perfect dislocation emmission into tne next grain. Other boundary sources were observed.	C
39	Ni-11.5Al	(TEM)	One figure shows triple point activity.	C
125	Ni-11.5Al	(TEM)	Several figures of likely boundary sources, one being of either double emission or an interior pileup reflecting off the boundary.	B
126	Ni-11.5Al	(TEM)	Shows 1 good figure of perfect dislocation generation across a grain, causing partial dislocation emission into the next grain.	A
127	43Ni-32Co-25V	ordered, 4% strain (TEM)	Shows 1 good figure of a superdislocation bowing out from a boundary which is covered by κ- phase.	B
128	Cu-23.7Ga	quenched from 780°C (TEM)	Profuse partial dislocation emission from grain boundaries due to transformation stresses.	A
129	Al-38.5Zn	quenched from 435°C (TEM)	Supposed generation from grain boundary particles, but very questionable.	D
130	Cu-10.8Si	(TEM)	Shows formation of κ- phase by partial dislocation emission from both sides of boundaries.	A
131	Be	microstrain region (TEM)	Conclude boundary generation may have taken place.	C
132	Be	as above	As above.	C
133	Nb	(TEM)	Shows 1 good figure of triple point activity.	B
134	Nb	(TEM)	One figure of triple point activity, but some doubt if created by applied stress.	B
135	α-Ti	fine-grained, near yield point (TEM)	One good figure shows dislocations emanating from a boundary, travelling across the grain and causing emission in the next grain. Study found that number of boundary sources increased with increasing boundary area (decreasing grain size).	A

TABLE 3 (continued)

REFERENCE	MATERIAL	EXPERIMENTAL DETAILS	COMMENTS	RELIABILITY
53	Ni(99.6)	40 μm gr.diam.,0.4-12% strain (TEM)	Some figures at lowest strains indicate possible boundary sources, but authors conclude interior sources operate.	C
136	Ni(99.98)	60 μm gr.diam., premacroyield region (TEM)	Observed substantial partial dislocation emission from boundaries at 3×10^{-4} strain, but micrographs not too convincing.	C
54	Ni(99.98)	30-120 μm gr.diam., premacroyield region (TEM)	Observed emission of both perfect and partial dislocations, primarily in the smallest grain size material. One very good micrograph shows 3 adjacent sources emitting loops into the grain interior. Boundary sources were much less in evidence around the macroyield point.	A

tacitly or expressly assumed that any dislocations or dislocation pile-ups associated with the boundary had originated at grain interior sources. This was often done even though the visual evidence suggested otherwise, likely because of the relatively new nature of the idea of boundaries acting as sources. In still other studies, pictorial evidence of likely boundary generation is incidental to the main purpose of the study and is not commented on at all. In compiling Table 3, an attempt was made to indicate such circumstances where possible. Several examples of boundary generation are shown in figure 19.

Leaving the implications to be discussed later, some of the points that can be extracted from Table 3 are:

1. The studies conducted inside the electron microscope have conclusively shown that both grain and twin boundaries are the major dislocation sources in thin foils. At the same time, extensive GBD movement can take place in the boundaries of such foils.
2. Boundary generation has been quantitatively documented in only one material, Fe-3Si, but the qualitative evidence for other materials shows that a wide range of metals and alloys possessing the three major crystal structures (BCC, FCC, HCP) are capable of boundary

Figure 19. Examples of dislocation generation from grain boundaries in

(a) Ti-6Al-4V (Odegard and Thompson, 109)

(b),(c) Fe-3Si (Tandon, 137)

(d) austenitic stainless steel (McDonald and Ardell,60).

(e) 304 stainless steel (Murr, 120)

(f) Ni (Malis et al, 54)

(g) Ni-11.5Al (Baro and Hornbogen, 126).

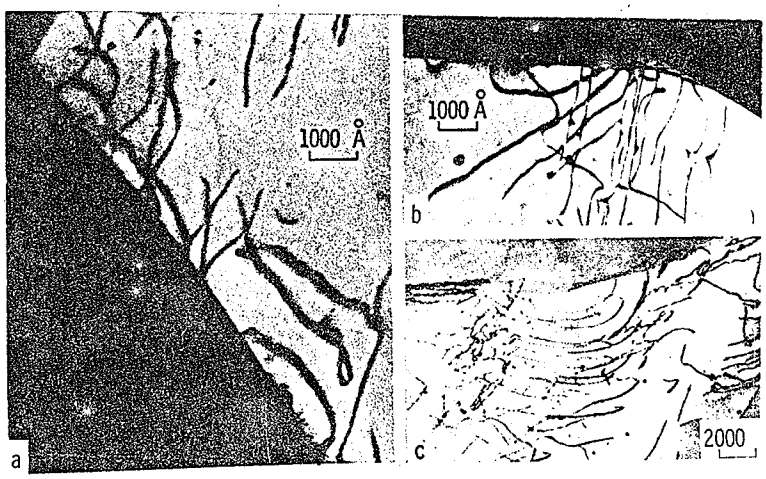

(a)

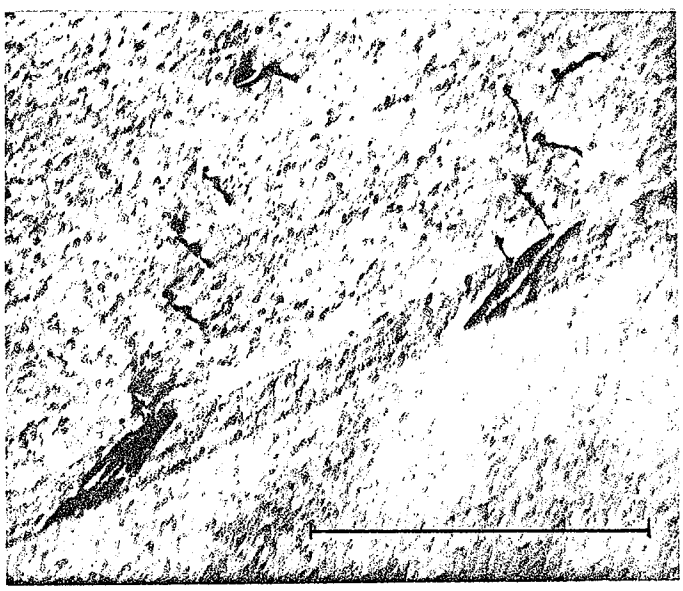

(b)

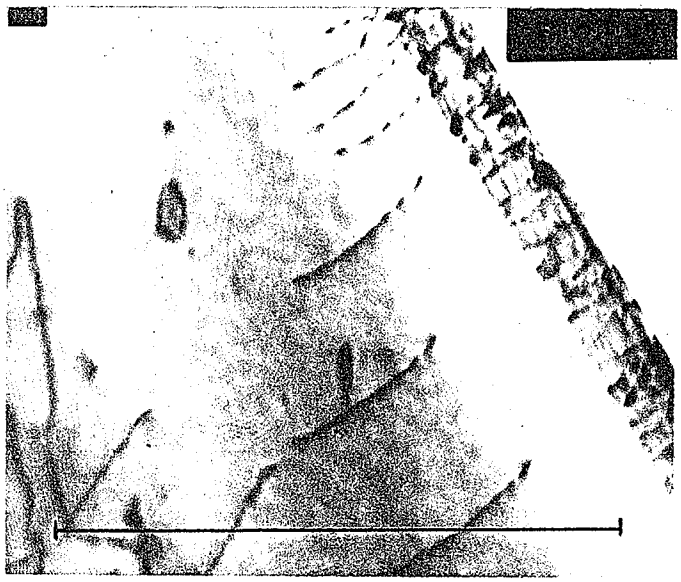

(c)

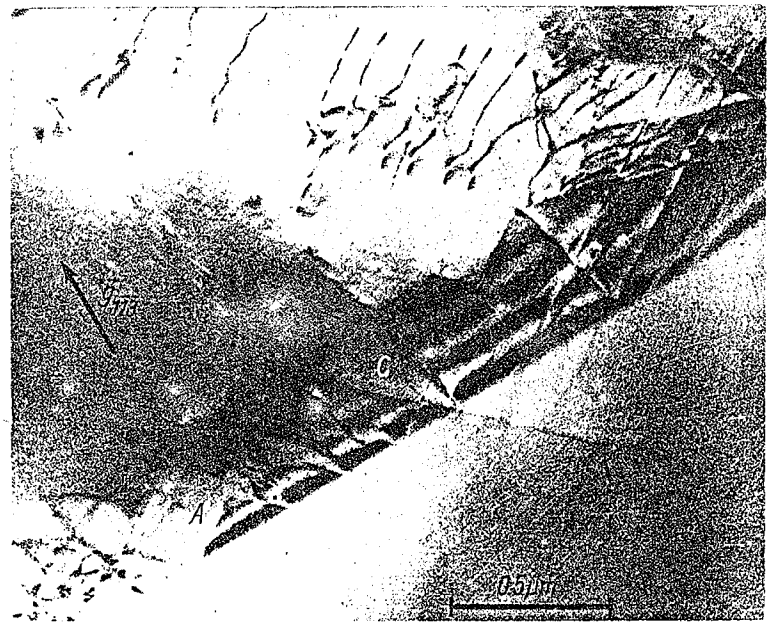

(d)

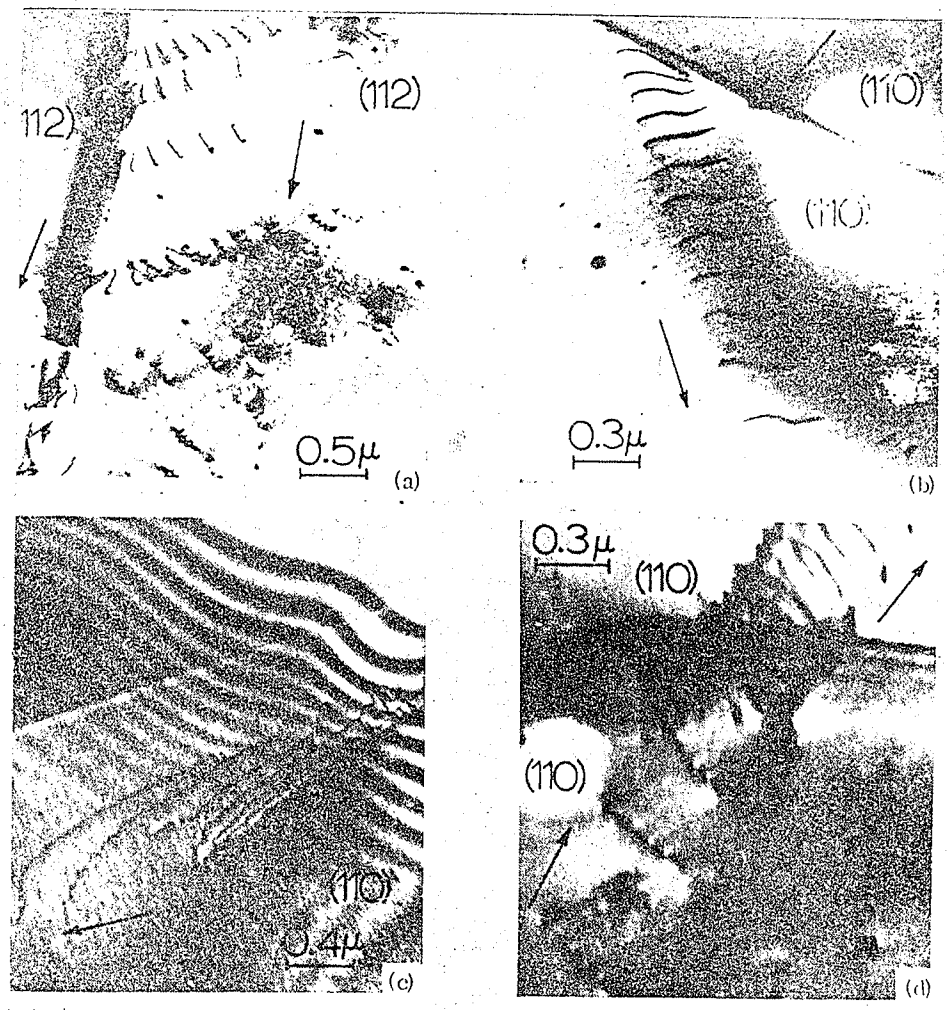

(e)

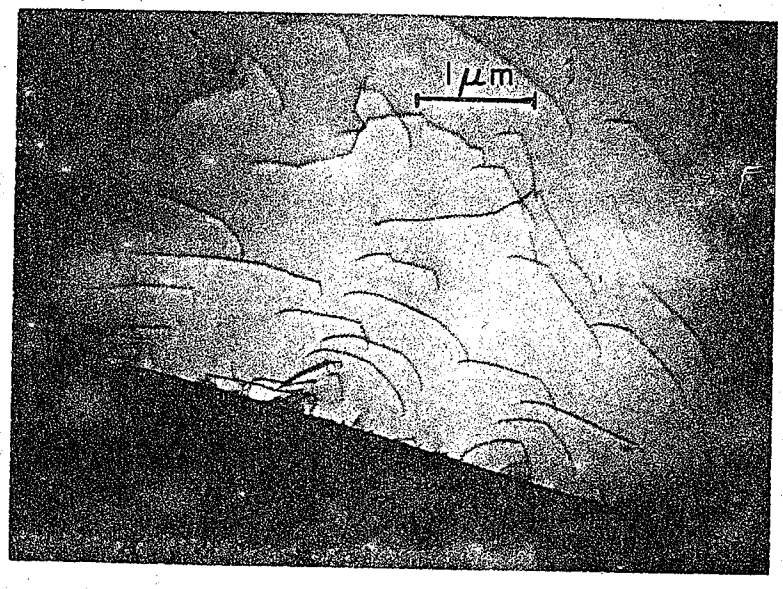

(f)

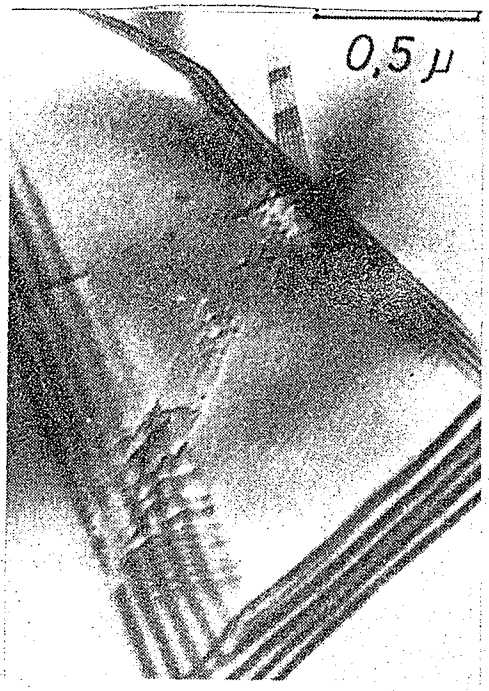

(g)

generation. Some of these have been indicated by both etch-pitting and electron microscopy, e.g. Nb (103, 134) and low carbon steel (116).

3. Boundary generation occurs preferentially at triple points (39, 42, 92, 98, 103, 105, 115, 117, 123, 133).
4. Generation occurs normally from only one boundary of a grain and from one side of that boundary (91, 105).
5. When generation does take place into both grains, it is collinear (or nearly so) (91, 105).
6. There is a higher percentage of yielded grains in large-grained material (90, 98).
7. Generation from boundaries appears to occur more readily in fine-grained material, e.g. less than 100 μm grain diameter, especially for pure metals (2, 105, 106, 110, 114, 117, 122, 135, 53, 136, 42).
8. Interior sources occur more and more frequently as grain diameter increases (103, 104).
9. Boundary sources in surface grains appear to operate at stresses slightly lower than those in interior grains (93).
10. There is some doubt as to whether the source operation stress is dependent on grain diameter (93, 106) or independent of it (90, 105).
11. Generation appears to occur preferentially in grains

of high elastic modulus (96).

12. Boundary generation can be caused or enhanced by elastic and plastic incompatibility and elastic anisotropy (100 - 102, 107, 108).
13. The classical theory of yield propogation across a grain boundary by means of dislocation pile-ups against it has been observed in conjunction with boundary generation (100, 101, 103, 112, 124, 126, 135).
14. Generation of partial dislocations can occur in metals of both low and high stacking fault energy (117, 2, 124, 126, 128, 130, 42).
15. Although the majority of evidence for dislocation generation from grain boundaries has been observed at or below the macroyield stress, a number of studies indicate that it can also occur at higher strains (117, 120, 60, 121, 127).

It is unfortunate that the bulk of the more quantitative data has been confined to only one material, Fe-3Si, and has been derived by only one experimental technique, etch-pitting. The difficulties of obtaining reliable quantitative data from electron microscopy of boundary generation will be discussed later, but suffice it to say at this point that they are both numerous and severe. It should be noted that some preliminary electron

microscopy of Fe-3Si in this laboratory does appear to confirm boundary generation in that material (137). Finally, it should be mentioned that several studies have hypothesized that boundaries could act as dislocation sources, in order to explain other experimental results (86, 134, 138-143).

3.2 GRAIN BOUNDARY DISLOCATION GENERATION MODELS

From the first detection of boundary dislocation generation, models of varying degrees of complexity have been proposed to explain how the generation process occurs. These models have been categorized by Tangri et al (179) as those which require low temperature GBD glide to activate the source, and those which may require GBD glide only to keep the source active. In other words, in the first category GBD glide is necessary before the source operation, while in the second it may only be necessary during the operation. This glide is over relatively short distances in the boundary and thus should not be confused with the proposed large scale gliding (sliding) that Gifkins and Langdon (108) have shown to be erroneous.

3.2.1 MODELS NOT REQUIRING GBD GLIDE

The earliest, and most well-known of these models is that of Li (144) and it is exceedingly simple. A grain

boundary ledge may be viewed as an adsorbed edge dislocation (figure 20a) which, under an appropriate stress, τ, may be expelled into the lattice (figure 20b). One characteristic of this model is the fact that a residual GBD will be left at the boundary if the Burgers vector of the GBD at the ledge is not that of a lattice dislocation. It is important to note that the ledge involved is actually the C-ledge defect discussed earlier, a defect which, unlike pure ledges, does not necessarily have to be present in the grain boundary. This is a major weak point in Li's theory that yielding could take place by emission of dislocations from all ledges to form a network near the boundary which would control subsequent dislocation movement. Also, the ledge itself must be oriented so that it lies along the intersection of a slip plane and the boundary plane, but Price and Hirth (145) mention that this is generally the case. The dislocations produced from such sources would be pure edge and, most important, the sources would be non-regenerative, that is only one dislocation would be produced from each one.

A similar use of C-ledges has been incorporated into two more complex models by Orlov (146), one regenerative and the other not. The non-regenerative model (figure 21a), denoted the Orlov I model, uses the two ledges (A and B) of a boundary facet which can travel into the crystal as

Figure 20. (a) A grain boundary ledge viewed as equivalent to the extra half-plane of an edge dislocation. (b) Annihilation of the ledge by emission of an edge dislocation into the grain interior (Li,144).

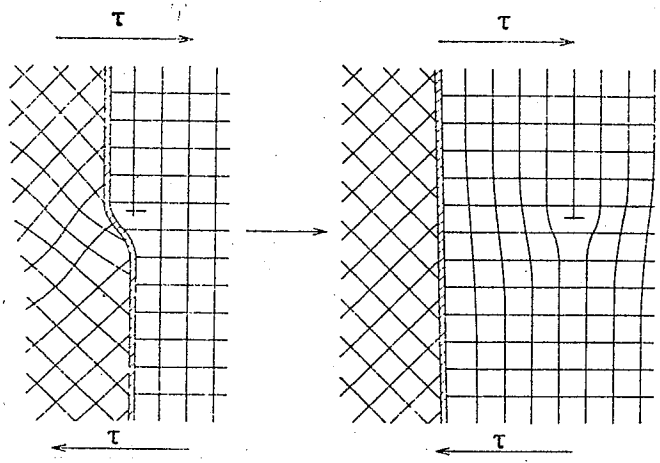
τ
τ
τ
τ
(a)
(b)

Figure 21. (a) Grain boundary facet AB on the surface of a crystal oriented so as to posess two primary slip planes, I and II.

(b) Annihilation of the facet by means of the two ledges travelling into the crystal as edge dislocations on the two slip planes.

(c) Formation of a new facet A'B' on the opposite surface of the crystal (Orlov, 146).

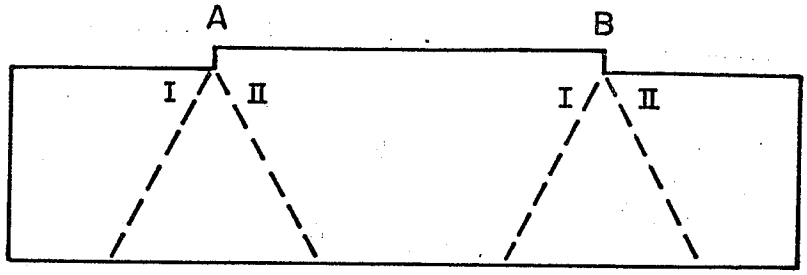

(a)

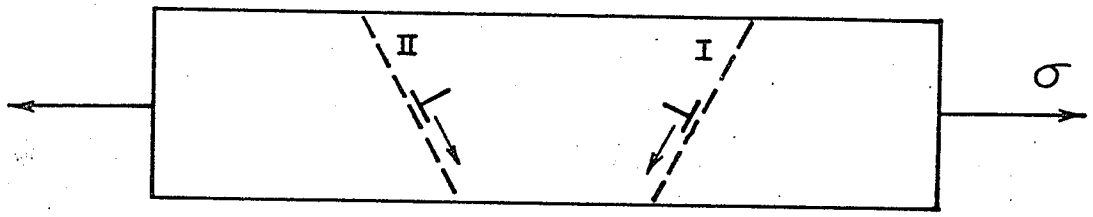

(b)

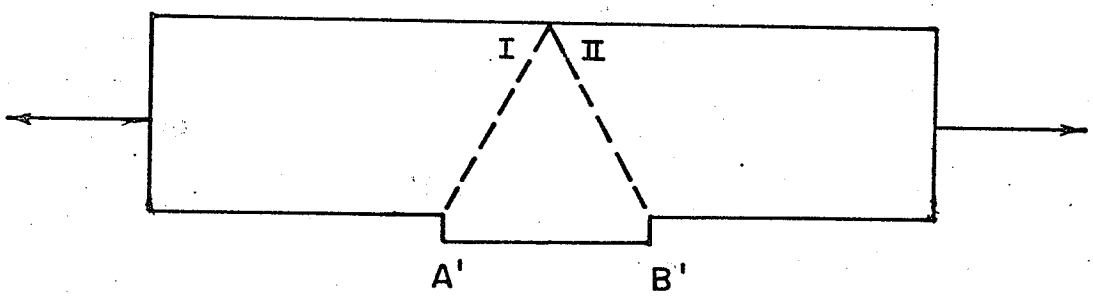

(c)

edge dislocations on either of two equally - likely slip systems (I and II). Under an applied stress, σ, the dislocations travel into the grain on both planes, as shown in figure 21(b). Traversing the grain, they form similar ledges on the opposite grain boundary (figure 21c). In a continued response to the stress, these ledges also emit edge dislocations, but on the opposite slip plane to that used to create the ledge. Again, these emerge on the top boundary and the process continues until the facet disappears (A compressive stress would have the opposite effect and the facet would grow until stopped by some obstacle). In essence, then, plastic deformation occurs through the repeated operation of single dislocation sources and the long range movement of the generated dislocations.

The regenerative model (Orlov II) is even more complex. Starting again with the facet AB and two equally-likely slip systems (figure 22a), we can see that the B ledge (abcd) travels into the grain as a dislocation loop (efgh) on plane I (figure 22b). This loop annhilates the original ledge and creates two new ledges, (cei) and (dbh). Since these are A-type ledges, they can travel into the grain as dislocation loops (ejkl) and (mnop) on plane II (figure 22c). The segments (kl) and (mn) of these loops recreate a B-type ledge (cqrd) as they meet

Figure 22. (a) Grain boundary facet AB with slip planes I and II.
(b) Removal of ledge B by emission of an edge dislocation on plane I.
(c) Re-creation of the ledge B by emission of edge dislocations on plane II (Orlov, 146).

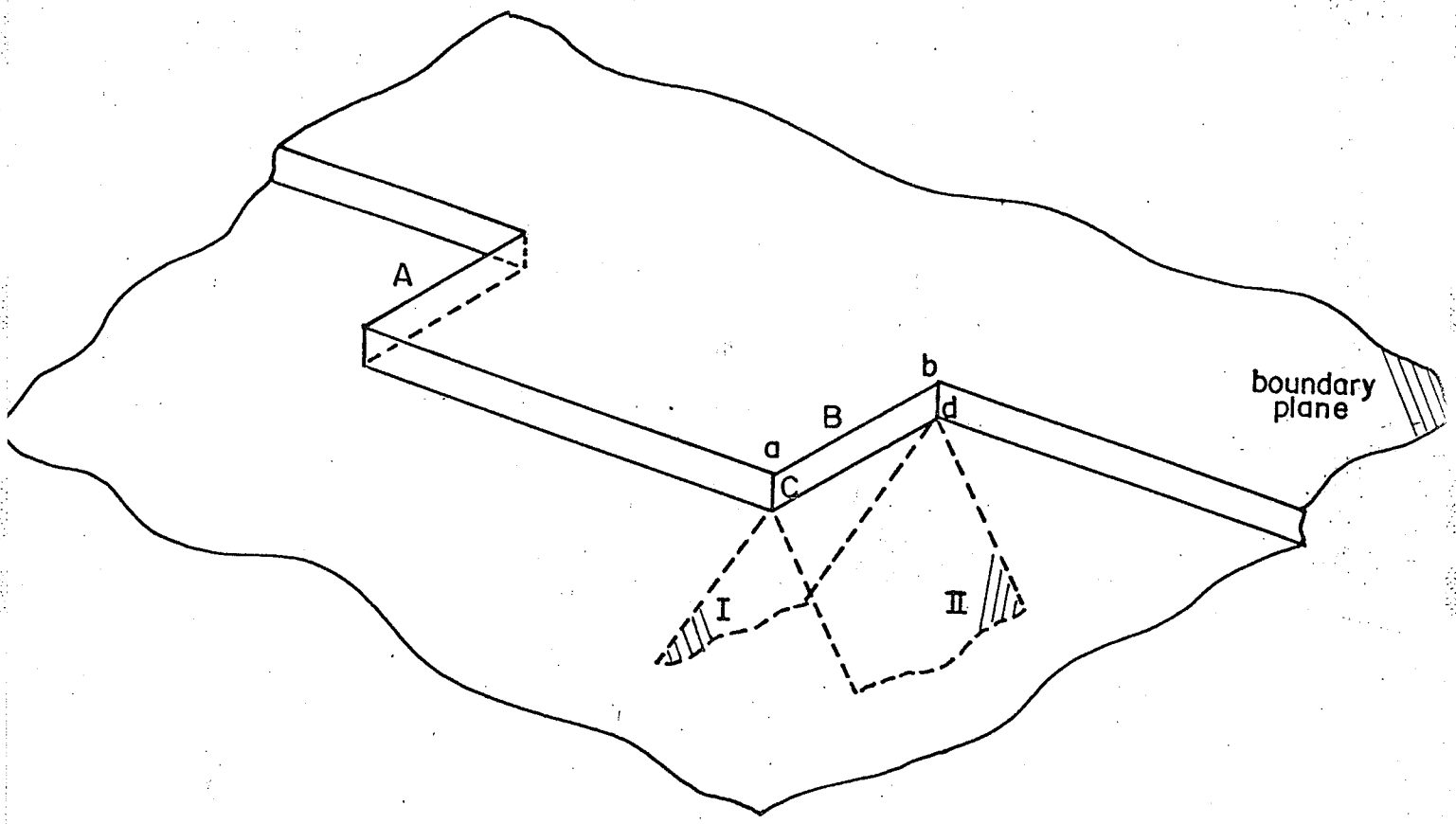
A
B
C
a
b
d
boundary plane
I
II

(a)

(b)

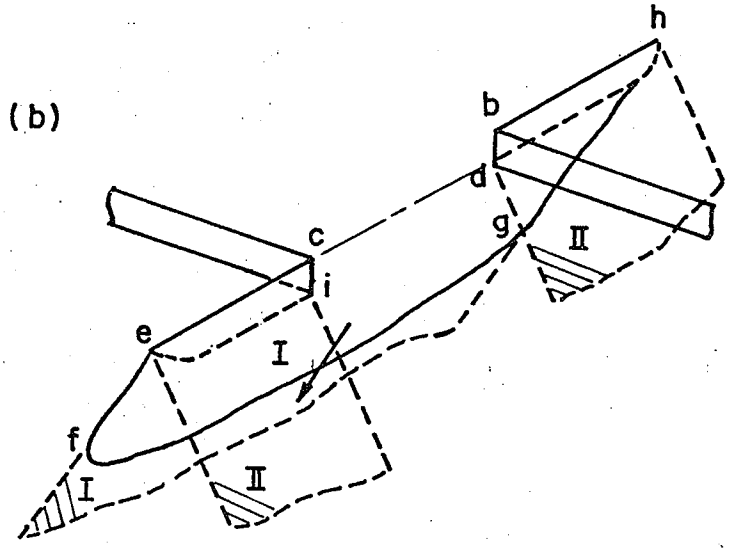
h
b
d
c
g
II
i
e
I
f
I
II

(c)

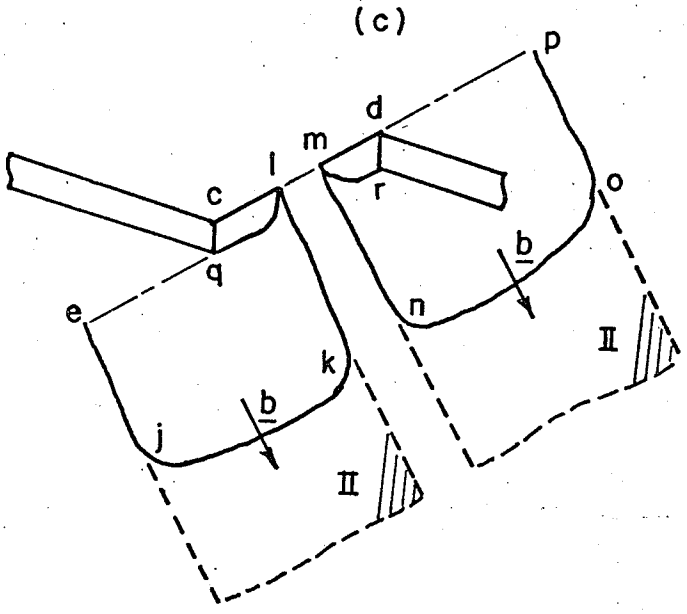
p
d
m
l
c
r
o
b
q
e
n
II
k
b
j
II

and annhilate each other. The entire process then begins anew. Since a similar process is occurring at A, the end result is four adjacent dislocation sources. It is also interesting to note that the process essentially results in grain boundary migration, i.e. the upper grain has grown at the expense of the lower one in figure 22.

Given the large number of grains in a polycrystal, it would seem reasonable to expect that some small percentage would be oriented so as to possess two equal slip systems. Other difficulties do arise, however. The first model requires that the free slip length of both dislocations be the same. Similarly, in the second model, any obstacle which stops any one of the four dislocation "trains" should hinder or even stop the operation of the entire process. For small facets this could quite easily be the interaction of the dislocations from each ledge. A similar cessation could occur if cross-slip and tangling occurred. As in the Li model, residual GBD's would be left at the boundary, since the ledge could only be oriented on one of the two slip planes. The accumulation of these would also hinder the source since they would not necessarily be glissile in the plane of the boundary. As before, the ledges would have to lie along the intersection of the slip plane and boundary.

Another model incorporating two slip planes has been suggested by Gleiter et al (125). In this model (Gleiter I), it was proposed that generation of an equal number of screw dislocations on each slip plane (figure 23) would enable continuity to be maintained at the boundary. No mention was made, however, of the details of this process.

A similar, more detailed model has since been proposed by Price and Hirth (145), although generation on only 1 plane is necessary. As shown in figure 24, the model simply proposes that, for every amount $\overline{b}$ (Burgers vector) the screw ledge shears, one screw lattice dislocation is emitted. Continuity at the boundary is maintained by the simultaneous creation of compensating GBD's which are glissile in the boundary (figure 25). The authors note that the generated loops will eventually intersect other portions of the boundary, creating ledges which will act as a drag on the continued propogation of the loop. If the character of the ledge is mixed, its area will decrease as the edge component vanishes due to Li-type behaviour. Although there seems no reason why pure ledges could not act as sources, the authors conclude that the GBD-macroledge defect would be more likely since it possesses a higher energy.

Figure 23. (a) Grain boundary with slip planes ABCD and ABEF intersecting along <110> at the boundary.
(b) Generation of screw lattice dislocations in equal numbers on both planes (Gleiter, 125).

Figure 24. Generation of a screw lattice dislocation from a grain boundary ledge by shear of the ledge by one Burgers vector (Price and Hirth, 145).

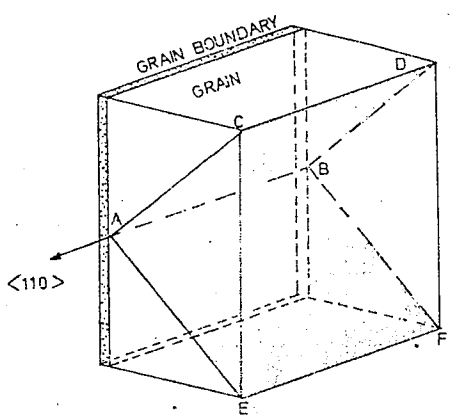

(a)

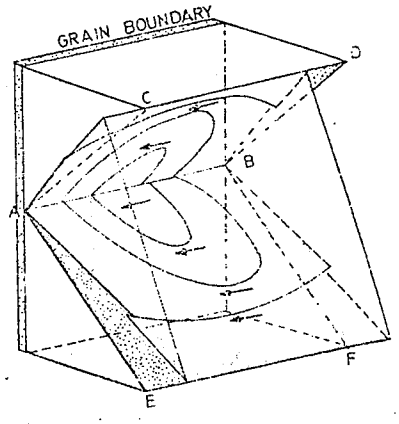

(b)

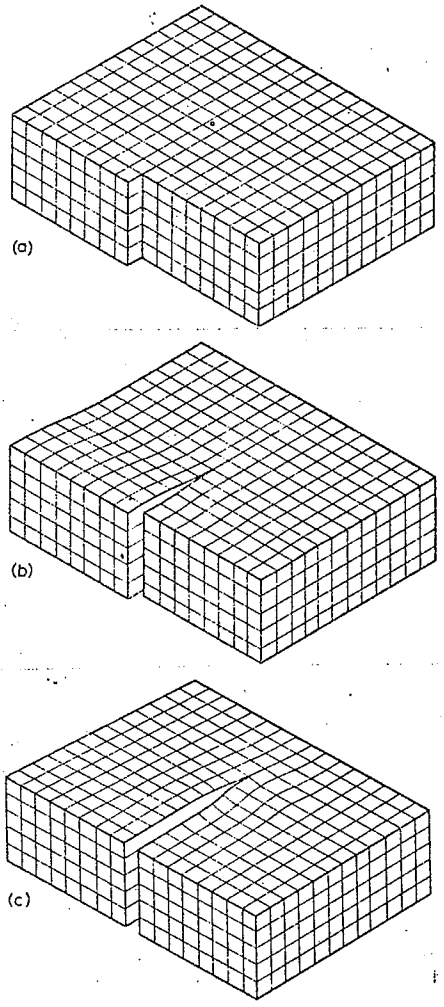

Figure 25. Creation of a compensating screw GBD by the shearing of a grain boundary so as to create a lattice screw dislocation.

Figure 26. Emission of screw dislocations into the grain interior by cross-slip of screw GBD's from the boundary plane onto a slip plane of the lattice.

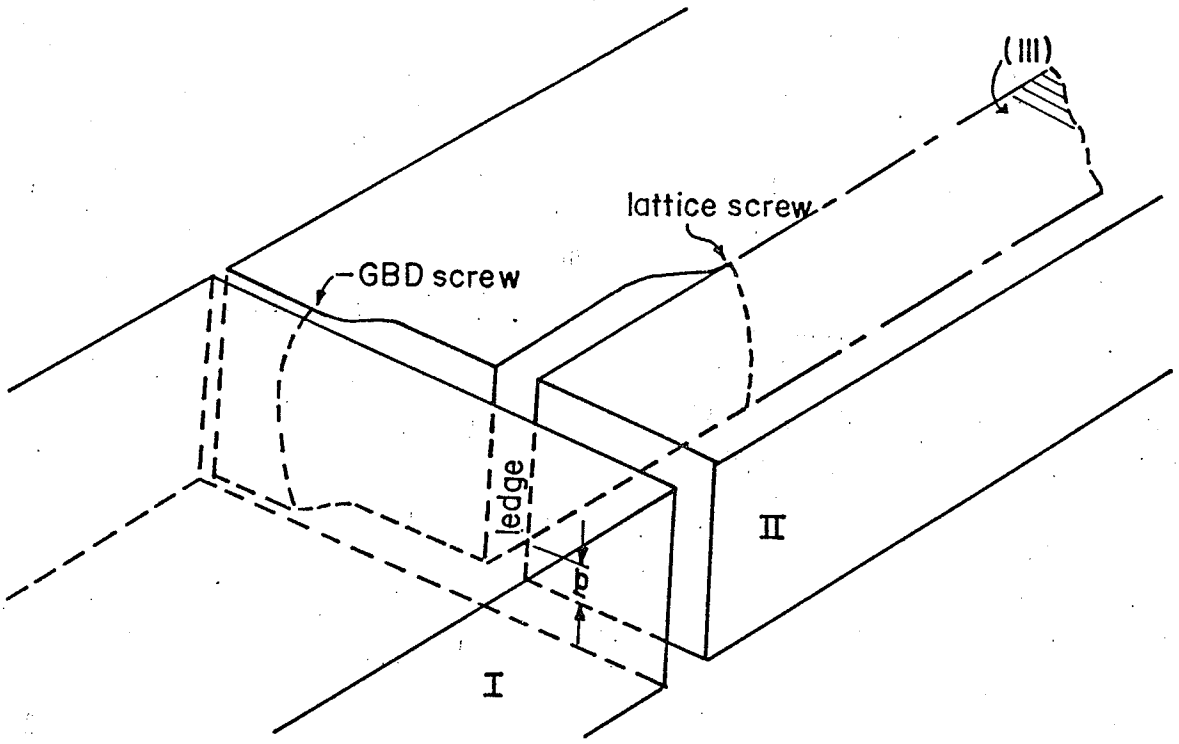
(III)
lattice screw
GBD screw
ledge
d
II
I

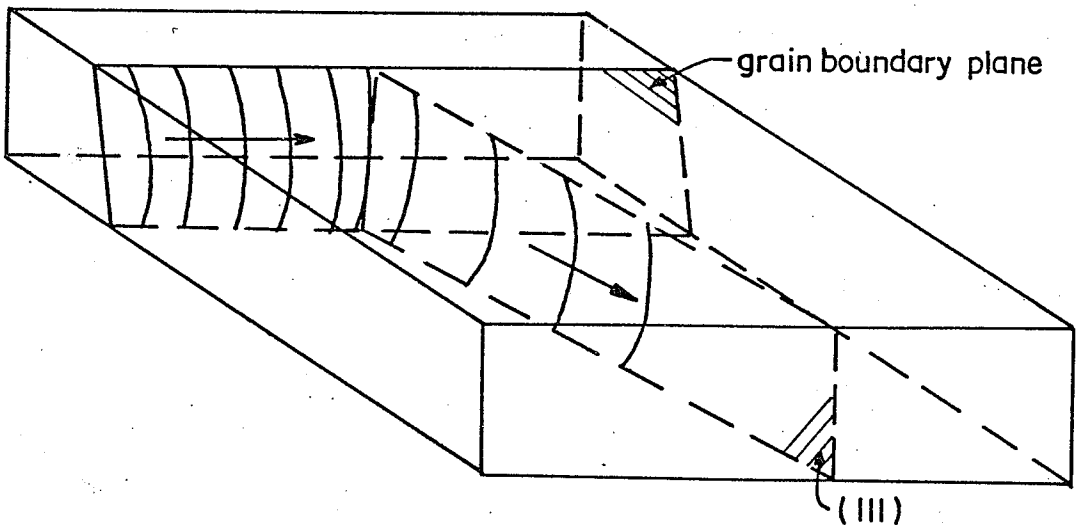
grain boundary plane
(III)

3.2.2 MODELS REQUIRING GBD GLIDE

The earliest of these models was that of Berghezan and Fourdeux (84) who simply proposed that glissile screw GBD's could cross-slip onto a lattice slip plane (figure 26). Presumably, if the first lattice dislocation(s) were stopped a short distance from the boundary, others could cross-slip onto adjacent slip planes. As in the Li model, the GBD Burgers vector would have to be that of a lattice dislocation or a residual GBD would be left behind.

This latter concept leads into the well-known model of Gleiter et al (39), which shall be denoted the Gleiter II model. As illustrated in figure 27, glissile GBD's of Burgers vector $\bar{b}_1$ travel along the boundary until a kink (K) is encountered. Under the stress concentration of the GBD's piled-up behind it, the first GBD would dissociate into a GBD with Burgers vector $\bar{b}_2$ (which would continue along the boundary) and a residual GBD which would be left at the kink. As more dissociations took place, the localized stress field caused by the accumulation of these residual GBD's could nucleate lattice dislocations and expell them into the grain interior. Perhaps because of the complexity of this process, it has been gradually revised (126, 147) to one of simple dissociation into a lattice dislocation of Burgers vector $\bar{b}_o$ and another GBD

Figure 27. Emission of lattice dislocations at a grain boundary kink (P) by dissociation of glissile GBD's (Gleiter, 147).

Figure 28. Emission of partial lattice dislocations at a grain boundary kink (K) through the reaction of glissile GBD's (Singh and Tangri, 136).

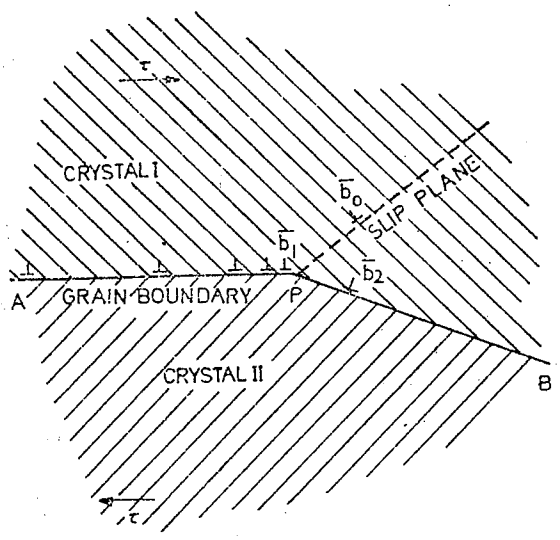
CRYSTAL I
CRYSTAL II
GRAIN BOUNDARY
A
P
B
$\vec{b}_1$
$\vec{b}_2$
$\vec{b}_0$
SLIP PLANE
τ
τ

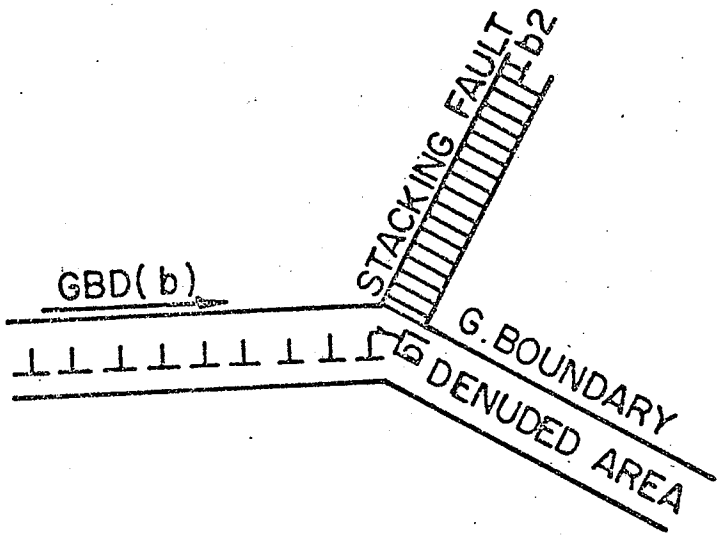
GBD(b)
STACKING FAULT
$\vec{b}_2$
G. BOUNDARY
DENUDED AREA

which may or may not continue along the boundary (an option that the original model did not offer). The implication of the model is that the original GBD Burgers vector must be larger than that of a lattice dislocation, a proposition which may not be all that likely to occur in view of the general experimental findings that GBD's possess Burgers vectors either less than or, at best, equal to those of lattice dislocations. In addition, large numbers of GBD's are required to move relatively large distances in the plane of the boundary to create the necessary pile-up effect.

Singh and Tangri (136) have adopted this model to account for generation of partial dislocations. This would result if continued GBD glide past the kink did not take place and the GBD's dissociated into two matching partials, one of which was held at the boundary (figure 28).

Malis et al (54) have avoided the difficulty of requiring GBD's with large Burgers vectors by suggesting GBD <u>combination</u> to form either perfect or partial dislocations. They have also proposed a means whereby only one partial of a Shockley pair would be emitted from the boundary. This involves the orientation of the applied stress with respect to the Burgers vectors of the partials. As illustrated in figure 29, the stress could be oriented

Figure 29. Possible orientations of the applied stress, τ, to the Burgers vectors of the Shockley partials of a dissociated dislocation (Malis et al, 54).

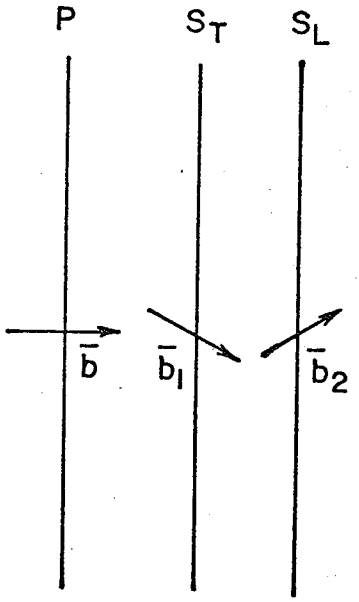

perfect → 2 Shockleys

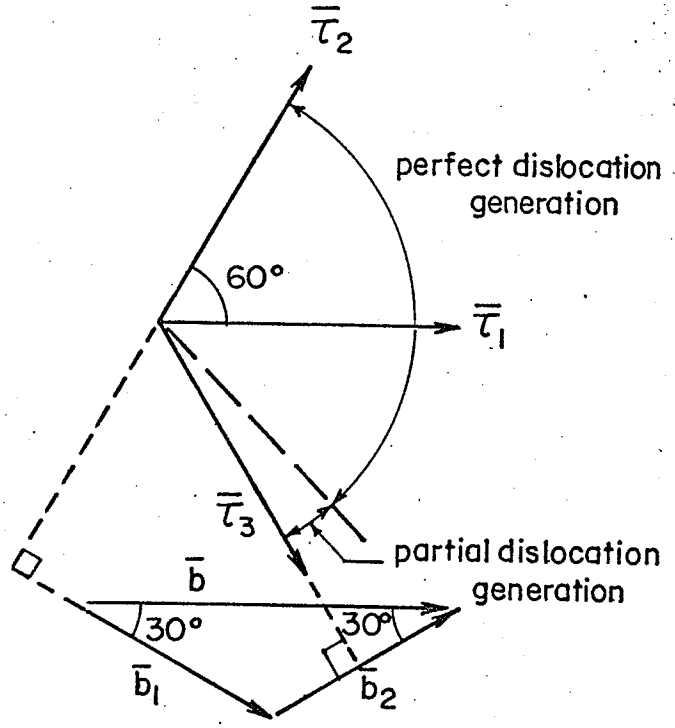

so as to create equal forces on the two dislocations (τ_1), or to have no force on either the leading partial (τ_3), or the trailing partial (τ_2). For this latter case, if the stress exceeds the critical tear stress required to separate the partials (148), the leading Shockley is emitted into the grain, creating a large, non-equilibrium stacking fault. Thus there would be no need to generate partial dislocations, it would only be necessary that a generated perfect dislocation be oriented correctly. Naturally, there would only be a small range of orientations where the resolved force would be small enough to effectively "pin" the trailing partial, and this is indicated in figure 29. In addition, the perfect dislocation would have to be slightly dissociated, but this has been calculated as being possible even in high stacking fault energy metals like Al (149). There is also considerable evidence that the stacking fault energy of a material is substantially reduced at or near grain and twin boundaries (150 - 152). One of these studies (152) shows what appears to be a classic experimental example of the above "pinning" effect on dissociated Shockley pairs in a coherent twin boundary of a Cu-.18Co alloy.

Some of the characteristics of these models which could be used in their identification have been compiled in Table 4. Because of weak contrast and/or high densities

TABLE 4

IDENTIFYING CHARACTERISTICS OF BOUNDARY SOURCE MODELS

A. MODELS NOT REQUIRING GBD GLIDE

MODEL	CHARACTERISTICS
Li(144)	- requires a C-ledge - produces edge dislocations - only one dislocation per ledge - diminished or no contrast after emission
Orlov I (146)	- requires a C-ledge - produces two adjacent edge dislocations on two slip planes
Orlov II (146)	- requires a C-ledge - multiple production of edge dislocations on two slip planes - accumulation of residual GBD's - likelihood of dislocation tangles near boundary in metals of medium-high stacking fault energy
Gleiter I (147)	- screw dislocations emitted in equal numbers on two slip planes
Price and Hirth (145)	- screw dislocations emitted on one slip plane - increased GBD density around source after emission begins - GBD-macroledges favored as sites - possibility of ledge shrinkage when of mixed character

B. MODELS REQUIRING GBD GLIDE

Berghezan and Fourdeux(84)	- screw dislocations produced - higher GBD density (in pileup form) on one side of source - strong GBD contrast (lattice Burgers vector)
Gleiter II (39)	- requires GBD pileups - emission occurs from boundary kinks - reduced or no GBD contrast on one side of emission site - strong contrast GBD's in pileup
Gleiter II modifications (136, 54)	- as Gleiter II, except; - strong GBD contrast not necessary - generation may be on one plane or on adjacent planes (overlapping stacking faults)

in the boundary, many of these identifications (such as residual GBD's or boundary ledges) are rather difficult to detect.

There is one other possible boundary source which has been mentioned in the literature (88, 64) and that is the operation of a Frank-Read source which is lying on the grain boundary plane. This source could be oriented so as to operate either out of the boundary plane (figure 30) or parallel to it (figure 31). For the former, the GBD segment A-B would bow out on the lattice plane in the direction shown. However, as the loop expands out from the nodal points and begins bowing back upon itself, the segments AC and BD would encounter the grain boundary and stop, thus preventing the original segment from regenerating itself. The AC and BD segments could react with the boundary and dissociate, as seen in figure 30(b), thus resulting in an expanded loop.

A similar problem exists for a dislocation segment, AB, bowing in the boundary plane (figure 31) onto a lattice slip plane which is parallel to the boundary plane. The ability of AB to sweep around to complete one cycle, critically depends on the size of the grain boundary segment CDEF and the location of AB within that segment. Thus, for figure 31, the expanding loop would encounter the boundary ledges CF and EF, again preventing regeneration.

Figure 30. Operation of a grain boundary Frank-Read source (AB) that is not parallel to the boundary plane.

Figure 31. Operation of a grain boundary Frank-Read source (AB) that is parallel to the boundary plane.

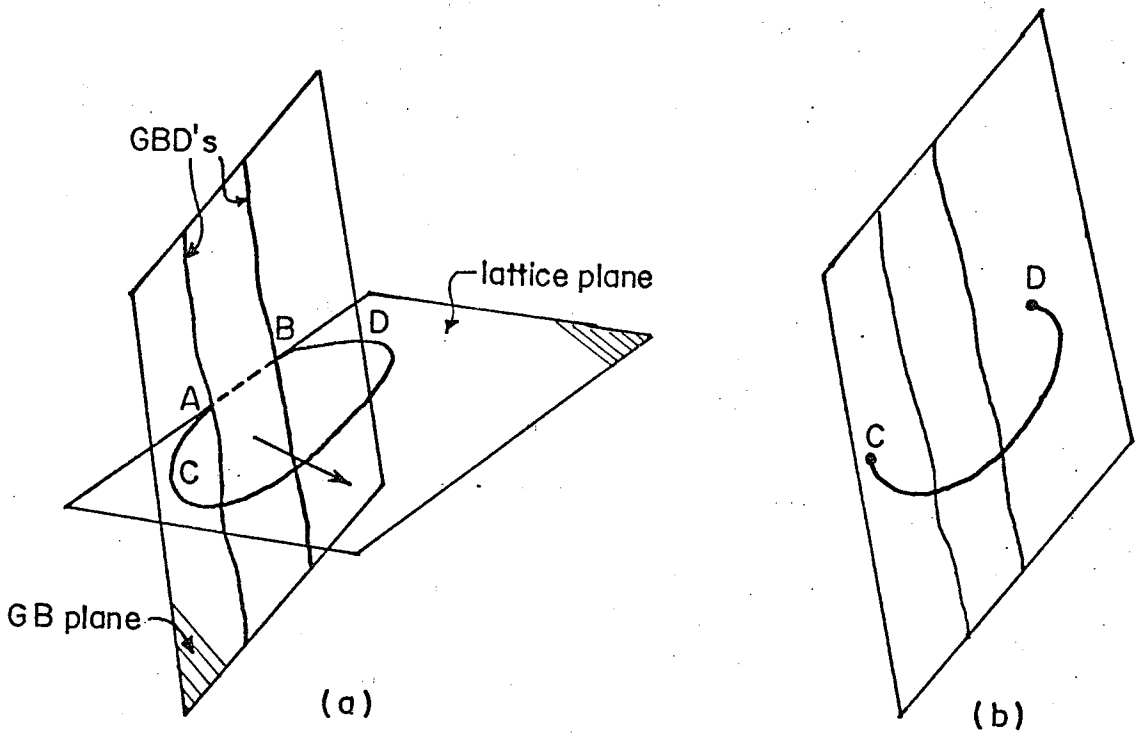
GBD's
lattice plane
B
D
A
C
GB plane
(a)
D
C
(b)

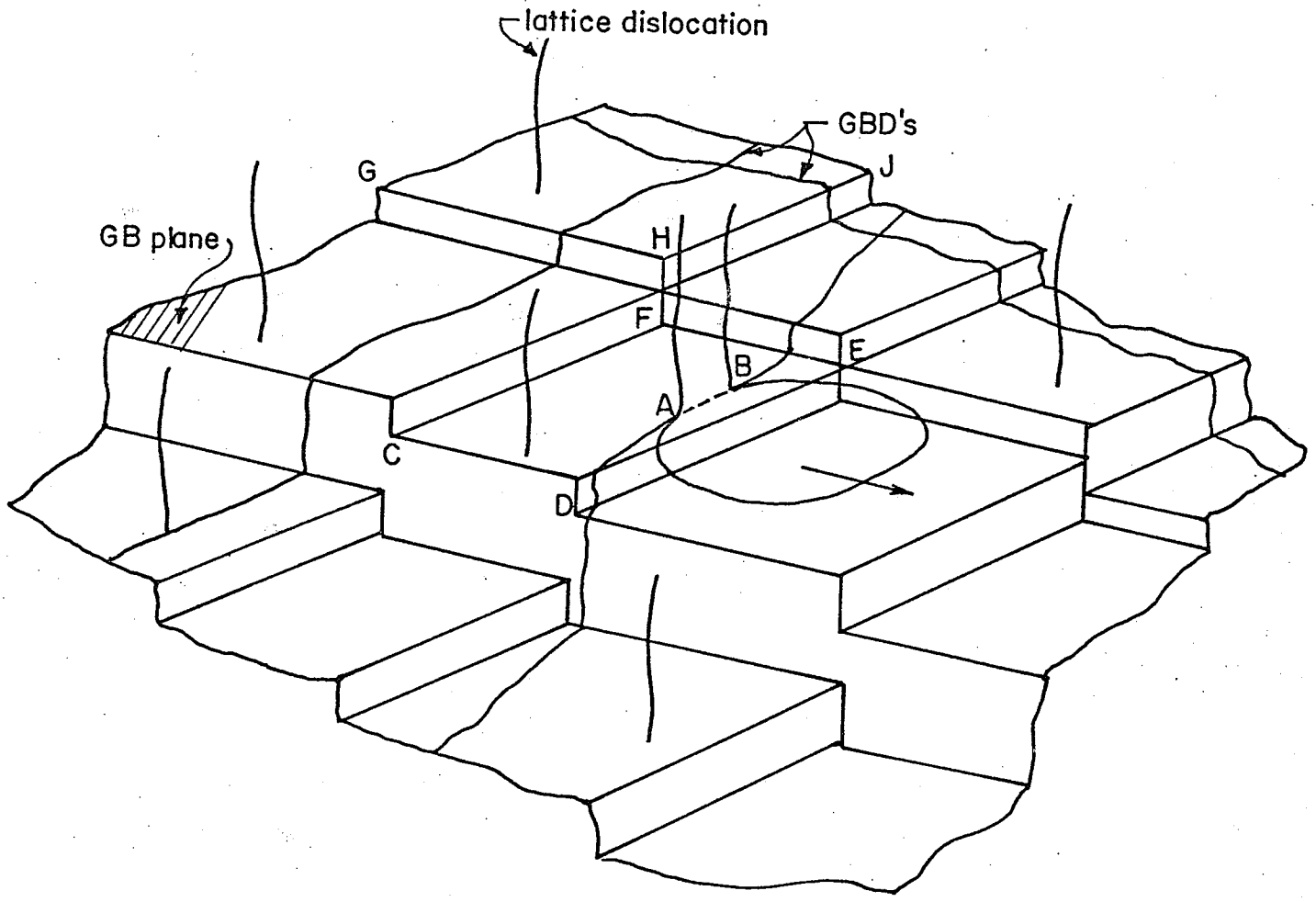
lattice dislocation
GBD's
G
J
GB plane
H
F
E
B
A
C
D

Such a source could, however, operate if it were on a segment such as GHJ or if AB were very small.

Finally, one other boundary source should be mentioned for completeness, although it is not truly pertinent to this study since it operates after initial yielding has taken place. Detailed work by Marcinkowski and co-workers (153 - 155) has examined the effects of lattice dislocations intersecting grain boundaries. The results indicate that the cutting of a boundary by a slip band results in the production of GBD's due to the differing orientations of slip planes in the two grains. As in the original Gleiter II model (39) such aggregations could nucleate further lattice dislocations due to their intense stress fields.

3.3 STRESS CONCENTRATION FACTORS FOR BOUNDARY GENERATION

There are two well-known means whereby plastic strain can be produced. The first is via the unpinning and movement of grown-in dislocations in the grain interiors. Their subsequent multiplication through such mechanisms as the Frank-Read source and double cross-slipping produces a sufficient mobile dislocation density to maintain the strain rate imposed by the testing machine.

The second is the nucleation of dislocations through stress concentrations achieved by large dislocation pile-ups or lattice spacing mismatch at the interfaces between second phase particles and the matrix. (The latter can also occur if large elastic moduli differences occur between particles and the matrix material).

As has been recently reviewed by Tangri et al (179), stress concentrations can also occur at the grain boundaries via GBD pile-ups, differing elastic moduli in the stress direction for adjacent grains, or from steps being present in the boundary. If sufficient concentrations to nucleate or generate dislocations are reached before either of the above operations can take place, or, if the above cannot maintain the strain rate, grain boundaries will act as dislocation sources. We have already seen ample experimental evidence that this does occur, therefore it is appropriate to detail the nature of such stress enhancement at grain boundaries.

3.3.1 THEORETICAL AND EXPERIMENTAL EVIDENCE FOR BOUNDARY STRESS CONCENTRATION

To begin with, the fact that dislocation generation from grain boundaries occurs in only some materials and/or microstructures would indicate that the operating stresses for boundary sources are generally higher than those for

Leaf blank to correct numbering

the common grain interior multiplication mechanisms. A classic example of this is the marked increase in yield stress achieved when lattice dislocations are fully pinned, leaving only boundary sources operable, e.g. (116).

For a starting point, we know that the stress required for homogeneous dislocation nucleation, that is, nucleation in the absence of any crystal defect, has been estimated as ranging from $G/2\pi$ (156) to $G/30$ (157), where G = shear modulus. Hirth (158) has calculated that this stress is reduced for nucleation at a surface (heterogeneous nucleation), and a grain boundary is very similar to an internal surface. Hirth considered the nucleation of both perfect and imperfect dislocations, which may or may not produce a step at the surface, for singular, non-singular and vicinal surfaces. The singular and non-singular correspond to atomically smooth and rough surfaces, respectively, while the vicinal surface is one of low index plane facets separated by monatomic ledges (159, 160). From the previous considerations it is apparent that the latter closely resembles a grain boundary surface. Hirth's calculations for copper and aluminum are shown in Table 5. He found no significant difference between the singular or non-singular surface, hence this distinction is omitted.

It can be seen that the nucleation stress for the

TABLE 5

CRITICAL SHEAR STRESS FOR HETEROGENEOUS NUCLEATION OF DISLOCATIONS IN COPPER AND ALUMINUM AT ROOM TEMPERATURE(158)

A. PERFECT DISLOCATION	CRITICAL SHEAR STRESS	
	AL	CU
1. Surface nucleation with step formation	G/11	G/8
2. Surface nucleation without step formation	G/16	G/15
3. Vicinal surface nucleation	G/22	G/28
B. IMPERFECT DISLOCATION		
1. Surface nucleation with step formation	G/10	G/12
2. Surface nucleation without step formation	G/13	G/24
3. Vicinal surface nucleation	G/17	G/48

most favorable case of the vicinal surface (which corresponds to the grain boundary) is of the order of G/25. Hirth pointed out that a reduction of 50% for the values in Table 5 occurs if Frank's expression (161) for the elastic energy of the dislocation loop is employed instead of Nabarro's (162). Thus an overall range would be G/25 - G/50.

It should be noted that the vicinal surface calculation involves a surface energy term. Since the grain boundary energy can be as much as four times smaller than the surface energy, it might be thought that a serious error would occur in applying the results of Table 5 to a grain boundary. However, for the case of Cu (surface energy roughly 3 times the boundary energy), approximate calculations indicate that this would only lead to a 10% increase in the value of critical stress.

If we now examine the models for boundary generation, we may first note that the binding energy of the GBD to the boundary must be overcome in <u>all</u> models. It is apparent that the Li, Orlov I and II and Price and Hirth models closely resemble the situation of surface steps in the above calculation. Although it is not clear, the Gleiter I model is also likely to fall into this category. Apart from those GBD's already present in the boundary, it has been postulated (39) that GBD's may have to be nucleated

within the grain boundary to form the pile-ups in the Gleiter II model which lead to lattice dislocation generation. This would likely also apply to the Berghezan and Fourdeux model. In addition it is possible that unfavorable dislocation reactions may be required at the head of the pile-up to emit the lattice dislocations. The Frank-Read source on the grain boundary differs from the above in that it only requires a single GBD, which could conceivably be left from the heat treatment and thus not have to be nucleated. (Indeed, such a source could be postulated as a GBD source for the above models). However, if we consider a facet size of 100 Å (13) (CDEF of figure 31) and assume that the facet must be roughly three times the source length to be regenerative, the operating stress must be G/15. Thus even a ten or hundred-fold increase in facet size would still require substantial operating stresses.

Keeping the foregoing theoretical estimates in mind, a perusal of Table 3 indicates that most of the boundary generation has been observed at very low stresses, generally below the macroyield point. A case in point for Fe - 3Si (91) showed that generation occurred at applied stresses from G/580 to G/730. Even for the few cases where clear generation has been seen well above the macroyield point, the applied stresses are still relatively low. For

example, the stress to deform fine-grained Armco iron to 5% elongation is G/800 (163). Of more pertinence to the present study, the applied stress value for boundary generation in Ni has been observed to be approximately G/3000 (54). Thus stress concentration factors of the order of 10 - 100 appear to be required for boundary generation.

3.3.2 STRESS CONCENTRATION FROM GBD's (K_n)

This stress concentration would arise from pile-ups of glissile GBD's. However, it is by no means obvious that GBD glide over even planar boundary segments is easily possible. Although the Burgers vector of the GBD may lie in the boundary plane, the previous study of boundary structure indicates that this plane is rather "rough" on an atomic level, unlike the smooth slip planes of the grain interior. Unfortunately, no work of any sort appears to have been conducted in this regard, perhaps because GBD glide is relatively easy and obvious at higher temperatures, where non-conservative motion can occur.

Assuming that glide over planar boundary segments is possible, it would be valuable to have some idea of their length in a given specimen. Unfortunately, this is experimentally difficult since the length can vary considerably and a tremendous variation can exist in any given specimen. About all that can be confidently stated is that different

types of heat treatments will likely produce preponderances of certain lengths, e.g. a long, high temperature anneal will likely produce large grains with straight boundaries that are as symmetric as possible with respect to the misorientation across them. It is essential to remember that the boundary is a curved surface in three dimensions, hence these slip lengths will be limited in two dimensions, as per figure 31.

Before examining the limited experimental evidence for small scale, low temperature GBD glide, it would be advantageous to recall the pertinent boundary defects discussed earlier. IGBD's do not appear to have been considered for this role, although they have been for high temperature sliding (165). The pure GBD, G-ledge and C-ledge all possess similar contrast and are therefore hard to visually distinguish. It is desirable that they could be, however, since the first two can move conservatively while the latter cannot.

The original work for the Gleiter II model (39, 125) contained several micrographs purportedly illustrating the GBD pile-up concept. Some are obviously of GBD's, but show no pile-up distribution. Others, by the regular spacing of the defects and their straightness are more likely GBD-macroledges. Two encouraging figures do show apparent bowing of GBD's around a particle and a

configuration resembling a Frank-Read source. The authors furthermore state that no such defects were observed in undeformed samples and that some of them increased in number with increasing deformation. Shortly thereafter, however, Gleiter, in a study of boundary migration (59) found similar configurations which he deduced to be monatomic steps. Similar spiral defects were identified by Schober and Balluffi (166) as Bardeen-Herring sources, i.e. sources of GBD's with their Burgers vector normal to the boundary (C-ledges). Furthermore, the spiral step configurations and other normal GBD's observed by Gleiter (59) occurred in undeformed specimens (both slowly and rapidly cooled), indicating their likely formation during heat treatment. As mentioned earlier, the situation is made even more complicated by glissile GBD's possessing a small step (G-ledge defect) and Gleiter found that even very small steps could produce noticeable fringe displacements in the boundary. Thus even Schober and Balluffi's identification could be erroneous.

Buzzichelli and Mascanzoni (63, 167) have also indicated evidence for GBD glide. In one study of the room temperature deformation of a steel (167), they purport to show Orowan loops left by GBD's gliding around particles in the boundary. Unfortunately, the figures are extremely vague and unconvincing. In a more detailed study (63),

they found GBD configurations in a rapidly cooled steel which appeared to indicate extensive glide. Similar configurations were duplicated in specimens deformed 0.3% at 250°C (figure 17a) but not between room temperature and 200°C. This latter result is somewhat contradictory, since all specimens received identical heat treatments and, as mentioned above, such configurations were seen in the undeformed state. Again, one good micrograph shows what the authors claim to be a Frank-Read source on the boundary, but which shows the fringe shifts characteristic of the Bardeen-Herring source. In any event the deformation temperature is 0.3 of the melting point, uncomfortably close to the region where true boundary sliding is considered feasible. The work of Malis et al (54) on pure Ni showed that the frequency of boundary generation increased in microstructures with higher densities of GBD's, but no mention was made of any visible correlation between sources and GBD pile-ups. Figure 19(g) shows a GBD pile-up connected with boundary generation, but it is difficult to decide whether the GBD's are causing the generation or are resulting from it. In summary, the experimental data does not enable any reasonably firm conclusions regarding GBD glide to be reached at this time. About all that can be said is that the extensive pile-up - like configurations discussed above

cover far too much boundary area to be caused solely by room temperature GBD glide.

If localized pile-ups occurred, the stress intensification could conceivably be estimated from the pile-up length, as done by Eshelby et al (168) for grain interior pile-ups:

$$K_n = \frac{\tau}{\tau_o} = \left(\frac{L}{x}\right)^{1/2} = \left(\frac{Gbn}{\pi \tau_o x}\right)^{1/2} \qquad (1)$$

where τ = intensified stress at a distance x ahead of the pile-up

τ_o = difference between the applied stress and the local frictional stress

b = GBD Burgers vector magnitude

G = shear modulus for the boundary region

n = number of dislocations in the pile-up

There are two difficulties associated with this calculation. One is simply the fact that equation (1) is only valid for points on the same slip plane ahead of the pile-up. Thus for the case of a slip plane lying at an angle to the boundary plane it is obvious that some decrease of the concentration will occur, the severity depending upon its inclination. Secondly, it has been pointed out earlier that GBD's produced in the boundary can have a variety of

Burgers vectors, most being substantially smaller than those of lattice dislocations. Also, since the shear modulus is a measure of the atomic bond strength in a given crystallographic direction, it would intuitively seem that this parameter should be lower for the relatively disordered boundary region (and likely different for different misorientations). The reduction in G and $\bar{b}$ would, for a given pile-up length, lead to a considerable increase in n, leading to the possibility of the pile-up being all but invisible and making the length difficult to judge. (It should be noted that little is known concerning the boundary frictional stress (169), which will be involved in τ_o). At the same time, lowering of these two quantities would make it favorable for GBD nucleation before lattice dislocation nucleation, since the nucleation stress for dislocations is directly proportional to both G and $\bar{b}$ (158). Such an occurrence has been experimentally observed in Fe (114) and Ni (42). Despite these difficulties, it is at least apparent from equation (1) that substantial enhancement of the applied stress could occur from GBD pile-ups, e.g. a pile-up on a boundary segment 1000 Å long would result in a value of $K_n = 10$ at a distance 10 Å in front of the pile-up. At a distance 100 Å ahead of the pile-up the value of K_n would be down to 3 and the effect would vanish entirely 1000 Å from the pile-up (only a tenth of a

micron). This latter figure demonstrates the relatively short range of the concentration.

3.3.3 STRESS CONCENTRATION FROM ELASTIC ANISOTROPY (K_E)

Most materials possess varying degrees of elastic anisotropy (170), that is, different elastic moduli in different crystallographic directions (a notable exception being tungsten, $\frac{E_{100}}{E_{111}} = 1.02$). Given the large number and varying orientations of the grains of a polycrystal, it is reasonable to expect that some small fraction of grains which are elastically "hard" in the direction of the stress axis will adjoin grains which are elastically "soft". The effect of such a pairing is illustrated in figure 32, where the term non-isoaxial is used to denote the differing crystallographic directions (and hence elastic strengths) in the direction of the applied stress. Under the applied stress, σ, each component of the bicrystal would want to extend by an amount proportional to the stress divided by the modulus for that component. Since E_A is greater than E_B, δ_A would be smaller than δ_B (figure 32b). However, the components are atomically bonded across the grain boundary, CD, and the extensions along this plane must be identical to preserve continuity. Thus A extends somewhat

Figure 32. The elastic extension of a non-isoaxial bicrystal under an applied stress, σ.

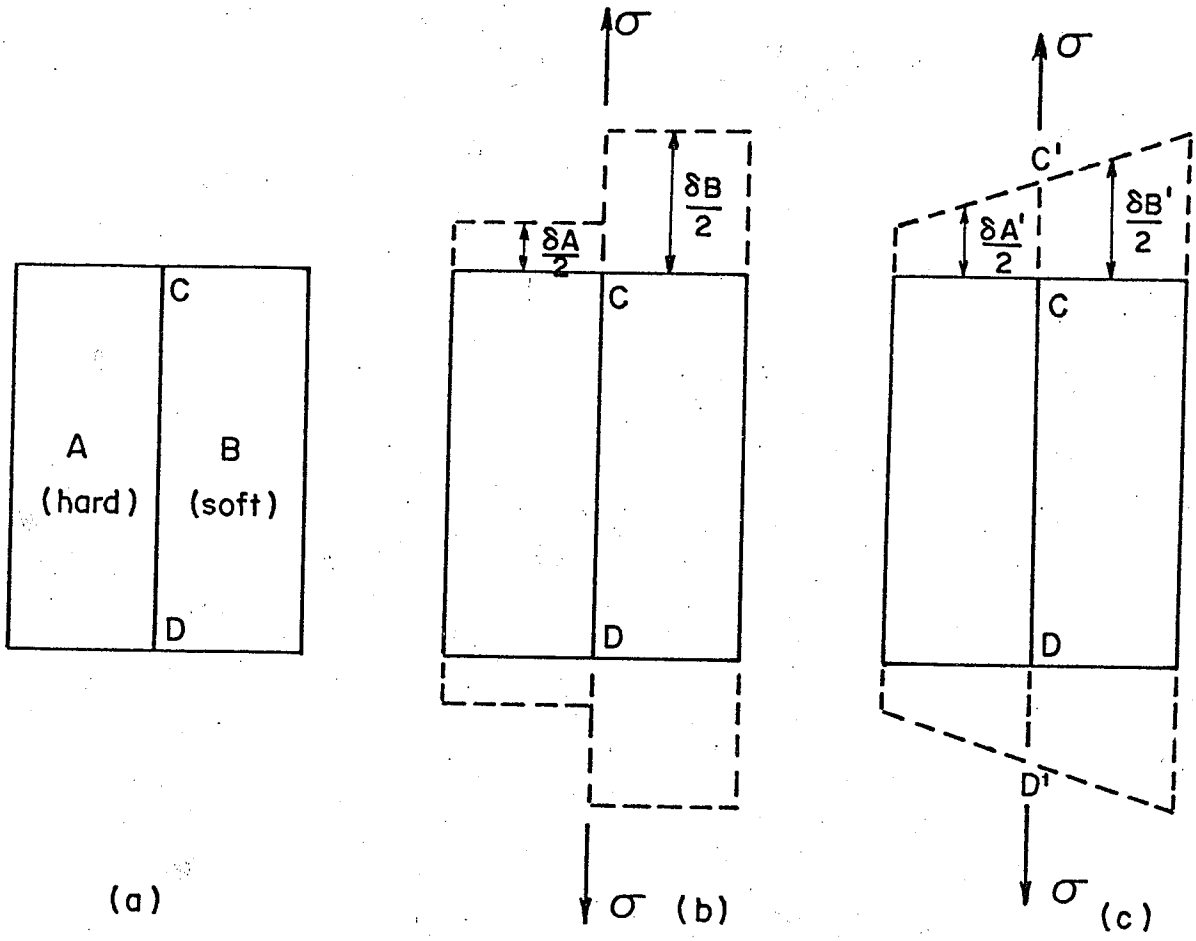
A
(hard)
B
(soft)
C
D
(a)
σ
δA/2
δB/2
C
D
σ
(b)
σ
C'
δA'/2
δB'/2
C
D
D'
σ
(c)

more and B somewhat less at this point (figure 32c).

Therefore, the stress acting on A must increase while that acting on B decreases, i.e. a "partitioning" of the applied stress occurs. The enhancement is maximum at the interface and drops to the level of the applied stress at a distance of roughly one-tenth the component width (169), making it a much longer-range effect than K_n. It is to be noted that this effect of elastic anisotropy occurs in addition to the normal incompatibility enhancement which occurs at the interface of any misoriented crystals of an anisotropic material even if the elastic strengths in the stress direction are identical (isoaxial crystals). A value for this type of enhancement of 1.6 may be calculated from Hook and Hirth's data on isoaxial Fe - 3Si bicrystals (100).

Data by Chuang and Margolin (102) appears to indicate that this factor could be as much as 4, but comparison of their experimental procedure with that of Hook and Hirth (100) indicates that some seriously incorrect assumptions were used in the calculation of the stresses which furnish the value.

Returning to the effect of elastic anisotropy, Carrington et al (96) conclusively demonstrated its existence by work which showed that a substantial majority of dislocation generations from Fe-3Si grain boundaries

occurred into elastically hard grains which were adjoined by substantially softer ones. The theoretical aspects of this factor have been studied by Hook and Hirth (101), Hasselman (173) and Abe (174 - 178). Hook and Hirth (101) state a simple relationship for K_E according to the relative areas of the crystals:

$$\frac{\sigma_A}{\sigma_T} = K_E = \frac{A_T}{A_A + \frac{E_B}{E_A} A_B} \qquad (2)$$

where A_A, A_B, A_T are the cross-sectional areas of crystal A, B and the total bicrystal, respectively. Studying this relationship, maximization of K_E requires that A_B be much greater than A_A, and it has been shown that this occurs when the ratio of A_A/A_B is 10 or greater (179). K_E then approaches the maximum anisotropy ratio, $A = E_{111}/E_{100}$. Thus for Cu, the maximum K_E is 3.08 and for Ni it is 2.26 (179). The validity of equation (2) in determining K_E is readily demonstrated by inserting the appropriate values of E_B/E_A from Hook and Hirth's data (101) for $A_A = A_B$, and comparing the calculated K_E with that calculated from their observed stresses on various operative slip systems. The two are identical.

Hasselman (173) came to a similar conclusion with regard to the maximum value of K_E when he studied

the effect of length to width ratio in elliptical grains of E_{max} surrounded by grains of E_{min}. Still another confirmation is possible using Kelly's formula for localized stress enhancement when a modulus difference exists between two grains (180):

$$\frac{\tau_m}{\tau} = K_E = \frac{1}{\alpha} \left(\frac{\Delta G}{G}\right) \left(\frac{d}{\rho}\right)^{1/2} \qquad (3)$$

where τ_m = maximum stress

τ = applied stress

ΔG = modulus difference

α = geometrical constant

d = grain size (presumably diameter)

ρ = grain boundary radius of curvature

Using a value of $\alpha = 3.7$ for an ellipsoidal grain (181), identical values of modulus difference, and identical grain length to width ratios, K_E values from (3) are the same as may be taken from Hasselman's curves (173).

Finally, Abe has extensively studied the effect of elastic anisotropy on theoretical polycrystal arrays (174 - 178) utilizing a number of variables, such as grain shape and varying degrees of anisotropy. Some of his pertinent findings are:

a) for a square grain network of alternating elastic strengths (figure 33a), the stress is discontinuous across boundaries parallel to the stress axis, as in the case of bicrystals. It is continuous across boundaries perpendicular to the stress axis except near intersection points such as 0. The elastic strain behaves in an opposite manner save that no triple point anomolies occur. These distributions are schematically sketched in figure 34.

b) the maximum stress occurs at boundary intersection points.

c) the stress discontinuity is most severe for square grains, least for circular grains.

d) as plastic flow begins, the elastic modulus discontinuity becomes "smeared" and the stress discontinuity vanishes.

e) although the maximum stress (and hence K_E) stays the same, various configurations can increase the stress differential across the boundary. Abe found this to occur when the grains became elongated in the direction of the stress axis, for triple point configurations such as figure 33(b) or for configurations such as figure 33(c),

Figure 33. Square - grained polycrystal array under an applied stress, σ, and $E_1 > E_0 > E_2$. (The significance of the dashed area in (a) is shown in figure 34).

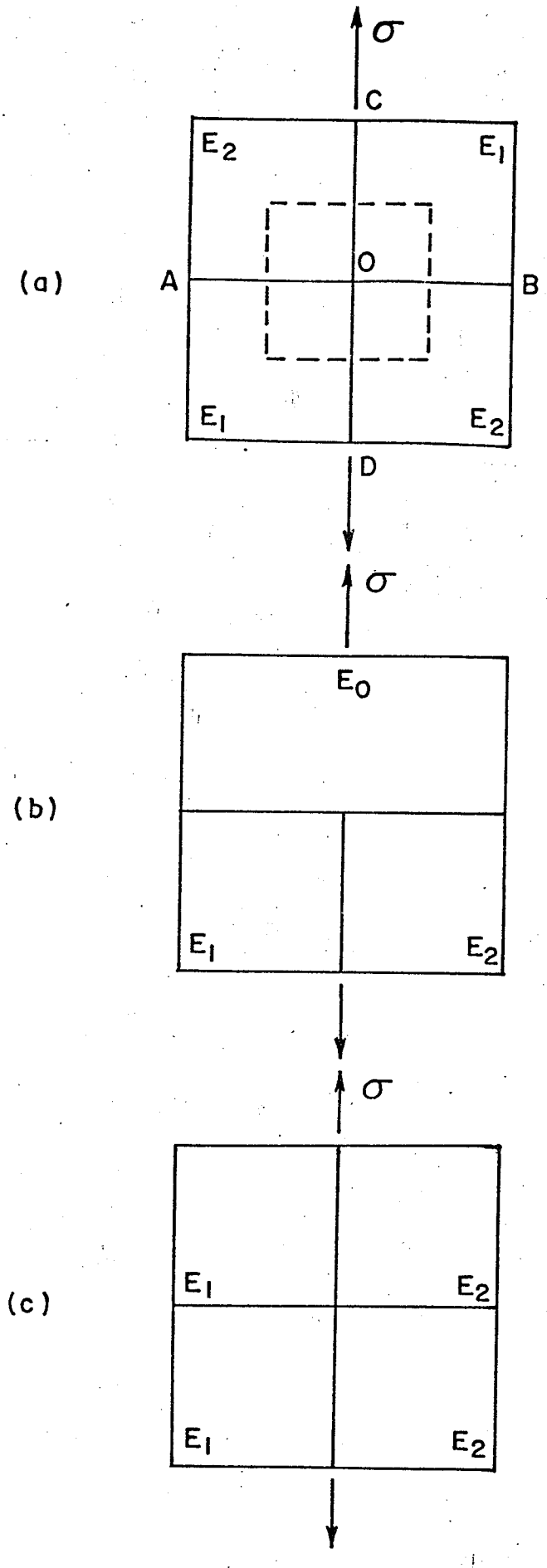
σ
C
E2
E1
O
A
B
(a)
E1
E2
D
σ
E0
(b)
E1
E2
σ
E1
E2
(c)
E1
E2

Figure 34. Distribution of (a) strain, and (b) stress, in the dashed area of figure 33 (a), under an applied stress, σ. The third dimension in each case is indicated by the axis on the left.

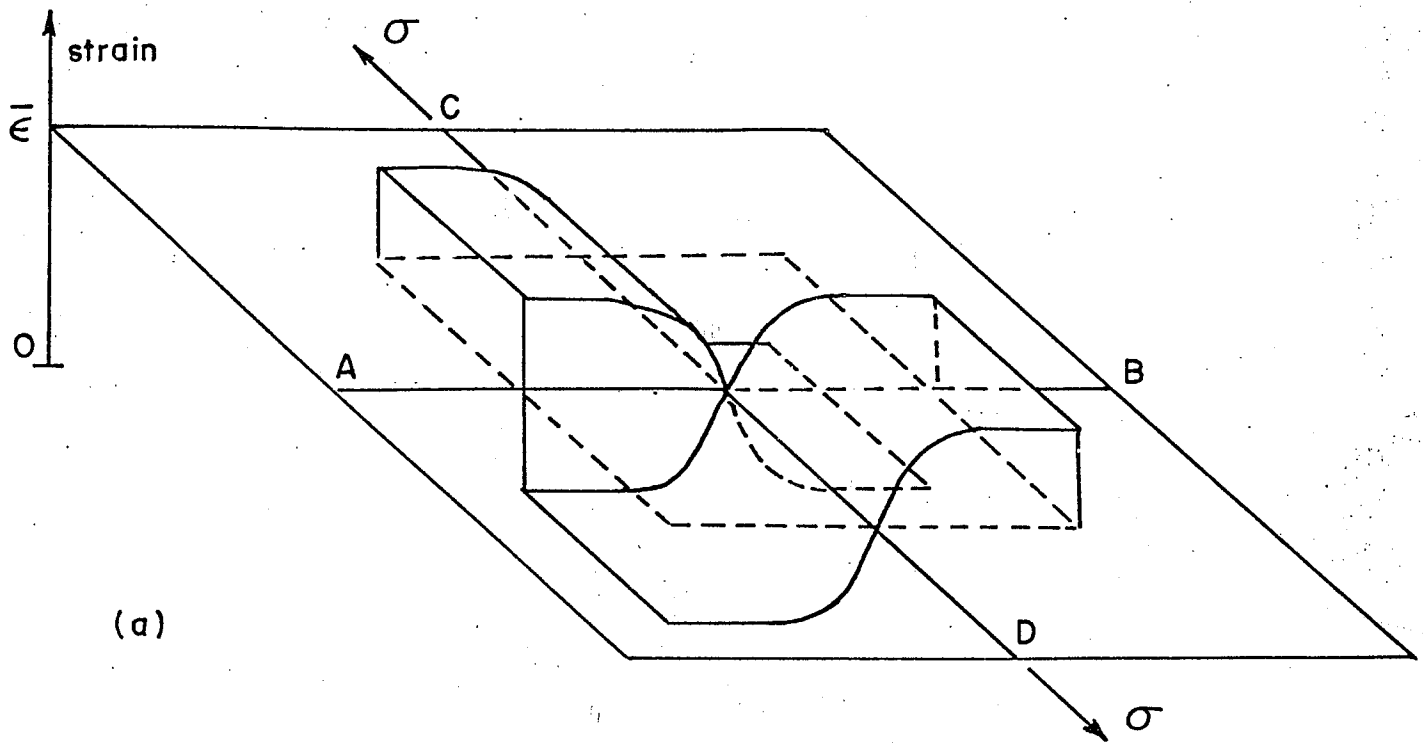
strain
$\bar{\epsilon}$
0
σ
C
A
B
D
σ

(a)

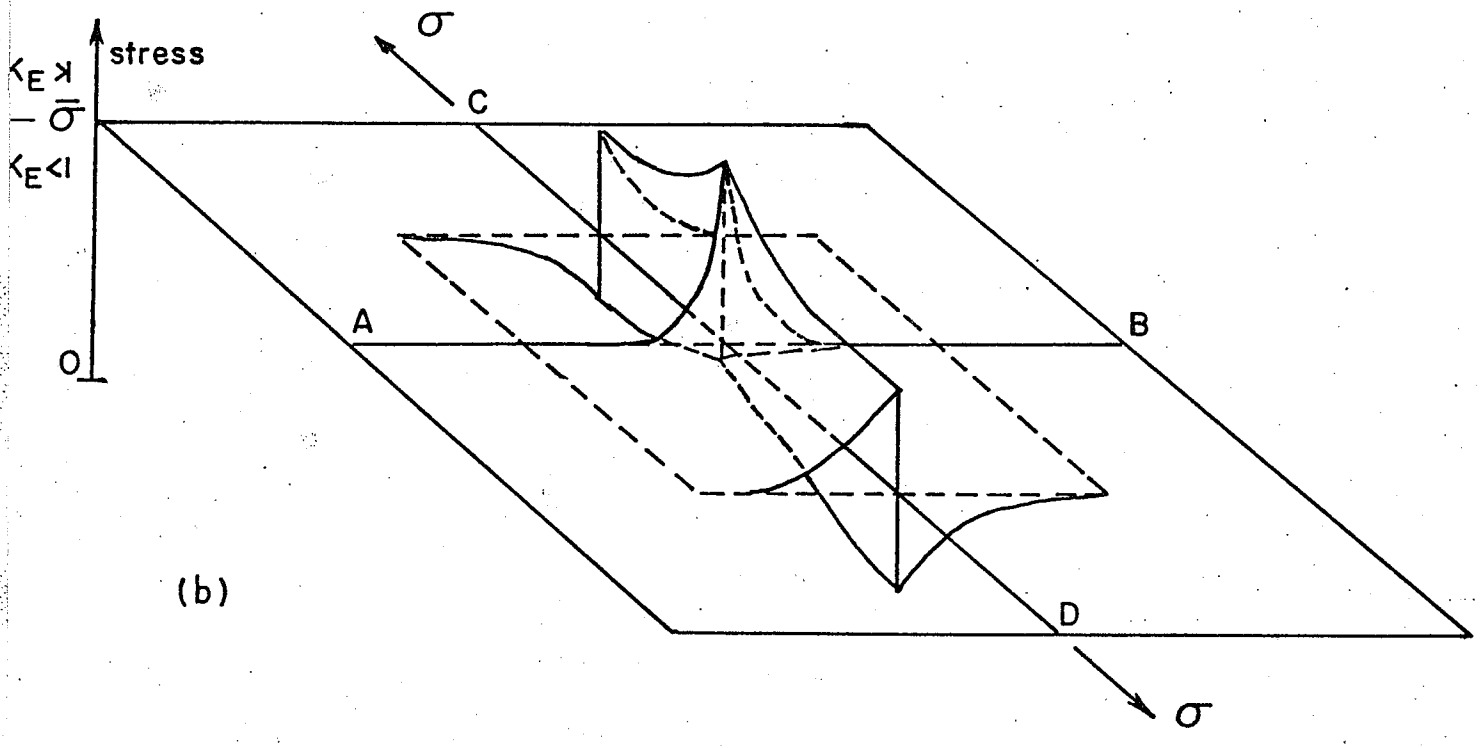
stress
$\langle E \rangle$
$\bar{\sigma}$
$\langle E < 1$
0
σ
C
A
B
D
σ

(b)

where moduli of grains in the direction of the stress axis were considered.

Thus it appears that the maximum value of K_E is likely the anisotropy ratio (although Hasselman (173) somewhat vaguely alludes to a further enhancement for the case of a large, hard grain surrounded by small, soft grains so that a "cascade-effect" occurs). A maximum value for a fairly anisotropic metal such as Cu is 3.3. Even if normal elastic incompatibility effects are included, this is only raised to around 5.

One other interesting effect of elastic anisotropy is that of dislocation attraction toward the soft grain accompanied by repulsion from the hard one, caused by image forces (171). In other words, the strain field of a dislocation in the hard grain extends across the boundary into the soft grain where the energy/unit displacement is lower. Thus the dislocation further lowers its energy by moving toward the boundary. In the context of boundary dislocation generation, this means that the generated dislocation will have an additional force to overcome besides lattice friction and boundary dislocation binding energy. An estimate of the profile of this force has been made by Tangri and Tandon (182).

3.3.4 STRESS CONCENTRATION FROM LEDGES (K_G)

The most significant stress intensification factor for boundary generation is the notch-effect created at ledges when under stress, since even the most well-annealed material is highly unlikely to have perfectly planar boundaries. Unfortunately, there has not been a great deal of work done in this area, although Gleiter et al (39) implied that it accounts for GBD generation at boundary ledges. The basic hypothesis was verified by Marsh (183), who considered steps on crystal surfaces and determined the stress concentration by photoelastic study of large scale models under a uniform stress (figure 35). The equivalence between the macroscopic steps of the models and the microscopic steps on real crystals is, of course, purely geometric, hence the label of this factor. Thus no account is taken of such factors as a pure step versus a GBD-macroledge.

The geometry considered by Marsh is shown in figure 35. He tested steps on a semi-infinite surface with values of $\phi = 45^{o}$ and 90^{o} (both common crystal steps) and found that the results followed a relation of the form:

$$K_G = 1 + K \left(\frac{h}{r}\right)^{1/2} \qquad (4)$$

Figure 35. Nomenclature of a crystal surface step under a uniform applied stress, σ, as considered by Marsh (183).

Figure 36. Standardized nomenclature for an elliptical crack in a solid under a uniform stress, σ (Paris and Sih, 184, 185).

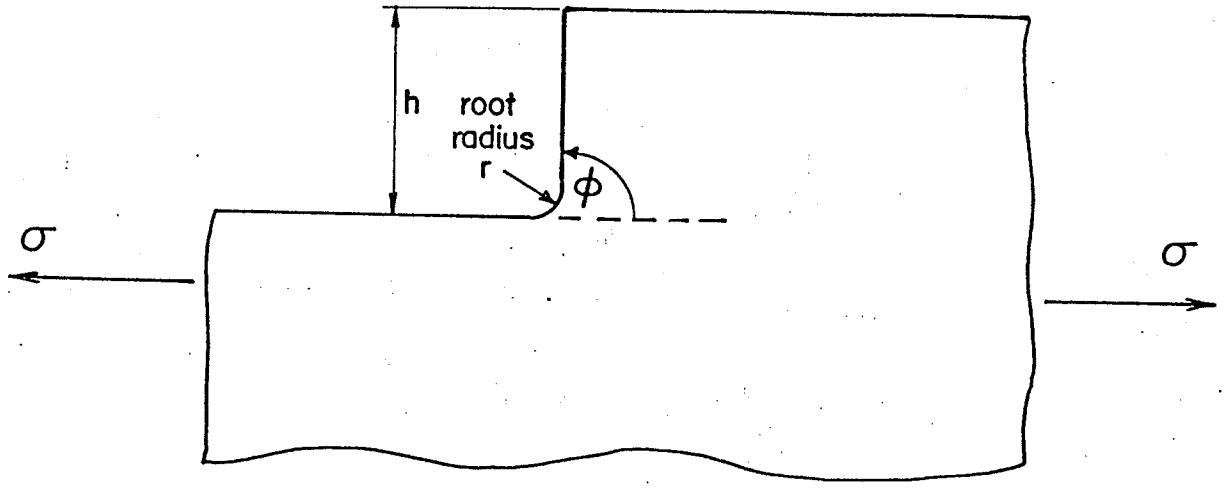
h
root
radius
r
ϕ
σ
σ

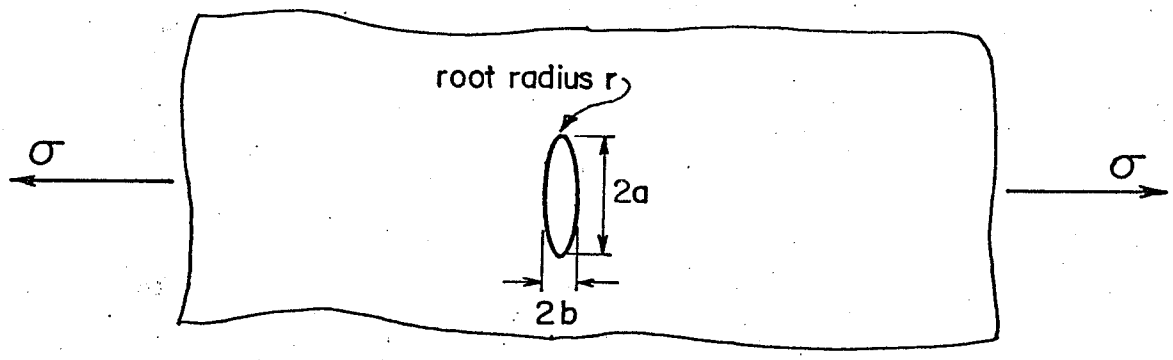
root radius r
σ
σ
2a
2b

It should be noted that in (183) this is erroneously expressed as $K_G = h + K (\frac{h}{r})^{1/2}$.

The results are shown (in an extended form) in figure 37. As can be seen, the results for the 90^o steps were quite close to the range of stress intensifications produced by normal Griffith cracks. This approximate equivalence can be further indicated by comparing equation (4) to one stated by Timoshenko and Goodier (184) for an elliptical crack:

$$K_G = \frac{\sigma'}{\sigma} = 1 + 2 (\frac{a}{b}) \qquad (5)$$

or especially to one stated by Paris and Sih (185):

$$K_G = \frac{\sigma'}{\sigma} = 1 + 2 (\frac{a}{r})^{1/2} \qquad (6)$$

Where σ' is the maximum stress at the root of the crack, and the remainder of the terms are as indicated in figure 36. Finally, the shear stress contours around the step (figure 38a) bear a resemblance to those around a crack (figure 38b), at least for steps with large values of h/r (roughly those greater than 100).

The steps used by Marsh were equivalent to those on a semi-infinite solid. For a boundary step this would

Figure 37. Stress intensification factor K_G for various step dimensions (after Marsh, 183).

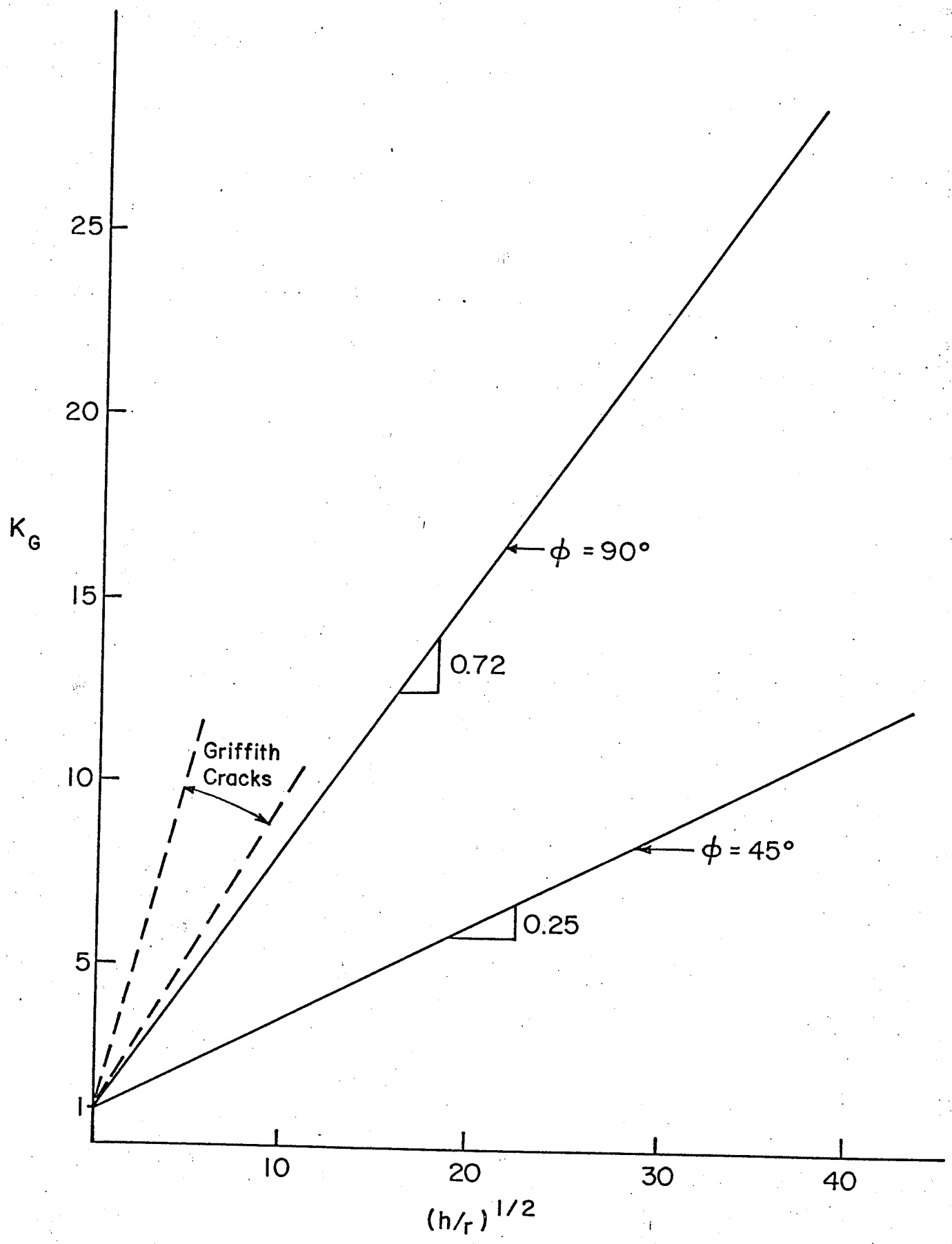
25
20
15
10
5
1
K_G
$\phi = 90°$
0.72
Griffith
Cracks
$\phi = 45°$
0.25
10
20
30
40
$(h/r)^{1/2}$

Figure 38. (a) Shear stress distribution around a step for an applied stress of 20 units.
(b) Shear stress distribution around a double-ended crack (Marsh, 183).

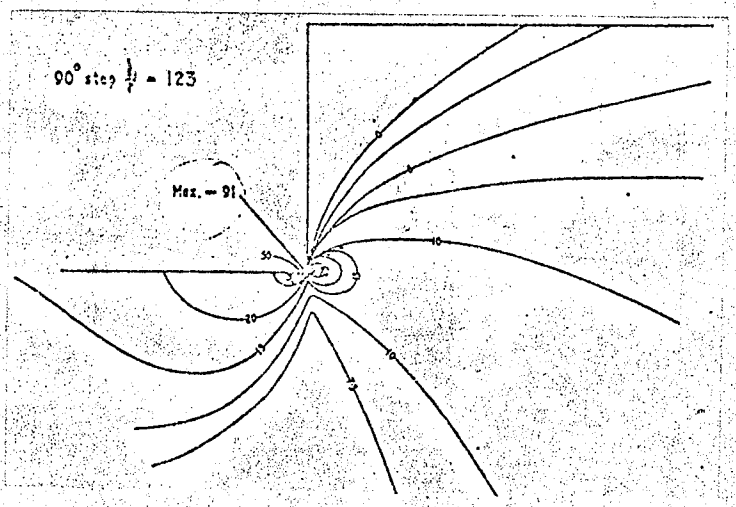

(a)

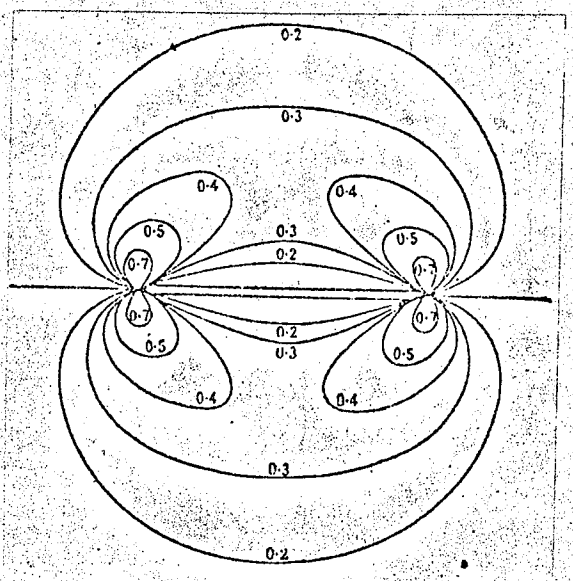

(b)

mean that neighbouring steps in the boundary plane (either parallel or perpendicular to the step in question) would be far enough away so as to have no influence on the stress concentration. Marsh experimentally found that this distance was a minimum of 5 times the step height. From earlier considerations it would appear that both cases could exist in typical random high angle grain boundaries, e.g. step heights of from 3 - several hundred Å have been seen (2, 120, 59). When the spacing of the ledges becomes small, it is quite possible that additional stress enhancement of up to five times for elliptical cracks spaced at a distance which is equal to their length.

Tangri et al (179) have estimated K_G for typical boundary steps in Cu and Ni by using as root radius values the interstitial holes in the FCC lattice (0.415 R for the octohedral hole and 0.225 R for the tetrahedral hole - R = atom radius). Their results are shown in Table 6 for step heights of 100 Å and 1000 Å. The important point is that values of K_G can be large enough to generate dislocations <u>without</u> the aid of either K_n or K_E, thus making it theoretically possible for boundary generation to occur in practically all metals (assuming for the present that the value of r used in (179) is reasonable). Indirect confirmation of this comes from evidence that

TABLE 6

K_G VALUES FOR VARIOUS LEDGE GEOMETRIES IN COPPER AND NICKEL (179)

h (Å)	r (Å)	$(h/r)^{\frac{1}{2}}$	K_G ($\phi=45^o$)	K_G ($\phi=90^o$)
100	0.5	14.1	4.5	11.2
100	0.3	18.3	5.6	14.2
1000	0.5	44.7	12.2	33.2
1000	0.3	57.7	15.4	42.5

surfaces (and likely surface steps) can act as sources of dislocations (187, 188). It can be seen from figure 38(a) that the range of the stress concentration is of the order of the step height, although it is apparent that the decay is quite rapid away from the root radius.

Finally, it is interesting that equation (3), used in the previous section to estimate K_E, can also be viewed in a different sense. That is, if the d and ρ in this relation were to refer to the microscopic geometry at a boundary step instead of the macroscopic geometry of the entire grain, the result would be a combination of the K_G and K_E factors. Thus, for Cu with $d = 1000$ Å and $\rho = 0.5$ Å, an enhancement factor of 18 results. This appears to have been done by Douthwaite and Evans (99), although they were not at all clear on defining the above parameters. They did state, however, that the stress concentration would be sufficient to nucleate dislocations, so it is obvious that they were certainly not considering the relation solely in terms of K_E.

In addition to the detailed picture of the grain boundary and its associated defects, we have now seen proposals for its operation as a dislocation source and experimental confirmation of such activity. This dislocation generation almost certainly requires a degree

of stress intensification at some point in the process, and there appear to be several factors which, singly or in combination, can furnish such an intensification. It would be useful if some experimental observations, as specific and quantitative as possible, could be made concerning this generation, and discussed via a coordinated consideration of all the factors presented thus far.

4 EXPERIMENTAL PROCEDURE

4.1 MICROSTRUCTURE DESIGN

From the foregoing considerations it is apparent that the probability of grain boundary dislocation generation can be enhanced by several factors. These would logically include such points as a very low density of grain interior sources or very strong solute pinning thereof. Even more important, however, the boundary must be capable of generation. Most of the models indicate that this would be favored by the presence of ledges, GBD-macroledges, GBD's, kinks and triple points (although the glissile GBD models would favor lower ledge and kink densities to form longer pile-ups). However, it is to be expected that the density of these should not become too high, lest mutual interaction strangle the sources. That is, for a high density of GBD's along with a high ledge density, the GBD's could not form pile-ups because of the ledges and the ledges could not act as sources because of the randomly-oriented GBD's on top of them. Thus some compromise microstructure is desirable, one between the two extremes of a heavily-deformed material (wherein the boundaries contain a tremendous number of defects) and a fully-annealed one (wherein the boundaries contain very few defects). One indication of such a compromise is the previously-noted tendancy for generation

to occur in relatively fine-grained material. These generally contain boundaries with a reasonable density, of the above defects, yet the material is almost completely recrystallized. An illustration is the previous Ni work by Malis et al (54), where fine-grained Ni of this general description showed substantial boundary generation. Longer heat treatments produced larger grain sizes, relatively defect-free boundaries and no boundary generation. Therefore, a similar procedure was followed in this study and the general mechanico - thermal treatment given was one which would produce a large amount of stored energy, followed by varying degrees of recrystallization and a minimum of recovery in the boundary region. Thus the general pattern was one of massive cold-rolling followed by a short time, low temperature anneal. The resultant fine grain sizes also aided the electron microscope requirement of reasonable lengths of boundary in a thin foil.

4.1.1 COPPER

The copper used in this study was of 99.999% purity, the major impurities being oxygen and arsenic. The as-received material, in the form of 1.25 cm diameter bar, was first cleaned in a solution of nitric acid and

water. It was then given a preliminary anneal of 1 hour at 600°C under a dynamic vacuum of 10^{-4} to 10^{-5} torr. The dynamic vacuum system (figure 39) was used for the majority of heat treatments for a number of reasons. First, the dynamic vacuum would remove any outgassing taking place. Second, the cooling rate obtained upon completion of the anneal was of the same nature for all materials. That is, the tube furnace was simply rolled back from the stainless steel specimen tube (figure 39). Third, because of the large size of this tube and the fact that a vacuum was present, the cooling rate for the material within it was relatively slow compared to, say, the normal air cooling of material enclosed in silica or Vycor tubing (e.g. from 500°C to 100°C in 30 min.). It was hoped that these similar, slow cooling rates would make any boundary segregation, however slight, be of roughly the same magnitude, and, at the same time, result in at least some solute pinning of grown-in dislocations.

The copper was then cold-rolled to a thickness of 5 mm, given another anneal of 1 hour at 600°C, then cold-rolled to a final thickness of 0.5 mm. Samples were annealed for 1 hour at temperatures of 250°, 350°, 450° and 550°C. They were electropolished in a solution of 1/3 nitric acid - 2/3 methanol at room temperature

Figure 39. Dynamic vacuum furnace used for Cu, Cu-1Sn and Ni heat treatments; A - specimen tube
B - tube furnace
C - vacuum system (mechanical and oil diffusion pumps).

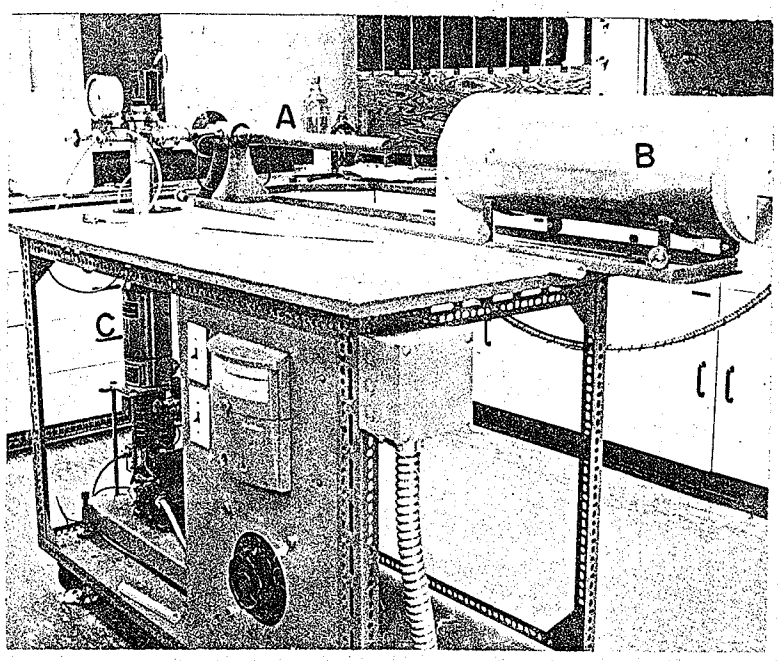
A
B
C

and at a voltage of 4 - 5 volts, then etched by brief immersion in a solution of 5 gm $FeCl_3$, 50 ml HCl and 100 ml H_2O. Average grain diameters for these preliminary treatments were estimated by comparison with ASTM non-ferrous standards. Thin foils for electron microscope examination were prepared (as detailed shortly) and examined to determine the most suitable microstructure as per the stated guidelines. The average grain diameter of this material was then also determined by the planimetric method.

4.1.2 COPPER - TIN

The alloy of Cu - 1 wt. % Sn used in this study was prepared previously (189) from the above Cu and high purity Sn. Roughly 80 gm., in the form of scrap pieces, were first cleaned in a HNO_3 - H_2O solution. They were then placed in Vycor tubing, evacuated to 10^{-5} torr, flushed five times with Argon and finally sealed with an Argon pressure of 100 mm. The material was then melted by placing it in a horizontal tube furnace for 30 min. at 1100°C. It was solidified by moving the tube to the mouth of the furnace for a few minutes, then air cooling. The resultant ingot was sectioned and polished on emery paper and cloth wheels impregnated with diamond paste. Small clusters of what appeared to be inter-

dendritic porosity were observed in some regions, so the material was resealed, remelted and recast in a vertical position. If anything, the porosity was worse, so the 12 mm. diameter ingot was hot-rolled at 750°C to 6 mm. thick strip. This confined the porosity to the outer edges of the strip, which were to be machined off in the preparation of tensile specimens. The oxide layer was ground off and the strip cleaned in HNO_3 - H_2O. It was then annealed in the vacuum furnace for 10 hours at 900°C and cold-rolled to 0.5 mm strip. Samples were then annealed for 1 hour at 500°C, 1 1/2 hours at 500°C, 30 min. at 550°, 575° and 600°C, and 40 min. at 625°C. Polishing, etching, thin foil examination and grain diameter determination were conducted in the same fashion as for the pure Cu, i.e. using the same polishing and etching solutions.

4.1.3 NICKEL

The nickel used was of 99.98% purity, with the major impurities being C < .01 wt % and Mn, Fe, Cu, Cr, S, Si, Mg, Ti and Co each < .001 wt %. It had been used in a similar, previous study of boundary generation (54), and it was decided to follow the treatment used there, if possible. However, this had involved cold reduction

to 0.125 mm, producing a material with an average of only 4 grains through the thickness. Since it has been often stated that a minimum of 5 grains is required (190) for true polycrystal deformation behaviour, it was decided to cold-reduce the as-received sheet from 1.5 mm to only 0.5 mm. (The same rationale was used for all specimen thicknesses). Samples were then annealed for 20, 30 and 45 min. at 500°C. Specimens were electro-polished in a solution of 1/3 HNO_3 - 2/3 methanol at 40 - 50 volts and etched by brief immersion in a 1:1 solution of HNO_3 and acetic acid. Thin foil and grain size studies were then conducted in the same manner as the previous materials.

4.1.4 ALUMINUM

The Al used was of 99.999% purity (major impurities likely C and O) in the form of 2.5 cm diameter rod sectioned into four quarter sections. Kasen (191) has derived a method for achieving fine grain sizes in super-purity Al, and achieved an avg. grain diameter of 30 microns in 99.9999 Al (which was unstable at room temperature, however). Using this method as a basis, the Al was cold-rolled to strip varying from 0.35 - 0.5 mm thick, with immersion in liquid nitrogen between

passes. Kasen then gave the material a very short anneal (a few seconds) in a salt bath at 400°C. However, since the reproducibility of a microstructure becomes more favorable with longer annealing times, the first heat treatments of the Al used in this study were conducted in a heated oil bath (Dow Corning Fluid 210 - H). Treatments of from 2 - 15 min. at temperatures from 170 - 200°C were given to the Al (which was kept in the liquid nitrogen as much as possible to preserve the maximum amount of stored energy). Specimens were electropolished in 70% methanol - 30% HNO_3 at 4 - 7 volts and etched by immersion for several minutes in a solution of 45% ethanol - 45% H_2O - 10% HF. When none of these treatments proved satisfactory, an annealing medium of a molten Pb bath in the stainless steel crucible of a salt bath furnace was used. The specimens were held in liquid nitrogen, dipped in the Pb, then quenched into water. Difficulty was occasionally experienced with the Pb forming an "envelope" around the Al, although no bonding occurred. Anneals of 2 sec. at 340°C, 1, 2 and 4 sec. at 365°C and less than 1 sec. at 400°C were carried out. The time for the latter anneal was difficult to estimate since it was conducted by dipping the specimen as quickly as possible in and out of the Pb.

This short time also led to a rather high mortality rate among the specimens, either from incomplete dipping or striking the sides of the crucible. As with the other materials, thin foil examination and optical metallography was then conducted. The eventual final mechanico - thermal treatments for the different materials are summarized in Table 7.

4.2 TENSILE TESTS

Tensile specimens for all materials were machined from the cold-rolled strip with a standard 3 cm. gauge length jig on a Tensilkut cutter. The widths were generally of the order of 1 cm. After cleaning and the final anneal, temperature-compensated Kyowa strain gauges were affixed, if necessary, and tensile tests conducted on a table model Instron testing machine (figure 40a). All tests were done using the Instron Servo Chart Drive Accessory, activated either by a strain gauge on the specimen or a strain gauge extensometer placed on the specimen during the tests (figure 40b). While the normal Instron chart drive system synchronizes the cross-head speed with a set chart speed (thus indirectly indicating specimen elongation), the Servo System directly indicates the strain on the chart. This occurs because the strain gauge (or strain gauge extensometer) forms

TABLE 7

FINAL MECHANICO - THERMAL TREATMENTS

MATERIAL	FINAL TREATMENT
99.999Cu	Annealed material rolled at room temperature to 90% reduction in cross - sectional area and annealed one hour at 450°C under a dynamic vacuum.
Cu-1wt%Sn	Annealed material rolled at room temperature to 95% reduction in cross - sectional area and annealed 40 min at 625°C under a dynamic vacuum.
99.98Ni	As received material (likely annealed) rolled at room temperature to 70% reduction in cross - sectional area and annealed one hour at 500°C under a dynamic vacuum.
99.999Al	As received material rolled at liquid nitrogen temperature to 99%+ reduction in area and annealed by dipping in molten Pb at 400°C, followed by water quenching.

Figure 40. Tensile testing apparatus:

(a) Table model Instron set for testing specimens with strain gauges attached;

A - external balancing and calibration box

B - Servo unit

(b) Specimen in grips with extensometer attached. Support bar (on platform) fits into slots in the grips for transportation and installation without bending the specimen.

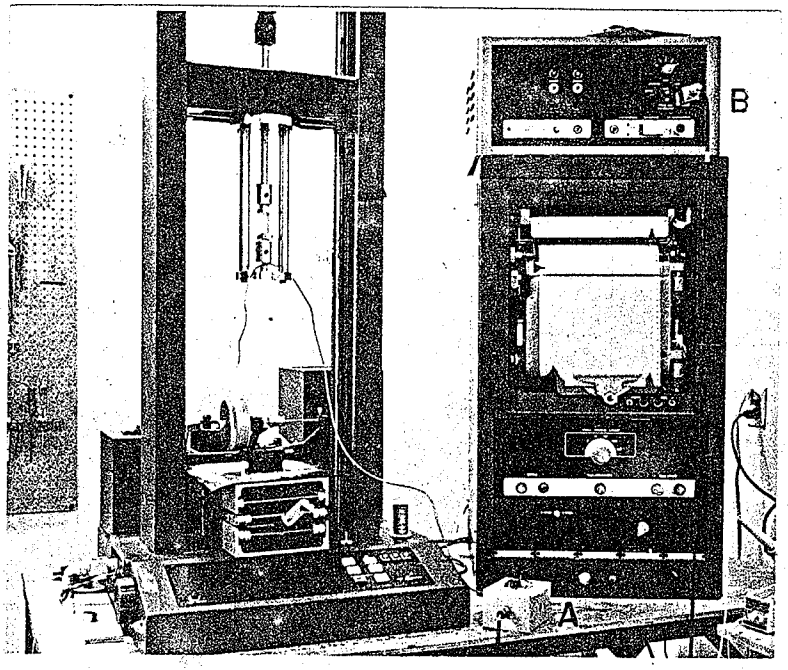

(a)

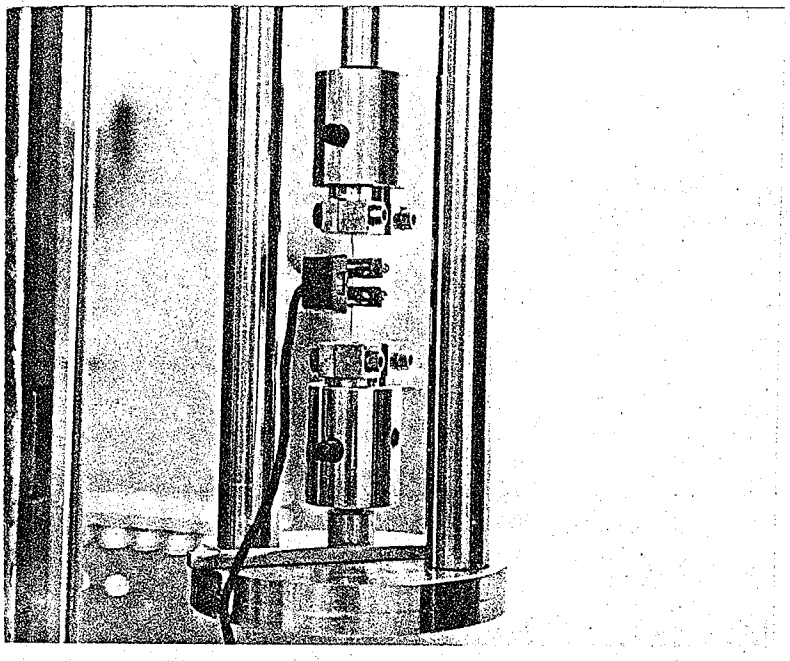

(b)

one arm of a Wheatstone Bridge and specimen elongation thus unbalances the bridge. This unbalance impulse is amplified and used to drive a gear system so as to directly move the chart. At the same time, a feedback loop continually rebalances the incoming signal. Hence a continuous load-strain diagram is obtained during a continuous tensile test.

The strain gauges attached to the specimens were used for the low plastic strain tests, since the sensitivity of the Servo System was much greater with this configuration. That is, the five-position attenuator on the strain gauge pre-amplifier of the system corresponded to full-scale strains (20 cm. of chart paper) of 5×10^{-4}, 1×10^{-3}, 2.5×10^{-3}, 5×10^{-3} and 1×10^{-2}. The same settings for the extensometer corresponded to full-scale strains (25 cm. of chart paper) of 1×10^{-2}, 2×10^{-2}, 5×10^{-2} and 1×10^{-1}. As seen in figure 40(b), a set of grips with a removeable support rod was used. After placing the specimen on the machine and removing the support rod, the strain gauge leads were soldered to the leads from the external balancing circuit (Wheatstone Bridge) of the Servo System. After zeroing and calibrating the load on the Instron console, the strain was zeroed on the Servo unit and calibrated by shunting a calibration resistor (in the external balancing circuit) into the

system. The tensile test was then conducted to the appropriate plastic strain, which was taken as the deviation from the elastic loading line.

For the higher strain tests (1×10^{-2}) and low temperature tests, the Instron G51-16M extensometer (1 cm. gauge length) was used. The procedure was much the same as above, save that the calibration was conducted before the test by attaching the extensometer to a special calibration micrometer and displacing the extensometer arms a set distance to correspond to full-scale chart displacement.

All tests were conducted at a cross-head speed of 0.005 cm/min in order to allow a reasonable amount of time for the low strain tests. Specimens of Cu were first pulled to plastic strains of 1.25 and 6.2×10^{-4} to determine if the microstructure was conducive to boundary generation. Then specimens were pulled to strains of 1, 3, 5 and 7×10^{-4}, 1, 2.5 and 5×10^{-3}, and 1×10^{-2}, all via strain gauges affixed to the specimens. In the same fashion specimens of Cu - 1 Sn were pulled to 3 and 7×10^{-4} and Ni and Al specimens to 3×10^{-4}. This room temperature testing corresponded to 0.22 of the melting point for the Cu and Cu - 1 Sn, and 0.17 of the melting point for the Ni. However, for the Al this would have been 0.32 of the melting point, right in the

range which was mentioned earlier for the onset of high temperature boundary behaviour, i.e. large scale sliding. Accordingly, tensile tests were conducted via the extensometer at -45° to -50°C (0.23 of the melting point) to a strain of 4×10^{-4}. This was achieved by immersion of the specimen and grips in a bath of dry ice and alcohol. Finally, specimens of all four materials were pulled to a strain of 1×10^{-2} with the extensometer to establish the macroyield deformation behaviour (the Al again at -45°C). It should be noted that, due to the somewhat unpredictable nature of the heat treatment given to that material, all Al tensile specimens were first polished, etched and optically examined over the entire gauge length for any signs of large unrecrystallized regions before testing. Parameters measured included σ_{my}, the microyield stress (first deviation from linearity), $\sigma_{0.2}$, the 0.2% yield stress, E, the modulus of elasticity (from both the loading and unloading lines).

4.3 ELECTRON MICROSCOPY

The very nature of grain boundary dislocation generation in the early stages of yielding hindered the quantitative collection of data concerning the density and distribution of lattice defects related to the phenomenon. That is, the defects were small enough to

require at least moderate electron microscope magnifications for detection, e.g. x10000 - x20000, producing a field of view on the microscope screen of the order of 10 microns of specimen surface. At the same time, the defects were as much as 100 microns apart. Thus, selection of random areas for density measurements would have been statistically prohibitive and plate collages would have required an enormous number of plates, to say nothing of the difficulty of co-ordinating the individual plates of such large collages. This low defect density also necessitated the examination of large areas of thin foil, (especially at the low strains) meaning that thin foils with very large electron transparent areas were desireable, if not necessary. Also, because of the relatively "soft" nature of the materials (particulary the Cu and the Al), great difficulties were anticipated in that deformation resulting from foil preparation could obscure the true, bulk deformation defects.

In summary, then, the electron microscope requirements were twofold; to produce thin foils with large electron transparent areas while at the same time minimizing foil handling, and to develop a reasonably fast, efficient means of scanning such large areas and recording the pertinent information. The attempts to

fulfill these requirements will be discussed in some detail because of their critical importance and their novel character.

4.3.1 THIN FOIL PRODUCTION

All thin foils were prepared with an Astromet Dual Jet Electropolisher (figure 41). The polishing conditions for the various materials are summarized in Table 8. The major point of interest in the Table is the "hybrid" technique. The normal procedure with thin foils prepared on the above unit had been to cut around the first perforation as carefully as possible with a sharp biological scalpel. However, as anticipated, this resulted in a very high level of spurious deformation and related defects. One alternative which was attempted was to simply "punch out" the perforation using a special punch that had been constructed for the purpose of making grids for the electron microscope holders (figure 42). This solution did not work. Foils of Cu, Cu - 1 Sn and Ni simply tore and buckled. The Al fared somewhat better, with tear - free, round discs being produced. However, they were found to become slightly concave and spurious deformation of a substantial level resulted from this.

Another alternative was the use of the PTFE

TABLE 8

DATA FOR THIN FOIL PREPARATION

MATERIAL	FIRST STAGE	SECOND STAGE	THIRD STAGE
Copper and Copper-Tin	Tensile specimen chemically thinned to 0.25 mm in 1/3 acetic acid -1/3 H_3PO_4-1/3 HNO_3 at 25°C with moderate agitation and water-wash.	Lacquered square electro-polished until perforation in 1/3 HNO_3-2/3 methanol at -30°C, voltage=4-5v.(Cu) or 5-7v.(Cu-1Sn), low jet flow. Withdrawn through liquid N_2 (1) and methanol washed.	Hybrid chemical polished in ½HNO_3-½H_2O. Apparatus washed in H_2O, then methanol Foil washed in trichloro-ethylene, methanol and ethanol.
Nickel	Specimen rubbed with 600 grit emery paper. Lacquered square electro-polished to 0.25 mm in 48% H_3PO_4-32% H_2SO_4-20% H_2O at 50°C and 9-10 v.(2). Low jet flow, water washed.	Electropolished in same solution until perforation (3). Moderate jet flow and ethanol washed.	Hybrid electropolished in same solution at high voltage (4). Washed as above.
Aluminum	Square electropolished to 0.25mm in 1/3 HNO_3-2/3 methanol at 25°C and 4-7 v. No jet flow, methanol washed.	Electropolished until perforation in 80% ethanol-20% perchloric acid(5) at 25°C and 18-20 v. Very low jet flow. Ethanol washed.	Hybrid electropolished in latter solution at high voltage(6). Washed as above.

(1) Rather critical, since a uniform dispersion of oxide particles obscures the thin area if notdone

(2) Can also use 77% acetic acid-23% perchloric acid at 22 v. or 60% H_2SO_4-40% H_2O at 5 v. Both are rather slow, however.

(3) Hole appearance very rapid, also solution somewhat opaque due to gas bubbles, therefore close watch must be kept.

(4) Can chemical polish in 50% acetic acid-30% HNO_3-10% H_2SO_4-10%H_3PO_4, but high temperature(90°C) judged unsafe due to possible dislocation rearrangement.

(5) This solution can also be used for the first stage, but action much slower.

(6) Room temperature chemical polish of 60% H_2O-40% HCl, 5 gm nickel chloride availible, but action rather slow for this technique.

Figure 41. Electropolishing apparatus for thin foil preparation; A - cooling bath
B - polishing solution
C - stainless steel jets with specimen

Figure 42. Punch used for attempts to obtain thin foils with reduced handling deformation.

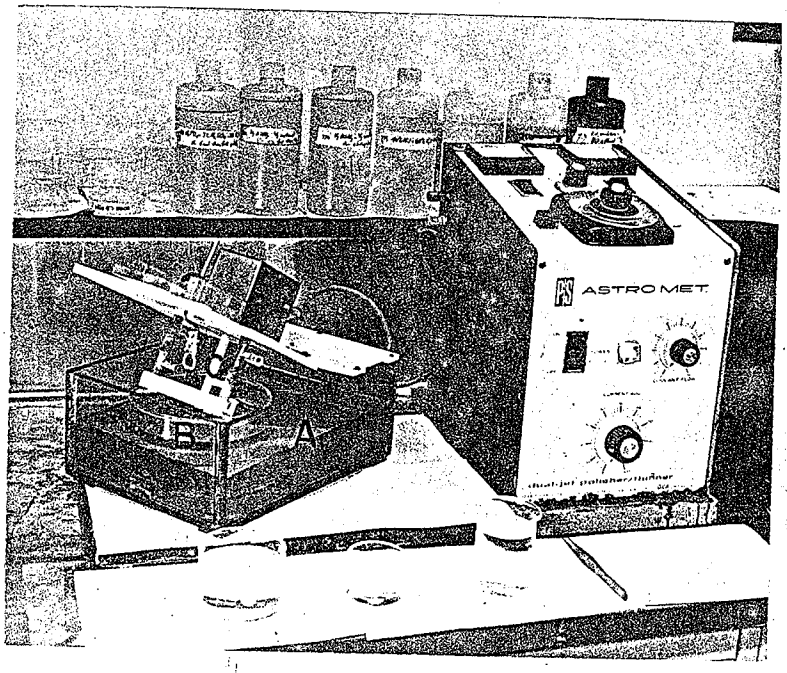
ASTRO MET.
B
A

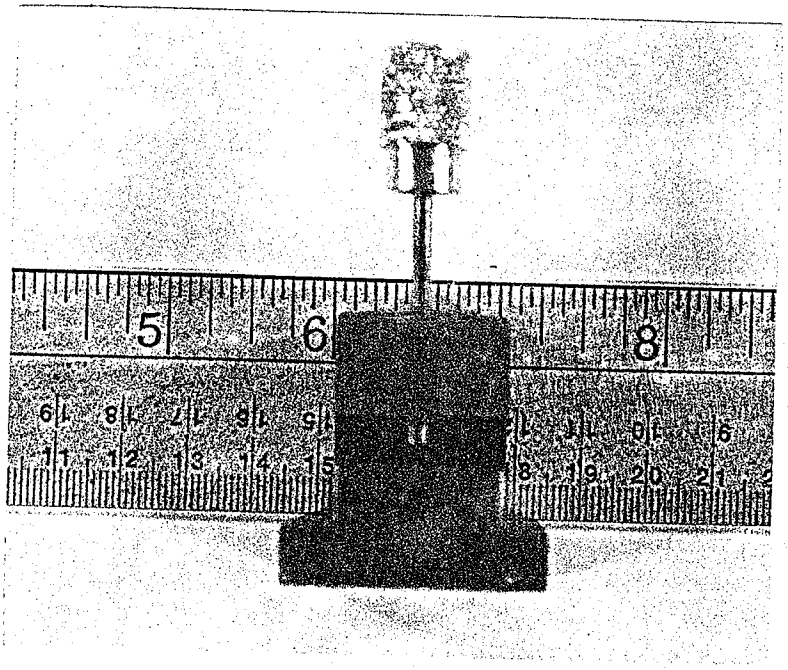
5
6
8

holder (figure 43) to produce thin foils from disc specimens. This looked very attractive, since foils produced by this technique are virtually free of spurious deformation. At the same time, a simple, rapid method had been derived for producing the strain - free discs needed for the holder. As reported elsewhere (192), the method was basically one of grasping the specimens with tweezers to which 3 mm diameter discs had been attached. Mineral oil was used on the disc faces to act as a sealant. The remainder of the specimen was then dissolved away in a chemical polish, leaving behind a disc of approximately the correct diameter (usually slightly smaller). In the latter stages of the study, special tweezers made of PTFE material with removeable inserts were constructed (figure 44). Thin foil production by the PTFE holder encountered several problems, however, when extensive attempts were made on both Al and Cu discs (the former punched, the latter prepared by the above method). The major one was that the disc-production method favored, and the goniometer electron microscope holder required, thinner discs (0.2 mm) than the optimum for the PTFE holder (0.5 mm). This meant polishing from only one side in the holder, which invariably resulted in a foil quality far inferior to foils produced by the dual jet method. Even without this, however, the most important

Figure 43. Electropolishing holder for disc specimens, made of PTFE material (Teflon).

(a) Holder showing; A - Pt electrode

B - main body of holder with removeable insert

C - cavity for disc.

Note: polishing from one side achieved by placing large PTFE disc over entire cavity.

(b) Specimen profile before and after polishing (Brammer and Dewey, 193).

Figure 44. Apparatus used in hybrid technique of preparing thin foils; A - PTFE tweezers with removeable 3mm inserts

B - holder used for washing thin foils

C - vacuum tweezers.

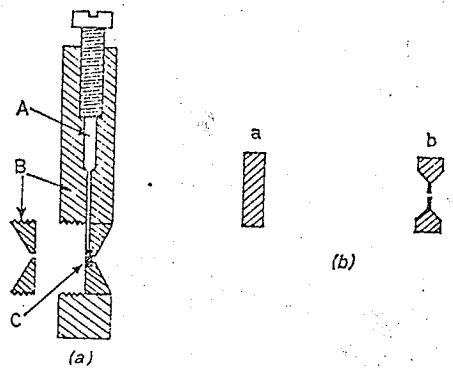
A
B
C
(a)
a
b
(b)

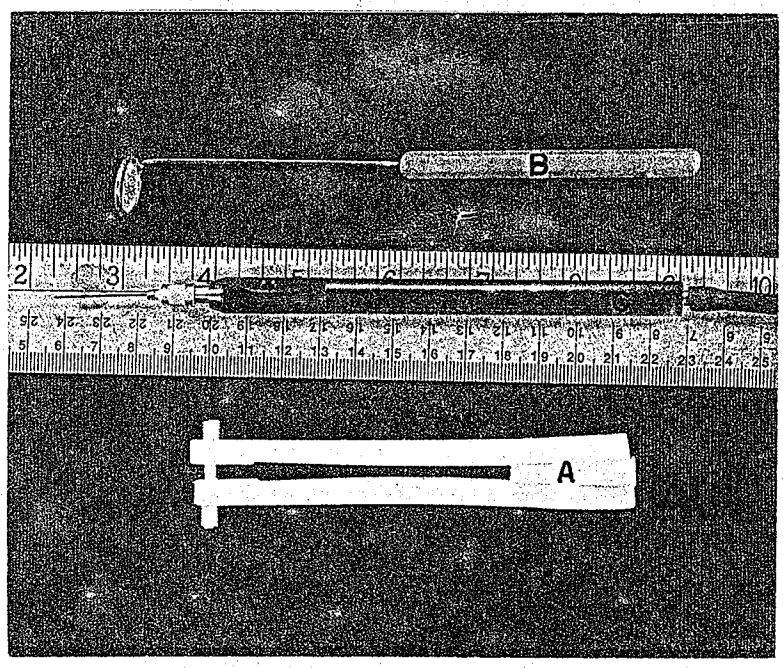
B
A

drawback was that the PTFE holder generally produces foils with much less electron transparent area than other methods using larger specimens. This problem has often been overcome to some degree by use of more sophisticated apparatus for disc polishing which incorporate photocell detectors, high intensity light sources and automatic devices for cessation of polishing upon perforation. Since such equipment was not available, it was decided to conduct the study as far as possible by the aforementioned procedure of cutting out the perforation as carefully as possible and studying only areas relatively free of spurious deformation. This was done, but the problems became insurmountable at the higher strains and for Al foils in any condition, annealed or deformed.

Fortunately, the suggestion of a colleague (194) resolved the impasse by leading to an adaption of the above disc - production method. The adaption was to follow the same procedure but applied to the perforation in the thin foil produced via the dual jet method. Initial thoughts were that the application of sufficient pressure to maintain a good seal would badly deform the foil, but, as illustrated in figure 45, it appeared that the concavity of the foil greatly reduced this possibility. That is, the most delicate area around the perforation was

Figure 45. Scaled cross - section of specimen - disc configuration for hybrid technique.

Figure 46. Typical Cu foils produced by cutting with scalpel (square) and by hybrid technique (disc). Millimeter scale at top.

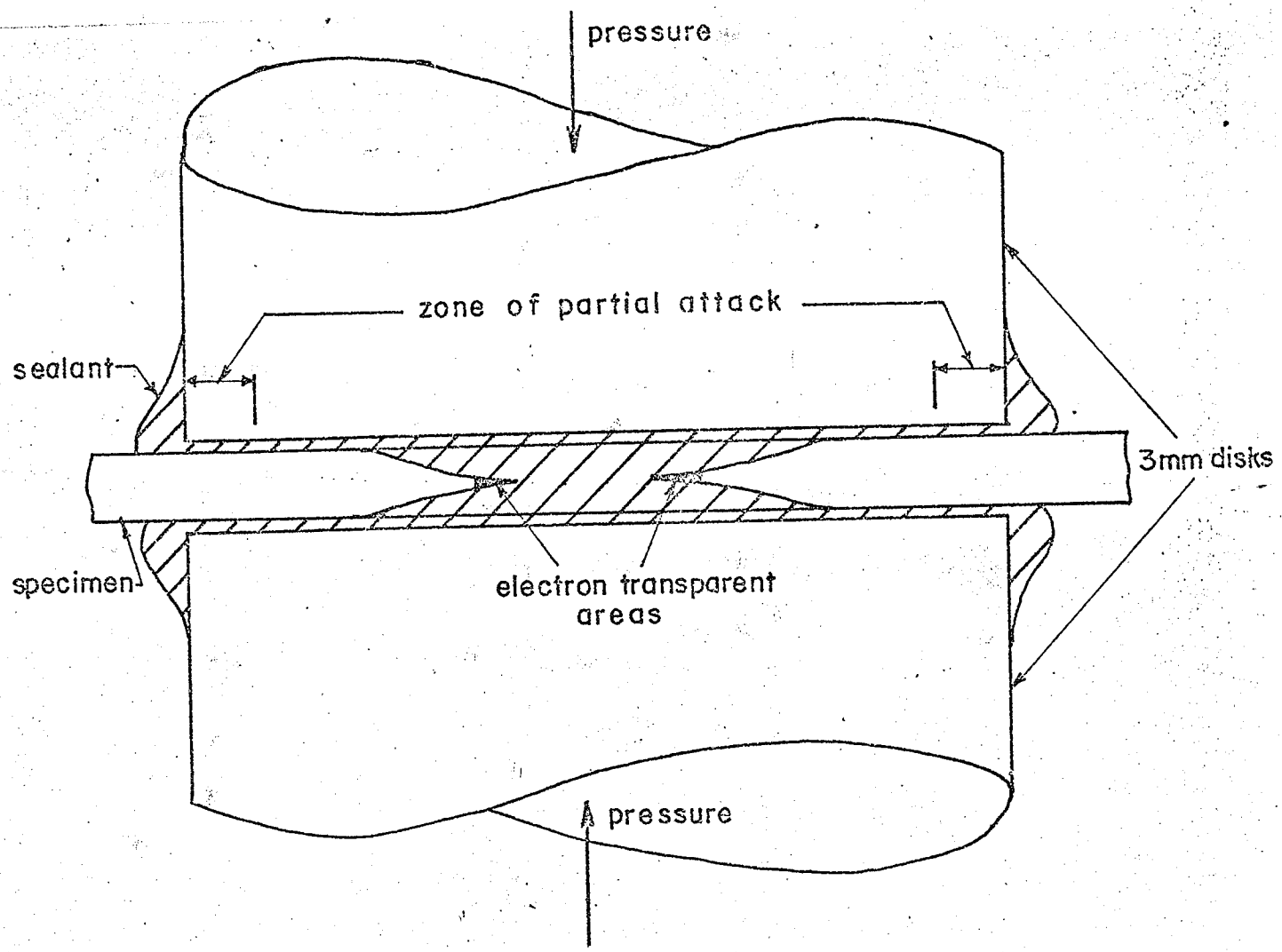
pressure
zone of partial attack
sealant
3mm disks
specimen
electron transparent areas
pressure

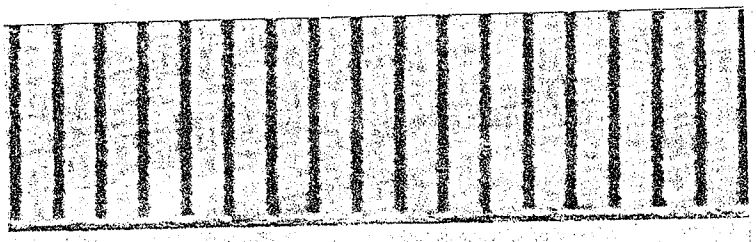

not in direct contact with the tweezers, but was only acted upon by the much safer hydrostatic pressure transmitted through the mineral oil. As simple as the idea sounded, its application nonetheless required a high degree of delicacy, for example, in the above-mentioned application of sufficient, but not excessive, pressure. In addition, centering of the perforation with respect to the discs was very critical, since some etching often occurred a short distance inwards (figure 45). To aid in this, reference marks were inked on each side of the square specimen. The dissolution of the remainder of the specimen should preferably take only a few minutes, since increasing time increased the likelihood of a breakdown in the oil seal at some point, invariably followed by attack of the electron transparent area. The washing procedure was also important, since it was found that any oil left on the foil greatly obscured the underlying structure. Unfortunately, the only solvent that appeared to satisfactorily dissolve the oil was trichloro - ethylene, which itself often left a residue on the foil, though not as bad a residue as the oil. This trichloro - ethylene film, when it did occur, could not be removed by prolonged washing in either methanol or ethanol. It was hoped that glycerin could be used as a sealant, since

it readily dissolved in alcohol, but it was also found to slowly dissolve in acid (e.g. HNO_3 and HCl) and the seal usually broke down before dissolution of the exposed portion of the thin foil.

Great care was also taken in handling the foil during the washing procedure. The disc was floated off the tweezers in the trichloro - ethylene onto a specially - constructed holding instrument (figure 44) normally used for electron microscope replica preparation. It was then transferred from wash to wash via this instrument and air dried. It was finally lifted from this holder by vacuum tweezers (figure 44) and placed in the microscope holder. The technique also proved amenable to electro-polishing via a pair of stainless steel tweezers with 2 stainless steel discs soldered to them. Figure 46 shows a comparison of typical foils from the cutting procedure and the "hybrid" procedure. This latter designation was given since it was felt that method combined the best aspects of the previous methods, i.e. the large thin areas of a foil obtained from a large specimen (dual jet method) and the minimal foil handling obtained from a disc specimen (PTFE holder). The value of the technique was important, not so much for the reduced magnitude of foil handling, but for the <u>location</u> of the handling -

induced deformations. Thus, there were still many cases of tearing and cracking at the foil edges and, less often, narrow bands of heavy slip passing through the entire thin area. The former was likely attributable to foil washing and the latter to excessive tweezer pressure or the insertion of the lock-ring on top of the foil in the microscope holder. The major reductions in handling came in the thicker regions where defect contrast was poorest and hence the possibility of making an erroneous classification greatest. This is only logical, since, for cut foils, travelling away from the perforation edge automatically meant travelling towards the heavily-deformed region extending from a cut edge, whereas, for hybrid foils, this same edge had been formed by stress-free chemical dissolution.

Although the results indicated that this technique had great potential, there are a number of obvious refinements that could be made. Of primary importance would be a framework of some kind into which both the thin foil and tweezers could be clamped, then adjusted so that the discs were centered over the perforation. The discs would then be brought in contact with the foil via some means whereby the clamping pressure could be regulated. With regard to electropolishing, it was found

that the stainless steel discs also were dissolved away. A possible solution would be to have discs made of carbon, or one of carbon and the other of PTFE material. Finally, the sealant and washing solution combination should be improved to provide better (and more consistent) foil visibility.

4.3.2 ELECTRON MICRO-MAPS

The technique devised for quantitative study of the premacroyielding process in the electron microscope was basically one of traversing suitable areas of the thin foils at moderate magnifications, noting configurations of interest and recording them on a "map" (referred to as an electron micro-map). The correlation between the foil and the micro-map was achieved by press-fitting plastic discs onto the x and y traversing controls of the Phillip's EM300 electron microscope (figure 47). The discs were graduated into tenths of a revolution. The magnitude of the correlation was established as follows:

1. The selected area (SA) magnification mode was set at the value which positioned the tilt axis of the specimen closest to the horizontal on the lower microscope viewing screen. In this situation, operation of the horizontal specimen traversing control resulted in a near horizontal displacement of the thin foil on the screen.

Figure 47. Graduated disc on electron microscope specimen traversing control for thin foil - map correlation.

Figure 48. (a) Correlation between thin foil and micro-map.
(b) Mapping of defects by following the indicated traverse and recording relevant defects on the micro-map.

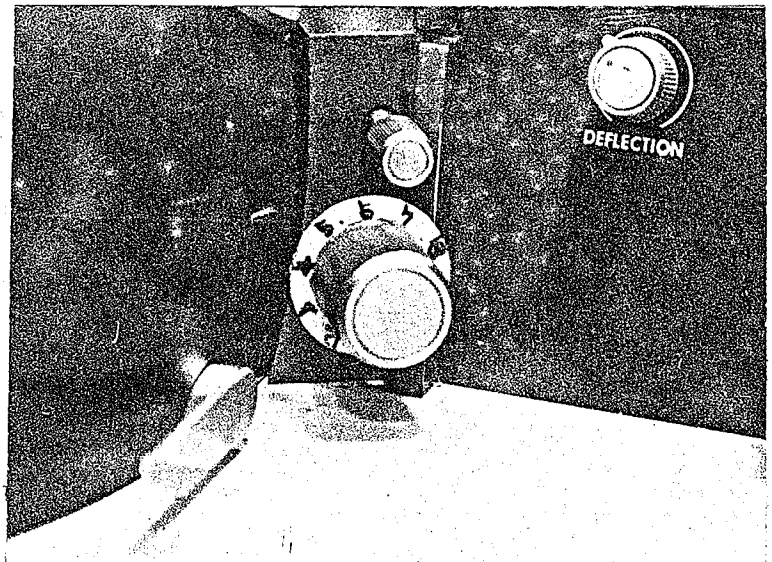
DEFLECTION

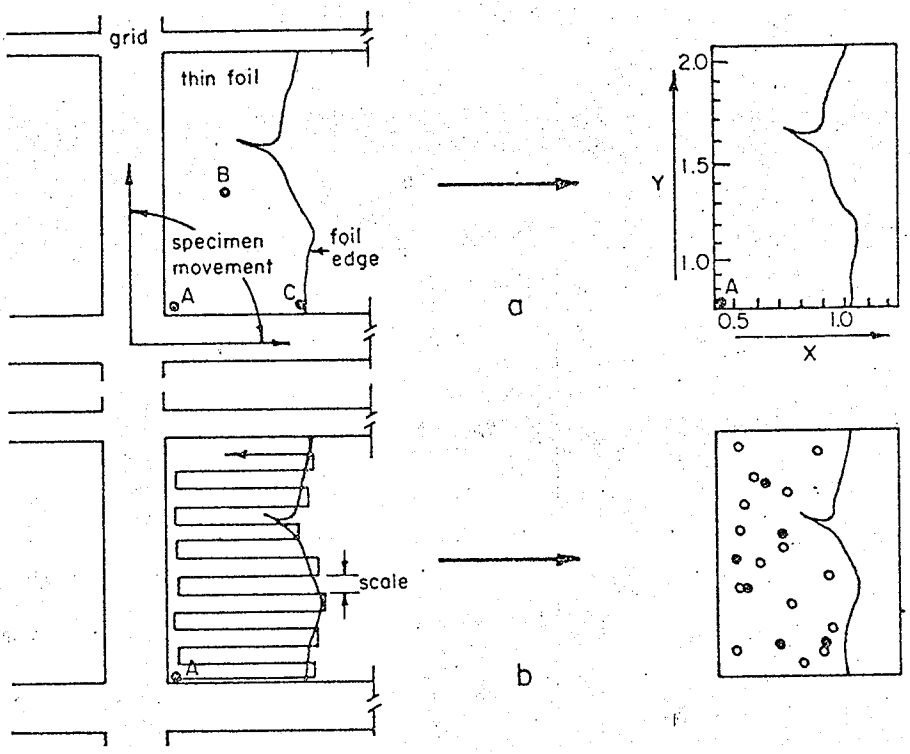
grid
thin foil
B
specimen
movement
foil
edge
A
C
a
2.0
1.5
1.0
Y
A
0.5
1.0
X
scale
A
b

2. A small particle in the thin foil was positioned on one of the photographic plate reference marks on one side of the screen, then moved across the screen to the matching mark on the other side. Knowing the distance between these marks (10.2 cm), the rotation of the control (0.07 revolution) and the magnification (x26,230), the correlation of the control to the thin foil was calculated as 0.1 revolution of the control equal to 5.5 μm of foil movement.

A general mapping procedure was then established as follows:

1. An area of the foil suitable for examination was chosen. If grids were used to contain the thin foil (as was normally the case), the specimen was rotated, while on the low magnification SCAN mode, so that the grid bars coincided with the horizontal and vertical displacements of the specimen. This was done at a tilt angle of 0^{o} to avoid distortion of the grids and the grid bar directions were set as the x and y axes of the map.
2. A convenient point, such as A in figure 48(a) was chosen, and its map co-ordinates determined as the readings on the horizontal and vertical controls (i.e. 0.4 and 0.7 revolution in figure 48(a) when A was located at the centre mark of the microscope screen. The map scales were then laid out accordingly. (It

should be noted here that if no grids are present, point A should correspond to some easily identifiable part of the thin foil for re-examination purposes).

3. The approximate centre of the thin area (point B) was levelled with respect to the tilt axis of the microscope, i.e. so that specimen movement on the screen upon tilting was minimized.
4. The foil edge was then mapped by switching to the SA mode, proceeding in the y-direction, and marking the x-co-ordinate of the edge at each increment, the increment size depending on the degree of map detail desired for the edge.
5. Starting from A, a traversing pattern, such as illustrated in figure 48(b) was followed, and relevant defects, their co-ordinates and their classification, were mapped. The scale of the traverse (figure 48b) was governed by the scale of the defects being mapped, through the magnification necessary to distinguish them.
6. As the traverse proceeded, the specimen was continually tilted in both directions about 0^{o} tilt to detect those defects out of contrast at the central 0^{o} position.
7. Where desired or applicable, plates or collages were taken according to whatever criteria were deemed necessary, e.g. simple observation, Burgers vector analysis, stereo

microscopy, etc.

The feasibility of the procedure was tested by a brief study of lattice defect densities in rapidly - and slowly - cooled Cu (195). The nomenclature and definition of the defects recorded in the present study, somewhat simplified from that of (195), are listed in Table 9. Those defects recorded in a given map were a matter of both interest and expediency. For example, for the former, twin boundary generation of lattice dislocations was generally not recorded after initial maps demonstrated that it appeared to be more a function of a factor (or factors) other than the specified plastic strain. For the latter, GB segments were only recorded over small portions of maps wherein this density was fairly high, and eliminated altogether when the density reached the point where almost all segments showed some defect activity. For much the same reason, the boundaries themselves were not fully recorded for most maps (although, again, small portions were recorded for several). Where possible, grain size estimates by the planimetric method were made on maps where the boundaries had been recorded. Grain boundary sources that were only a few hundred Å apart were classified as one P-orF-defect. This was done to enable a consistent classification to be made, something which could not

TABLE 9

MICRO-MAP NOMENCLATURE

Note: numeric subscripts used on maps to designate different defects, e.g. IA_2.

SYMBOL	DEFINITION
IA	Denotes areas of grain interior dislocation activity not obviously connected to the grain boundaries.
GB	Denotes grain boundary segments (semi-planar portions) containing observeable boundary defects (GBD's, ledges, etc.).
TP	Denotes emission* of lattice dislocations from a boundary triple point.
F	Denotes emission of stacking faults (partial dislocations) from a grain boundary (including any from triple points).
P	Denotes emission of perfect lattice dislocations from a grain boundary (including triple points).
TBF	Similar to F-defects, but referring to a twin boundary.
TBP	Similar to P-defects, but referring to a twin boundary.

* Aside from obvious cases of dislocations bowing out from the boundary (figure 19, p.68), this will include dislocations which are merely in contact with the boundary when there is little or no dislocation activity in the nearby grain interior.

be done for adjacent sources when the source site was not visible (e.g. figure 19f) or the sources were very close together.

As intimated previously, the major difficulty in this procedure was the necessity to exclude from the study lattice defects due to foil handling. The origin of a given defect or defects was particularly difficult to determine in thicker regions of the foil where contrast was severely reduced or when the specified plastic strain was relatively high. To aid in this, the following observations were regarded as generally characteristic of thin foil regions that had been subjected to high handling stresses:

1) The presence of cracks or tears in the foil edge.
2) The presence of deformation bands, accompanied by slip traces which indicated their formation in the thin foil (196).
3) The presence of a high density of extinction contours which indicated a high degree of foil rumpling.
4) The presence of extensive dislocation arrays or tangles not expected from the level of stress (if any) reached in the bulk specimen.
5) The presence of a number of long dislocations nearly parallel to the foil surface (196).

Any region of the thin foil which contained an

appreciable number of any of the above mentioned characteristic features was designated as a Deformed Zone and was not employed for mapping. As the transition between such zones and the normal thin areas was found to be gradual, defects lying in the vicinity of these zones were carefully studied in relation to the surrounding matrix before mapping. Finally, after thorough examination of the micrographs, defects suspected to be due to handling were distinguished with asterisks and were ignored for defect density calculations. Some isolated spurious defects were occasionally observed outside Deformed Zones and similarly excluded. Any lattice defect whose origin or nature was deemed particularly contradictory or unclear was so indicated by a question mark and its status decided only after considerable thought. It is a well-known fact that lattice defects annhilate at the foil surface much more easily in the thinnest regions (196), therefore, where possible, it was attempted to choose areas of a similar proportion of thin to thick regions.

The micro-maps were recorded on graph paper to a scale of 1 cm. = 0.1 revolution of the control (rendering a map magnification of X1800). A few of the Al maps were drawn to half this scale because of the larger grain size in that material. Tracings of the map were made and, together with pertinent micrographs, assembled into a

collage which was regarded as a completed map. For greater clarity these were made somewhat oversized (27.5 by 35 cm.), but for this thesis were reduced and photographed to fit standard-sized pages (21.25 by 27.5 cm.), thus producing varying maps magnifications. For the calculation of defect densities, the areas of the maps were measured with a planimeter and, where appropriate, the grain boundary lengths were measured with a distance recorder normally used for regular maps.

It should be pointed out that the maps possessed rather poor accuracy with regard to exact locations due to two factors; play in the specimen traversing controls and some geometric distortion upon tilting (even when the foil was levelled with respect to the tilt axis).

Thus any given defect, grain boundary or foil edge could be perhaps as much as several microns from its true location and the maps should not be used for such calculations as exact interdefect distances or radii of curvature for boundary segments.

It must also be emphasized that the defect densities are comparative only. Many defects were undoubtedly lost to the foil surface in thinner regions. In thick regions, many were undoubtedly overlooked (especially in the foils of higher strain). There may have been defects from spurious deformation which resembled,

in all respects, those from bulk straining, or they may have been present in the annealed material (incomplete recrystallization). Some of the defect definitions were obviously rather general e.g. IA's and GB's, and there were often large variations in the numbers of individual defects within these areas from one case to another. However, this generality (along with such factors as the previously mentioned classification of closely adjacent sources as one source) enabled large lengths of boundary in a large number of foils to be studied quantitatively in at least some respects. Finally, and most importantly, they were determined for a very thin slice of the deformed metal, i.e. a section through (approximately) only 1% of the total volume of a grain of average diameter.

4.3.3 GENERAL MICROSCOPY

In addition to the mapping, a number of individual boundary generations were carefully studied in both mapped regions and areas outside these. Because of varying foil conditions and defect contrast, no set amount of data was obtainable from every configuration. Amongst the information that was sought was :

1) The intensity of the generation (number of dislocations generated and the distance travelled into the grain),

2) Any evidence for either single sources or multiple adjacent sources,
3) Character of the generated dislocations (edge, screw, mixed),
4) Burgers vectors of the dislocations, in the sense of whether or not they were identical for all dislocations in a given configuration,
5) For faults, confirmation via bright field-dark field fringe asymmetry,
6) Any related boundary defects (GBD, IGBD, GBD-macroledge, etc.) or topography (ledges, triple points, kinks),
7) Any evidence for boundary type (coincidence, low angle, etc.),
8) Any configurational data confirming or refuting boundary origin of the dislocations, i.e. as opposed to grain interior or twin boundary sources,
9) Any evidence for the presence of elastic strain concentrations,
10) Any evidence for enhanced generation in particularly - oriented grains,
11) Source location with respect to grain size or shape,
12) Any possible connection to foil handling.

Although most of the electron microscopy techniques associated with the above are quite well-known, e.g. for 3) - 5), it would be appropriate to comment on that used for 9) since it does not appear to have been used extensively

prior to this study. Briefly, the presence or absence of significant elastic strain concentrations was detected by the relative sharpness of Kikuchi lines in selected area diffraction patterns. These lines result from the inelastic scattering of electrons and, because they are rigidly "fixed" to the specimen with regard to the diffraction pattern, they have been often used for accurate orientation determination or orienting foils for taking stereomicrographs (196). However, a few authors have also noted that these lines should be sensitive to the presence of elastic strain (197, 198), much in the same fashion as are x-ray powder photograph lines or diffraction peak profiles. Accordingly, diffraction patterns with strong Kikuchi lines were taken for some boundary sources. They were taken with a very small diffraction arpeture at three locations; at the source, at the grain boundary away from the source, and in the grain interior. Of course the latter two were taken, as much as possible, away from any other possible source of elastic strain.

5 RESULTS

5.1 MICROSTRUCTURES

As mentioned, final heat treatments of 1 hour at 250, 350, 450 and 550°C were given to the cold-rolled Cu. The ASTM average grain diameters ranged from 10 - 35 microns. Electron microscopy examination of the structure from the 250°C treatment showed a substantial number of grown-in dislocations in the grain interiors. The 350°C treatment produced relatively clean interiors and many boundary segments with substantial numbers of defects. There was, however, a very high density of annealing twins which was undesireable due to spurious dislocation generation occurring from them (to be discussed shortly). This was greatly reduced in the 550°C treatment, but the grain boundaries were quite defect-free. Thus the 450°C treatment was accepted as the best compromise of a reasonably annealed structure with defected grain boundaries and a tolerable density of annealing twins. Its ability to produce grain boundary generation of lattice dislocations was confirmed by electron microscopy of the specimens deformed to 1.25 and 6.2 x 10^{-4} (figure 49).

The Cu - 1Sn presented a somewhat different problem. Examination of the first trial treatment (1 hour at 500°C) showed a very high annealing twin density along with many

Figure 49. Grain boundary emission of $\frac{a}{2}$<110> perfect lattice dislocations onto {111} slip planes; (a), (b) Cu, plastic strain of 1.25×10^{-4} (c) Cu, plastic strain of 6.2×10^{-4}. GB = grain boundary, TB = twin boundary

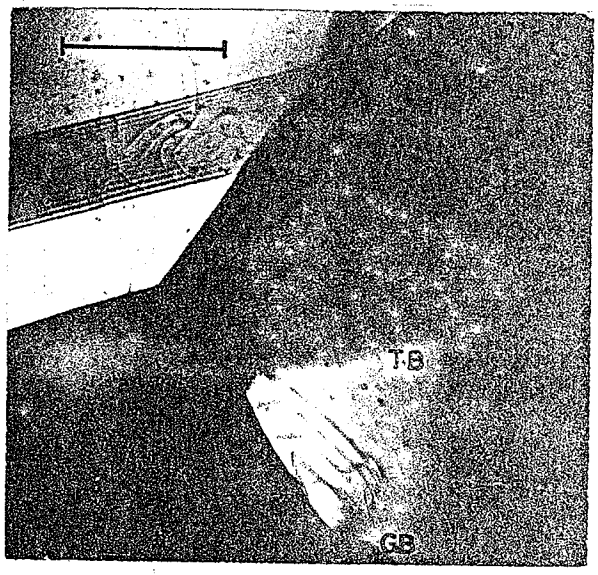

(a)

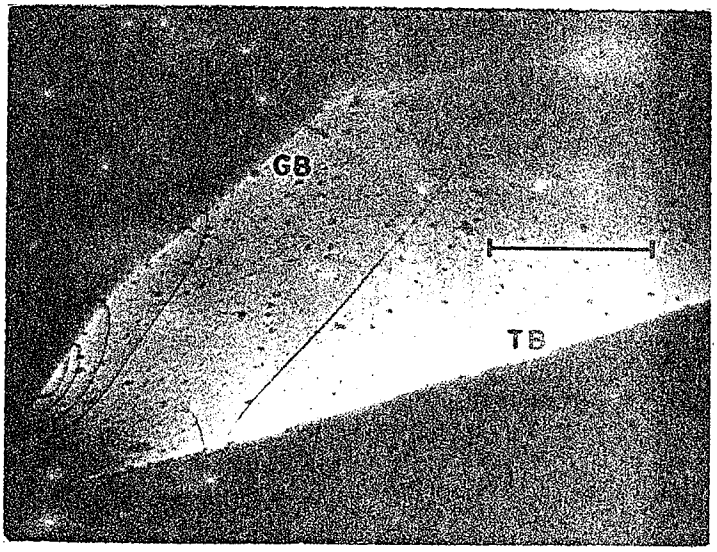

(b)

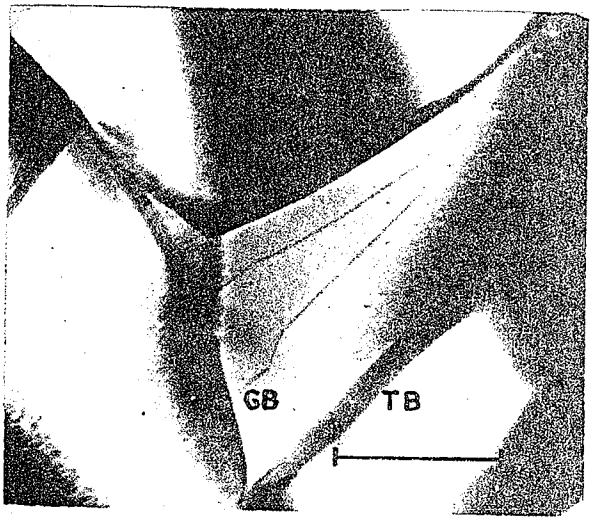

(c)

grown-in dislocations. Slightly decreasing the time and increasing the temperature proved helpful in that the interiors became cleaner, while the boundaries still contained some defected segments. However, the cleaning of the grain interiors appeared quite slower than that of the grain boundaries, so the 40 min. at 625°C treatment was accepted as another compromise between tolerating the occasional cluster of grown-in dislocations and boundaries containing some number of defects. The annealing twin density was much the same as the Cu.

Because of the reduced cold-working from the previously-used treatment (54), the Ni required a somewhat longer time (45 min.) to produce an acceptable microstructure similar to the Cu and Cu - 1Sn.

The initial treatments of the cold-rolled Al in the oil bath were unsuccessful, with the best recrystallized structure possessing an average grain diameter of roughly 100 microns, rather too large for a reasonable amount of grain boundary length in a given thin foil. The initial treatments in the Pb bath improved on this only slightly, but the quick dipping at 400°C produced better results, with many portions of the microstructure being of reasonably small grains.

These microstructures are shown optically in figure

50 (Cu, Cu - 1Sn, and Ni) and figure 51 (Al). The average grain diameters via the planimetric method were 18 microns for the Cu, 22 microns for the Cu - 1Sn and 25 microns for the Ni. At the same time, it can be seen that the extremes of individual grain diameters was quite large in each, being of the order of 1 to 50 - 100 microns (the lower range for the Cu - 1Sn, the higher for the Ni and the Cu falling somewhere in between).

The notion of an average grain diameter was rather difficult to apply to the Al. Not only was there a very large variation in individual grains (1 - 450 microns), but large variations in average diameter for areas of the same specimen (figure 51 b-d) and overall variations from one specimen to another (figure 51a vs 51b-d). It should be noted that the Al was very difficult to fully etch and thus figure 51 is somewhat misleading in that some grains have undoubtedly not been revealed.

5.2 TENSILE DATA

The main parameters calculated from the stress-strain curves are presented in Table 10. Because of only moderate equipment accuracy, occasional microstructural variation and/or a somewhat limited number of tests, they are presented for completion only. The lower σ_{my} for Ni,

Figure 50. Microstructures of;

(a) Cu - etchant of aqueous $FeCl_3$

(b) Cu-1Sn - etchant as above

(c) Ni - etchant of equal parts HNO_3-acetic acid.

Markers = 100 microns.

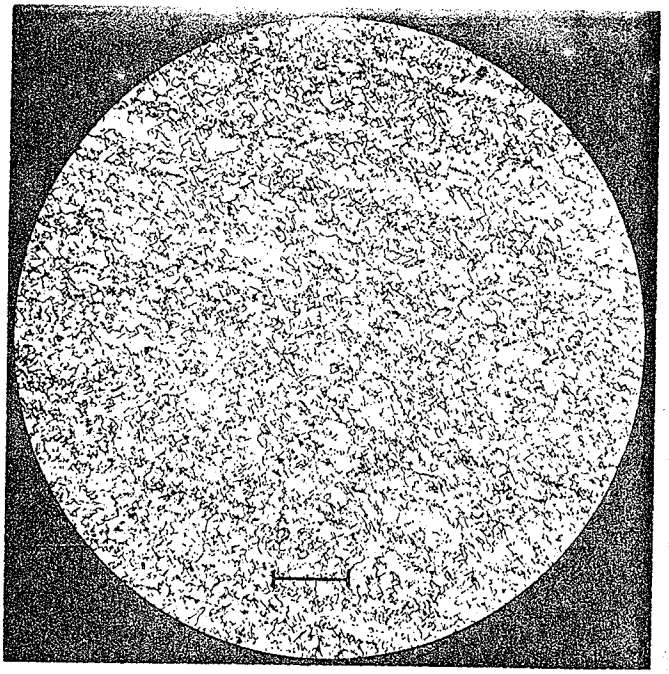

(a)

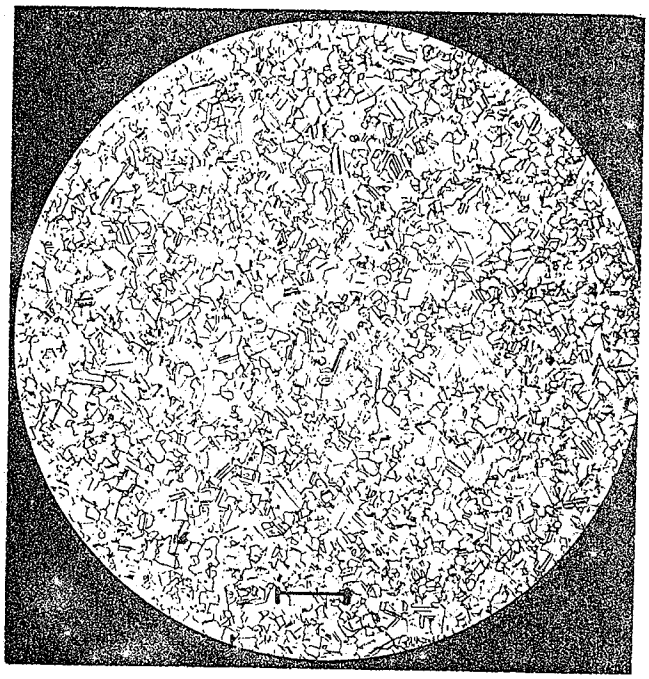

(b)

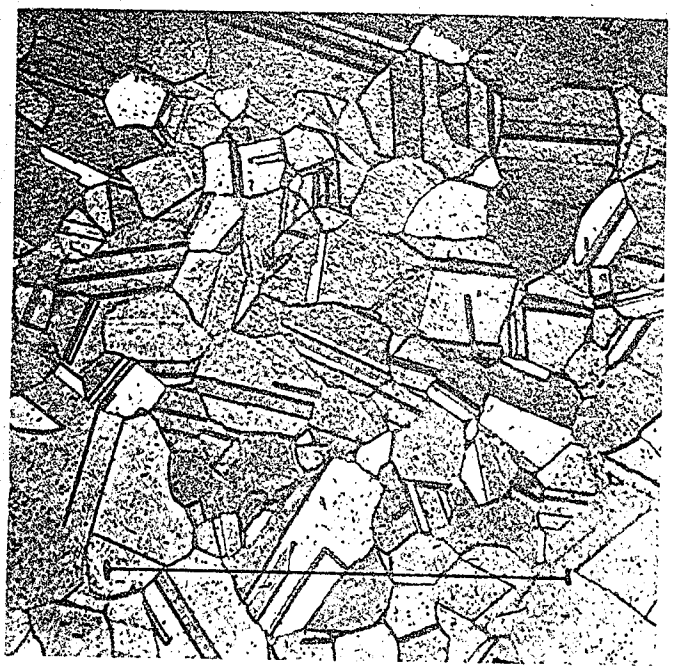

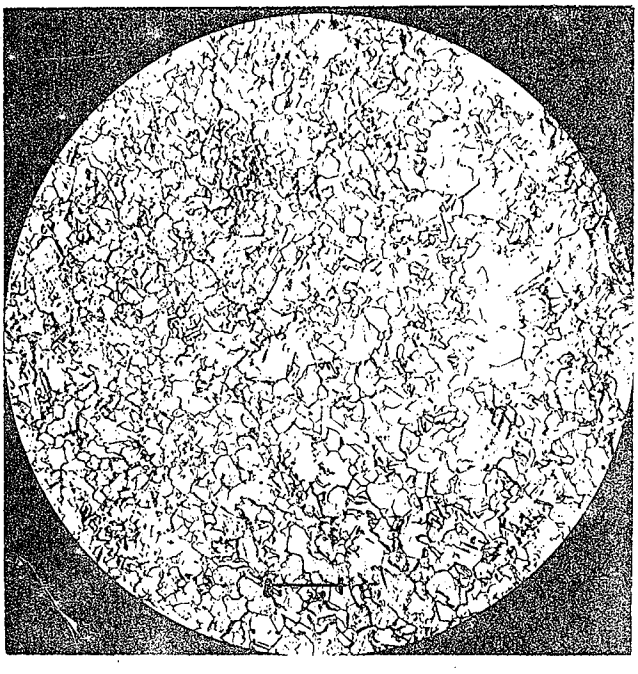

(c)

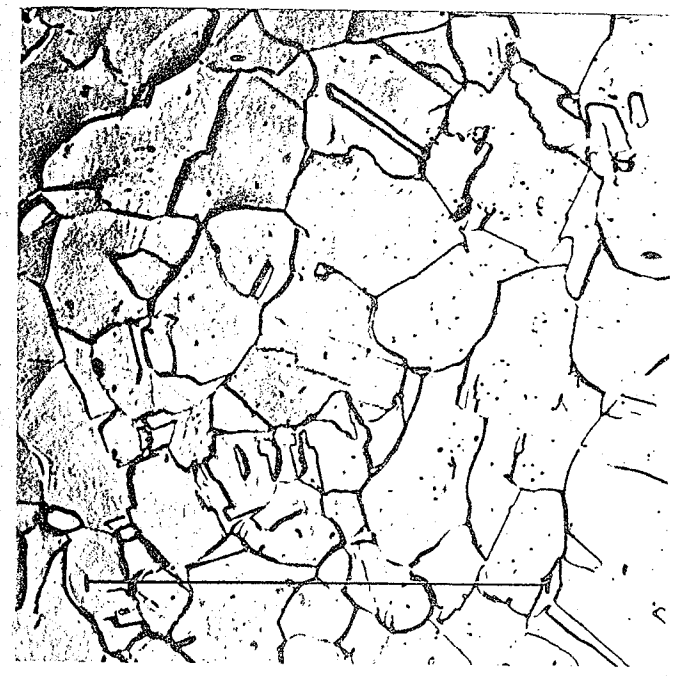

Figure 51. Microstructures of Al (etchant of 10% HF-45% HCl-45% H_2O). (a) and (b)-(d) are from different specimens. Markers = 100 microns.

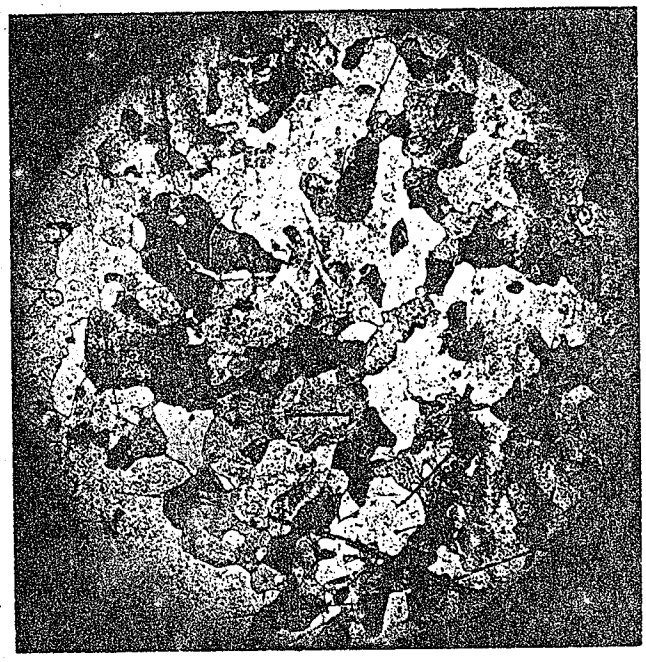

(a)

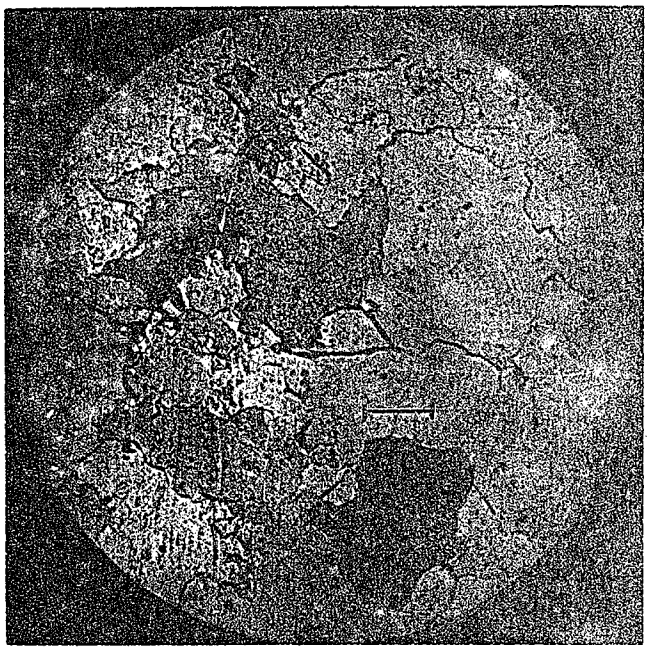

(b)

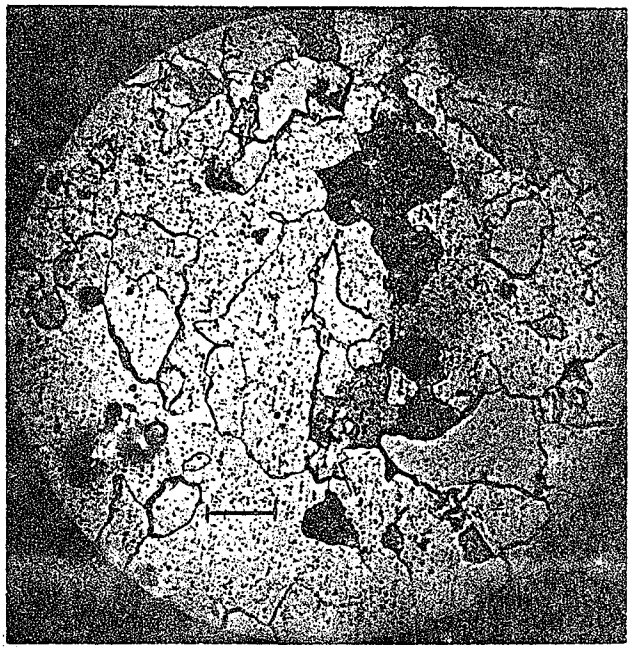

(c)

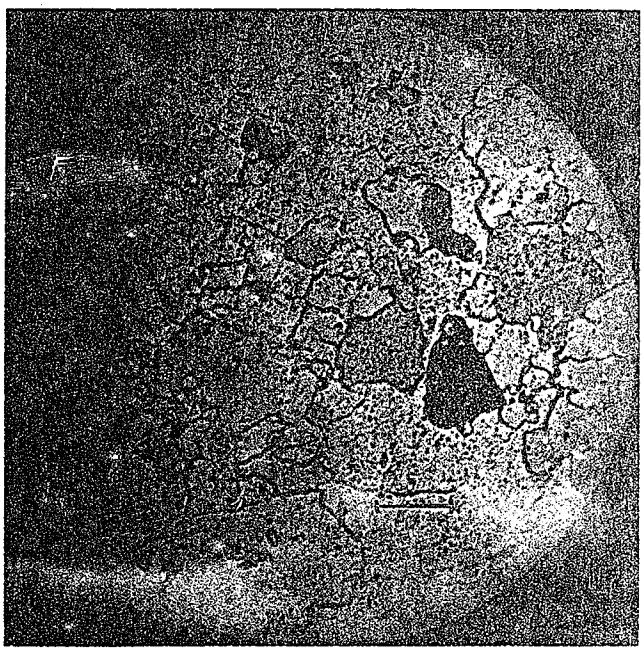

(d)

TABLE 10

TENSILE DATA

- bracketed numbers indicate number of tests used for average value
- EXT indicates extensometer used
- RT = room temperature

Copper

$\bar{\sigma}_{my} = 1.3$ kg/mm^2(22) $\bar{E} = 12.0 \times 10^3$ kg/mm^2(20)
$\bar{\sigma}_{0.2} = 5.6$ kg/mm^2(4)
$\bar{\sigma}_{0.2}$(EXT) $= 4.7$ kg/mm^2(1)

- breakdown with respect to full scale strain of $\bar{\sigma}_{my}$ (measure of recording sensitivity)

@ full scale $= 5 \times 10^{-4}$, $\bar{\sigma}_{my} = 1.4$ kg/mm^2(6)
@ full scale $= 1 \times 10^{-3}$, $\bar{\sigma}_{my} = 1.2$ kg/mm^2(10)
@ full scale $= 2.5 \times 10^{-3}$, $\bar{\sigma}_{my} = 1.1$ kg/mm^2(2)
@ full scale $= 5 \times 10^{-3}$, $\bar{\sigma}_{my} = 1.1$ kg/mm^2(1)
@ full scale $= 1 \times 10^{-2}$, $\bar{\sigma}_{my} = 2.0$ kg/mm^2(3)
@ full scale $= 2 \times 10^{-2}$, $\bar{\sigma}_{my}$(EXT) $= 2.35$ kg/mm^2(1)

Cu-1Sn

$\bar{\sigma}_{my} = 2.9$ kg/mm^2(2)
$\bar{\sigma}_{0.2}$(EXT) $= 10.5$ kg/mm^2(1)
$\bar{E} < 21.4 \times 10^3$ kg/mm^2(4) - from unloading line because E_{load} values were either greater than E_{unload} or could not be measured.

Nickel

$\bar{\sigma}_{my} = 1.05$ kg/mm^2(4) $\bar{E} = 26.4 \times 10^3$ kg/mm^2(1)
$\bar{\sigma}_{0.2}$(EXT) $= 6.2$ kg/mm^2(1)

Aluminum

$\bar{\sigma}_{my}$ (RT) $= 1.1$ kg/mm^2(3) $\bar{E} = 9.0 \times 10^3$ kg/mm^2(3,RT)
$\bar{\sigma}_{my}$ (230°K) $= 0.6$ kg/mm^2(4,EXT) $\bar{E} = 6.5 \times 10^3$ kg/mm^2
$\bar{\sigma}_{0.2}$(230°K) $= 1.2$ kg/mm^2(1,EXT) (2,EXT,230°K)

Figure 52. Stress - strain curves of a low plastic strain, obtained from specimens with a strain gauge attached.

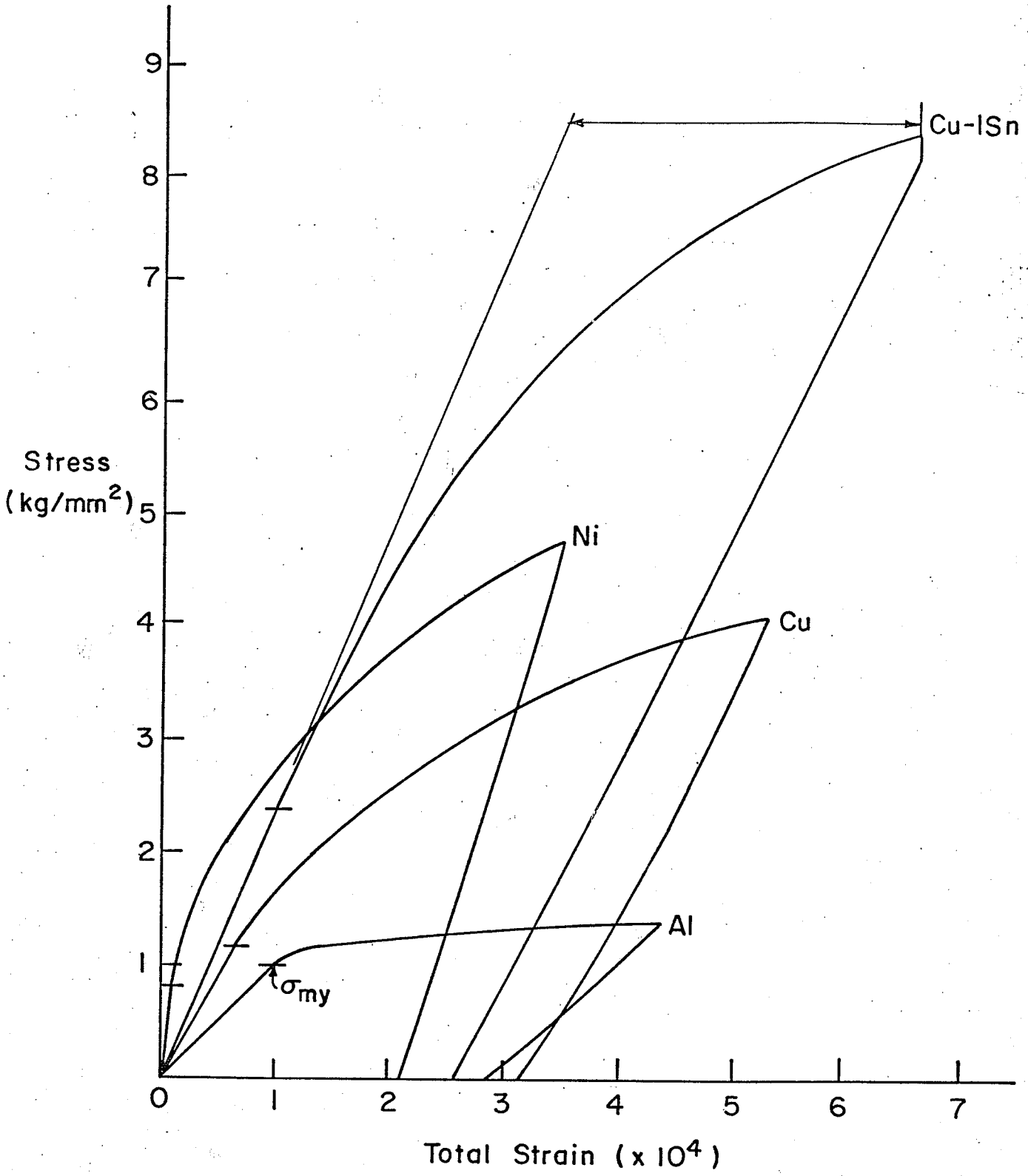
Stress
(kg/mm²)
9
8
7
6
5
4
3
2
1
0
1
2
3
4
5
6
7
Total Strain (x 10⁴)
Cu-ISn
Ni
Cu
Al
σmy

Figure 53. Stress - strain curves of a high plastic strain, obtained from specimens with an extensometer attached.

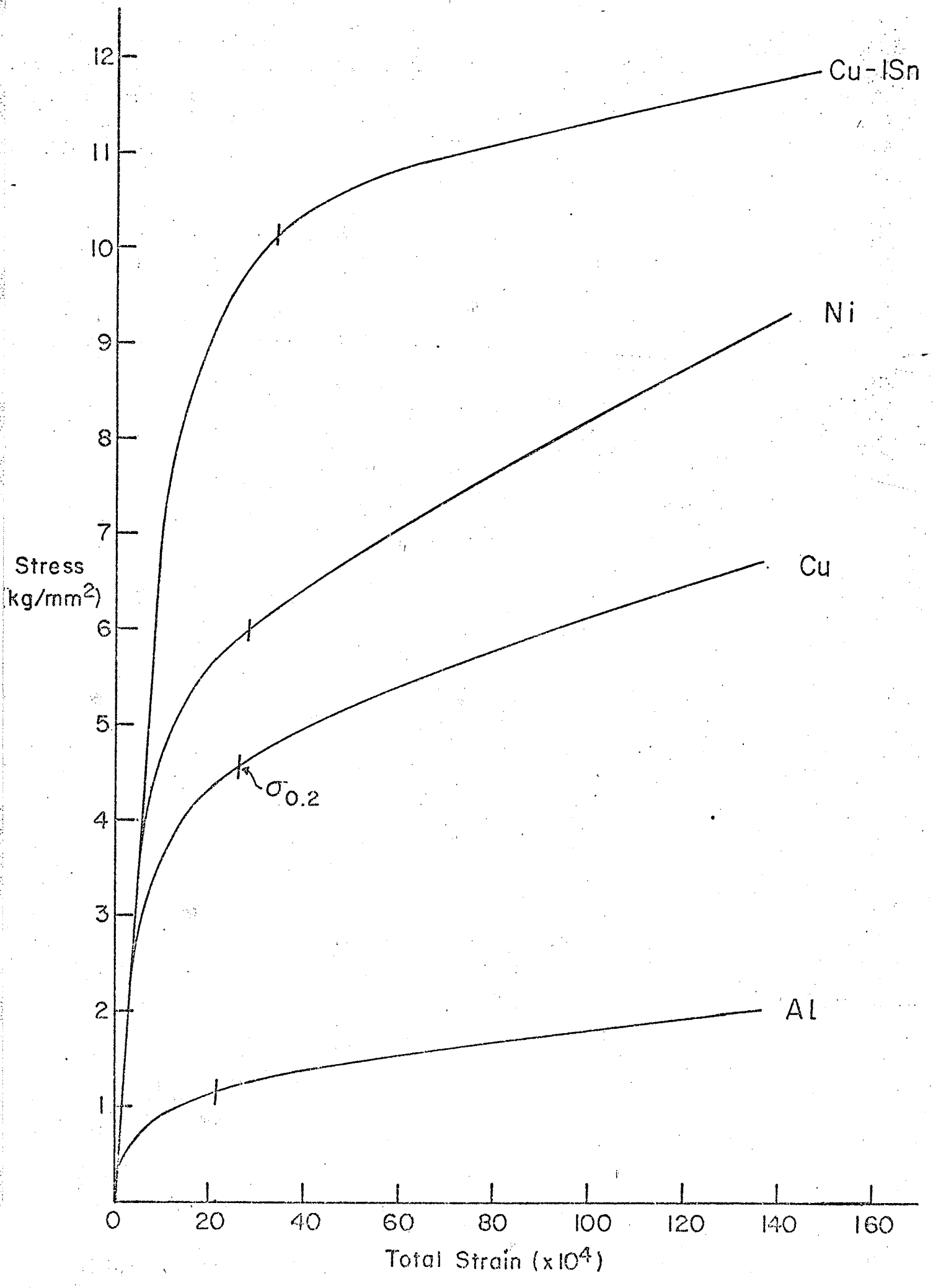
12
11
10
9
8
7
6
5
4
3
2
1
Stress
(kg/mm²)
Cu-ISn
Ni
Cu
Al
σ0.2
0
20
40
60
80
100
120
140
160
Total Strain (x10⁴)

compared to the Cu, is rather surprising in view of the consistently higher flow stresses in Ni at higher strains. This is seen in the typical stress-strain curves for both low and high strain regimes, shown in figures 52 and 53, respectively. It should be noted that the majority of modulus values calculated from the unloading curve were significantly greater than those from the loading curve. Therefore, the occasional cases where the reverse occurred were not used for the calculations. Also, E and σ_{my} values were calculated only if there was a reasonable linear portion.

5.3 ELECTRON MICROSCOPY

Before presenting the results for each material, some general comments are appropriate with regard to micrographs, dislocation generation and general boundary defect densities. All micrographs in these maps are at the same orientation with respect to the maps (allowing, of course, for the slight rotational differences between different magnifications). All distance markers are 1 micron unless otherwise indicated and arrows are used to represent the deduced direction of the dislocation generation where deemed necessary. (These latter two considerations apply to all micrographs in the thesis).

It appeared that not every case of foil handling or spurious deformation could be distinguished by any amount of examination according to the criteria listed previously. This was demonstrated by the observation, in every annealed material, of at least one case of what resembled bulk deformation activity. Examples for Cu and Al are seen in figure 54, others are noted in the micro-maps. With regard to spurious deformation, all microscope examination was conducted with a liquid nitrogen-cooled device around the specimen to prevent any structural degeneration due to specimen contamination.

One very notable phenomenon was the generation of dislocations from both coherent and incoherent segments of twin boundaries. The generation was of both perfect and partial dislocations (figure 55 and Map 1), with the latter occurring almost exclusively from along the coherent boundaries (Map 1). The puzzling aspect of such generation was that it gave no strong indication of being dependent on specimen strain, whereas the grain boundary dislocation generation did.

It occurred in annealed as well as deformed material and showed no regular increase with increasing strain. This is illustrated in Table 11 (a compilation of the defect densities from the various micro-maps) by

Figure 54. Examples of dislocation emission from grain boundaries in annealed material.

(a) Cu

(b) Al (although this configuration was near an extensive Deformed Zone).

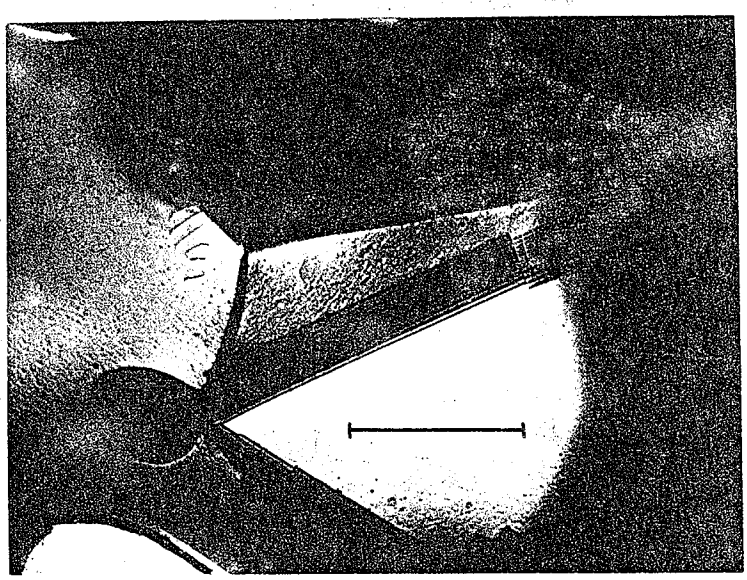

(a)

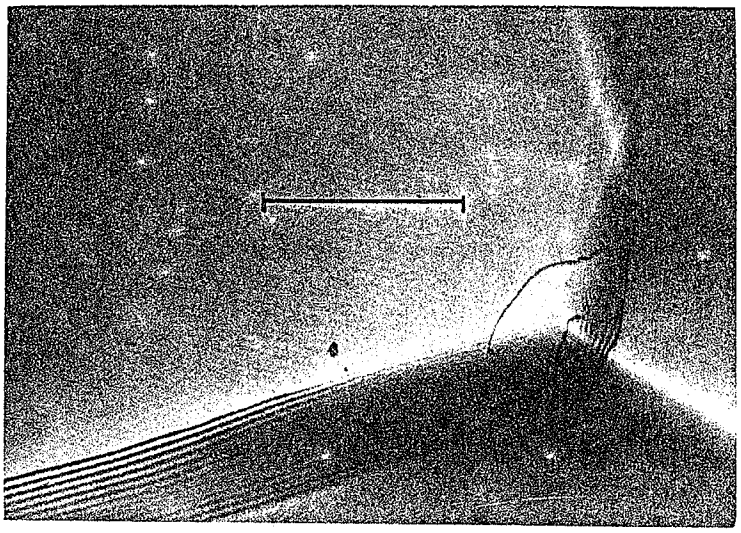

(b)

Figure 55. Emission of (a) $\frac{a}{2}$<110> perfect, and (b) $\frac{a}{6}$<112> partial dislocations from incoherent annealing twin boundaries;

(a) annealed Cu

(b) Cu, plastic strain of 5×10^{-4}.

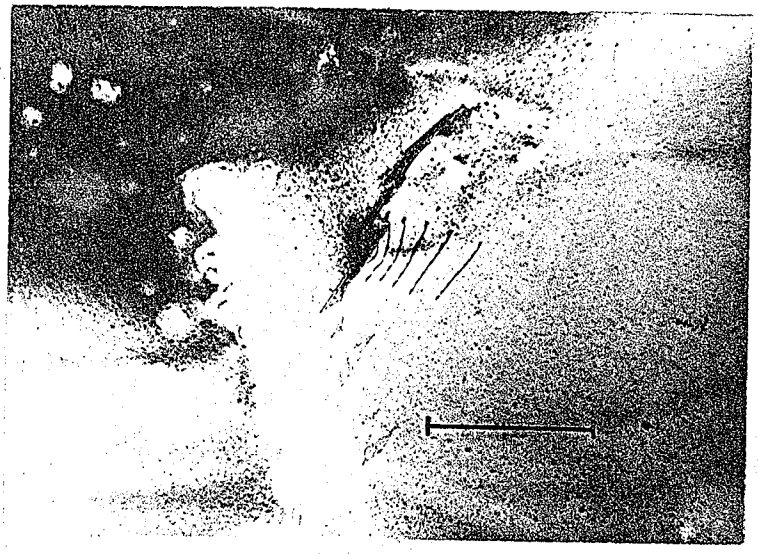

(a)

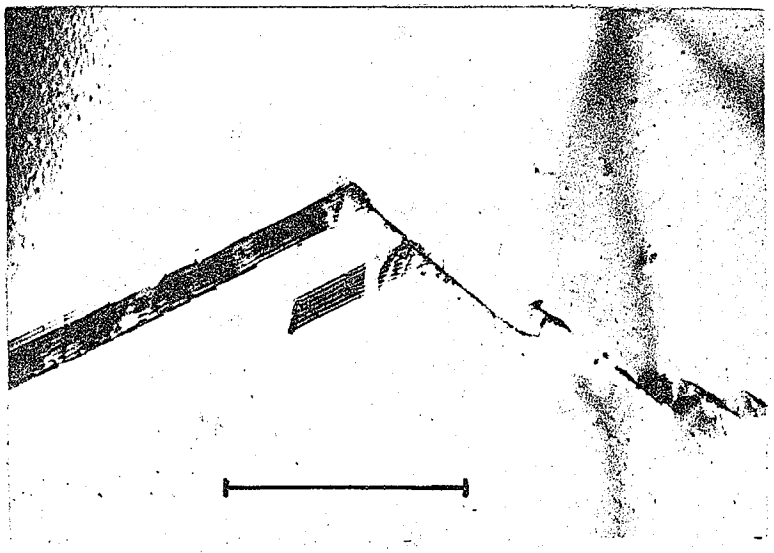

(b)

TABLE 11

MICRO-MAP DEFECT DENSITIES

- all densities x $10^{-4}/cm^2$

(?)-indicates some doubt as to strain value due to poorly-defined stress-strain curve

NM - not measured for this foil

H - hybrid technique of foil preparation used

* - recorded over less than total map area

** - number of activated grains/(number of whole grains plus one-half of partial grains)

ann.=annealed, WQ=water quenched, ε_p=plastic strain

MATERIAL/ MAP NO.	STATE	MAP AREA (μm^2)	BOUNDARY LENGTH(μm)	ACTIVATED GRAINS**	GB	F	P	TP	IA	TBF	TBP
Cu(Map 1)	ann.	3787	NM	NM	7.9	0	0	0	0	13.2	0
	ann.	3818	NM	NM	2.6	0	0	0	0	23.6	2.6
	ann.	4969	NM	NM	0	0	0	0	0	6.0	6.0
total or avg.		12574			3.2	0	0	0	0	13.5	3.2
	WQ	13090	NM	NM	9.9	0	0	0	0	3.8	2.3
	WQ	10270	880	0	19.5	0	0	0	0	2.9	0
total or avg.		23360	880	0	14.1	0	0	0	0	3.0	1.3
	$\varepsilon_p=1\times10^{-4}$	10393	NM	NM	7.7	0	0	0	0	1.0	0
	" "	10483	NM	NM	5.7	0	1.9	0	0	5.7	0
(Map 2)	" "	8666	NM	NM	12.7	0	3.5	0	0	4.6	2.3
total or avg.		29542			8.5	0	1.7	0	0	3.7	0.7
	$\varepsilon_p=3\times10^{-4}$	4272	NM	NM	32.8	2.3	11.7	9.2	2.3	0	9.4
(Map 3)	" "	7545	NM	NM	25.2	1.3	2.6	1.3	1.3	2.6	7.8
	" "	6333	NM	NM	NM	3.2	1.6	1.6	1.6	NM	NM
total or avg.		18150			27.9	2.2	4.4	3.9	3.3	1.7	8.5
(Map 4)	$\varepsilon_p=5\times10^{-4}$ (?)	10908	NM *	NM	22.9*	3.7	5.5	NM	2.8	10.1	7.3
	" "	10554	375*	1/14	50.6	2.8	5.7	2.8	0	NM	NM
	" "	14119	412	2/8	NM	4.2	1.4	1.4	2.1	NM	NM
	" "	9817	NM	NM	NM	1.0	6.0	2.0	3.1	NM	NM
total or avg.		44600	787	3/22	31.5	3.1	4.9	2.1	2.0	10.1	7.3
	$\varepsilon_p=7\times10^{-4}$ (?)	13574	NM	NM	39.0	0	8.8	NM	5.2	0	6.6
(Map 5,H)	" "	14180	737	9/19	NM	0	6.3	0.7	4.9	NM	NM
total or avg.		27754	737	9/19	39.0	0	7.6	0.7	5.0	0	6.6
(Map 6,H)	$\varepsilon_p=1\times10^{-3}$	5272	270	5/7	NM	3.8	NM	NM	11.4	0	0
(Map 7,H)	"$=5\times10^{-3}$	7726	610	20/24	NM	0	NM	NM	NM	NM	NM

TABLE 11 (continued)

MATERIAL/ MAP NO.	STATE	MAP AREA (μm^2)	BOUNDARY LENGTH (μm)	ACTIVATED GRAINS	GB	F	P	TP	IA	TBF	TBP
Cu-1Sn											
(Map 8,H)	ann.	8090	NM	NM	3.7	0	1.3	0	2.6	2.6	0
(Map 9,H)	$\varepsilon_p = 3 \times 10^{-4}$	7575	500	6/23	6.6	2.6	3.9	2.6	10.6	NM	NM
(Map 10,H)	" $= 7 \times 10^{-4}$	6060	NM	NM	52.0*	0	54.5	5.0	9.9	NM	NM
Ni											
(Map 11,H)	ann.	6363	NM	NM	48.8	0	0	0	0	0	0
(Map 12,H)	$\varepsilon_p = 3 \times 10^{-4}$	3212	NM	NM	NM	0	18.7	3.1	6.2	0	6.2
	" "	2242	165	3/7	NM	0	17.9	17.9	9.3	0	0
total or avg.		5454	165	3/7		0	18.4	7.3	7.3	0	3.7
Al											
(Map 13,H)	ann.	13800	390	0	0	0	0.7	0.7	0	0	0
	ann.	10165	340	0	0	0	0	0	0	1.0	1.0
total or avg.		23965	730	0	0	0	0.4	0.4	0	0.4	0.4
(Map 14,H) @230°K	$\varepsilon_p = 4 \times 10^{-4}$ (?)	39800	1496	8/24	1.8	0	1.8	0.3	3.0	0	0
	$\varepsilon_p = 3 \times 10^{-4}$	4540	209	1/4	2.2	0	0	0	2.2	0	0
(Map 15)	" "	6060	341	3/5	0	0	13.2	5.0	6.6	0	0
total or avg.		10600	550	4/9	0.9	0	7.5	2.8	4.7	0	0

comparing TBF and TBP densities for slow- and fast-cooled Cu (the latter included from (195) for this comparison only). Contrary to what might logically be expected in terms of generation due to cooling stresses, the densities are substantially greater in the slow-cooled Cu. Twin boundary generation (both partial and perfect) was observed in all materials (even the Al, where only a very few annealing twins were found). The incidence of partial dislocation generation appeared higher in the Cu and Cu - 1Sn than in the Ni. The generation did seem to show a dependence on the method of foil preparation. For example, for cut foils the densities were: Cu, annealed - $16.7 \times 10^4/cm^2$, $\varepsilon_p = 1 \times 10^{-4}$ - $4.4 \times 10^4/cm^2$, $\varepsilon_p = 3 \times 10^{-4}$ - $10.2 \times 10^4/cm^2$, whereas for hybrid foils they were: annealed Cu - 1 Sn - $2.5 \times 10^4/cm^2$, annealed Al - $0.4 \times 10^4/cm^2$, annealed Ni - zero, Ni, $\varepsilon_p = 3 \times 10^{-4}$ - $3.7 \times 10^4/cm^2$.

There were definitely overall preponderances of certain grain boundary line defects, at least ones that were visible at moderate magnifications. IGBD networks, such as illustrated in figure 56, were rarely observed. Somewhat more often, defects were seen that showed distributions similar to those discussed in sec. 3.3.2 concerning GBD glide (figure 57).

Large pure ledges or large GBD-macroledges were

Figure 56. Apparent IGBD network in annealed Cu-1Sn.

Figure 57. Semi-regular configurations of boundary defects;
(a) Cu, plastic strain of 7×10^{-4}
(b) annealed Al
(c) Ni, plastic strain of 3×10^{-4}.

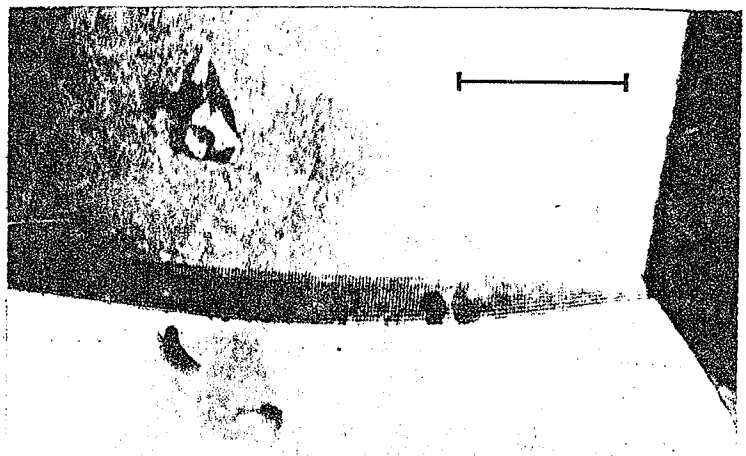

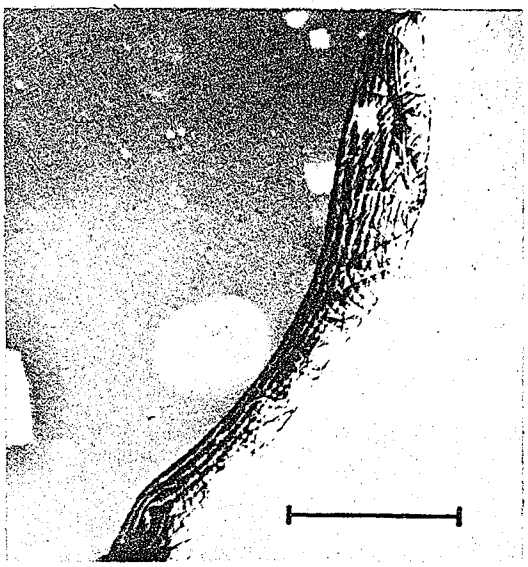

(a)

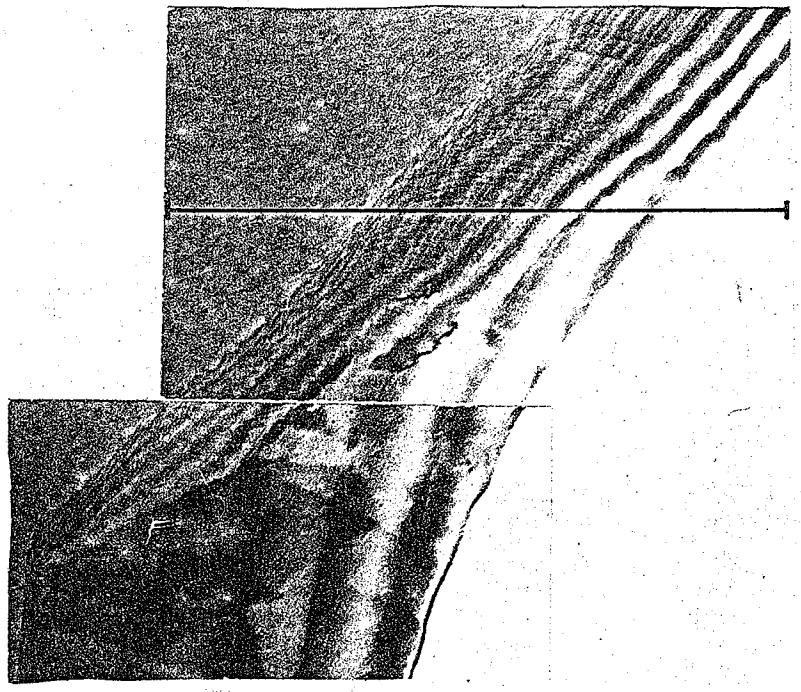

(b)

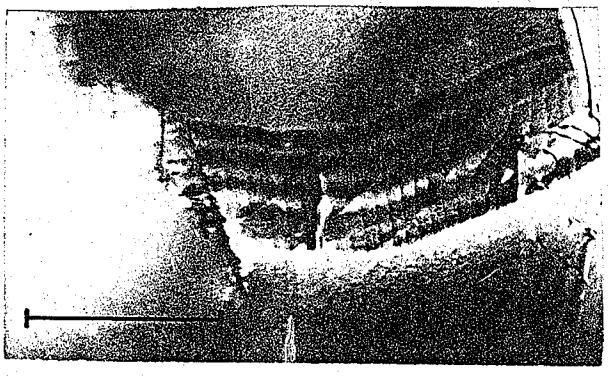

(c)

only infrequently spotted. Randomly-oriented GBD's were quite frequent, particularly at higher strains. By far the most abundant line defects were the straight (or only slightly curvilinear) GBD-macroledges in which only the GBD strain field was visible and the ledge was too small to be directly resolved. These can be seen in most micrographs in this section.

It is important to note that misleading fringes appear in many micrographs in somewhat of a "fingerprint" configuration over a portion or all of the print. These are not from thin foil contrast but from some part of the reproduction process, i.e. either in the electron microscope plate or the printing procedure. Examples are seen in figure 54(b), figure 57(a) (top left), figure 57(b), (upper portion) or figure 57(c) (upper right). These can be particularly misleading where they cross the images of grain boundaries, since they can be mistaken for finely-spaced dislocation networks of weak-contrast.

It should be pointed out that, although some of the densities in Table 11 are based on comparatively small areas, the entire foil was examined in choosing the map areas. Mapped areas were, in almost all cases, representative of the entire foil (excluding Deformed Zones).

5.3.1 COPPER

Micro-Maps 1 - 7 illustrate the yielding behaviour of the pure Cu. The variations in defect density with strain are seen in Table 11. GB's (boundary segments showing defect activity), steadily increased from a fairly low value in the annealed material to the 7×10^{-4} strain, at which point their measurement was discontinued because almost every segment possessed some defects. In addition, it was noted that, on the whole, this was accompanied by an increase in the number of defects in a given segment, e.g. GB_1 of Map 1 vs the P_7 - boundary of Map 5. At $\varepsilon_p = 1 \times 10^{-4}$ (Map 2) signs of microyielding (aside from the GB increase) were few, consisting of only the occasional, isolated boundary generation (total of $1.7 \times 10^4/cm^2$). At $\varepsilon_p = 3 \times 10^{-4}$ (Map 3), this generation was much more widespread ($6.6 \times 10^4/cm^2$) and a significant amount (roughly 30%) was of partial dislocations. Some signs of interior dislocation activity also appeared. Map 3 also illustrates a moderate tendancy for both GB-segments and boundary sources to occur in the same general region. At 5×10^{-4} (Map 4) the boundary generation had increased (total of $8.0 \times 10^4/cm^2$), but not as drastically as in the previous strain increment. Partial dislocation generation was still a significant factor (37%) and

Micro-Map 1. Annealed Cu (cut foil).

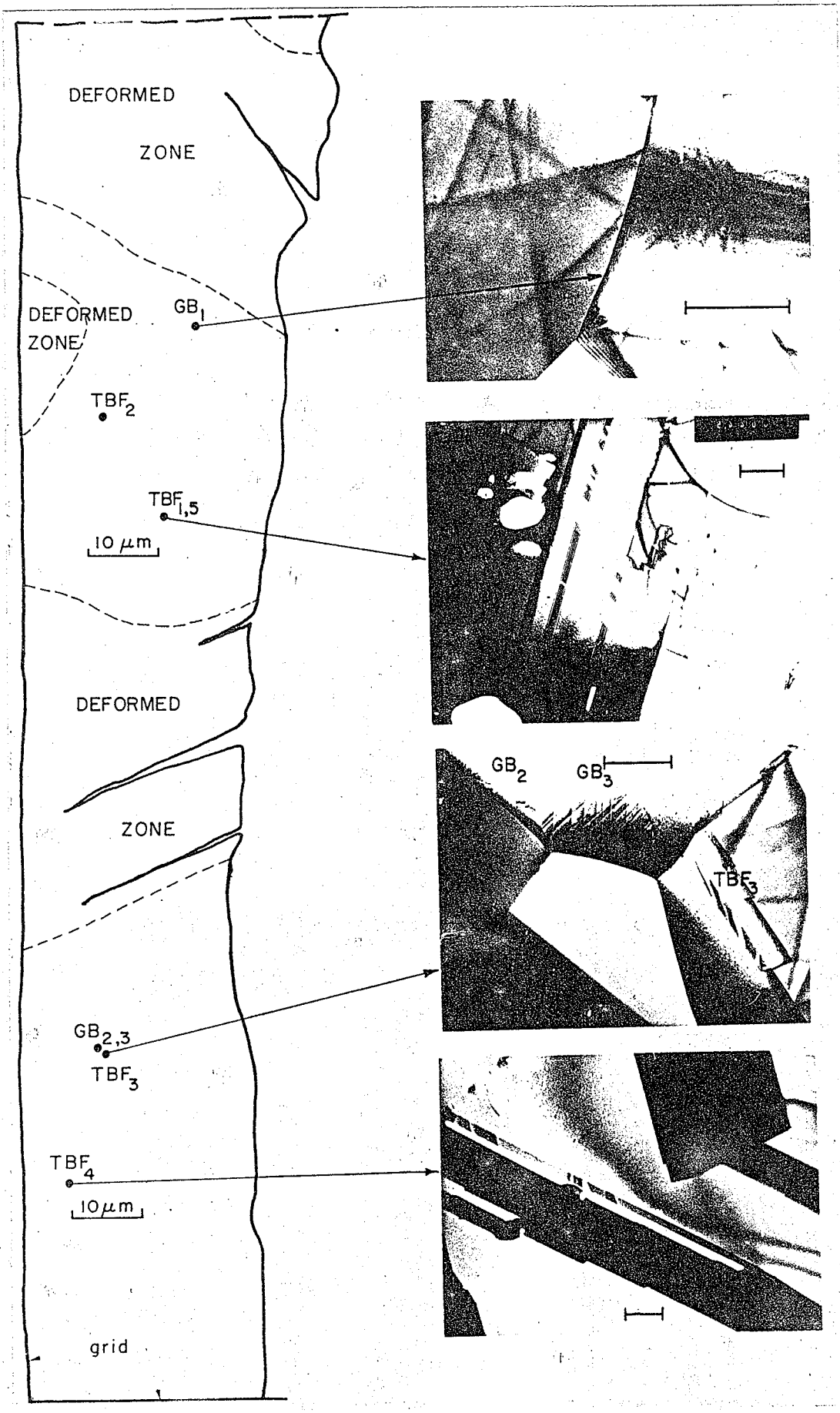
DEFORMED
ZONE
DEFORMED
ZONE
GB1
TBF2
TBF1,5
10 μm
DEFORMED
ZONE
GB2,3
TBF3
TBF4
10μm
grid
GB2
GB3
TBF3

Micro-Map 2. Cu, plastic strain of 1×10^{-4} (cut foil). The P_4(?) defect was judged to be a remnant of the recrystallization process. The P_2 activity was (as shown) only a single dislocation bowing out of the boundary.

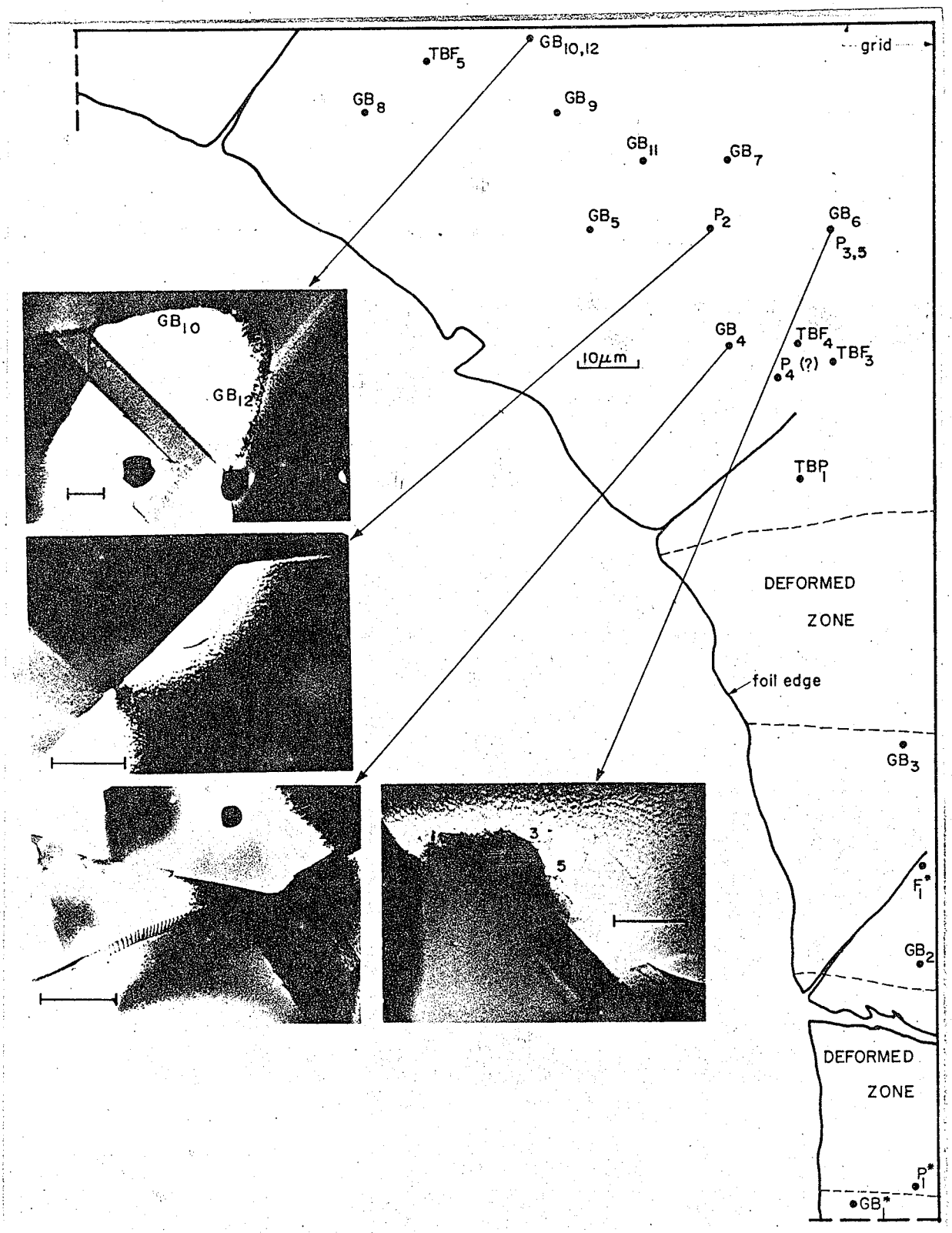
grid
TBF5
GB10,12
GB8
GB9
GB11
GB7
GB5
P2
GB6
P3,5
GB10
GB12
10μm
GB4
TBF4
TBF3
P4 (?)
TBP1
DEFORMED
ZONE
foil edge
GB3
1
3
5
F1*
GB2
DEFORMED
ZONE
P1*
GB1*

Micro-Map 3. Cu, plastic strain of 3×10^{-4} (cut foil). The P_1-defect occurred in one of the smaller grains observed.

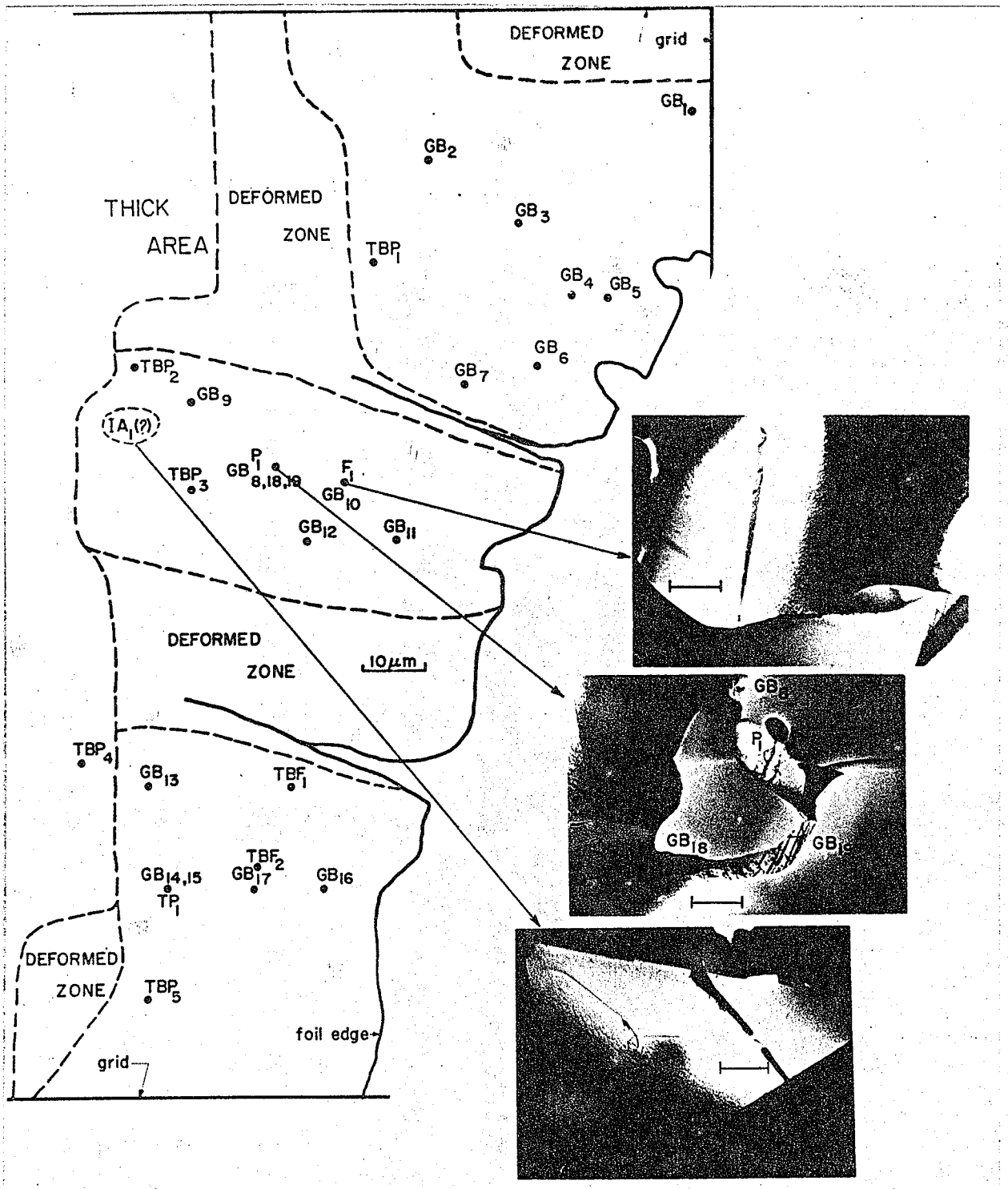
DEFORMED ZONE
grid
GB1
GB2
GB3
THICK AREA
DEFORMED ZONE
TBP1
GB4
GB5
GB6
GB7
TBP2
GB9
IA1(?)
P1
GB8,18,19
F1
TBP3
GB10
GB12
GB11
DEFORMED ZONE
10μm
TBP4
GB13
TBF1
TBF2
GB14,15
GB17
GB16
TP1
DEFORMED ZONE
TBP5
foil edge
grid
GB8
P1
GB18
GB19

Micro-Map 4. Cu, plastic strain of 5×10^{-4} (cut foil). P_7 is one of the few apparent generations observed from large ledges (at A). Note the F_{1-3} -defects occurring on two slip planes. Only a portion of F_5 is shown since it was of a substantial length.

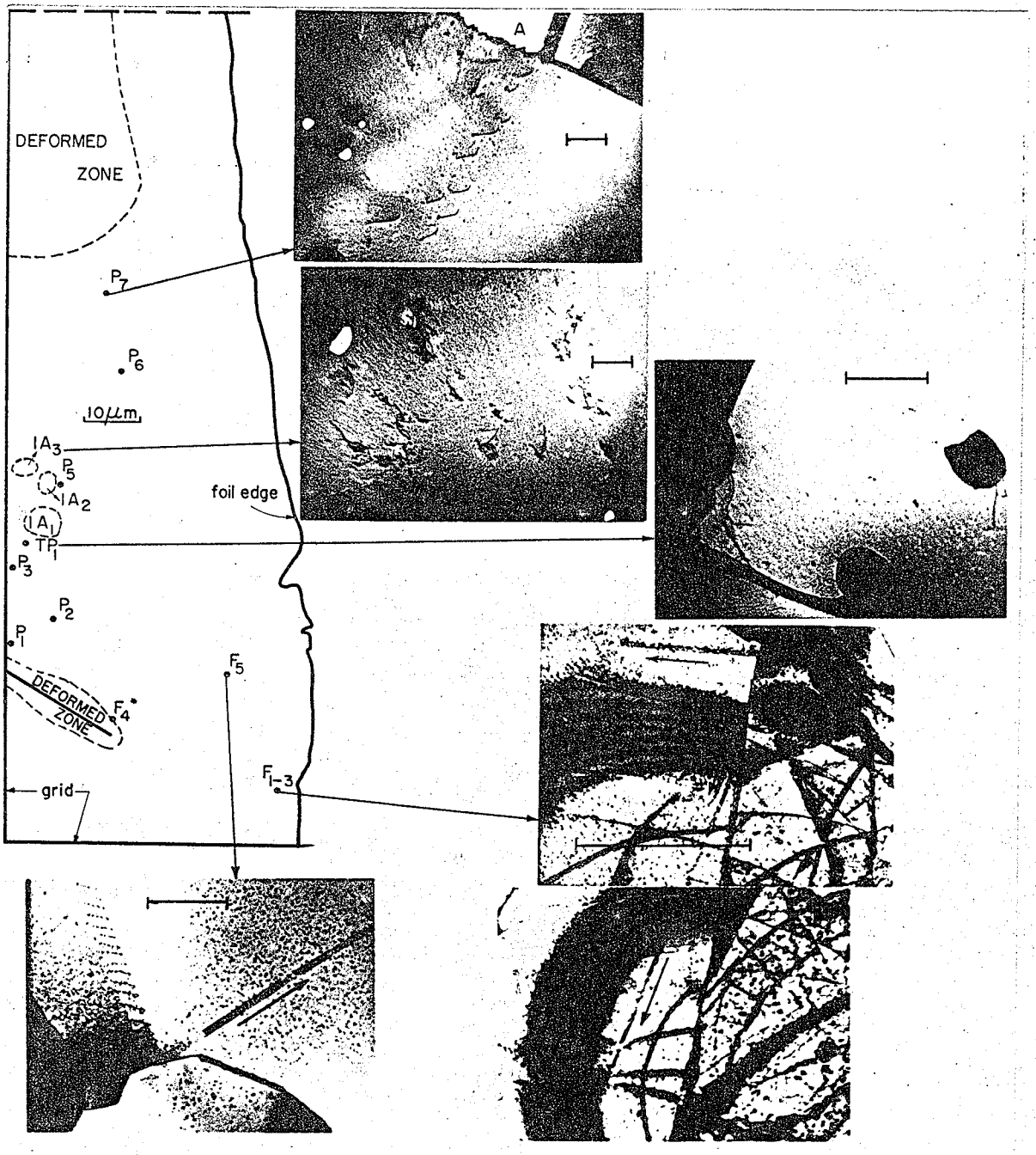
DEFORMED
ZONE
A
P7
P6
10μm
IA3
P5
IA2
foil edge
(A1)
TP1
P3
P2
P1
F5
DEFORMED
ZONE
F4
grid
F1-3

interior activity, though nominally decreased, was of a more intense nature, e.g. IA_3 of Map 4. By $\varepsilon_p = 7 \times 10^{-4}$ (Map 5) total boundary generation had decreased somewhat due to the complete lack of observed partial dislocation generation. Interior activity was greatly increased and showed definite signs of occurring within the same region, as did the P-defects (though not necessarily together). It is noted that this was a hybrid foil and the decrease in Deformed Zones from those of Maps 1 - 4 was dramatic. The boundaries themselves were recorded for this map and the anisotropy in grain size and shape is obvious. Application of the planimetric technique to such maps produced an average grain diameter identical to that obtained optically. Map 6 demonstrates that interior activity was quite widespread by the 1×10^{-3} strain although the dislocation distribution within the IA's was somewhat diffuse, as seen. The presence of extensive interior activity led to difficulty in distinguishing true P-defects and they were therefore not recorded. Somewhat surprisingly, at least one, and likely two, F-generations were observed. The spread of interior activity is emphasized by Map 7, $\varepsilon_p = 5 \times 10^{-3}$ (into the macroyield region). The accumulation of dislocations was much more intense and the first signs of cell formation were apparent. However, boundary generation was <u>still</u> observed, even of partial

Micro-Map 5. Cu, plastic strain of 7×10^{-4} (hybrid foil).

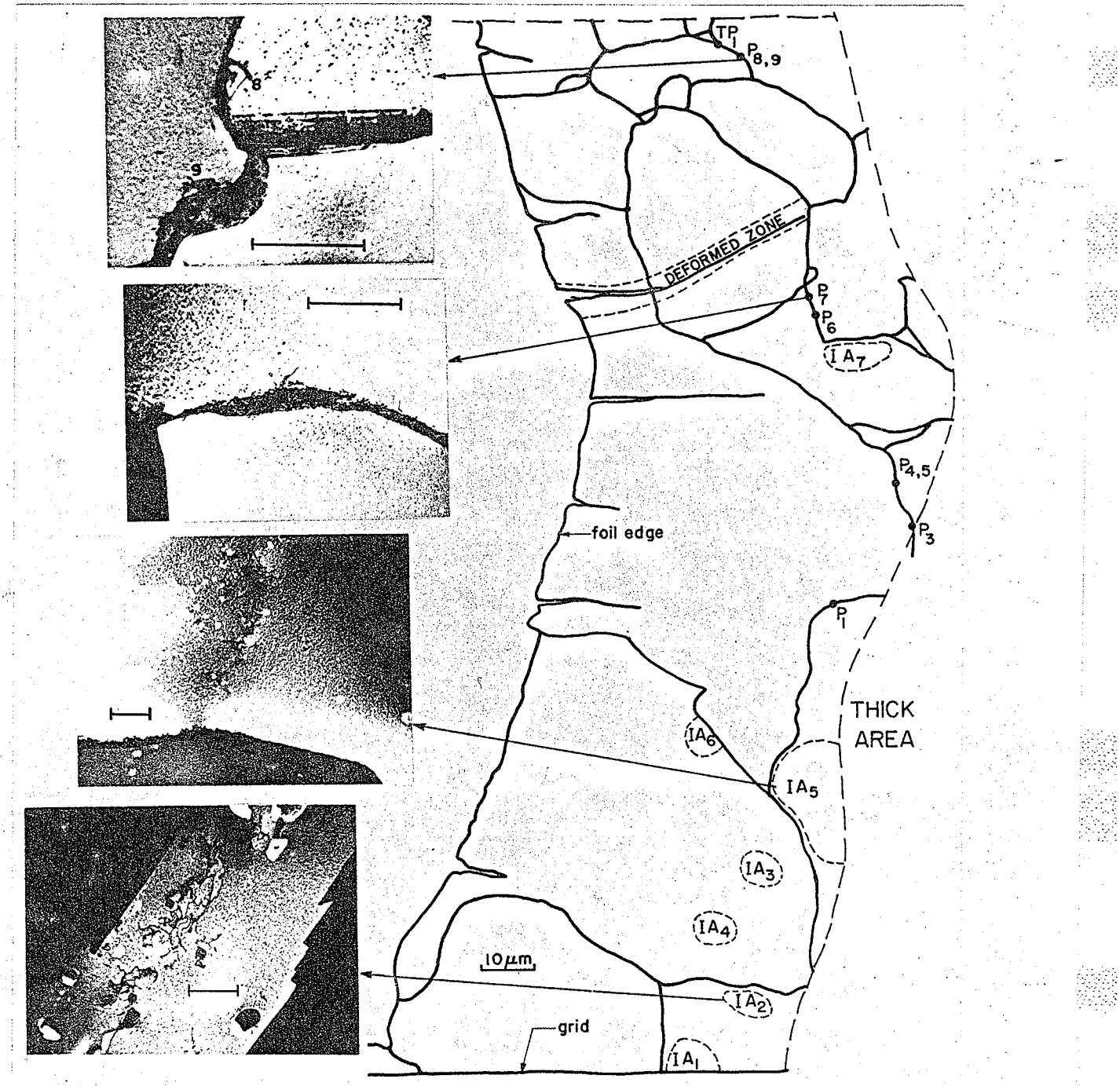
TP1
P8,9
8
9
DEFORMED ZONE
P7
P6
IA7
P4,5
P3
foil edge
P1
THICK
AREA
IA6
IA5
IA3
IA4
10μm
IA2
grid
IA1

Micro-Map 6. Cu, plastic strain of 1×10^{-3} (hybrid foil). F_2(?) is questionable as it emanated from the intersection of three twin boundaries. It was counted as a boundary source, since this was the only case of its kind and thus did not resemble other twin boundary sources.

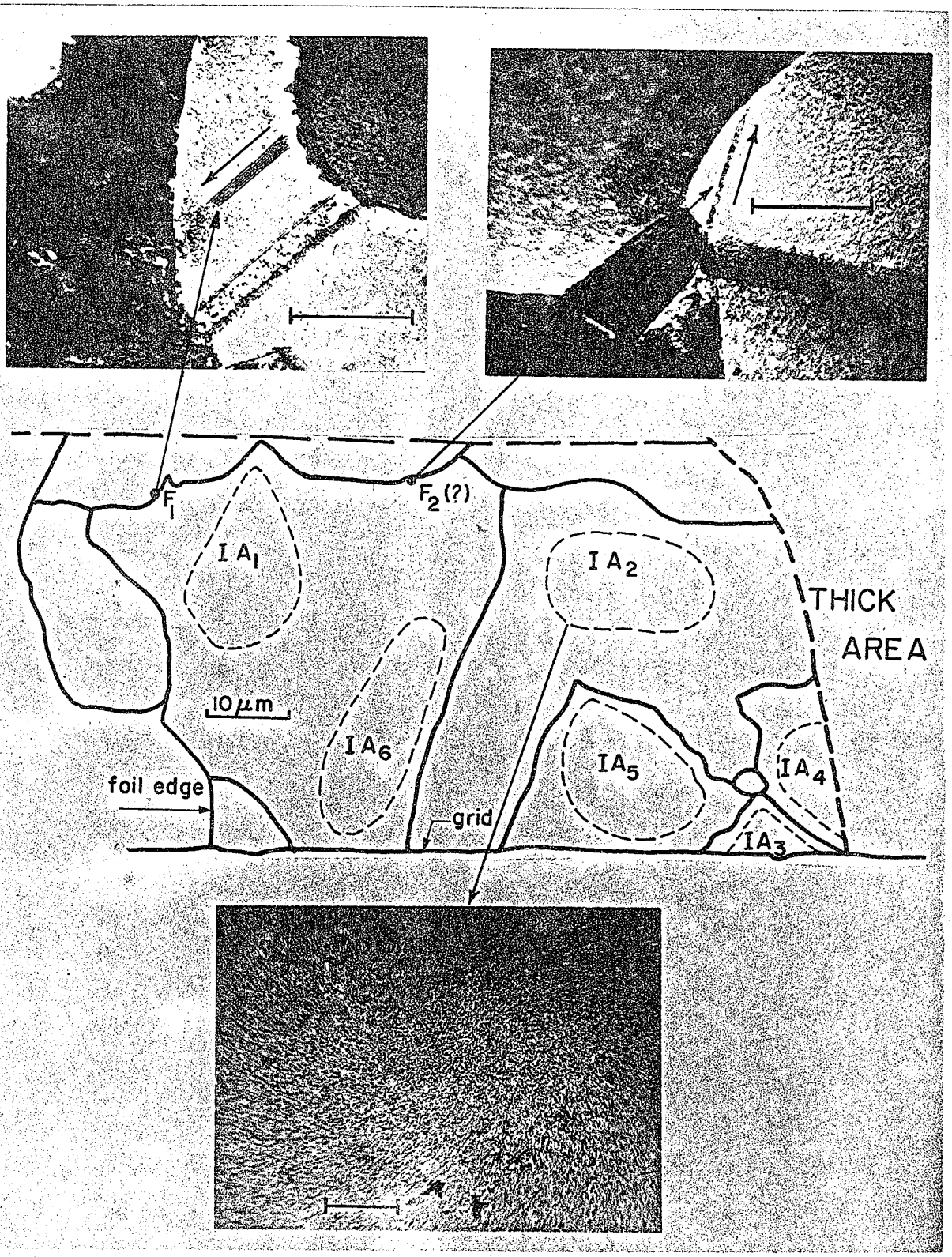
F1
F2 (?)
IA1
IA2
THICK
AREA
10 μm
IA6
IA5
IA4
foil edge
grid
IA3

Micro-Map 7. Cu, plastic strain of 5×10^{-3} (hybrid foil).

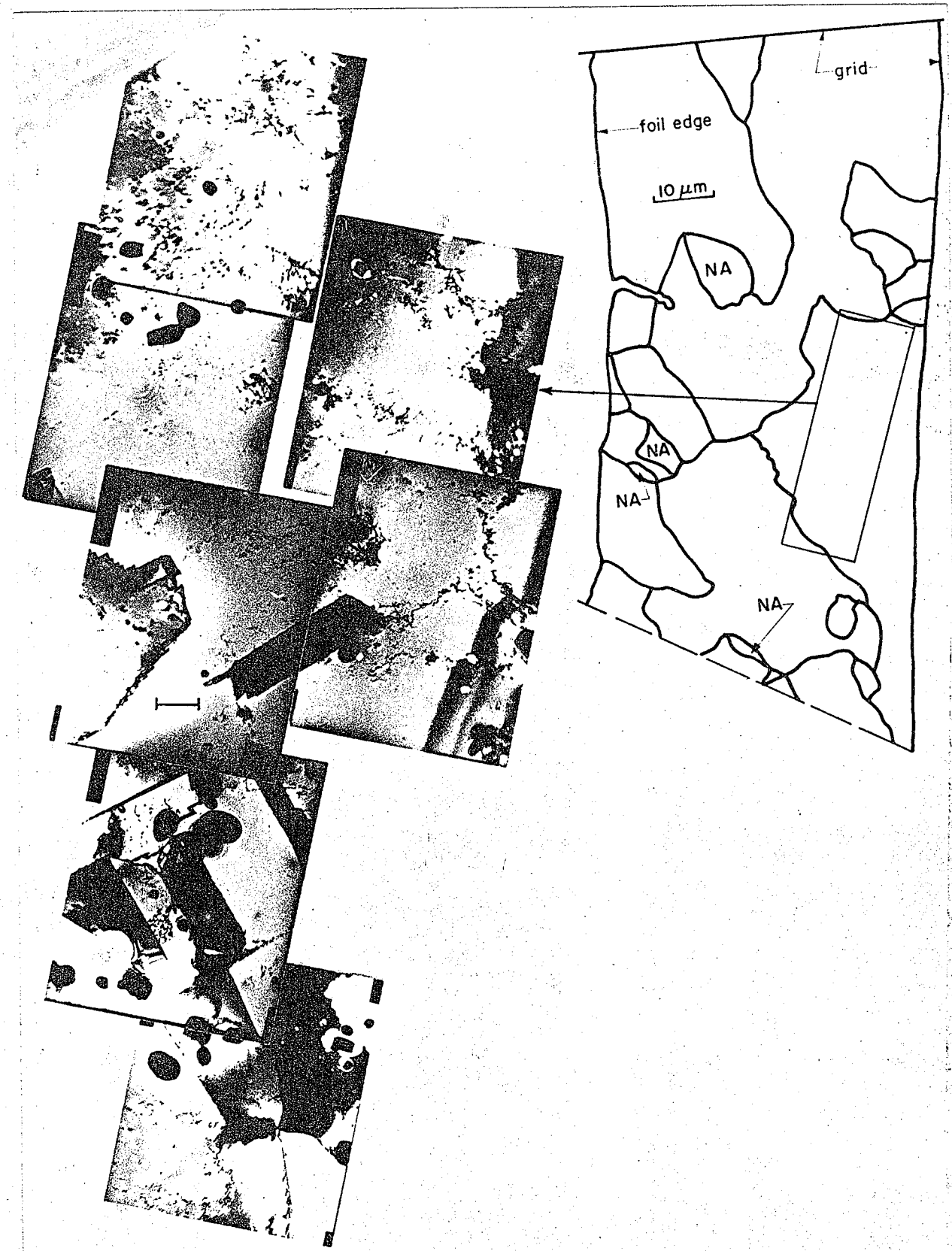
grid
foil edge
10 μm
NA
NA
NA
NA

dislocations (figure 58). The NA designations on this map refer to the few grains which were not active at all. Thus the percentage of yielded grains is very high compared to earlier strains (Table 11).

5.3.2 Cu - 1Sn

The annealed Cu - 1Sn (Map 8) showed a moderate density of GB-segments. The most notable aspect was the presence of the scattered grown-in dislocations (at A and B) mentioned earlier in this section. Even so, they were classified as IA (?) (indicating uncertainty as to their origin) for reasons which will soon become apparent. In addition, at least one P-defect was observed although this was annealed material.

At $\varepsilon_p = 3 \times 10^{-4}$ (Map 9), the GB increase was quite small. Boundary generation was substantial ($6.5 \times 10^4/cm^2$), with 40% being of partial dislocations. The puzzling aspect of this map was the large number of relatively intense IA's. Some areas of comparable activity were present in the annealed material (though none were in Map 8), but not as numerous as here. Large numbers of the dislocations in these areas gave the appearance of being segments of grown-in networks. Thus the difficult question of whether these were caused by bulk specimen

Figure 58. Two partial dislocation sources in Cu, plastic strain of 5×10^{-3}. The direction of emission is deduced mainly from the dislocation spacing and curvature. Note also the TBP emission from a coherent twin boundary.

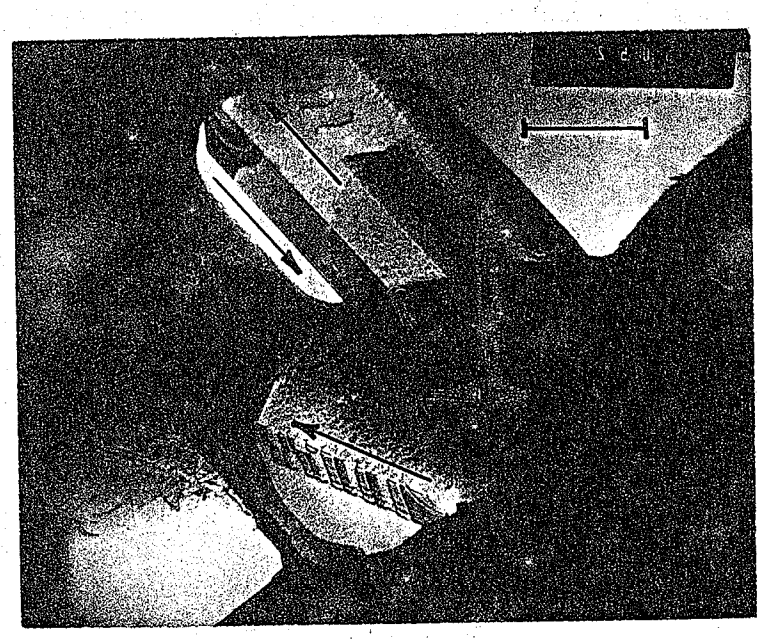

Micro-Map 8. Annealed Cu-1wt%Sn (hybrid foil).
P_1^* was given this designation (indicating a spurious origin) because of the nearby Deformed Zone. Though not visible in these prints, GB_3 showed signs of a faint IGBD network.

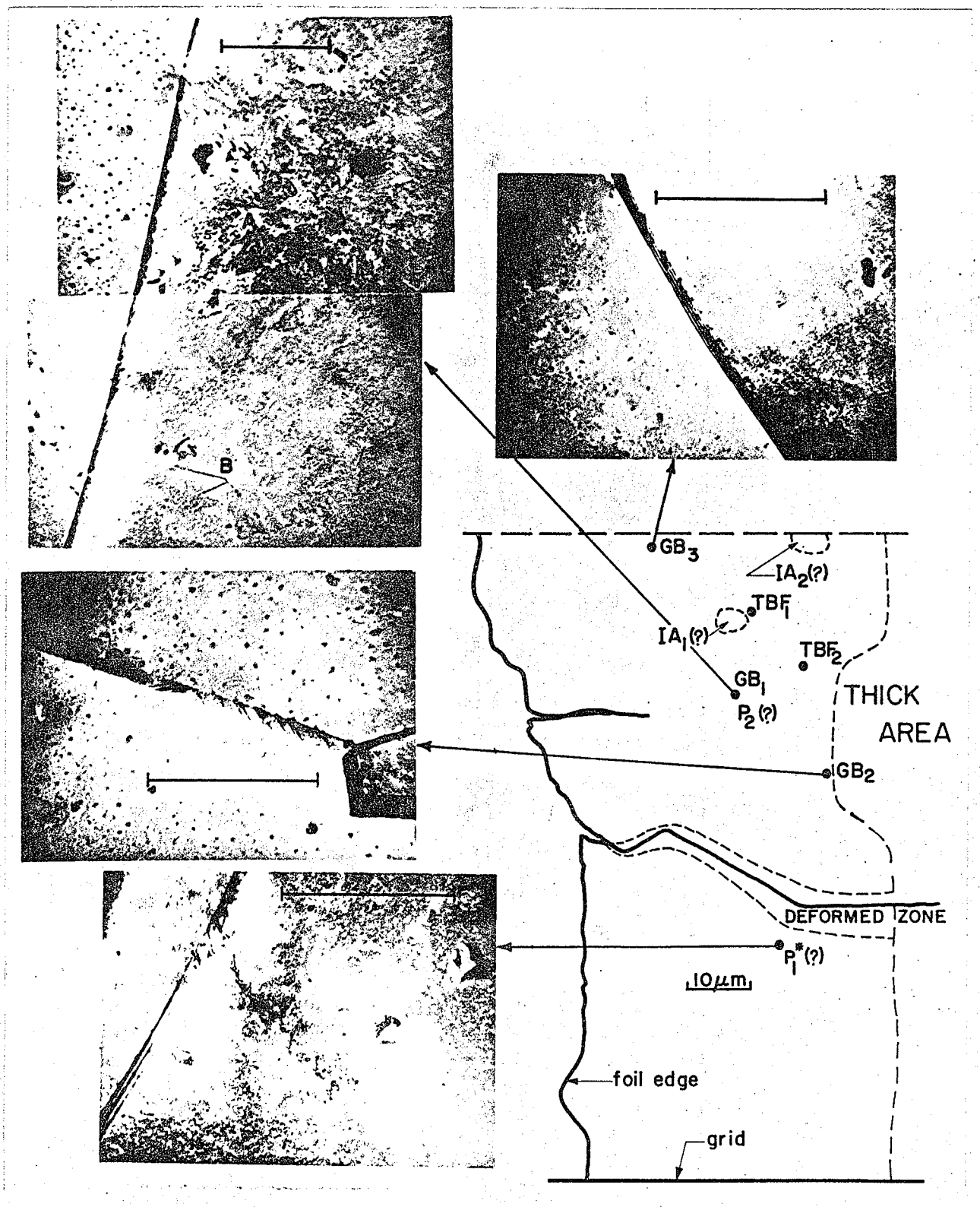
B
GB3
IA2(?)
TBF1
IA1(?)
TBF2
GB1
P2(?)
THICK
AREA
GB2
DEFORMED ZONE
P1*(?)
10μm
foil edge
grid

Micro-Map 9. Cu-1Sn, plastic strain of 3×10^{-4} (hybrid foil). The large arrow indicates the approximate direction of the applied stress. TP(?) could have originated spuriously from the circular depression, but the presence of the GBD-macroledges in the boundary (not clearly visible) led to its classification as a true source. F_1 emanates from a twin - grain boundary intersection and is thus erroneously located on the map. It should be about 0.5 cm to the right. P_2 is a good example of two sources (A and B) that are separated yet have been classified as one to maintain the consistency of classification. The dislocation characters of these sources are 10^{o} from screw.

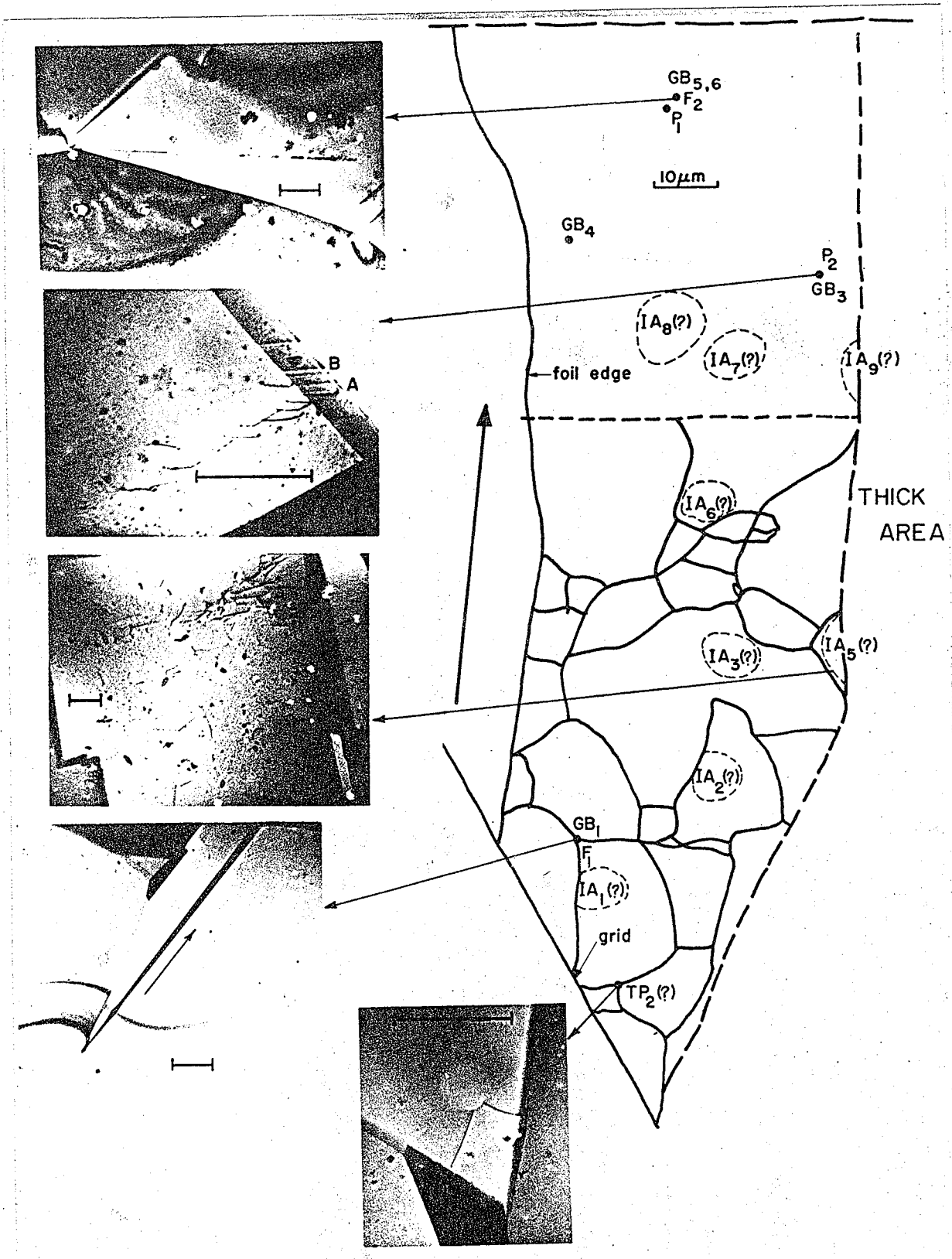
GB5,6
F2
P1
10μm
GB4
P2
GB3
IA8(?)
IA7(?)
IA9(?)
foil edge
B
A
IA6(?)
THICK
AREA
IA3(?)
IA5(?)
IA2(?)
GB1
F1
IA1(?)
grid
TP2(?)

deformation, foil handling, the heat treatment or some combination of any of these.

The 7×10^{-4} strain (Map 10) did little to clarify this matter. IA's were again present in numbers greater than in the annealed material but less than in the 3×10^{-4} material. This strain exhibited two distinct deformation modes. A foil made from near the end of the specimen gauge length showed a uniform distribution of fairly intense dislocation activity, both in grain interiors and grain boundaries (figure 59). A foil made from nearer the center of the specimen showed a much different behaviour (Map 10). There were many GB-segments, but most possessed a relatively moderate defect density. The most striking aspect was the tremendous increase in boundary generation (all of perfect dislocations), many of which were almost classic examples in their retention of a planar array well into the grain. They occasionally were clustered on a very local scale (P_{1-6} and P_{30} were on the same boundary segment) or on a somewhat broader scale (the region of P_{15} to $P_{7,8}$ to P_{17}). Some F-defects were observed outside of the Map 10 area and a few were seen in the region of intense activity mentioned above (figure 60). As seen in figure 61, many perfect dislocation loops were seen to emenate from tne grain boundaries of this

Figure 59. Collage of extensive dislocation activity, both at boundaries and in grain interiors, in Cu-1Sn, plastic strain of 7×10^{-4}.

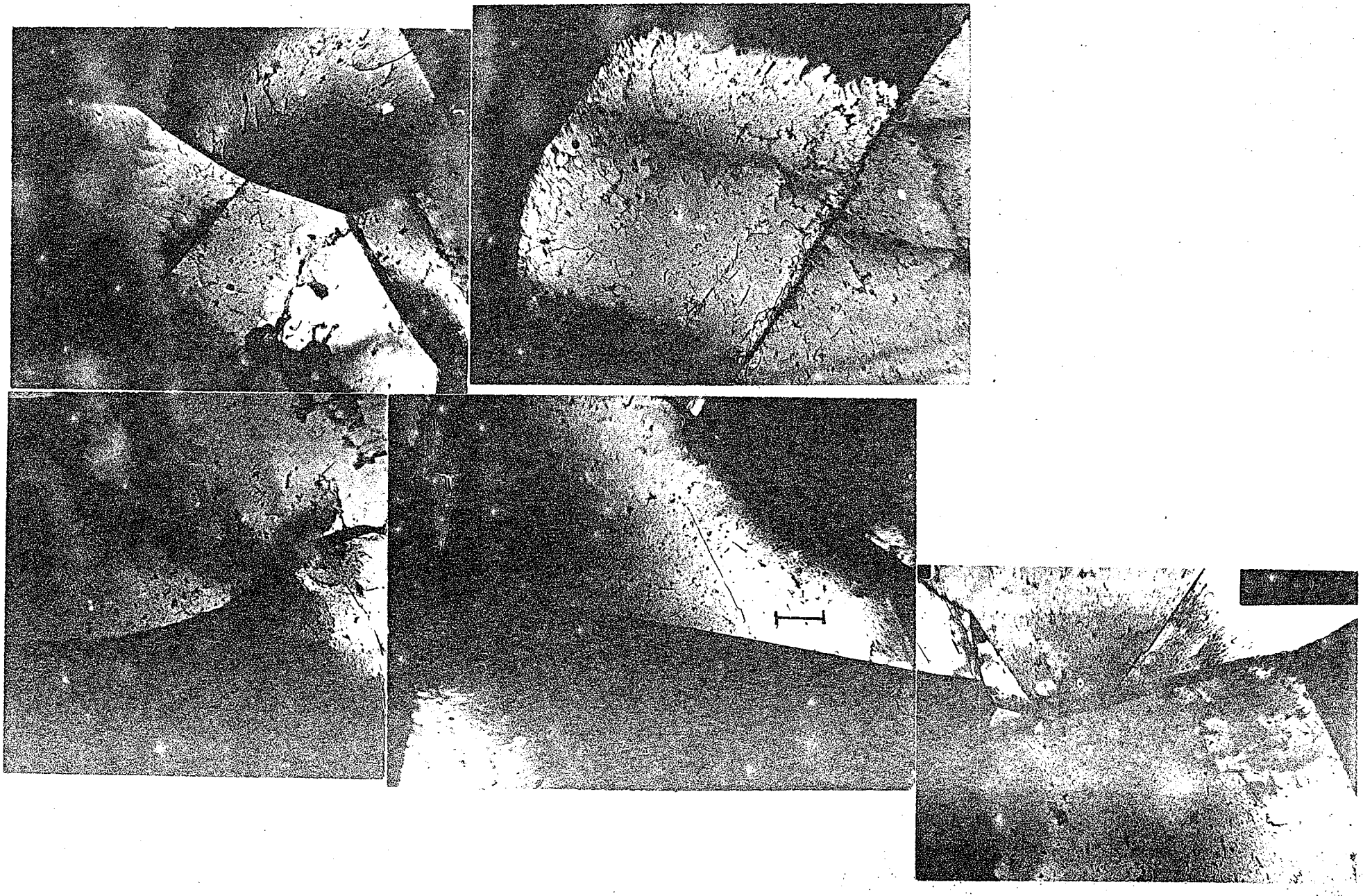

Micro-Map 10. Cu-1Sn, plastic strain of 7×10^{-4} (hybrid foil). The large circles on P_{1-6} are images of the objective arperture over the main beam and the strongly diffracting beam for a two-beam disappearance condition for the dislocations, which occurred at a tilt angle close to that for this plate.

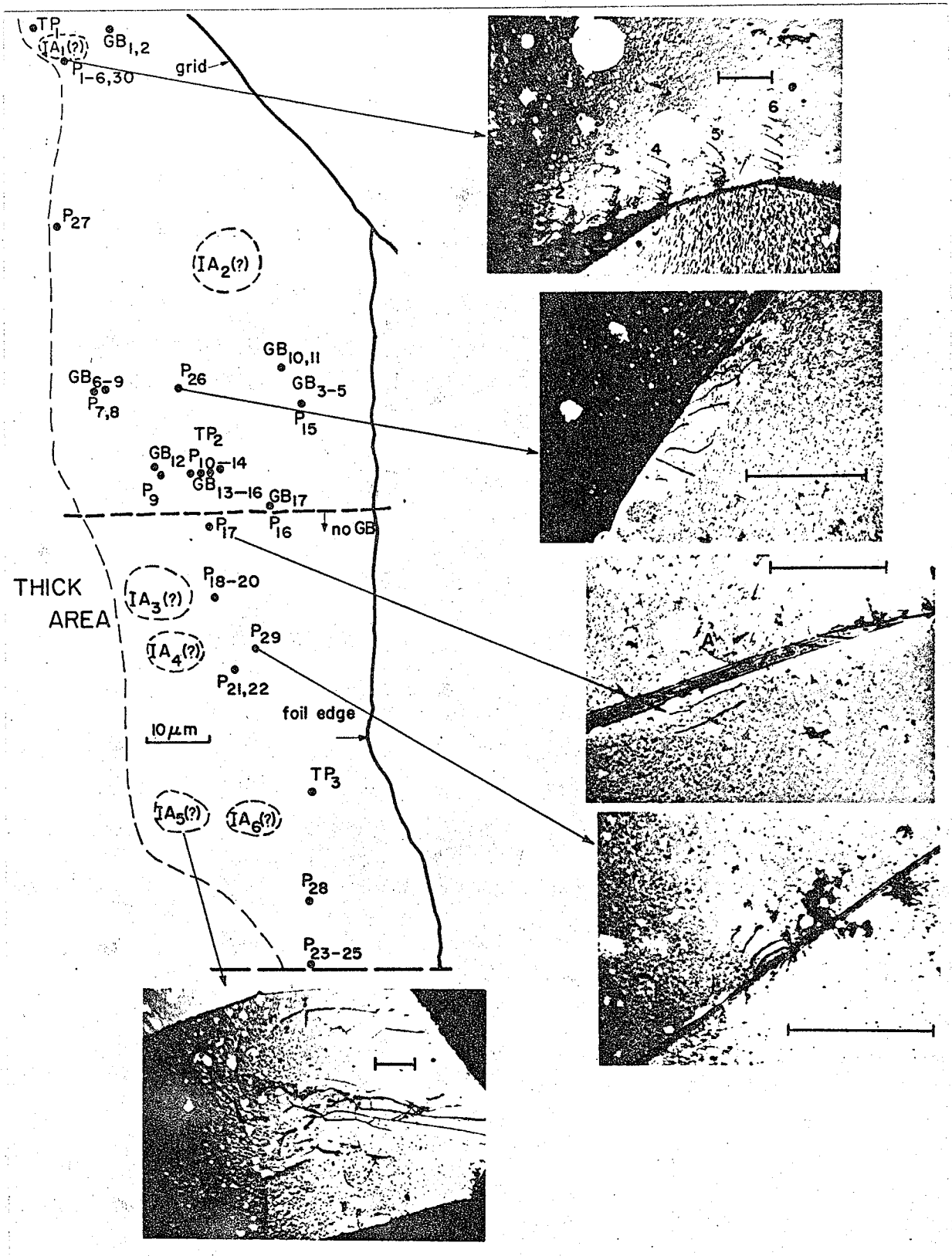
TP1
IA1(?)
GB1,2
P1-6,30
grid
P27
IA2(?)
GB10,11
GB6-9
P26
GB3-5
P7,8
P15
TP2
GB12
P10-14
P9
GB13-16
GB17
P17
P16
no GB
THICK AREA
IA3(?)
P18-20
IA4(?)
P29
P21,22
foil edge
10 μm
TP3
IA5(?)
IA6(?)
P28
P23-25
3
4
5
6
A

Figure 60. Emission of partial dislocations in the same Cu-1Sn foil as figure 59, plastic strain of 7×10^{-4}.

Figure 61. Emission of perfect dislocations in the same Cu-1Sn foil as figures 59 and 60, plastic strain of 7×10^{-4}.

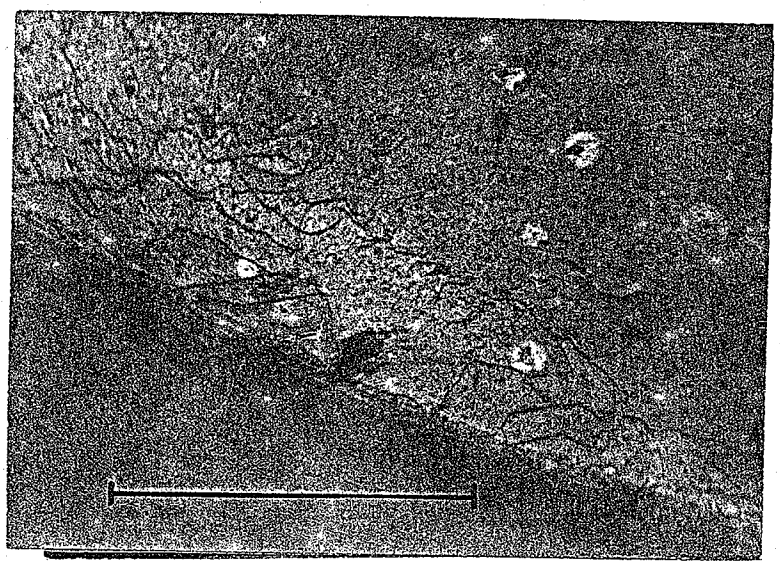

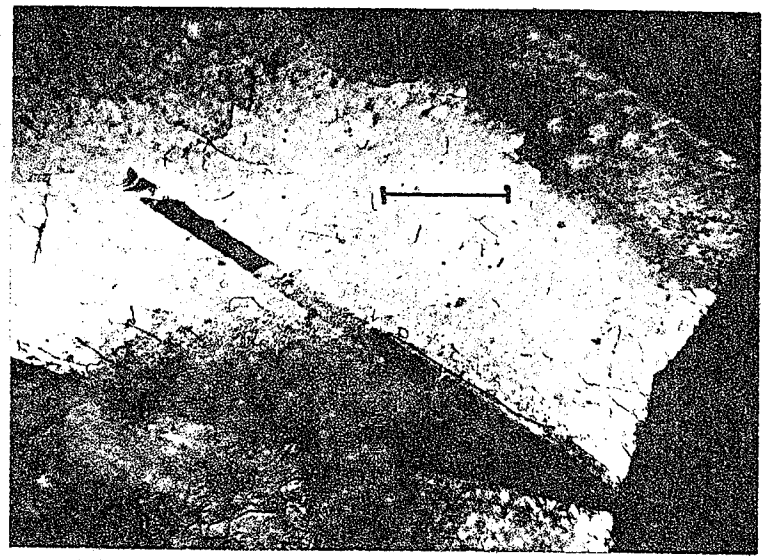

region, but in a different fashion than in Map 10.

5.3.3 NICKEL

The annealed Ni (Map 11) showed a very high density of GB - segments with some, such as GB_8, possessing a fairly high defect density. Occurrence of the GB's in groups was also noticeable. As in the other materials, an unexplainable P-defect was observed (P_1), although the dislocations are somewhat faint. It should be noted that the defect was rather close to the Thick Area where contrast was negligible and nothing (including possible Deformed Zones) could be seen.

The Ni deformed to 3×10^{-4} (Map 12) showed a large amount of P-activity distributed somewhat uniformly. No F-defects were observed here or elsewhere, contrary to the previous findings (54), although it should be pointed out that the Ni was the least examined material and that TBF's were observed. The P-defects tended to consist of only 1 or 2 dislocations, e.g. P_4, P_5. The GB density was much too high to record and some segments, such as that of P_5, appeared to be totally obscurred by defects. Despite the small generations shown here, more intense generation was observed elsewhere in the Ni (figure 62).

Micro-Map 11. Annealed Ni (hybrid foil).

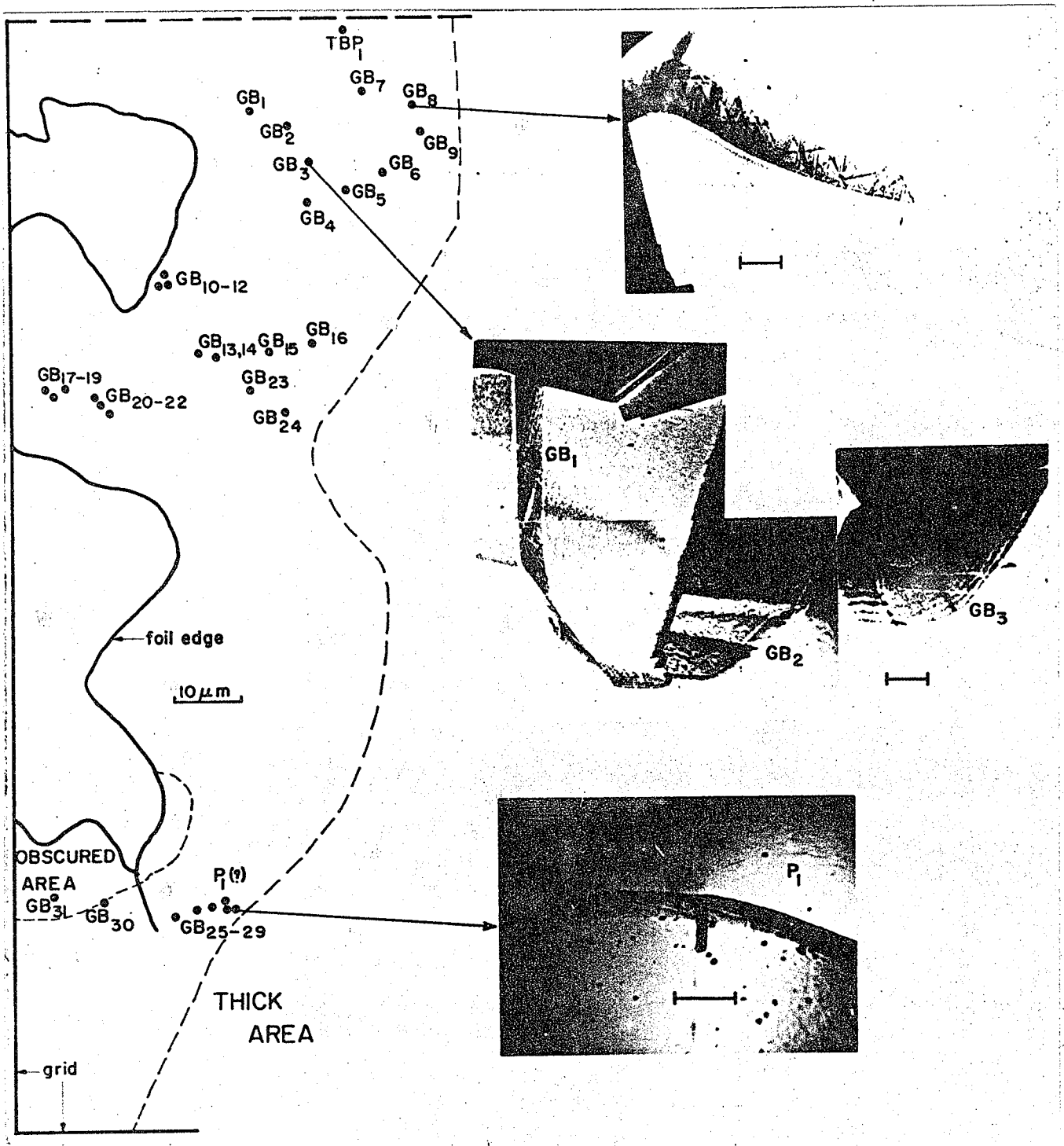
TBP1
GB7
GB8
GB1
GB2
GB9
GB3
GB6
GB5
GB4
GB10-12
GB13,14
GB15
GB16
GB17-19
GB20-22
GB23
GB24
foil edge
10 μm
OBSCURED
AREA
GB31
GB30
P1(?)
GB25-29
THICK
AREA
grid
GB1
GB2
GB3
P1

Micro-Map 12. Ni, plastic strain of 3×10^{-4} (hybrid foil). P_7 is the single dislocation just bowing out from the boundary (barely visible). TP_1, P_1 and P_2, as per requirements, were classified as one source (further emission may be taking place at A). The few dislocations of P_4 were from an unusual small grain which was surrounded by a much larger grain. A similar grain was also observed in a Cu specimen.

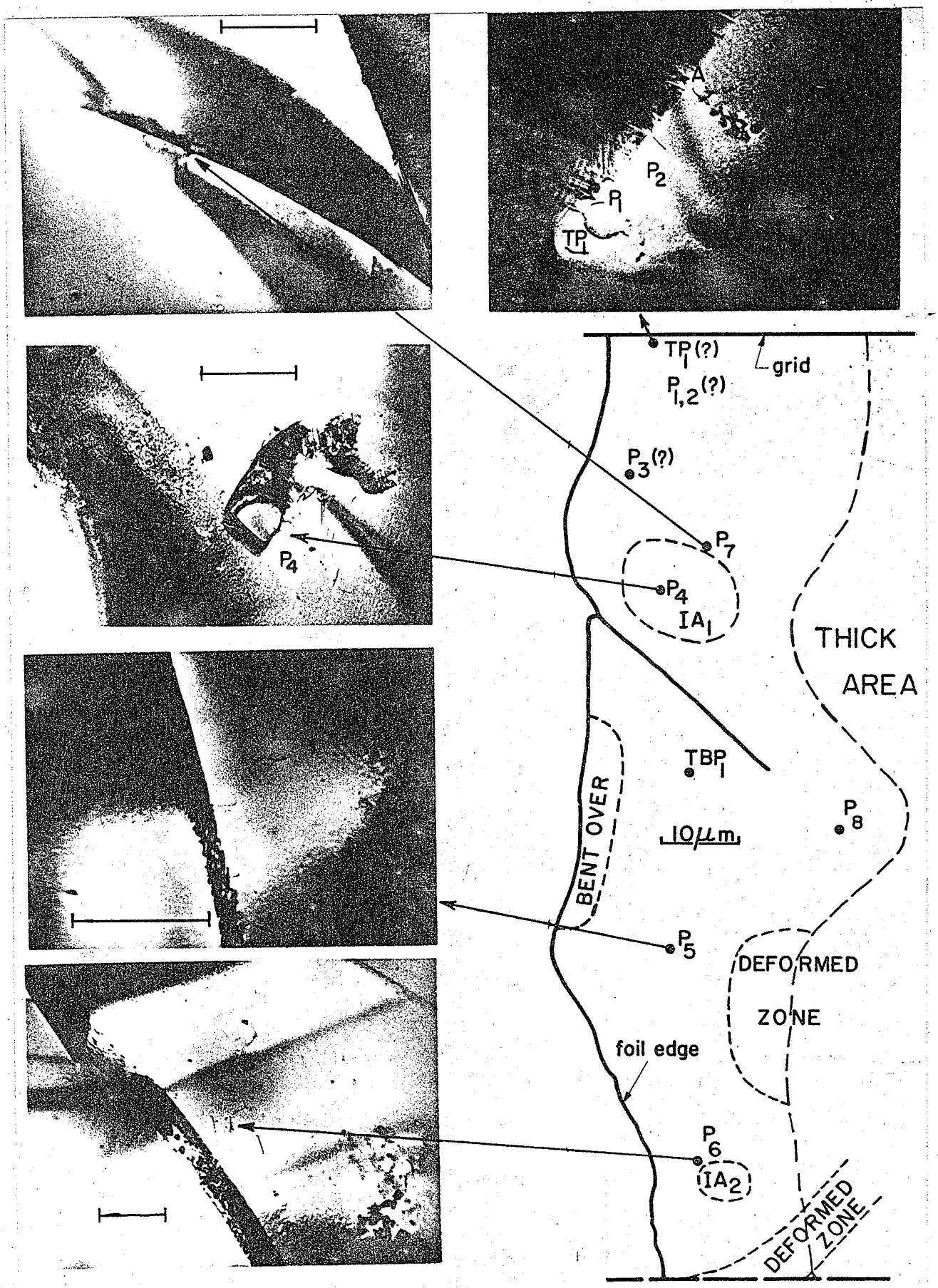
A
P2
R
TP1
TP1(?)
grid
P1,2(?)
P3(?)
P7
P4
P4
IA1
THICK
AREA
TBP1
BENT OVER
10μm
P8
P5
DEFORMED
ZONE
foil edge
P6
IA2
DEFORMED
ZONE

Figure 62. TP activity in Ni, plastic strain of 3×10^{-4}.

Figure 63. Partially recrystalliized region in Al, plastic strain of $3\text{-}5 \times 10^{-4}$ at $230^{\circ}K$.

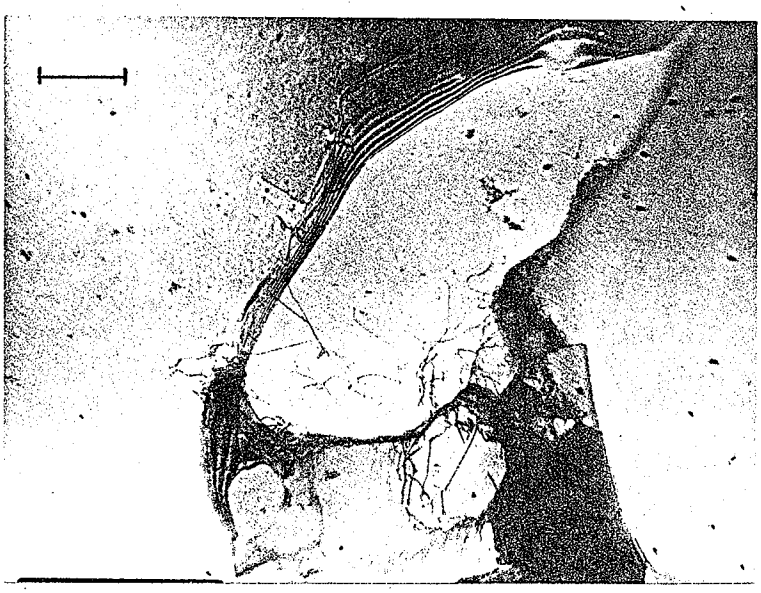

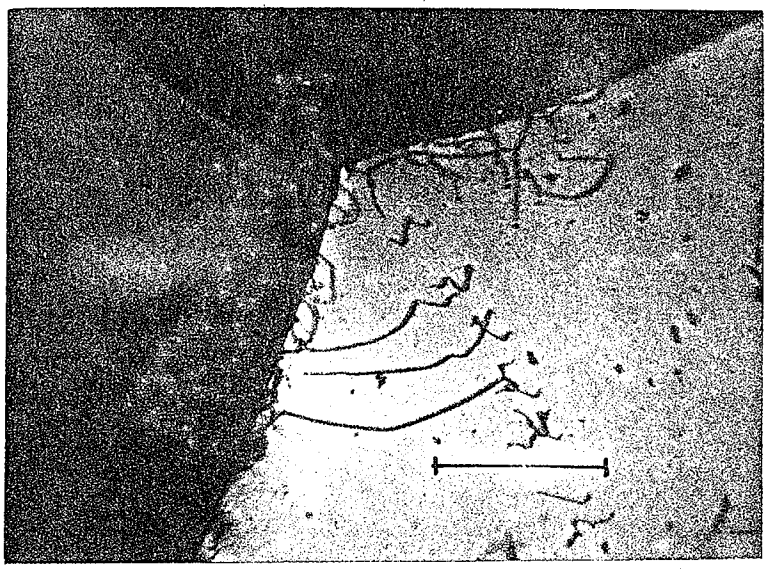

5.3.4 ALUMINUM

The annealed Al (Map 13) was most notable in that, over the entire area searched, not one GB-segment was observed. This observation generally held even in severe Deformed Zones, although some defected segments, such as figure 56(b), were seen in or near these areas. TP_2* and P_1* of Map 13 serve as good illustrations of spurious defects. They are located near a Deformed Zone and a large hole in the foil. There is good evidence of local foil buckling (the semi-circular contours), and there is at least some indication that P_1* is oriented along these contours. There are no similar characteristics for TP_1 but it should be remembered that there was evidence in many Al specimens, both optically and in the electron microscope, for the occurrence of small areas where recrystallization was not quite completed (figure 63).

Some GB-segments started to appear in the Al strained to 3-5 x 10^{-4} at 250^{o}K (Map 14). This strain uncertainty, incidentally, was due to the fact that the extensometer was used and, unlike the stress-strain curves of figure 52, this stress-strain curve was very foreshortened with regard to strain (1 cm corresponding to 4 x 10^{-4} strain). In addition, the elastic loading line was quite irregular. These few GB-segments were of fairly high defect densities and showed extensive networks resembling the previously-

Micro-Map 13. Annealed Al (hybrid foil).

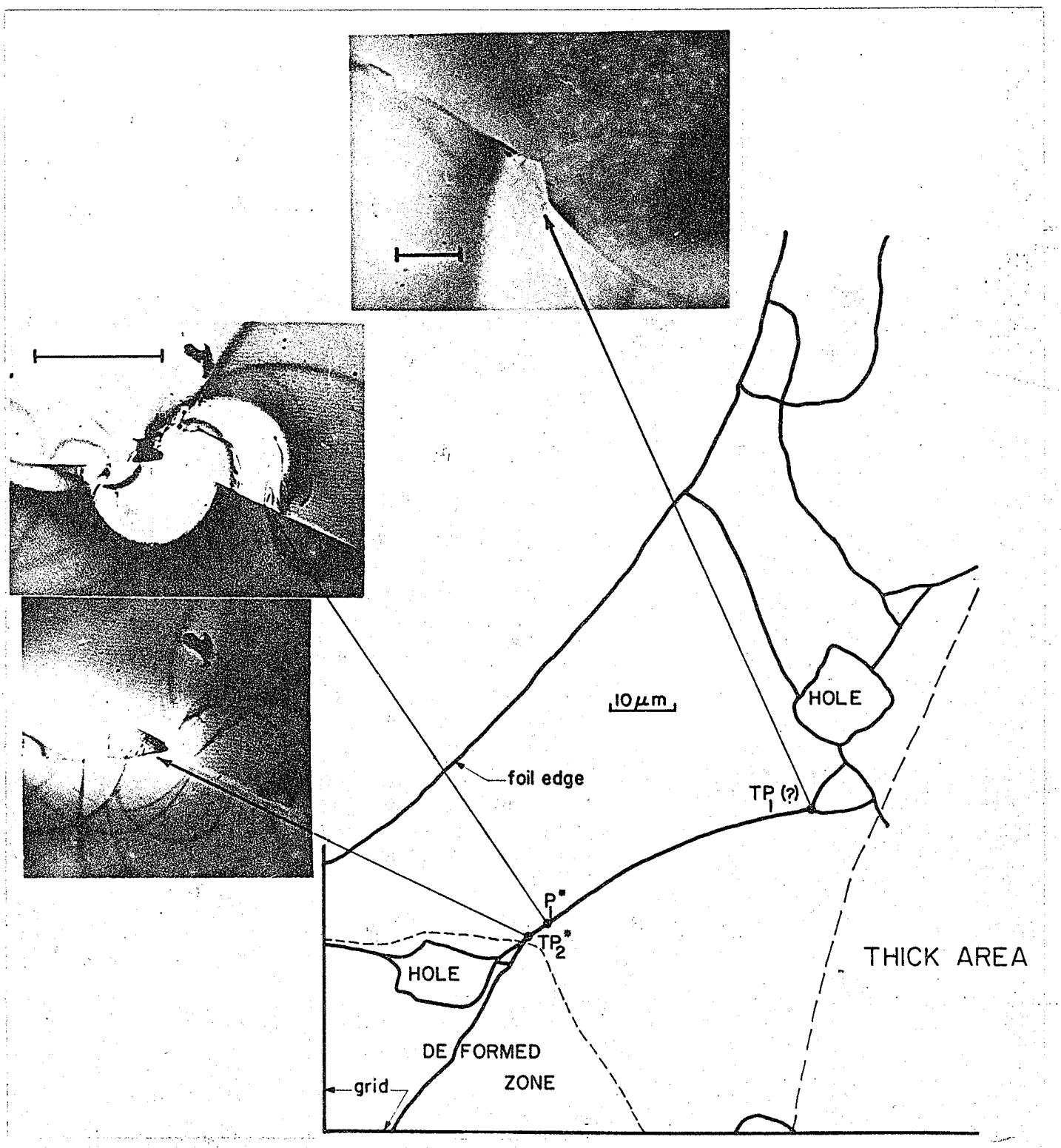
10 μm
HOLE
foil edge
TP1 (?)
P1*
TP2*
HOLE
THICK AREA
DEFORMED
ZONE
grid

Micro-Map 14. Al, plastic strain of 3-5 x 10^{-4} at 230$^{\theta}$K (hybrid foil). P_{3-6} consisted of only one or two dislocations starting to bow out from the boundary (although the nearby interior dislocations may have originated at the boundary). TP_1, P_1 and P_2 are obvious sources, but may be spurious because of the nearby Deformed Zone and their close resemblance to the source of figure 54(b). P_2 posessed a screw character.

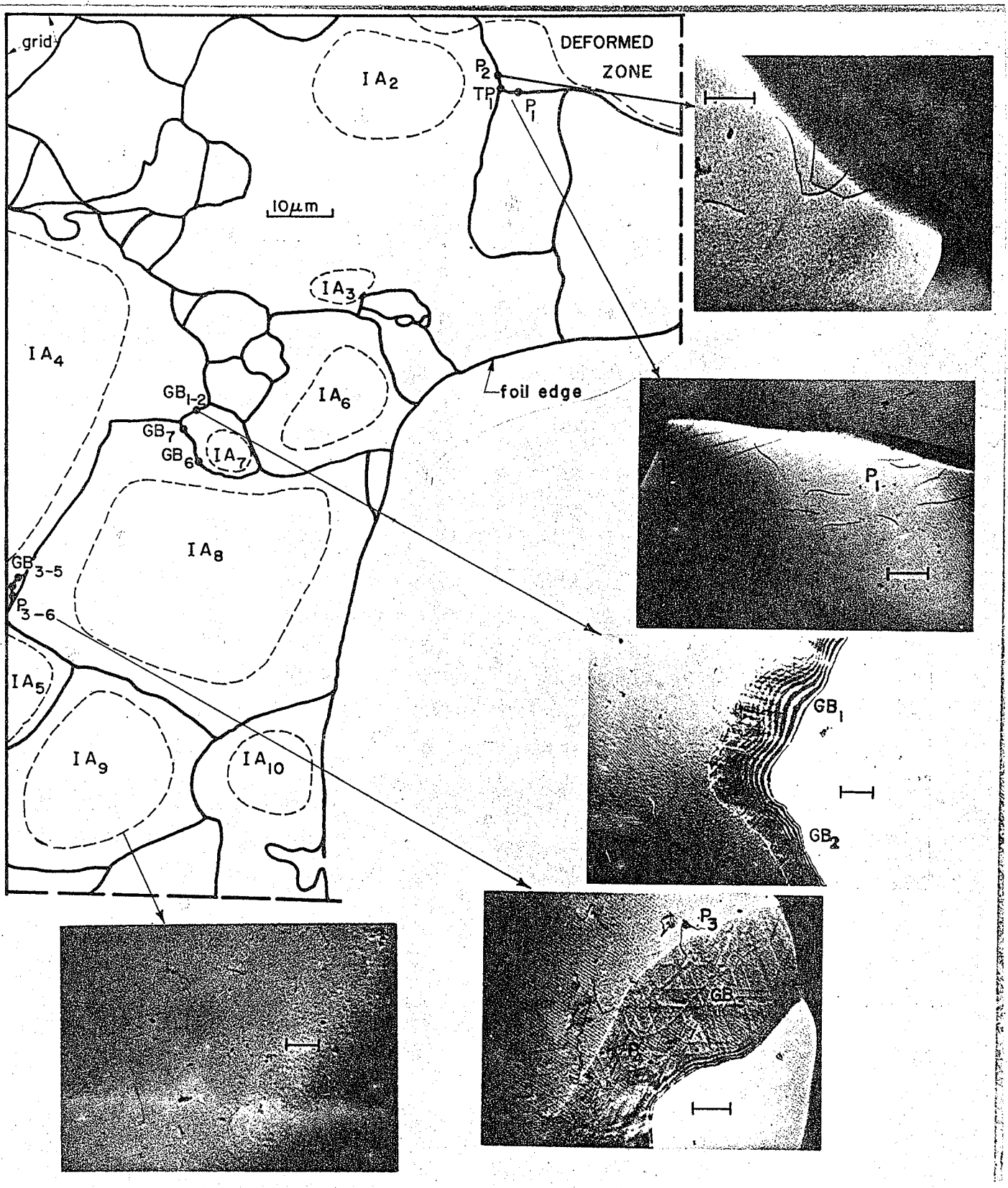
grid
DEFORMED
ZONE
P_2
TP_1
P_1
IA_2
10μm
IA_3
IA_4
GB_{1-2}
IA_6
foil edge
GB_7
GB_6
IA_7
IA_8
GB_{3-5}
P_{3-6}
IA_5
IA_9
IA_{10}
P_1
GB_1
GB_2
P_3
GB_3

mentioned regular configurations of GBD's, C- or G-ledges. IA - defects were the dominant ones in this material, being quite widespread. The dislocation distribution within each was generally in the form of small, scattered tangles.

Map 15 is of Al deformed at room temperature to a 3×10^{-4} strain (specimen strain gauge used). It is both puzzling and intriguing. The puzzling aspect is with regard to the authenticity of <u>any</u> of the boundary generation. This was one of the few "punched" thin foils and all but a few areas showed obvious signs of spurious deformation. One of these, unlike the Map 15 area, showed almost <u>no</u> activity. However, in favor of the activity being authentic, is the absence of overt signs of foil handling. There was an extensive Deformed Zone to the left, but extensive tilting showed there was none in the immediate vicinity to the right or below the activity. One notable feature was the occurrence of at least some of the generations (particularly $P_{2,3}$) at unusual variations in the boundary dimensions. Such curvilinear boundary topography was largely unique to the Al and is also evident in the boundaries of Map 14. The intriguing aspect of this activity is that these would be rather unusual cases of boundary generation if indeed they are legitimate. They are all quite intense (even the IA regions) and 3

Micro-Map 15. Al, plastic strain of 3×10^{-4} at $25^{o}C$ (cut foil).

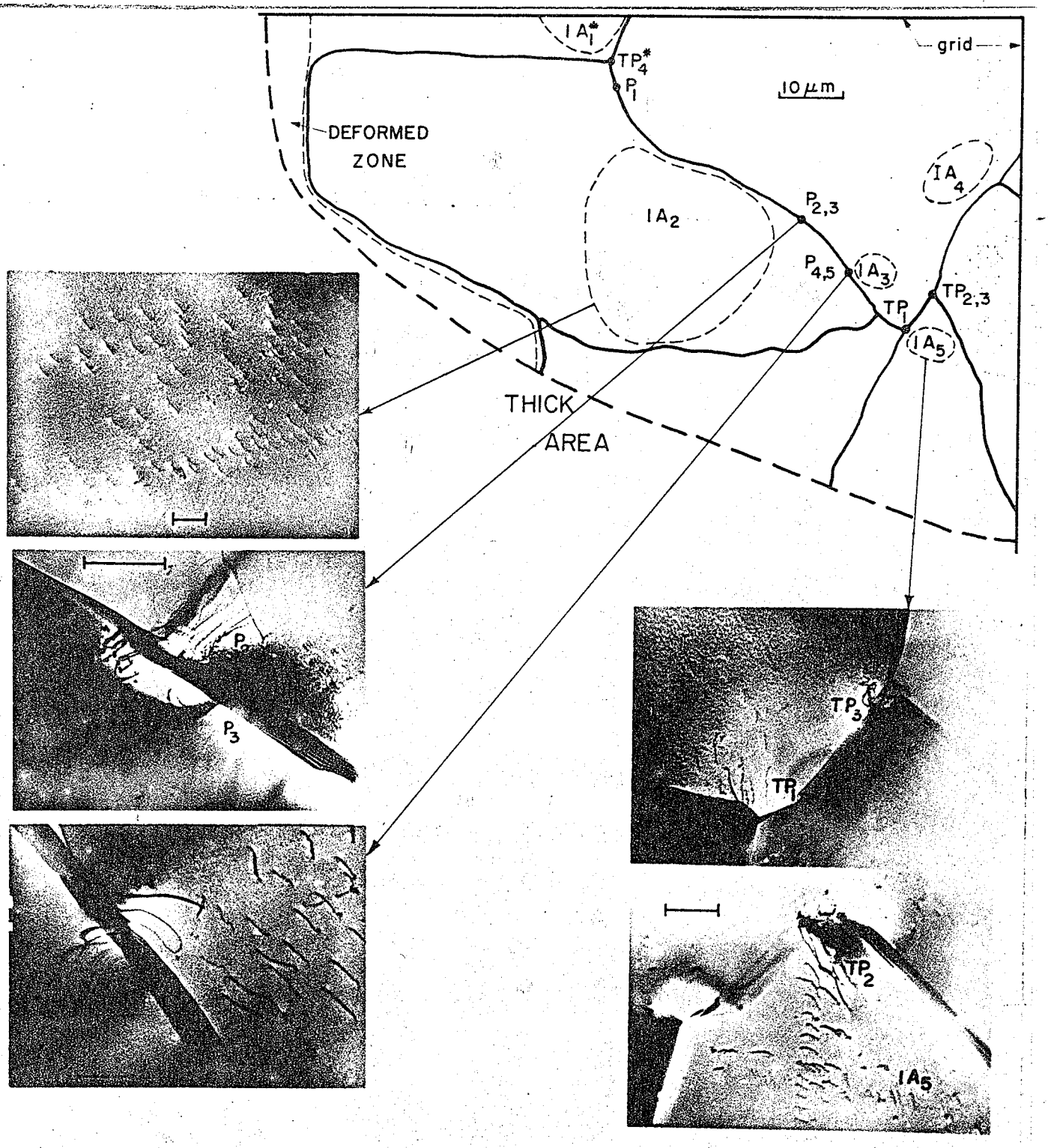
IA1*
TP4*
P1
grid
10 μm
DEFORMED
ZONE
IA2
P2,3
IA4
P4,5
IA3
TP2,3
TP1
IA5
THICK
AREA
P2
P3
TP3
TP1
TP2
IA5

of the 5 sites generate into both grains, quite uncommon amongst any of the other sources observed in any material. Almost all of them show signs of high strain concentration.

Finally, to aid in the comparison between different materials at the same strain, some of the more pertinent data has been extracted from Table 11 and is presented again in Table 12.

5.3.5 INDIVIDUAL BOUNDARY SOURCES

Almost all of the generations from the micro-maps, plus any others that were photographed outside of these areas, were analyzed according to the guidelines stated in sec. 4. The results of some of this analysis are compiled in Table 13. Such data as distance generated into the grain and number generated were relatively easy to measure and were recorded for most. Other factors were rather more time-consuming or difficult to apply, hence they were performed for a limited number of generations.

Perhaps somewhat surprisingly, both the length and number for Cu appeared to show no strong dependence on strain. Similarly, there was no outstanding differences for these parameters between the different materials, save for the Al deformed at room temperature (cf. Map 15). One difference that is quite apparent is that between the generation of perfect and partial dislocations. Note also

TABLE 12

COMPARATIVE DEFECT DENSITIES

- all x $10^{-4}/cm^2$
- note that only the low temperature Al data is included

ANNEALED MATERIAL

	Cu	Cu-1Sn	Ni	Al	
GB	3.2	3.7	48.8	0	(all others zero)

PLASTIC STRAIN OF 3 x 10^{-4}

	Cu	Cu-1Sn	Ni	Al
GB	27.9	6.6	NM	1.8
F	2.2	2.6	0	0
P	4.4	1.3	18.4	1.8
TP	3.9	2.6	7.3	0.3
IA	3.3	10.6*	7.3	3.0

PLASTIC STRAIN OF 7 x 10^{-4}

	Cu	Cu-1Sn
GB	39.0	58.0
F	0	0
P	7.6	54.5
TP	0.7	5.0
IA	4.3	9.9*

* - recall the suspect nature of these configurations

TABLE 13

DATA FOR INDIVIDUAL SOURCES

AVERAGE DISTANCE OF EMISSION INTO THE GRAIN(microns)

- bracketed numbers indicate number of defects used for average value
* - indicates emission was completely across grain
- includes all strains

	P-defects	F-defects
Cu	0.9(31)(1*)	3.2(25)(14*)
Cu-1Sn	1.0(38)(0)	5.8(4)(2*)
Ni	0.4(16)(0)	-----
Al(230°K)	1.2(7)(0)	-----
Al(290°K)	1.4(8)(0)	-----

AVERAGE NUMBER OF DISLOCATIONS EMITTED

- includes all strains

	P-defects	F-defects
Cu	4.0(29)	12.9(20)
Cu-1Sn	5.0(38)	20.0(4)
Al(230°K)	3.3(7)	-----
Al(290°K)	17.6(8)	-----
Ni	3.9(16)	-----

AVERAGE DISTANCE EMITTED AND AVERAGE NUMBER FOR Cu

	P-defects		F-defects	
strain	length	number	length	number
$1x10^{-4}$	0.4(5)	3.0(5)	3.0(1)	~40(1)
$3x10^{-4}$	0.6(11)	3.3(10)	4.9(5)	10.0(5)
$5x10^{-4}$	2.4(7)	6.3(7)	2.9(13)	13.1(8)
$7x10^{-4}$	0.2(5)	2.4(5)	-----	-----

PERCENTAGE OF PARTIAL DISLOCATION EMISSION

- measured over equal areas, all strains included

Cu - 18/75 = 24 %

Cu-1Sn- 2/36 = 6 %

TABLE 13 (continued)

BREAKDOWN OF TRIPLE POINT SOURCES

- includes all strains

	% TP's	P-defects	F-defects	GB triple points	GB-TB triple points	% of each
Cu	43	12(31)	12(25)	9	15	(38/62)
Cu-1Sn	21	5(38)	4(4)	4	5	(45/55)
Ni	37	6(16)	----	3	3	(50/50)
Al	too few defects of reasonable authenticity					

ratio of GB triple points to GB-TB triple points

- total of 4 runs
- areas surveyed for each material not equal

(a) counting around a grain

	GB	GB-TB	% of each
Cu	15	35	(30/70)
Cu-1Sn	21	45	(32/68)
Ni	16	30	(35/65)

(b) counting along random boundaries

	GB	GB-TB	% of each
Cu	12	39	(24/76)
Cu-1Sn	15	36	(30/70)
Ni	14	21	(40/60)

(c) total

	GB	GB-TB	% of each
Cu	27	74	(27/74)
Cu-1Sn	36	81	(31/69)
Ni	30	51	(37/63)

CHARACTER OF EMITTED DISLOCATIONS

- all materials, all strains

P-defects - 7 pure edge, 8-10^{o} from edge, 4-20^{o} from edge, 2-35^{o} from edge, 3-45^{o}, 2-30^{o} from screw, 1-10^{o} from screw, 1 pure screw

F-defects - 2-20-25^{o} from edge, 3-30^{o} from edge

BURGERS VECTORS OF GENERATED DISLOCATIONS

- Cu and Cu-1Sn, all strains

P-defects - 40 sources all identical, 2 mixed

F-defects - 6 sources all identical , 12 mixed

the larger number of F-defects that completely traversed the grain. It is also apparent that generation of partial dislocations was a significant portion of the total boundary generation, at least for the Cu.

The breakdown of TP-generations definitely shows that there was more of a tendency for F-defects to occur at these points than there was for P-defects. Triple point generations also accounted for a fairly significant portion of the total generations (43% in Cu, 21% in Cu - 1Sn and Al, 27% in Ni). The breakdown involving grain boundary triple points (GB triple points) and grain boundary - twin boundary triple points (GB - TB triple points) would, of course, have been influenced by the relative proportions of each. These ratios were determined for the Cu, Cu - 1Sn and Ni and are included in the Table. The counting for this was conducted in two ways; counting completely around a single grain or counting along random grain boundaries. As seen, both gave approximately the same ratios. Comparing these ratios to the TP generations, it is apparent that GB triple points are consistently more likely to act as sources, but not by a very wide margin. Finally, there was no marked association of F-defects with sharp kinks. Of the 13 that were not from triple points, only 4 were from boundary kinks, the remainder being from smooth segments.

Dislocation characters were determined by obtaining

a good 2-beam vanishing condition using, if possible, low index operating reflections ($\bar{g}$ = 002, 111, 220). This was done because Loretto and France (199) found that apparent disappearance can occur for larger $\bar{g}$ values, such as 311, even for $\bar{g}\cdot\bar{b} = .1$ ($\bar{g}\cdot\bar{b} = 0$ being the true disappearance condition). As shown in the P_{1-6} defects of Map 10 (p.190), these beams were superimposed on a plate of the defect wherein the dislocations were visible. This was done at a tilt angle as close as possible to the disappearance condition to avoid changes in the orientation of the dislocation lines that can occur over large tilt angles. The most serious difficulty was often that of determining the <u>true</u> dislocation orientation, i.e. at the source itself. Thus, most determinations were conducted on Cu - 1Sn boundary sources, since only in this material were sources well-delineated. For example, the corrective rotation necessary between the diffraction pattern and defects of P_{1-6} was roughly 90^{o}. Hence the Burgers Vector of these dislocations was roughly parallel to the two superimposed circles, indicating that the orientation was 20 - 30^{o} from screw, using those dislocations nearest the boundary. However, closer examination showed that they were actually emenating from GBD-macroledges that were almost at right angles to $\bar{b}$, i.e. they were 10^{o} from pure edge dislocations.

An angular error arises from the fact that the slip plane lies out of the plane of the foil. Calculations on typical sources indicate this error to be small for dislocations with edge or screw character and a maximum of 8 - 12^{o} for dislocations with 45^{o} character. The F-defect determinations also have to consider the fact that partial dislocations may vanish for $\bar{g}.\bar{b} \neq 0$ (196). Another reason for using the boundary source itself for character determination is that dislocations often rearrange themselves in the thin foil, destroying their original orientation.

Table 13 also demonstrates that essentially each boundary source of perfect dislocations (P-defects) involved ones with identical Burgers vectors, whereas a majority of those involving partial dislocations (F-defects) were of dislocations with different Burgers vectors. However, it should be pointed out that this latter was generally a case of only a few dislocations of one Burgers vector, with all of the remainder possessing another, e.g. figure 66(a) shows an F-defect with six dislocations of one character and two of another.

Some other points that were determined were:

1) The configurations of the generated dislocations often made it uncertain as to wether they emanated from a single line on the boundary or closely adjacent lines, e.g. figure 64(d), due to a wide zone of strong contrast,
2) Generation was observed to occur from boundaries with

no defects (figure 67a), a moderate number of defects (figure 64g) or a high number of defects (figure 65c).

3) Of 130 generations examined, only 14 were from the same point on the boundary into both grains (4F, 10P) but it should be noted that 6 of the P-defects were from the uncertain Al foil of Map 15. A good example of such an F-defect is Figure 67(d). In only one case was the pair definitely close to being collinear. Somewhat more often, generation would occur into both grains, but at points separate from each other, e.g. the boundary of figure 64(b), (c), (d), (e).

4) Although not extensively studied, there appeared to be no obvious trend to boundary generation occurring in either very small or large grains, or in pairings of the two. This also proved true for the relation of active boundaries to the stress axis.

5) The orientations of both source and neighbour grain with respect to the stress axis were determined for three cases. In one, the stress axis was < 110 > in both (P_{17} of Map 10 - stress axis vertical). In another it was < 122 > in the source grain and 10^{o} from < 001 > in the neighbour (figure 65b - stress axis vertical). The third had the stress axis being < 001 > in the source grain and 10^{o} from < 112 > in the neighbour (the main and right hand grains of fig. 64a - stress axis vertical). The accuracy of such estimations was somewhat dubious

Figure 64. Localized grouping of boundary sources in Cu-1Sn, plastic strain of 7×10^{-4};

(a) expanded view of region showing some source locations

(b)-(g) close-ups of individual sources

Note: (d) and (e) are the same area, but under different diffracting conditions.

Dislocation characters are (b)-45°, (e) lower source, pure edge, (f) AB source, 10° from edge.

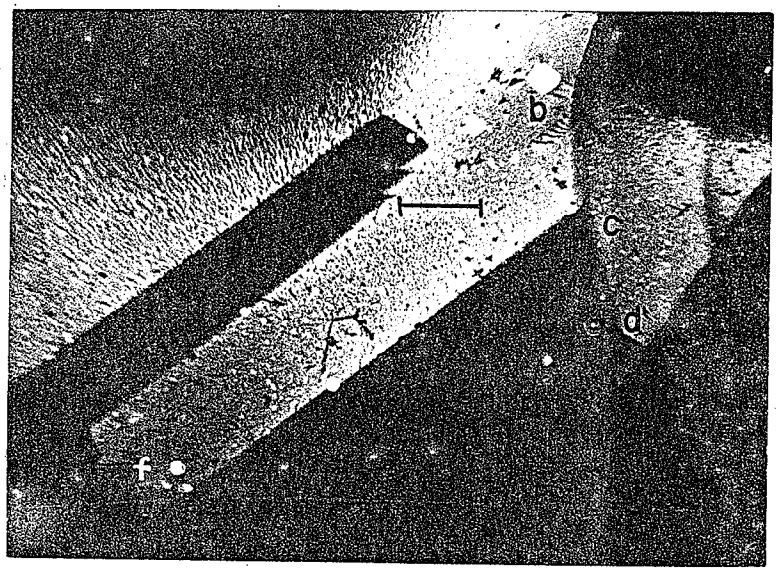

(a)

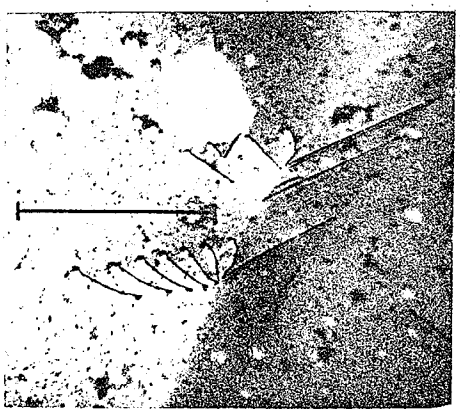

(b)

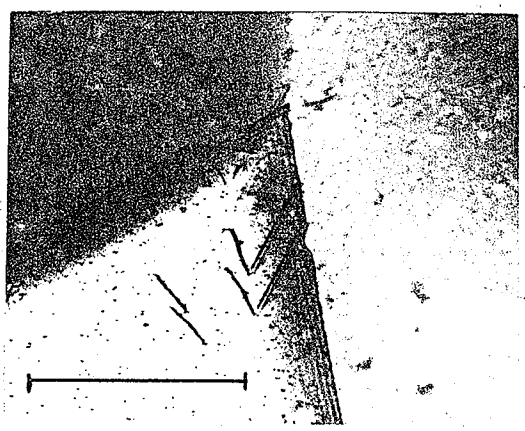

(c)

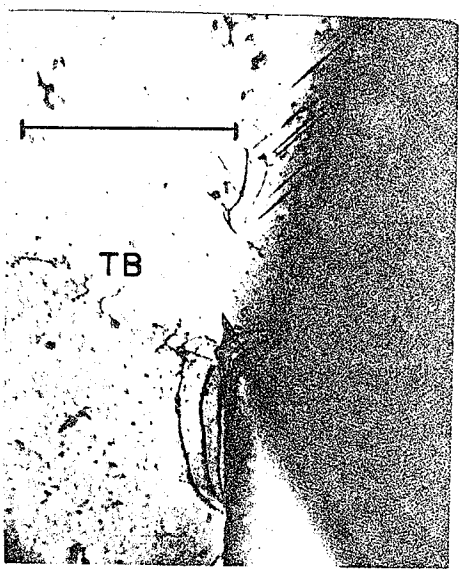

(g)

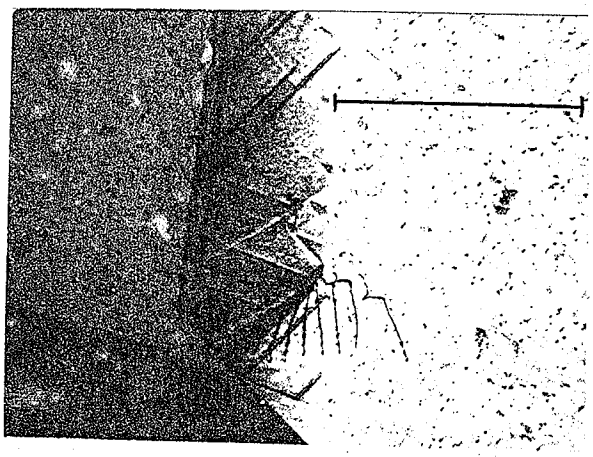

(d)

(f)

(e)

Figure 65. Examples of perfect dislocation emission from grain boundaries;

(a) Cu, plastic strain of 5×10^{-4}

(b) Cu-1Sn, plastic strain of 7×10^{-4} (30^{o} from screw orientation)

(c) Ni, plastic strain unknown (pure edge orientation).

(d) Cu-1Sn, plastic strain of 3×10^{-4} (dark field micrograph, $\bar{g} = \bar{1}13$, pure edge).

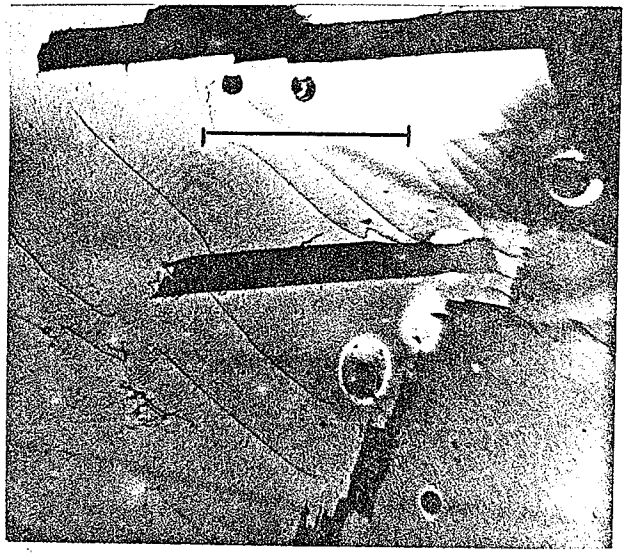

(a)

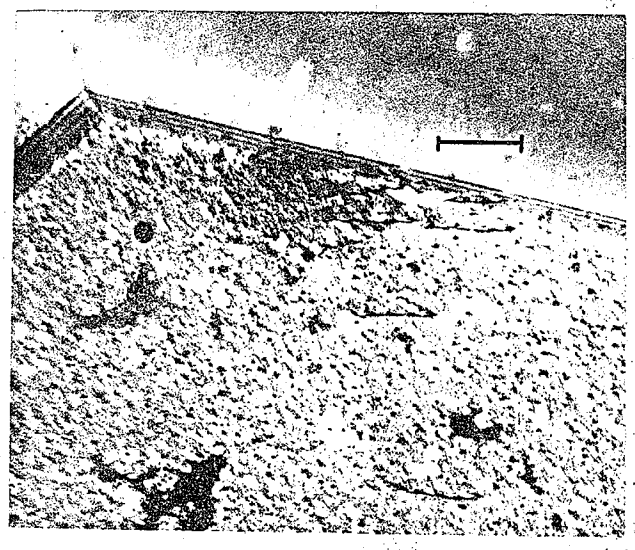

(b)

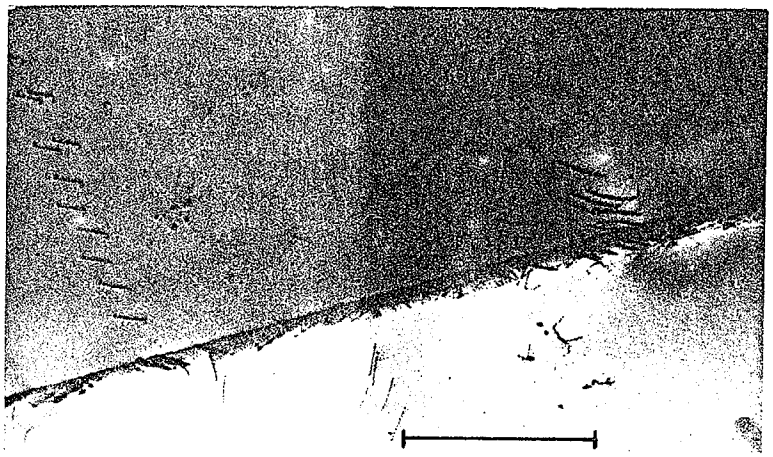

(c)

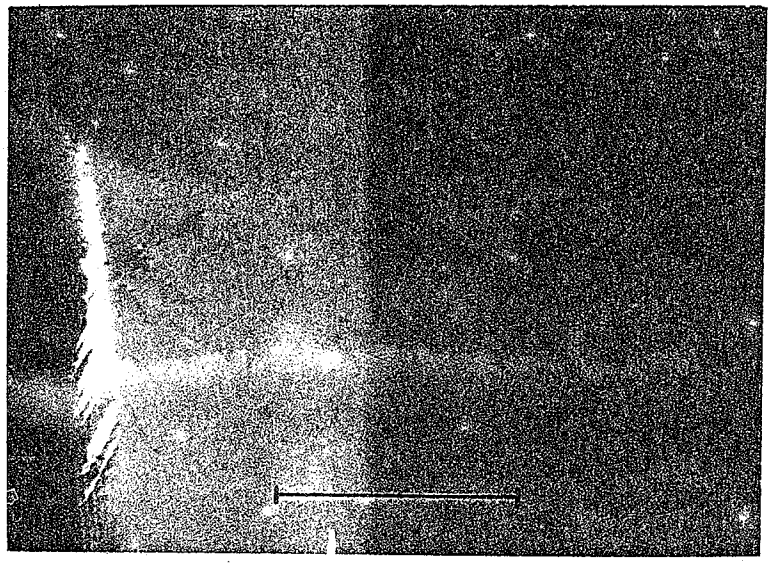

(d)

Figure 66. Examples of partial dislocation emission from grain boundaries;

(a) Cu, plastic strain of 5×10^{-4} (major set of partials is 30^{o} from edge)

(b),(c) Cu, plastic strain of 5×10^{-4}

(d) Cu, plastic strain of 3×10^{-4}.

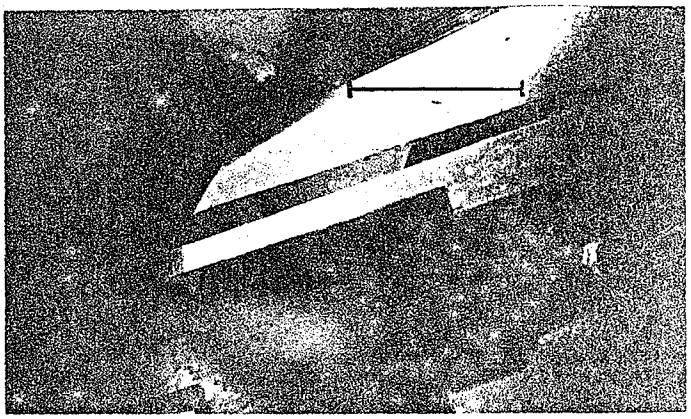

(a)

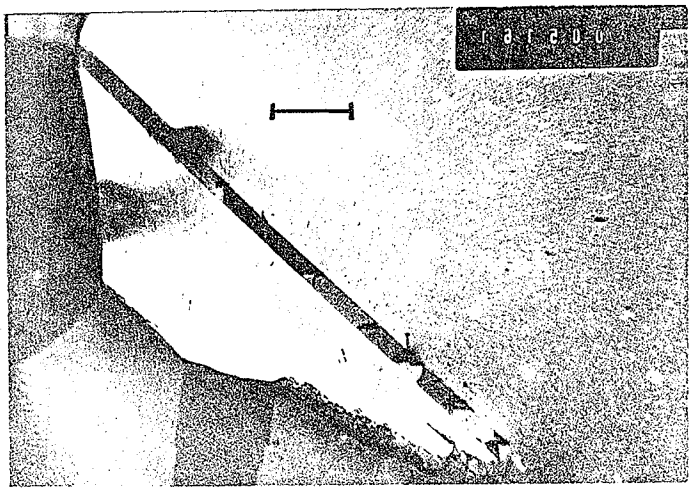

(b)

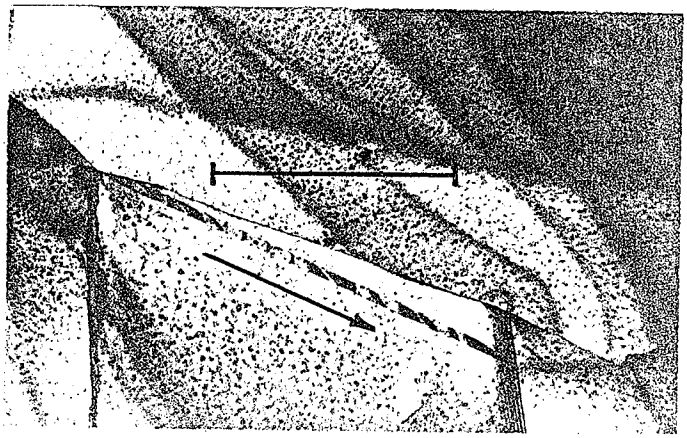

(c)

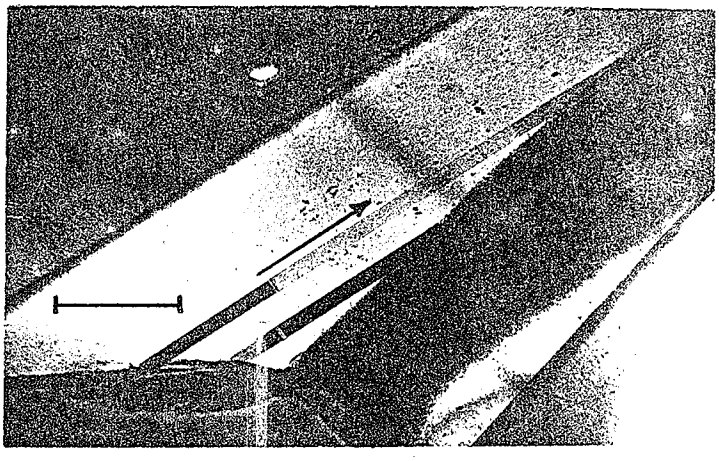

(d)

Figure 67. Examples of emission of partial dislocations from grain boundaries ;

(a) Cu, plastic strain of 5×10^{-4}

(b) Cu-1Sn, plastic strain of 7×10^{-4} (roughly 25^{o} from edge)

(c) Cu, plastic strain of 5×10^{-4} (30^{o} from edge)

(d) Cu, plastic strain of 5×10^{-4}.

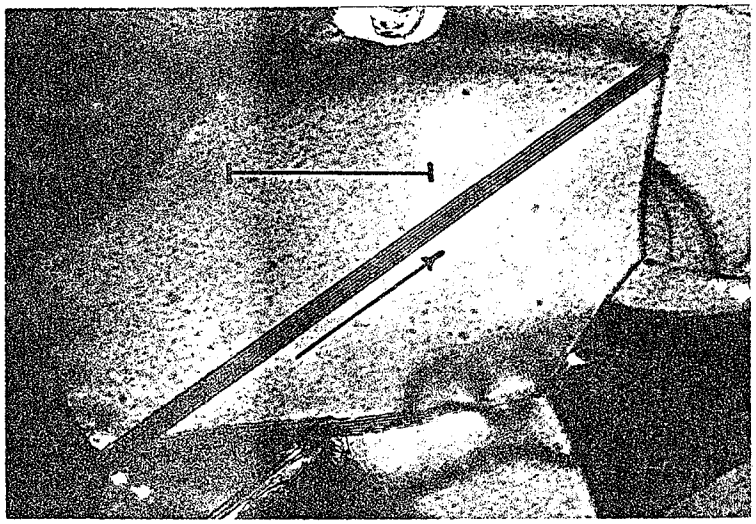

(a)

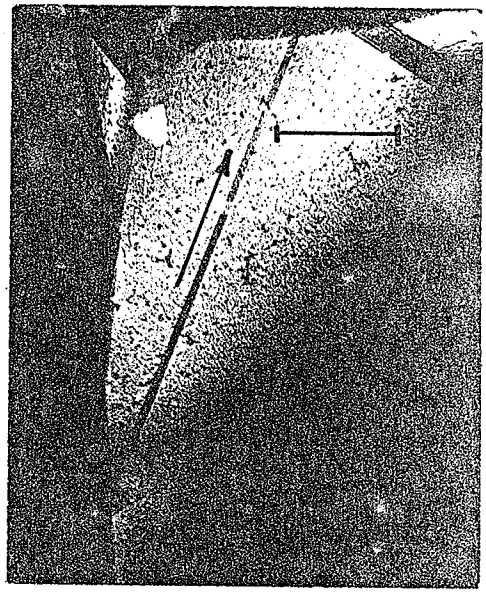

(b)

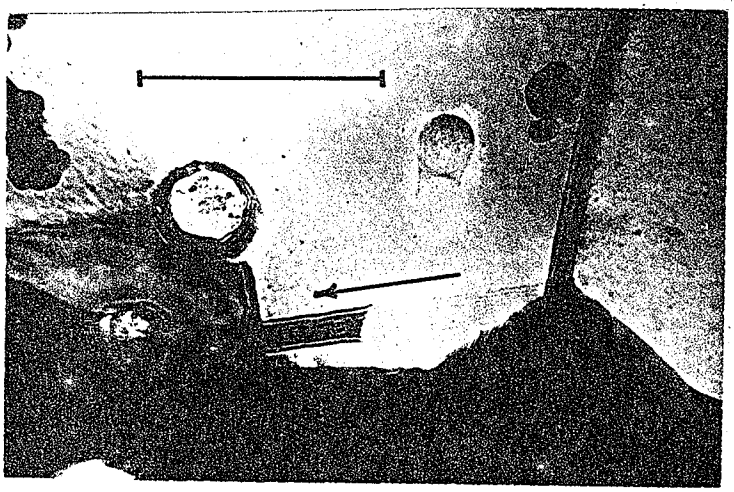

(c)

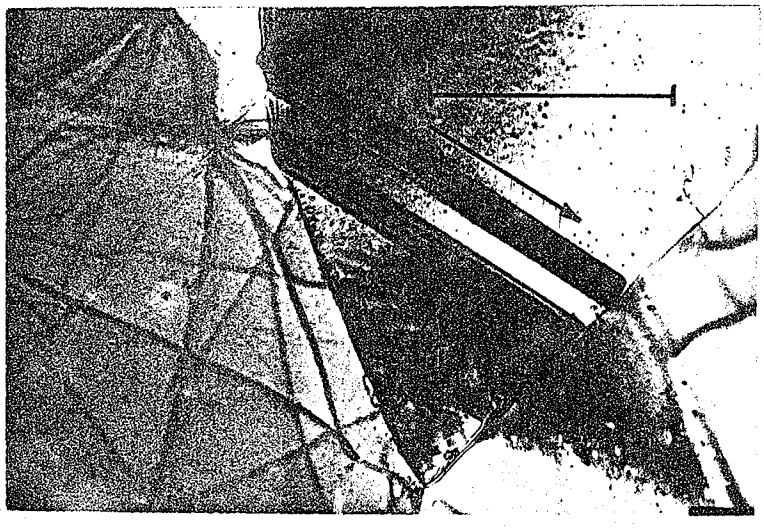

(d)

Figure 68. Enlarged views of partial dislocation sources;

(a) Cu-1Sn, plastic strain of 3×10^{-4} (dark field micrograph, g = $11\bar{1}$, T = top surface of foil)

(b) same defect, bright field

(c) emission site for F_1 of map 9 (p.187) (arrows at right indicate $\bar{1}1\bar{1}$ directions)

(d) emission site for F-defect of figure 67(b), faults out of contrast but emit from AB.

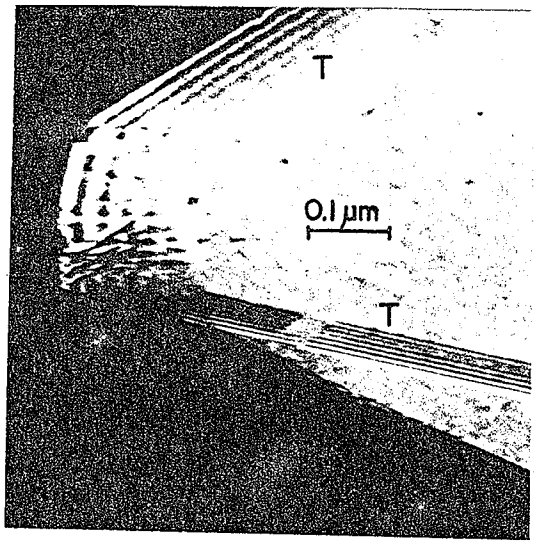

(a)

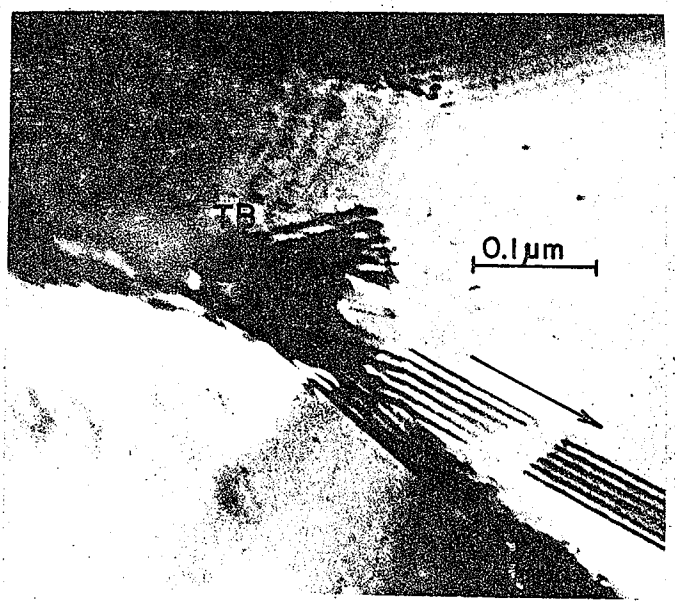

(b)

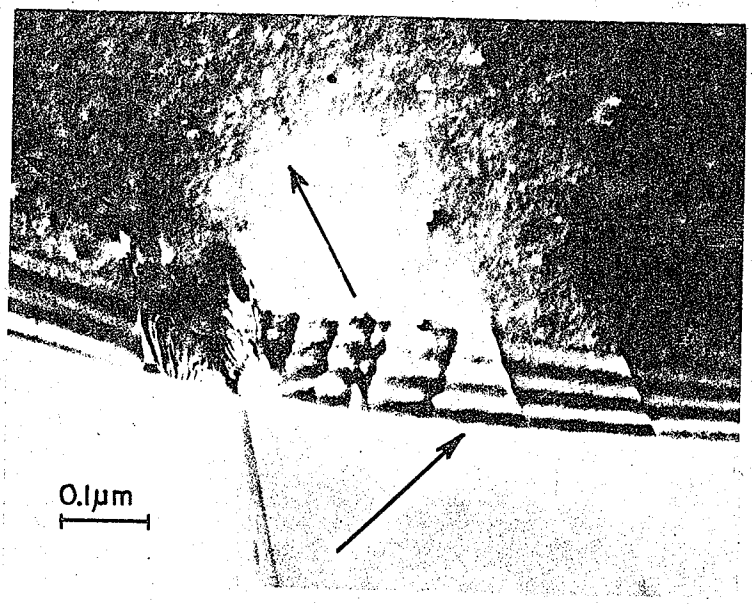

(c)

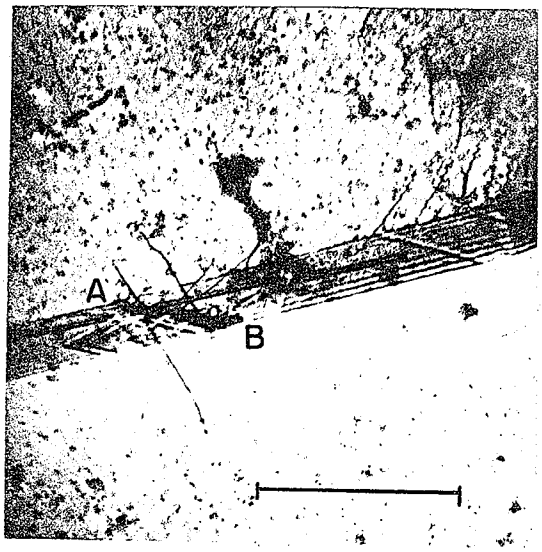

(d)

due to the fact that the stress axis was optically noted with respect to the perforation in the thin foil and this information used to estimate it on the area being examined. Hence a circular perforation would have been completely useless in this regard.

6) Of 11 instances where the 0^{o} tilt foil normals were determined for both source and neighbouring grains, 2 cases of a common normal were found. The upper and lower grain of figure 67(c) were misoriented either 8 or 82^{o} about < 001 >! Neither are near any coincidence orientation (using Pumphrey and Bowkett's compilation, 200). The misorientation for F_1 (Map 9) was about < 110 >, which was around 3^{o} from the $\Sigma = 17$ coincidence orientation.

7) Numerous F-defects were checked by the standard bright field-dark field technique of stacking fault identification and all showed the required asymmetric fringe reversal. An example is the faults of figure 68(a), (b), where the outer fringes change from both dark in the bright field (figure 68b) to one dark and one bright in the dark field (figure 68(a). The unchanging fringe marks the fault intersection with the top of the foil and the reversed fringe the bottom.

Figures 64 - 67, which have already been mentioned several times, are a compendium, as it were, of many of

the more obvious boundary generations not already presented in the maps. Figure 16 is a particularly good example of both obvious generations and their clustering on a very localized scale in the Cu - 1Sn at $\varepsilon_p = 7 \times 10^{-4}$. Figure 64(a) is an overall micrograph and figures 64 (b) - (g) show no less than 10 generations in this small area, 7 into the major grain of the micrograph and 3 into neighbouring grains. (Subsequent examination showed 5 more sources to the upper left of figure 64(a) and 1 more to the right of figure 64 (g), a total of 16). It appeared at first that the sources of (b) and (f) were identically aligned, thus indicating the possibility of an interior source operating against both boundaries (the only such case found, it should be noted). However, careful examination appeared to show a slight misalignment between them and there was also no sign of any dislocation activity whatsoever between them. Figure 64(b) is a particularly clear example of the necessity of studying the boundary itself rather than the generated dislocations for character determination. As with the three adjoining F-defects of Map 4 (p.179), figure 64(g) shows apparent generation on two slip systems. One consisted of the vertical dislocations and the other consisted of the almost horizontal dislocations just starting to bow out from the GBD-macroledge, AB. Figure 64(e)

also shows 2 generations, with the more regular one emenating from a quadruple point (one TB is almost out of contrast).

In figure 65, the two sources of figure 65(b) came from two apparent GBD-macroledges that were the only defects in the boundary. The strain for the generations of figure 65(c) was indeterminate, since the specimen was accidentally bent in the annealed condition and therefore not strained. The general appearance of the thin foil indicated the strain was likely of the order of a few percent or less. In figure 66(d), it should be pointed out that the two F-defects originate from a boundary where it adjoins a very tiny grain, and the smaller generation actually occurs from the intersection with the grain boundary of a twin boundary within this grain. (The F-defects of figure 66a-c and figure 67b originate from GB-TB triple points). The F-defect of figure 67(a) occurs near to, but not at, a GB triple point. The fault-like defect below the right hand generation of figure 67(d) is a coherent twin boundary. It should be noted that the faults of figure 67(c) are out of contrast between the visible portion and the triple point from which they emanate.

Some cases of apparent GBD pile-ups at sources turned out to be misleading upon closer examination. A case in point was F_2 of Map 9 (p.187) which appeared (at

a different tilt angle) to have GBD's from the boundary segment just above it piled-up against its point of origin. However, the GBD's can be seen in the dark field of figure 68(a) to be actually piled against a twin boundary intersection (which is visible in figure 68b). The area around the generation point of the faults is actually quite clean. Figure 68(a) incidentally, illustrates the findings of McDonald and Ardell (60) re boundary fringe attenuation (p.41). Thus the top of the grain boundary is as indicated in figure 68(a). One case where a GBD pile-up does appear to have occurred is seen in figure 68 (c), where dissociated GBD's (shown by changes in fringe intensity) seem to have moved along the boundary from right to left and piled up at the twin-grain boundary intersection. This is a close-up of the generation point for the F_1 defect of Map 9. The trace of the faults generated from this point may be faintly seen under the directional arrow. A third example of the point of origin for partial dislocations is seen in figure 68(d), which corresponds to the faults of figure 67(b). Here the faults are out of contrast, but the intersection line AB is clearly visible.

As previously mentioned, very few extremely large grain boundary ledges (either pure or associated with a GBD) were observed. One of these cases of very large ledges (3000 Å or so) is seen in figure 69. Although the

Figure 69. Large grain boundary ledges showing strain enhancement, Cu, plastic strain of 3×10^{-4}.

Figure 70. Partial dislocation pileup against a grain boundary. Small white circles are objective arpeture images for dislocation character determination (main set of partials 30^{o} from edge).

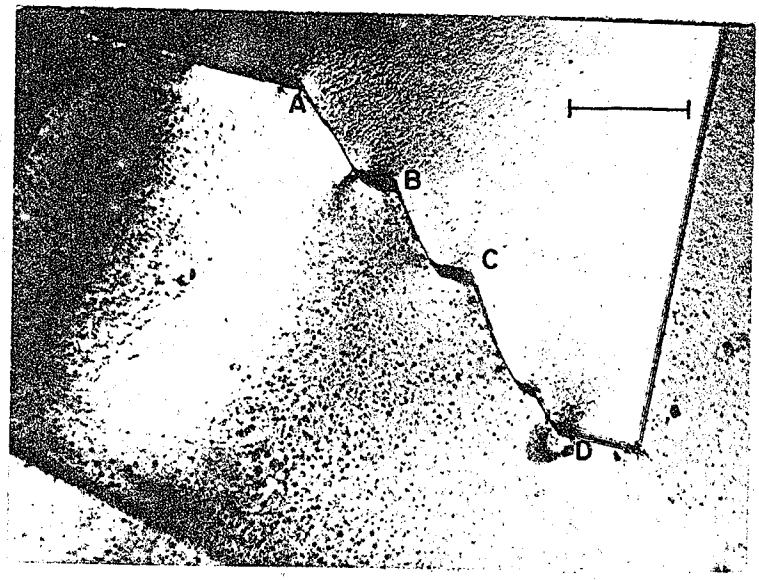
A
B
C
D

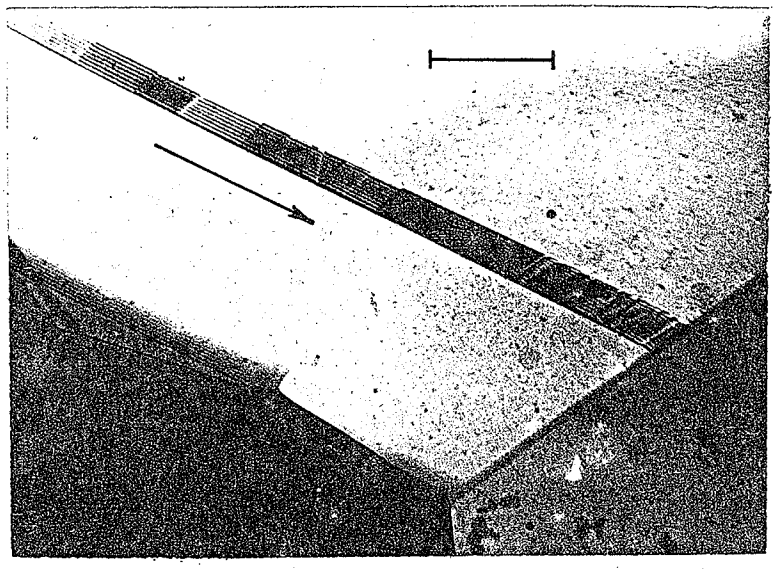

boundary resembles an annealing twin boundary, both extensive tilting and consideration of its placement relative to nearby grain boundaries demonstrated that it was almost certainly a grain boundary. This case is particularly notable in that strain concentrations at the corners of the ledges are clearly visible, yet no dislocation generation has occurred.

No cases were seen of the classical concept of dislocations piling up against a grain boundary and causing dislocation nucleation in the next grain. (It should be remembered, however, that few generated dislocations travelled completely across the grain). Pile-ups did occur (figure 70 - the end of the F_1 - generation of Map 9), but they showed no sign of causing any significant strain concentration at the boundary.

Finally, a few boundary generations were checked via the Kikuchi line technique. Figure 71 shows the diffraction patterns from the grain interior, along the boundary away from the generation and at the generation itself, for the F-defect of figure 67(c). Figure 72 shows patterns from a point on the boundary away from the sources of figure 65(c) and from a point adjacent to the right hand emissions. In both cases there are differences in some of the Kikuchi line widths that are detectable to the eye (particularly in figure 72). Figure 71 shows increasing

Figure 71. Selected area diffraction patterns for the F-defect of figure 67(c);

(a) in the grain interior

(b) along the upper right grain boundary away from the triple point

(c) at the triple point.

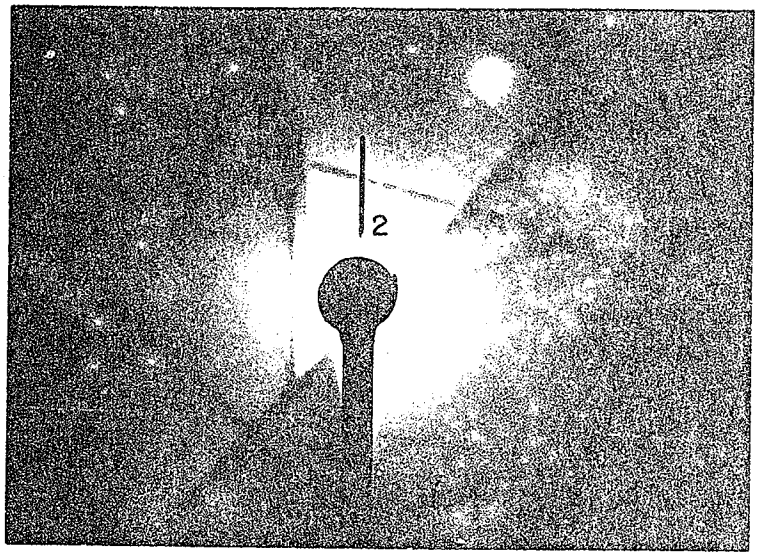

(a)

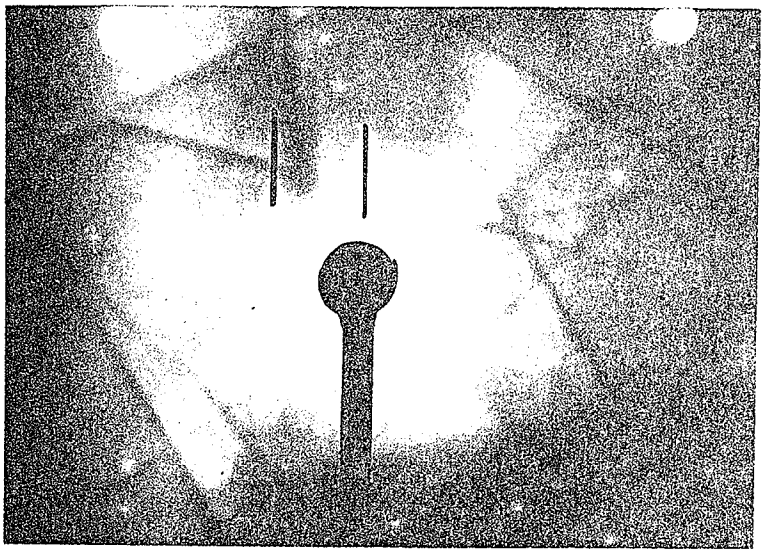

(b)

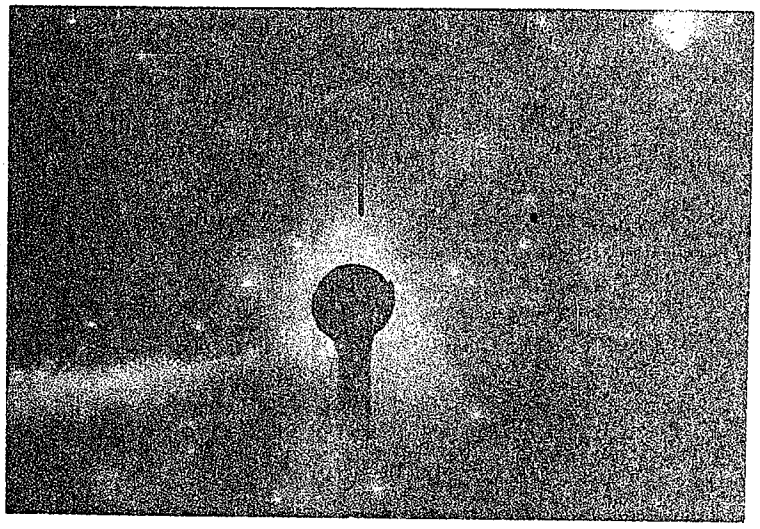

(c)

Figure 72. Selected area diffraction patterns for the P-defects of figure 65(c);

(a) along the grain boundary away from the source

(b) at the right - hand sources.

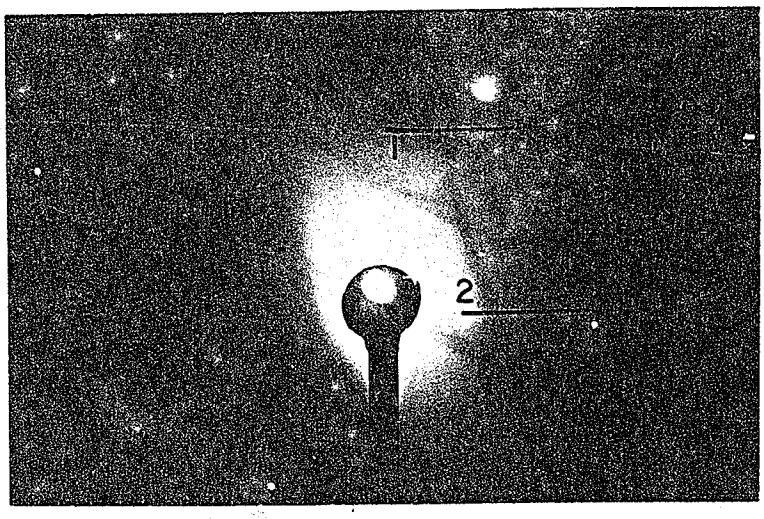
1
2

Figure 73. Densitometer traces across Kikuchi lines from figure 71;

(a) Traverse 1 - drive speed = 8.1 cm/min, chart speed = 6 cm/min

(b) Traverse 2 - drive speed = 1 cm/min, chart speed = 3 cm/min.

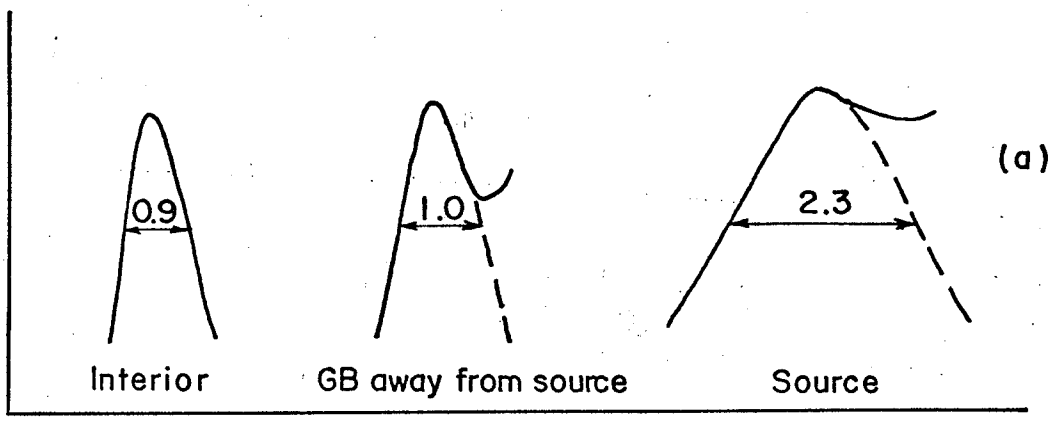
0.9
1.0
2.3
(a)
Interior
GB away from source
Source

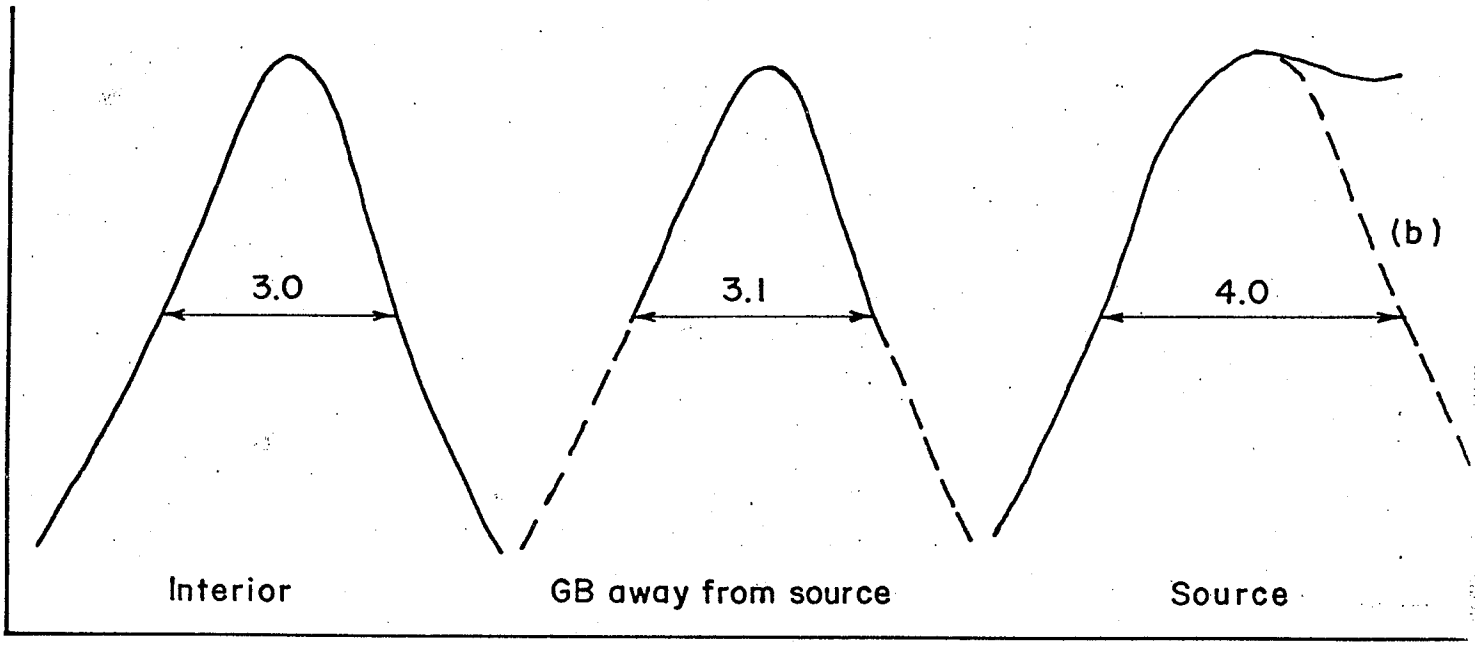
3.0
3.1
4.0
(b)
Interior
GB away from source
Source

Figure 74. Densitometer traces across Kikuchi lines from figure 72;

(a) Traverse 1 - drive speed = 8.1 cm/min, chart speed = 6 cm/min

(b) Traverse 2 - drive speed = 13.2 cm/min, chart speed = 6 cm/min.

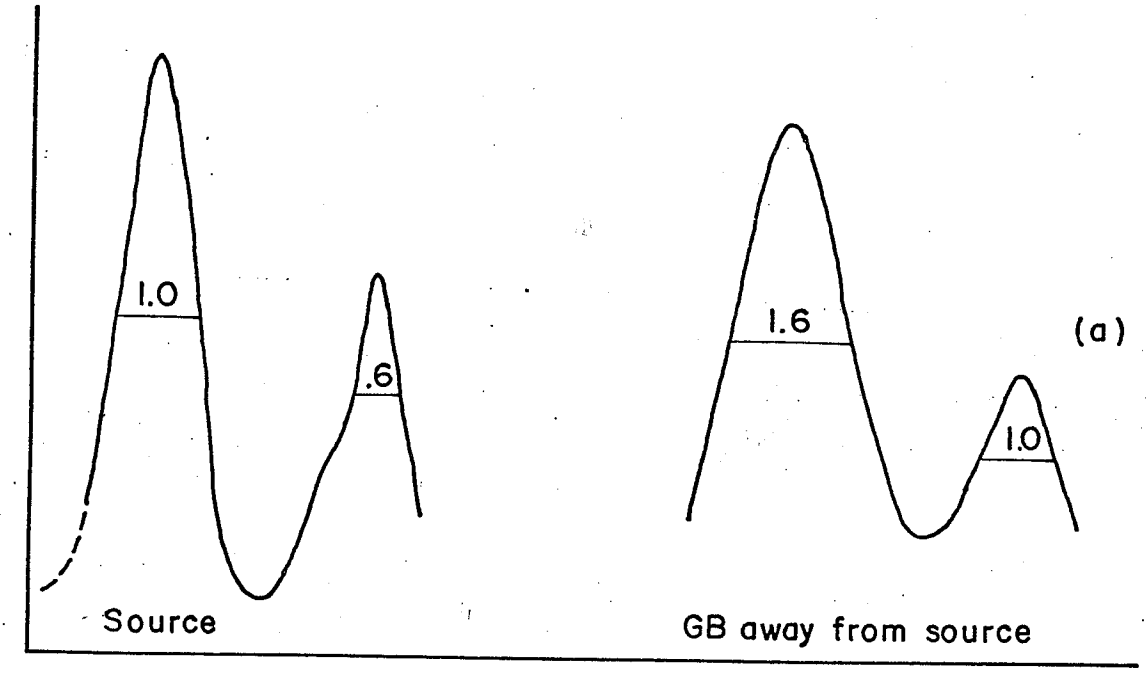
1.0
.6
Source
1.6
1.0
GB away from source
(a)

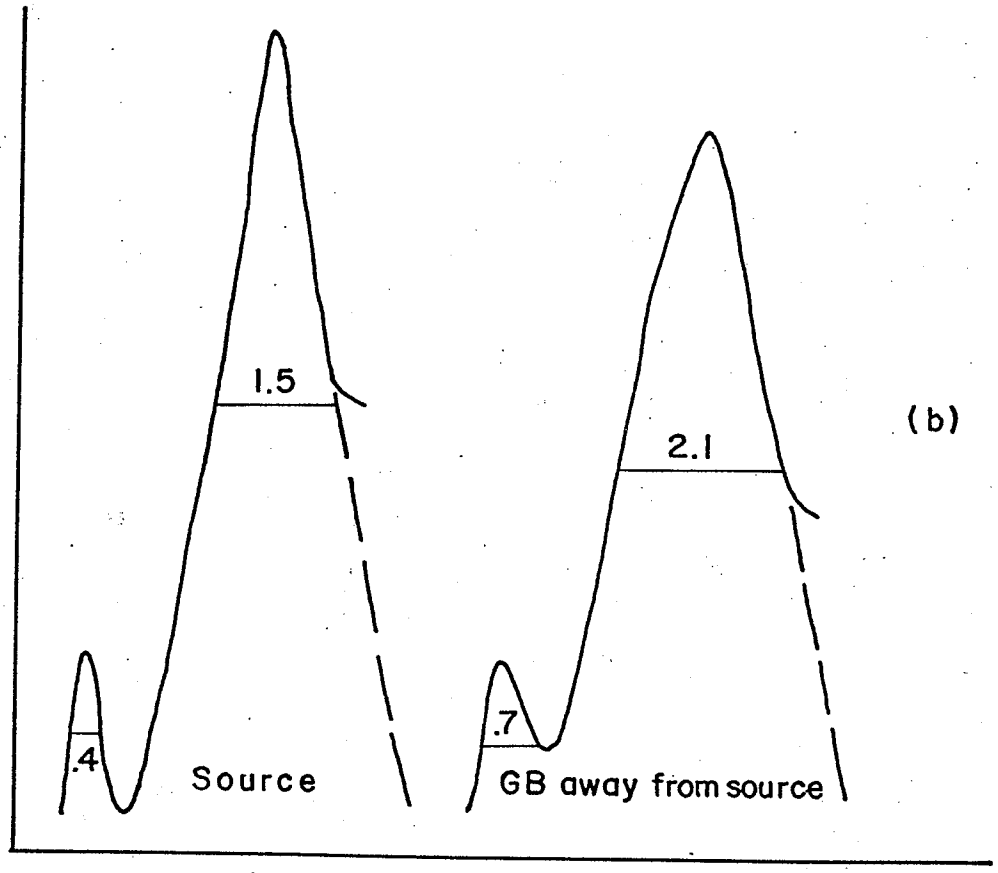
1.5
.4
Source
2.1
.7
GB away from source
(b)

width (and hence elastic strain) in the order grain interior, boundary away from the source and the source itself. This is not the case for figure 72 which shows a broader width for the boundary away from the source. To check these qualitative observations, a number of traverses were made over portions of the original plates on a densitometer. The results (shown in figures 73 and 74) confirm the visual observations. The locations of the traverses are indicated on figures 71 and 72. The few other instances in which this technique was applied showed much the same trend, that is, a decided increase in elastic strain from the interior to the boundary, but no definite trend on the boundary itself vis à vis the source and locations away from the source.

6 DISCUSSION

We have seen ample evidence for the generation of lattice dislocations from grain boundaries in the premacroyield region, the magnitude of this activity in different materials and the characteristics of individual boundary sources. We shall now examine the implications of this evidence with respect to several factors. These will include the validity of the dislocation generation models and stress concentration factors discussed earlier, the proportion of total strain contributed by emission of dislocations from boundaries, and the effect of various parameters, e.g. solute content, on all of these.

The conclusions based on this data will, in turn, be used to speculate on the finer details of boundary dislocation source operation and its role in deformation under different conditions. First, however, some comments should be made concerning the initial microstructures of the materials tested, since the number and distribution of lattice defects in this state will also affect yielding. Because of the boundary defect comparisons made at different strains and in different materials, the validity of the strain detection should also be commented upon.

6.1 MICROSTRUCTURES

At the outset, it should be pointed out that the basic criterion used for microstructure determination proved reasonably correct. That is, treatments leading to the presence of relatively high energy grain boundaries (from the point of view of both their intrinsic and defect structures) led to at least some grain boundary generation of lattice dislocations in all materials. That this included high purity FCC metals (the Cu and Al) tends to confirm the trend established in Table 3 that such generation can be a phenomenon which occurs in all metals under the right conditions. This mechanico-thermal principle of obtaining high energy boundaries entailed certain difficulties, such as the occasional presence of undesireable "debris" due to the somewhat less than complete recrystallization. These included, at various times, small unrecrystallized regions, semi-cellular dislocation walls, and a relatively high grown-in dislocation and annealing twin density. (The treatments used also precluded any accurate determination of solute segregation, as we shall see shortly.) The full anneals (complete recrystallization) required to eliminate this "debris" would likely have seriously impaired or eliminated altogether the boundary generation observed here, as noted at the outset of the experimental procedure.

6.2 TENSILE DATA

The tensile data of Table 10 was in reasonable agreement with literature values. Thomas and Averbach (201) found the yield stress based on 10^{-5} strain to be 1.7 kg/mm^2 for 99.999 Cu of 25 μm average grain diameter. For the same material, σ_A (the stress for earliest detection of plastic strain, roughly equivalent to σ_{my} in this study) was found to be 1.2 kg/mm^2. Using more sophisticated techniques, Bilello and Metzger (202) found that σ_A was roughly 0.3 kg/mm^2 for 50 μm 99.999 Cu. The value of σ_{my}=1.3 kg/mm^2 for Cu in this study is comparable to these σ_A values, considering the relative accuracies of the techniques involved, i.e. σ_A is expected to be substantially lower than σ_{my} since it is the stress at which load-unload microstrain loops fail to close, rather than a deviation from an elastic loading line which was itself often difficult to distinguish. Also, the strain sensitivity used in (202) was likely much greater than that obtainable in this study. Ni data for σ_A is somewhat scarce, but Holt (203) found a value of 0.25 kg/mm^2 for 48 μm Ni of identical purity to that used here. Considering that Holt's strain sensitivity was somewhat less than that of (202) (10^{-6} versus 10^{-8} for (202)), this would tend to confirm the result, seen in

Table 10, of σ_{my} for Ni being slightly lower than that for Cu, even though the flow stresses for the Ni were generally higher. It should be noted that Brown (204) also points out a similar anomaly for Cu, where OFHC Cu has a σ_A value more than an order of magnitude lower than Cu of substantially higher purity.

In Al, Rosenfield and Averbach (205) determined a yield stress at 10^{-6} strain of 0.6 kg/mm^2, again comparable to, if somewhat less than, the values found in this study. It should also be noted that modulus of elasticity values for all materials agree well with those of Tegart (206); for Cu, 12.5 x 10^3 kg/mm^2 (12.0 x 10^3 kg/mm^2 in this study), for Ni, 20.5 x 10^3 kg/mm^2 (26.4 x 10^3 kg/mm^2 here), and, for Al, 7.2 x 10^3 kg/mm^2 (9.0 x 10^3 kg/mm^2 here).

The point of these comparisons is to indicate that the strain detection was reasonably accurate for the purposes for which it was employed, i.e. comparisons of defect densities at a given plastic strain between different materials, and variations in defect densities in a given material at different strains.

6.4 CONSIDERATION OF THE MODELS FOR GENERATION OF DISLOCATIONS FROM GRAIN BOUNDARIES

The phenomenon of grain boundary dislocation generation may be examined from two major viewpoints. The first

shall focus on the individual source, the second on the contribution of the totality of these sources to the plastic deformation process. The separation between the two cannot be clearly defined since the former logically leads into the latter as the influence of various variables are considered.

We shall start with a consideration of the observed boundary sources in terms of the models reviewed earlier, particularly in terms of those characteristics that furnish the best chance of deciding which models are, or are not, viable (Table 4, p.86). Where appropriate, this viability (or lack thereof) will be commented upon in terms of the structural model of the boundary.

Regarding the Orlov models, there is no concrete evidence for emission of dislocations onto 2 slip planes intersecting at a ledge along the boundary. A few cases of two slip systems being activated were seen, notably F_{1-3} of Map 4 (p.179) and figure 64(g) (p.209), but neither could have been the operation of Orlov models as per the above characteristic since they did not share a mutual intersection line at the grain boundary. One might also speculate that the complexity of the Orlov models works against them. That is, the boundary imposes very rigid geometric restrictions on operations conducted within its rather narrow domain, particularly with regard to the continuity of atomic bonding across the boundary.

Therefore, the more complex the model (the more steps involved in its operation), the more likely it would seem to risk running afoul of these restrictions. The same lack of double emission rules out the Gleiter I model, although cross-slipping and tangling of the screw dislocations emitted by this source could easily mask such emission. The Price-Hirth model was not confirmed, despite its attractions as a relatively simple regenerative model. Only 1 defect analyzed for character was of a screw orientation, and that was the somewhat suspect P_2 defect of Map 15 (p.200). More important, no signs were observed of any of the compensating GBD's which are required for operation of this source.

There was limited evidence for the models requiring GBD glide, notably the Gleiter II model modified for generation of partial dislocations (54). This was the F-defect of figure 68(c) (p.213), in which there was a definite appearance of dissociated GBD's having moved along the boundary from right to left and piled-up at the twin-grain boundary intersection. At the head of this pileup, the GBD's may have either combined or dissociated into partial dislocations which were emitted into the interior (F_1 of Map 9) and GBD's (likely the trailing partials) which remained at that point. There is also evidence for the creation of other GBD's which moved a short distance further left along the boundary. In view

of the presence of a long length of defect-free boundary to the right of the pileup, no comment can be made on the origin of the dissociated GBD's. If they were present on the boundary in the annealed state, however, it is noted that the source could not be classified as regenerative, since there would be no obvious means of providing more GBD's. It should also be pointed out here that no other signs of GBD pileups were observed at kinks or triple points, even though some defects would have matched well with a pileup, e.g. the F-defect of figure 67(a) (p.212).

The Li model of edge dislocation generation was thus the only one supported by positive evidence in a large number of cases. The findings of Table 13 indicated a marked preference for edge dislocation generation. In addition, the Li model may be modified to account for dislocations of mixed character (as shall be seen later). Almost all defects emanated from what appeared to be ledge-dislocation associations. Although many sources seemed to demonstrate a regenerative nature (which the Li model does not possess), closer examination often showed this to be erroneous. For example, the ends of the generated dislocations of figure 64(d) (p.209) do not lie on a straight line, as should be the case if they were on the same plane, thus they must lie on planes some distance apart. This distance varied, but the largest separation

(between the third and fourth dislocations) was of the order of 300Å.

Two very good examples of the Li model appear to be the P_3- and P_4- defects of Map 14 (p.198). The P_3- defect may have been a case of the classical Li model in which the C-ledge was simply expelled into the grain as a lattice dislocation, leaving no defect contrast behind (although a small, pure ledge could have been present). The P_4- defect, on the other hand, appeared to have left behind a residual GBD on the ledge from which it originated. A similar operation to that of Li-type sources is, of course, the simple bowing out of pure GB segments as discussed in figures 30 and 31 (p.88). This is expected to occur occasionally, resulting in a single dislocation travelling into the interior (as with P_3 and P_4 above), but with no associated ledge at the boundary.

As noted in Table 13, a substantial portion of the dislocation generation can be of partial dislocations, a phenomenon which persists at relatively high strains. The stress orientation concept to explain this (54) has the advantage of being applicable to all cases, regardless of the type of source. Thus, even though it was originally conceived as an extension of the Gleiter II model, it can, in fact, be applied to any dislocation, nucleated or simply expelled from

the boundary, which posesses the proper orientation of Burgers vector. The 5 cases of such generation that were analyzed for character (Table 13) are all roughly 30^{o} from an edge orientation. Again, one must keep in mind the possibility that partials can disappear for values of $\bar{g}.\bar{b}\neq 0$, a fact complicated by the presence of overlapping faults in all 5 cases. Even considering this, the occurrence of such nearly-identical characters seems more than coincidental and may, in fact, be explained by slight modification of the stress orientation concept. This modification arises from the fact that, although there may be no direct component of the applied stress acting on the trailing partial of a dissociated pair, there will be an indirect component. That is, the stress, in moving the leading partial away from the trailing one, increases the faulted area between the two and therefore increases the attractive force between them which is due to the free energy of the fault. This will cause the trailing partial to move, providing this attractive force exceeds the lattice friction force before the stress for wide, non-equilibrium splitting of the partials is reached. (The analogy would be similar to pulling a cylinder across a surface, with another cylinder attached to the first via a rubber sheet.) There should be one case when even this attractive force should not be felt by the trailing partial, and that is for the case of the

trailing partial posessing a screw character. Since the attractive force of the faulted area acts normal to the dislocation line (figure 75 , it would be normal to the Burgers vector and not act upon the trailing partial. As seen in figure 75, this would then mean that the leading partials expelled into the interior should show a character of 30^{o} from edge, as was observed.

There would then be three classes of F-defects:

1) The one discussed above, where there is no significant effect of either F_{app} or $F\gamma$ on the trailing Shockley partial (S_T),
2) There is no effect from F_{app}, but the orientation is only close to screw, therefore $F\gamma$ has some effect,
3) Both F_{app} and $F\gamma$ have some effect due to the Burgers vector of S_T being slightly deviant from the ideal orientation in both respects.

Only 1) will produce a permanent separation (permanent until the direction of the applied stress changes due to grain rotation, etc.), while the F-defects produced by 2) and 3) will be increasingly less stable. This stability will be a function of the magnitudes of F_{app} and $F\gamma$ relative to the lattice friction force and any attractive force between the trailing partial and the grain boundary. (The latter will be discussed in more detail later). Thus the formation of

Figure 75. Illustrating the orientation of the Burgers vectors for the leading (S_L) and trailing (S_T) Shockley partials which are necessary for the creation of F-defects at grain boundaries.

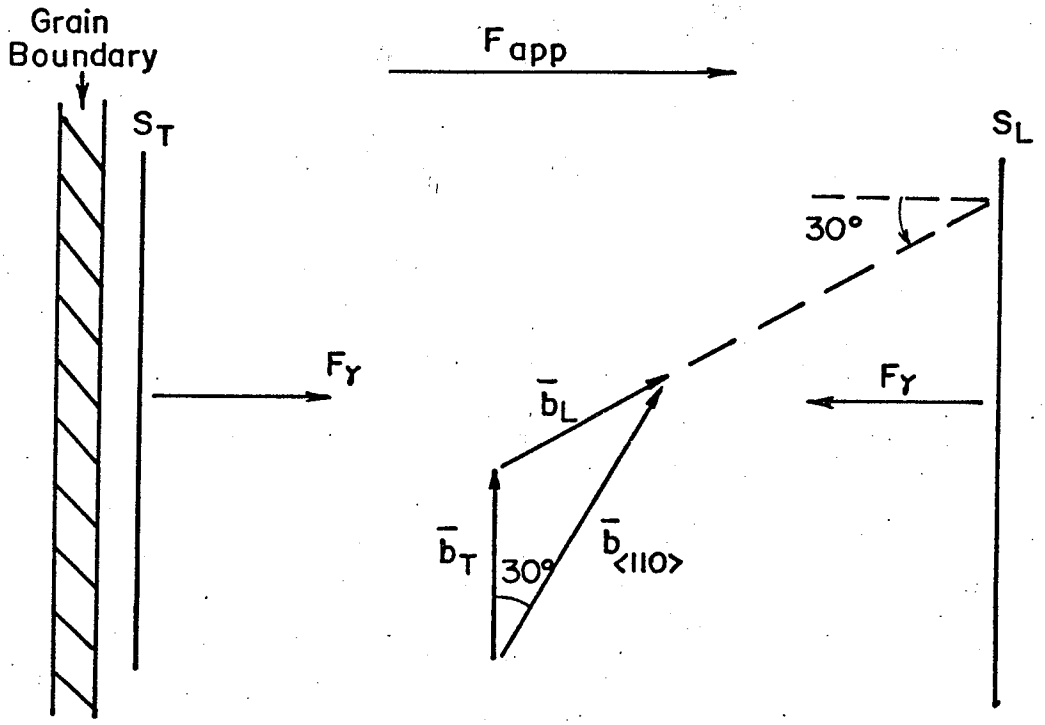
Grain
Boundary
F_{app}
S_T
S_L
30°
F_Y
F_Y
$\bar{b}_L$
$\bar{b}_T$
30°
$\bar{b}_{\langle 110 \rangle}$

F-defects diminishes with increasing strain. At the same time, it is obvious that the statistical probability of the orientations increases from 1) to 3). Thus many of the overlapping faults that do occur at lower strains will "unfault" at higher strains. Counteracting both of these trends to some extent would be the tendancy for more F-defects with increasing strain as more boundary sources become operative and the number of favorable stress-Burgers vector orientations increases. The result would be a peaking of the proportion of F-defect occurrence at some intermediate strain, which was indeed observed (Table 11).

Summarizing to this point, there was substantial evidence for the operation of boundary source models of a nonregenerative nature, but very little for those of a regenerative nature. This does <u>not</u> rule out the existence of regenerative sources, since the absence of identifying characteristics can always be explained. (For example, the compensating GBD's required for the Price-Hirth model could easily dissociate into the IGBD network, effectively rendering them invisible.) What does appear to have been established, however, is that regenerative sources play a very minor role in low temperature grain boundary generation of dislocations.

6.4 CONSIDERATION OF STRESS CONCENTRATION FACTORS

In examining the evidence for stress concentration factors, it should be reiterated that such concentration is necessary, i.e. the experimental observations indicated that dislocation nucleation accounted for the major portion of boundary source operation. This was particularly clear in the Al, which posessed defect-free boundaries in the annealed state, yet showed defected boundary segments and dislocation generation therefrom in the deformed state. For the Cu and Cu-1Sn, the density of boundary defects (GB-segments) in the annealed state was not sufficient to account for any substantial portion of the sources observed, even with the unrealistic assumption that all these boundary defects were GBD's capable of simply moving off the boundary as lattice dislocations. In addition, there were substantial increases in the number of GBD's (as seen in GB-segment increases) before the operation of boundary sources into the grain interior, pointing to nucleation of GBD's in a fashion similar to lattice dislocations, as suggested by Tangri and Tandon (182). At the same time, the stresses at which such nucleation must have occurred indicated that total enhancements of the order of 50 for Cu-1Sn, 60 for Cu, 100 for Ni, and 110 for Al were required.

As already noted, there was no evidence to indicate

a substantial or widespread stress concentration due to GBD pileups, i.e. K_n. There were some configurations (figure 57, p.173, $GB_{1,2}$ of Map 14, p.198) which, by their semi-regular distribution of defects, indicated movement of boundary dislocations (pure GBD, C-ledge or G-ledge). However, their presence in annealed material as well as deformed, and their extent over boundary lengths of the order of several microns (regardless of boundary curvature), suggests the involvement of non-conservative movement in their formation. This would indicate formation during the heat treatment.

There is also no concrete evidence that elastic anisotropy (K_E) plays a major role in boundary source operation. If maximization of this factor was critical for the operation of large numbers of boundary sources, the following should be observed (as described in sec.3.3.3):

1) A tendancy for sources to emit dislocations into the smaller grain of a pair of grains where there is a large size disparity. (Resulting from a maximization of equation (2),p. 104). No such tendancy was observed, although isolated examples of this and the opposite behavior were both seen (P_1-Map 3, p.178, for the former, and figure 66(d), p.211, for the latter),
2. A tendancy for the active sources to be located on boundaries parallel to the stress axis and very seldom on those

normal to it, since the stress differential should only occur across the former and be zero across the latter. This was not observed, although irregular boundary curvature and uncertainty of the stress axis orientation would have made such a trend more difficult to detect. As a rather more accurate check, a brief study was made of micrographs of etch-pitted Fe-3Si (K_{Emax}=2.14), that had been stressed(137) into the premacroyield region and had yielded by operation of grain boundary sources. The location of the stress axis on the micrographs was accurately known. No trend was discovered - 12 active boundaries were roughly normal to the stress axis, 7 were parallel and 8 were of a mixed nature. If anything, the boundaries normal to the stress axis gave the qualitative impression of having the highest source densities,

3) Generation of dislocations into the elastically harder grain of a grain pair. (This is where the higher stress occurs, cf. figure 32, p.103). For the three cases in which this was done by estimating the crystallographic direction along the stress axis, the results were inconclusive, with one pair having the sources in the harder grain, one having them in the weaker grain, and one with both grains having the same elastic hardness.

The effect of K_E should not be entirely discounted since

(unlike the case for K_n) it is a factor that is always present to some degree. This degree may be influenced by the amount of texture in the material, and it should be pointed out that a high percentage of {001}<001> cube recrystallization texture was likely present in the Cu and Cu-1Sn (207). This may have produced many grain pairs with both grains being oriented close to <001> in the direction of the stress axis, thus minimizing their elastic hardness differences and hence, K_E.

This appears to leave K_G as the principal stress concentration factor, without which substantial grain boundary dislocation generation would have been impossible. Unfortunately, concrete evidence was somewhat scarce for this factor as well. There was ample observation that boundary sources accounting for a large majority of boundary dislocation generation were located at defects showing contrast characteristics indicative of ledges. Unfortunately, these ledges were seldom actually seen, either through fringe displacement or a macroscopic change in the plane of the boundary. Since the fringe displacements would be greater than the actual ledge height due to geometric distortion (59), lack of observation of any such displacements indicated the ledges were rather small. For a representative magnification of X30000, moderate geometric distortion and assuming displacements greater

than 1mm may not have been visually detected, a maximum ledge height of 150 - 200 Å for the boundary sources is obtained. At the same time, some very large ledges were seen (figure 69, p.218, height ∿3000 Å) from which no generation occurred, even though boundary sources were observed elsewhere in the foil. Such cases will also have to be considered in the formation of a more detailed model of boundary sources.

It should be noted, at this point, that both the Li-type model and K_G, as the principal source model and stress concentration factor respectively, fit well with the physical model of boundary structure. Thus, this model predicts that ledges are not only always present on grain boundaries, but that for the type of mechanico-thermal treatments used here, they should be present in numbers far greater than any other boundary defect.

6.5 EFFECTS OF MATERIAL PARAMETERS (SFE, etc.) ON BOUNDARY SOURCE CHARACTERISTICS

It would now seem appropriate to broaden our consideration of individual boundary sources to include the effects occasioned by the differences in SFE, solute, elastic anisotropy and initial boundary defect density, for the materials tested.

There is a decided difference in the matrix SFE of, on the one hand, the Ni (220ergs/cm^2 (208)) and the Al

(163 ergs/cm^2 (208)), and, on the other hand, the Cu (41 ergs/cm^2 (209)), and the Cu-1Sn (a few percent less than the Cu (210)). This appeared to effect boundary sources in two respects. The first relates to the incidence of F-defects, with none observed in the Ni and Al, and many observed in the Cu and Cu-1Sn. This may be explained in terms of the model for emission of partial dislocations from grain boundaries discussed earlier. That is, the SFE has been observed to decrease greatly very close to an interface (150 - 152). It would seem reasonable that the value to which it decreases be somewhat proportional to the matrix value of SFE. If this is the case, the permissible deviation of the trailing partial's orientation from pure screw which would still allow wide separation, should decrease as the SFE adjacent to the boundary increases. In other words, the Ni and Al would require orientations very close to pure screw to produce an F-defect, while the Cu and Cu-1Sn would tolerate a much wider range of orientations.

The effect of SFE was also apparent in the longer distances the partial dislocations travelled into the grain interior (Table 13, p203). This may be explained by consideration of the previous model of F-defect formation. It is apparent that the formation of an F-defect requires

a larger stress than that for a P-defect because of the attractive force due to the increased separation. The additional stress has been estimated by Tangri et al (179) as G/170 for Cu and G/70 for Ni, a rather sizeable value. Thus, after a perfect dislocation is nucleated to relax a stress concentration, it may be propelled into the grain, overcoming lattice friction and any attractive forces with the boundary as it does so. For a leading partial dislocation, however, such emission is delayed until the above additional stress is added. Thus when the partial is, in effect, "released", it will be under a greater impetus than that experienced by the perfect dislocation and will travel correspondingly farther.

It is somewhat puzzling that a large difference exists in the proportion of partial dislocation generations for the Cu and Cu-1Sn (24% and 6%, respectively) in view of their similar SFE's. This difference may be ascribed to the presence of solute/impurity atoms at the grain boundary. This presence has often been quoted as making the movement of boundary defects more difficult during annealing, thereby stabilizing them, e.g. Li and Chou (211). Thus there would be more relatively high energy boundary defects in the Cu-1Sn than in the Cu, i.e. more defects which could emit dislocations at a given stress. Counteracting this, however, is the fact that this same solute concentration

could hinder the dislocation emission through pinning. The former consideration would mean that, in the Cu-1Sn, the extra stress needed for F-defect creation at some ledges made such sites unattractive for operation in view of the large number of sites available. In the Cu, on the other hand, the smaller number of available sites meant that many F-defects had to be created to contribute the proportion of the total strain required from the boundary. The latter consideration would explain the density differences for both GB-segments and the total of F- and P-defects in the Cu and Cu-1Sn at ε_p = 3 and 7 x 10^{-4}. That is, at ε_p = 3 x 10^{-4}, the relatively fewer Cu sources could nonetheless generate more readily and therefore were observed in greater numbers, while at ε_p=7 x 10^{-4}, the much more numerous Cu-1Sn sources had finally overcome the pinning of the solute and thus greatly outnumbered the Cu sources. There was substantial variation in the degree of elastic anisotropy amongst the metals tested, with Cu (and likely Cu-1Sn) having a maximum K_E of 3.08, that for Ni being 2.26 and that for Al being 1.20 (97). A major role for this parameter could have accounted for the fact that the incidence of confirmed boundary sources in Al was very low, but the different heat treatment for that material had unfortunately given it a markedly different boundary defect density and solute distribution than the

other metals. The treatments were similar for the Cu and Ni, yet the Ni showed a higher source density than the Cu, indicating that some factor other than anisotropy was responsible for the difference. As mentioned previously, elastic anisotropy produces maximum stresses at triple points, but it should be pointed out that the increase over the K_E value obtainable elsewhere on the boundary appears to be only of the order of 5 - 10% (176 - 178). If this additional enhancement, small as it is, resulted in a preference for triple point generation, the relative proportions should decrease in the order of Cu, Cu-1Sn, Ni and Al. Table 13 shows that the respective proportions were actually 43%, 21% and 37% for Cu, Cu-1Sn and Ni, again indicating the presence of other factors (the Al had too few defects for a meaningful comparison). Perhaps all that can be safely predicted with regard to anisotropy is that, other factors being equal, increased elastic anisotropy will produce more boundary source operation, likely with a higher proportion from triple points.

The difference in initial boundary defect density appears to be the principal cause for the high density of activated sources in Ni and, at the same time, the cause of the reduced number of dislocations generated and the reduced distances they travelled. That is, there were likely many C-ledges and random GBD's on the annealed Ni

boundaries that possessed lattice dislocation Burgers vectors. These could have been emitted into the grain interior at quite low stresses, since dislocation nucleation was not involved in their emission. This would help rationalize the relatively low stress at which boundary generation occurred in Ni (as indicated by σ_{my} or σ_A values), with the high total enhancement factor (~100) needed for boundary dislocation nucleation in that metal. Such nucleation might still have occurred, e.g. P_1 of Map 12 (p194), but it would have been relatively rare, as was observed. This is by no means a linear phenomenon, that is, increasingly higher initial defect densities on the boundaries will not necessarily lead to increasingly greater ease of boundary generation. As the defects become more numerous, a point will be reached where mutual interactions will prevent their emission from the boundary and render boundary source activation more difficult, not less.

6.6 BOUNDARY GENERATION IN THE PREMACROYIELD REGION

The previous considerations of boundary sources and the parameters influencing the operations of these sources now enables a more comprehensive picture of the premacroyield region to emerge. First, however, it should be noted that the marked independence of strain shown by dislocation emission from annealing twin boundaries would

indicate that it was primarily due to either foil handling or the heat treatment and thus will not be commented on.

For the Cu, the initial state of the boundaries was one of a comparatively low density of defects (Table 11, p.170) which were nonetheless capable of dislocation generation at rather low stresses. Thus the first plastic strain, from σ_{my} to $\varepsilon_p = 1 \times 10^{-4}$, (Map 2) was likely contributed by a combination of generation from the most favorable of these sources (hence only P-defects were observed and a high percentage of them were from triple points), along with movement of favorably oriented segments of the grown-in dislocation network in the grain interiors. Other boundary sources nucleated dislocations which did not travel into the grain interior, producing an increase in the density of GBD's (GB-segments). At a plastic strain of 3×10^{-4} (Map 3), all three of the above had increased. The GB density increased more than the total F- and P-defect density since, if the "emission" sources only form a small fraction of the "nucleation" sources, any increase would lead to an increasing disparity in total numbers. Dislocation multiplication occurred in a few grain interiors (IA defects). At 5×10^{-4} strain (Map 4), the GB density had again risen dramatically. Emission of dislocations from grain boundaries had become more widespread and showed

signs of occurring preferentially in certain regions (as had been seen for the GB-segments at lower strains). A larger portion of the emissions was of partial dislocations and the prominence of triple point activation was reduced as more and more sources on the boundaries between triple points became operative. The interior activity became more intense in nature. As the strain further increased to 7×10^{-4} (Map 5), many of the overlapping stacking faults (F-defects) unfaulted, greatly reducing their density. At the same time, many interior segments were multiplying, thus a smaller proportion of the strain was required from the boundary region and the source density there remained relatively constant, with new source activation only required to offset those sources exhausting themselves (due to their non-regenerative nature). The IA-defects were located in the same general regions, indicating (as did the boundary sources) a non-homogeneous distribution of yield initiation sites. The strains of 1 and 5×10^{-3} (up to and past the macroyield point - Maps 6 and 7), merely confirmed the increasingly minor slip contributions of grain boundary sources. However, there was ample evidence to indicate that such generation still occurred, but was generally much harder to detect due to the masking effect of widespread interior activity in almost all grains.

It must also be kept in mind that at least some of the interior activity could have resulted from boundary generation, yet would have been undetected because of the boundary source(s) exhausting themselves, i.e. there would have been no configuration of emitted dislocations to indicate the connection between grain boundary and interior dislocation tangle.

The transition of the yield process from markedly non-homogeneous (e.g. Map 5) to homogeneous (Map 7) during premacroyielding, appears to confirm a type of two-stage yielding model, as suggested by Bonfield and Li (131). The first stage consists of movement of grown-in dislocations, grain boundary generation and subsequent work hardening in a small percentage of grains. This would have taken place from the microyield point to approximately $5 - 7 \times 10^{-4}$ in Cu (note the change from 10% to 50% activated grains between these 2 strains, Table 11). The second stage consists of dislocation multiplication within many grains (mainly through activation of interior sources in the case of Cu). Yield initiation does <u>not</u> spread via the classical dislocation pile-up - propogation model, which has been increasingly questioned as having any integral part in the yield process (120, 211).

Thus, for the Cu, the overall role of grain boundary sources in the premacroyield region is rather difficult to

ascertain. Boundary sources were certainly instrumental in the first portion of this region, wherein a small percentage of grains yielded, but it is very difficult to accurately determine their influence in the latter portion, where the remainder of the grains were activated. In view of the high purity of the material and consequent high mobility of the grown-in dislocations, the influence of grain boundary dislocation generation in this latter portion was not likely very great.

This was not the case for the Cu-1Sn, where the presence of the Sn solute produced higher stresses than in the Cu at a given strain, resulting in a marked σ_{my} and flow stress increase. The σ_{my} increase (2.5 times that of Cu) resulted from the combination of partial solute pinning of grown-in dislocations and relatively few boundary sources which could operate at low stresses. (The latter resulting from the solute pinning of nucleated dislocations, as discussed earlier). By the 3×10^{-4} strain (Map 9), a number of the sites of lowest operating stress had been activated, providing roughly the same strain contribution as in the Cu at this strain. The GB-segment increase, on the other hand, was much less than in the Cu, probably due to the solute atmospheres at the ledges making nucleation more difficult. The increase in flow stress was thus primarily due to the greater stress required to unpin and

move the most weakly - pinned segments of the grown-in dislocation network. The indications of roughly similar proportions of the 3×10^{-4} strain contributed by boundary and interior sources for the Cu and Cu-1Sn would predict similar IA - defect densities (and characteristics), as was the case for the boundary sources. That this was not seen for the IA densities (Table 12), demonstrates that most of these defects in the Cu-1Sn were therefore portions of the grown-in dislocation network and not due to dislocation multiplication within this network caused by the applied stress.

By the 7×10^{-4} strain (Map 10), it was apparent that boundary source operation was playing a major role in the yield process, i.e. there were a large number of active boundary sources and no apparent increase in interior dislocation activity. The distribution of sources was more non-homogeneous than in the Cu, as shown by the number of sources along the grain boundaries of figure 64 (p.209). The boundary sources likely provided the impetus for the onset of macroyielding, as shown in the widespread boundary and interior activity occurring at the same strain in a different region of the specimen (figure 59, p.189). Some interior multiplication from the grown-in network could also be expected by this stage. With the stronger pinning and higher equilibrium segregation furnished by a furnace-

cooling treatment, the observed yield drops in Cu-Sn alloys (212) could be explained as the sudden activation of a very large number of boundary sources.

The Ni and Al were only tested at the one strain of 3×10^{-4} ($3 - 5 \times 10^{-4}$ in the Al). It was apparent that the Ni first yielded primarily through emission of single dislocations from the boundaries, but, by the 3×10^{-4} strain (Map 12), interior movement and multiplication, along with some boundary source operation, accounted for substantial portions of the strain. The boundary defect density, which was initially high, had increased greatly, and these defects would likely have interfered with source operation at higher strains. The Al was not at all suited for grain boundary dislocation generation, since there was no pinning of the grown-in network and no sources with a low operating stress on the boundaries.

Thus the movement and multiplication of interior dislocations governed yielding from the outset, although the small, unrecrystallized regions may have had some influence on σ_{my} and the work hardening behaviour. However, it is indicative of the pervasiveness of boundary sources that some bona fide nucleation of both GBD's and lattice dislocations still occurred (P_{3-6}, Map 14, p.198). The TP_1, P_1 and P_2 - defects of Map 14 and those of Map 15 supply many intriguing prospects (e.g. for higher temperature

source operation), since they were unquestionably boundary sources, but the uncertainty of their origin would make commenting on these prospects particularly hazardous at this time.

6.7 CONSTRUCTION OF A MODEL FOR GRAIN BOUNDARY DISLOCATION SOURCES

To this point we have established the major type of boundary source (Li-type) and the major stress concentration factor (K_G) resulting in source operation. We have described the role played by the operation of these sources in the yielding of several materials and the influence of a number of parameters on that role. In constructing a more detailed model of these sources, it must be kept on mind that use of the word "source" does not necessarily imply a regenerative nature.

The basic factors which a source model must take into account are that boundary sources operate at stresses requiring concentration factors of the order of 50-100, and do so from quite small ledges or ledge-dislocation combinations. Table 6 (p. 117) indicates that the maximum K_G obtainable at a ledge of 100 Å height is about 15. Thus even with a maximum K_E factor of 2 or 3 present, the total enhancement is 30-45, and some additional enhancement will be necessary.

One possible means of providing this is through a variable value of the ledge root radius, r, since the ledge height appears to be limited. Such an argument would be supported by the relaxed structural unit model. This model indicates that the detailed structure of a ledge corner is governed primarily by the relaxation of atoms into the lowest

energy configuration as the different structural units " mesh " at the ledge corner. The units involved and the ledge geometry are a function of the misorientation between the two grains and the location of the boundary between them. Both of these, in turn, are a function of the mechanico-thermal treatment. Thus, a non-homogeneous distribution of grain misorientations and boundary orientations would imply a similar distribution of the ledge root radii. This would then logically account for the operation of certain boundaries before others, and the preferential occurrence of active boundaries in localized regions, both a result of the non-homogeneous nature of the mechanico-thermal treatment. The difficulty with unlimited variation of the ledge root radius is that, on a ball model of atoms, it could decrease (theoretically) to an extremely small value at the juncture of the two atoms at the ledge corner. This would produce very high stress concentrations at virtually every ledge. There would then be nucleation of dislocations at every ledge on every boundary, which is not observed. A possible resolution of this difficulty would be a lower limit of roet radius, with variations only above this value (so that the non-homogeneous distribution of sources could still be accounted for). In this regard, Tegart (213) has

stated that this should be the atomic spacing, approximating to the large dashed circle of figure 76. Another reasonable possibility would be that of the small dashed circle of figure 76, which is approximately the size of the octahedral interstitial hole located immediately to the right of this circle. A similar possibility would be the tetrahedral interstitial hole (which is not in the plane of figure 76).

Since this still leaves a maximum K_G factor of around 15, the additional stress concentration must originate elsewhere. A significant portion of this could come from the interaction of closely-spaced ledges of finite dimensions, i.e., where the approximation to a semi-infinite solid is no longer valid. Thus the value of K_G for a given ledge would be enhanced by the presence of nearby ledges. This would occur in groups of ledges, such as at A and C of figure 77 and not at isolated ledges such as B and D.

These configurations would then account for the non-aligned nature of the dislocations observed at many generation sites (figure 64d, p.209, figure 65c and 65d). They would also explain the broad contrast of the GBD-macroledges from which these dislocations often emanate as being due to residual GBD's at each ledge or dislocations which had been nucleated, but had not left the boundary, e.g., source C, figure 77 shows one example of the latter.

Figure 76. Illustrating a <100> grain boundary ledge in the FCC lattice with possible root radii of either the atomic radius (large dashed circle) or that of the small dashed circle. The latter is approximately that of the octahedral interstitial hole (after Tangri, 214).

Figure 77. Schematic illustration of dislocation emission at groups of small grain boundary ledges under an applied stress, τ. Source A is exhausted, while source C is not.

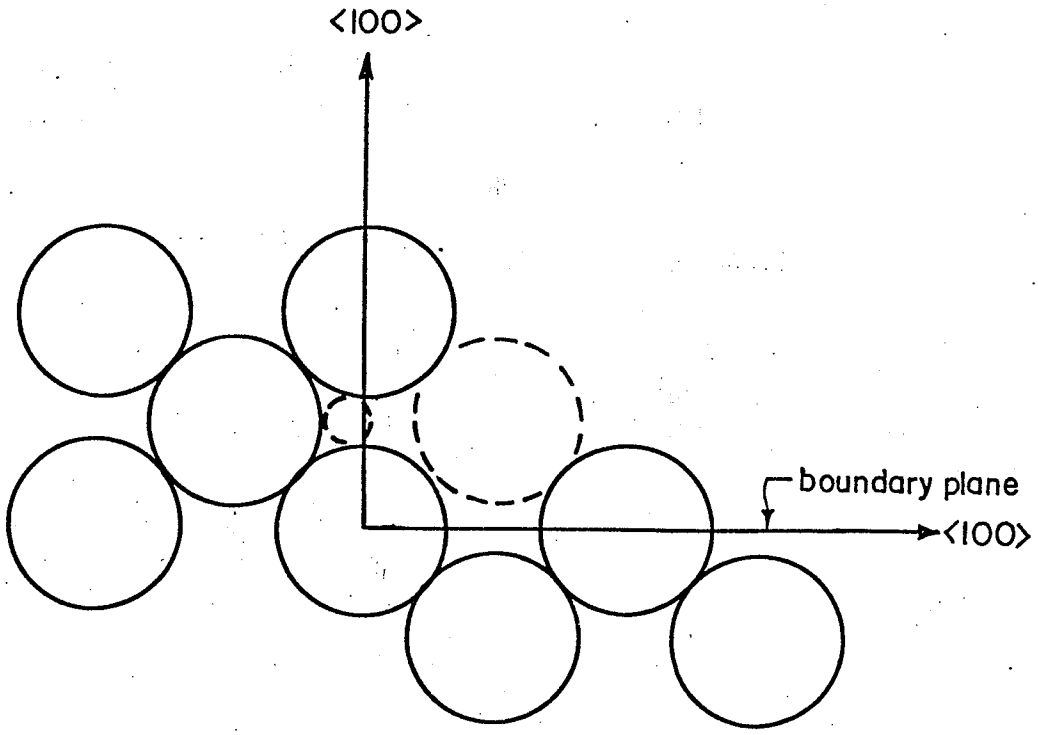
<100>
boundary plane
<100>

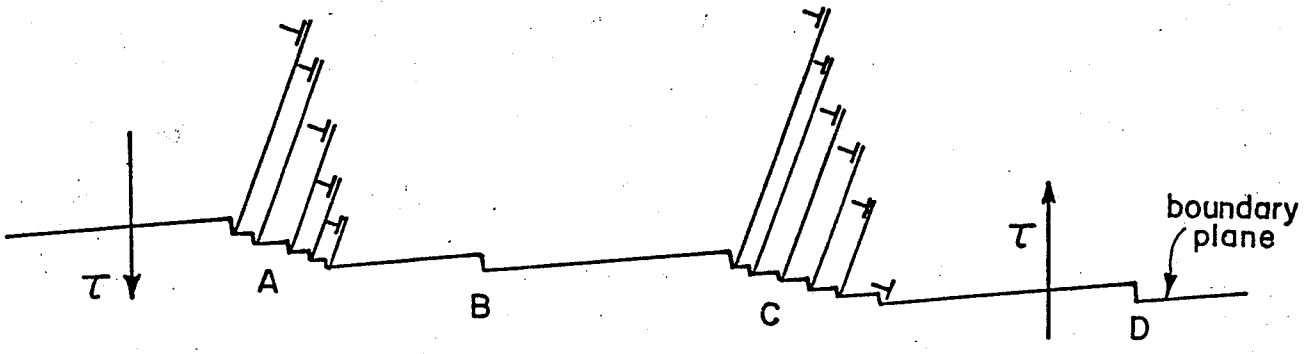
τ
A
B
C
τ
boundary plane
D

Further enhancement would come from K_E, which would normally be present to some degree in an anisotropic material, and possibly even from K_n, but not in the manner discussed previously. This K_n might arise from 2 or 3 glissile GBD's piled-up at each ledge corner such that a cumulative pileup effect is felt (at B in figure 78) which results from all the GBD's in the configuration. Since these GBD's are not all in the same plane and are separated into small groups, the effect would not be as intense as for the normal case of a dislocation pileup on one plane. Glide of these GBD's would be easier than in the lattice if the Peierl's-Nabarro force along the boundary plane was less. A reduced shear modulus along the boundary plane would indicate this, since the Peierl's-Nabarro stress is directly proportional to G. We know that the boundary region is one of some disorder and we also know that G can decrease substantially with increasing temperature, e.g., by as much as a factor of 10(215). Since increasing temperature results in increasing disorder in the perfect lattice, there may be an analogy between the reduction in boundary modulus and that due to temperature. Even if such an analogy were only partially correct, the modulus reduction could be significant. It should be noted that the Peierl's-Nabarro stress increases with decreasing dislocation width (and hence decreasing

Burgers vector). Thus GBD's of larger Burgers vector would be moved more easily.

The combination of these various additional stress concentration factors (enhanced K_G, K_E and K_n) could produce total concentrations of 15 ÷ 135, even if each were only of the order of 1 - 3, using the original K_G value of 15. It must be remembered that the enhanced stress would consist primarily of the component due to K_G and, as such, would decrease to approximately the value of the applied stress at a distance from the boundary of the ledge height.

It might be pointed out here that the Kikuchi line technique (p.219) appears to hold promise in the gross detection of the elastic strain due to these concentrations. The preliminary attempts in this study demonstrated that the boundaries, as expected, possessed higher elastic strains than the interior. More important, the tests detected variations in this strain along the boundary. This would furnish a means of distinguishing between sources which were exhausted (the strain relaxed below the level of the rest of the boundary, figure 72) or those which could generate more dislocations (a strain level above the rest of the boundary, figure 71). Refinements of this technique could also lead to the possible identification of sources of high potential before they are activated.

One possibility that should not be discounted is the presence of GBD's at ledge corners triggering the nucleation process. That is, the intense strained region near the core of the GBD might supply the final impetus needed to shear the atomic bonds at the ledge corner, which would be already severely strained by the concentrated applied stress. Distinguishing such GBD's would be very difficult because they would provide much the same electron microscope contrast as that provided by nucleated dislocations which had not left the boundary or by compensating GBD's (both of which are discussed next). All of these would have been classified as GBD-macroledges in this study.

Figure 79 demonstrates the need for compensating GBD creation with nucleation of lattice dislocations at pure ledges (figure 79a). Such GBD's may be of C-ledge character (figure 79b) or possess both C- and G-ledge character (figure 79c). The only other possibility is for nucleation into <u>both</u> grains (figure 79d) if the slip planes in each were suitably aligned with the ledge. This would be a rather rare occurrence, but possible examples may be the (d) micrograph of figure 19(e)(p.68), or the P_{17}-defect of Map 10 (p.190), with A indicating the dislocation being emitted into the neighbour grain to P_{17}. It should be noted that these double emissions would appear more often in etch-pit studies because

Figure 78. Illustrating the possible pileup effect of glissile GBD's at closely spaced ledges under an applied stress, τ, such that the effect is maximized at ledge B.

Figure 79. (a) Pure grain boundary ledge, AB.
(b) Lattice dislocation generation with C-ledge compensating GBD.
(c) Dislocation generation with both C- and G-ledge compensating GBD's.
(d) Dislocation generation into both grains.

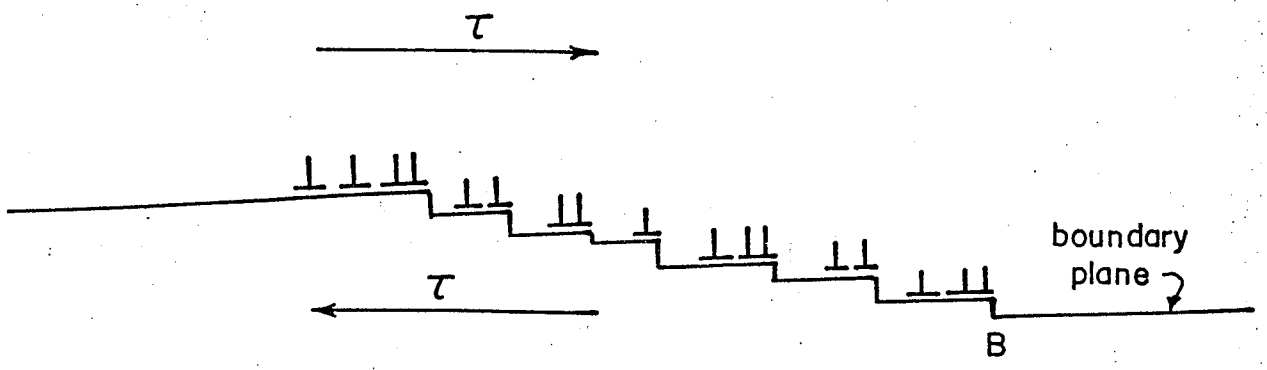
τ
boundary plane
τ
B

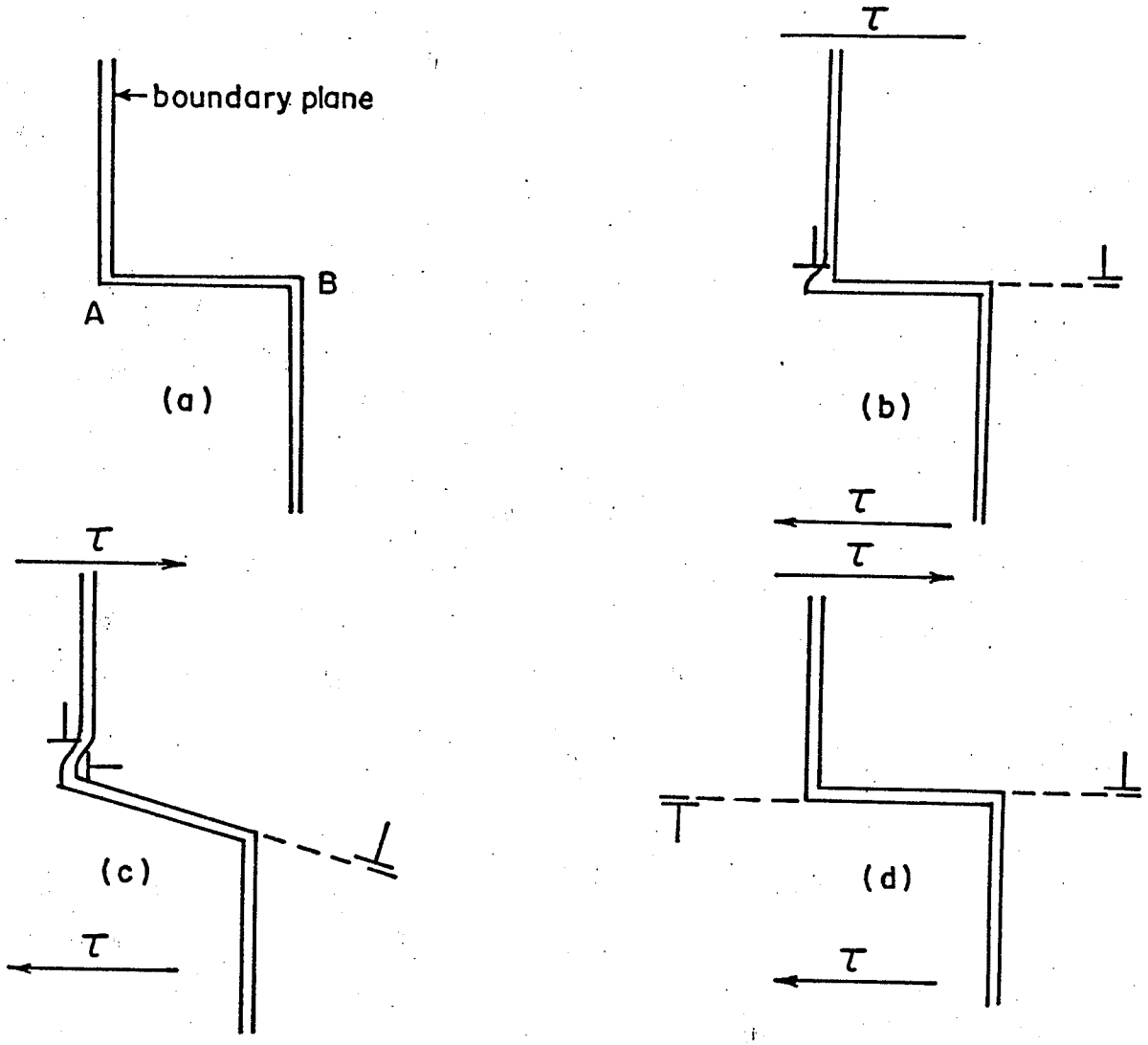
boundary plane
A
B
(a)
τ
(b)
τ
τ
(c)
τ
(d)
τ

the low optical magnifications used would not distinguish between adjacent sources (such as figure 64c). Nucleation of mixed character dislocations could arise from the applied stress acting at less than 90^{o} to the ledge length (which is out of the plane of the paper).

As previously mentioned, Table 12 (p.202) indicates the Cu and Cu-1Sn possessed similar boundary defect densities in the annealed state, as shown by GB-segment densities. At the strain of 3×10^{-4}, the boundary source densities were also similar, but the GB density was markedly higher in the Cu. This could be a consequence of the reduced shear modulus leading to a reduced value of nucleation stress (G/25 - G/50) in the vicinity of the boundary for the Cu. This lower stress should mean that many dislocations would be nucleated at ledges in the Cu at low strains. A large portion of these would not have sufficient impetus to escape the "capture cross-section of the boundary", i.e., those forces tending to retain the dislocation at the boundary, resulting in the large increase in GBD density from the annealed material. Segregation of solute to ledges in the Cu-1Sn alloy might raise the local shear modulus substantially. This would mean a higher nucleation stress, hence fewer dislocations nucleated at the lower strains. The fact that the density of emitted dislocations (boundary sources) was similar to that of the Cu,

indicates the Cu-1Sn ledges were more "efficient" sources, perhaps through a decrease in the above-mentioned retentive forces. It is thus seen that the creation of GBD's and lattice dislocations occur by the same process. A consequence of this fact would be that GBD-macroledges of strong contrast (due to the nucleated dislocations retained at them) would lie along the same crystallographic directions. These directions would be simply that of the ledge segments with the lowest root radii. This was indeed the case and can be seen, for example, in the right-hand grain boundary of figure 64 (p.209), the boundaries of figures 65(c) and 65(d), and the boundary of figure 68(d). This was in marked contrast to the more random orientations of GBD-macroledges seen in annealed material, e.g., GB_3 of Map 1 (p.176) or GB_8 of Map 11 (p.193). These latter GBD-macroledges would have resulted from lattice dislocations which had been swept up by the grain boundary during annealing and thus would show no preferred orientations like the above.

As mentioned above, achieving the stress required for nucleation does not always produce dislocation emission. Tangri and Tandon (182) have proposed that an image force due to elastic anisotropy could retain a generated dislocation at the boundary. Sample calculations for Cu indicate, however, that this force alone could not retain the dislocation at the

boundary, since the applied stress (enhanced by K_G and K_E) would always be greater than such an image force. In addition, such a force would only be significant when maximum elastic moduli differences occurred between two grains. There are, however, a number of other forces available to retain the dislocations near the boundary. One would be the attraction of the long-range strain field of the dislocation to the regions of opposing strain in the boundary. This would have a marked influence over a distance of at least a few hundred Angstroms out from the boundary (the width of the strong contrast which arises from the most severely strained regions of the dislocation (196)). A similar attraction would be the reduction in core energy ($\sim$ 50%) postulated by Ashby (51). An approximate estimate of this attraction may be made as follows. A relationship of the form,

$$K_G = \frac{10}{x/h} - 9 \qquad \ldots\ldots \qquad (7)$$

is assumed (182), where K_G is the total enhancement and x is the distance from the edge of the boundary region, which is assumed to be 20 $\mathring{A}$ wide. Thus at x = 10 $\mathring{A}$ and h = 100 $\mathring{A}$ (ledge height) K_G = 91, which is sufficient for nucleation. At x = 100 $\mathring{A}$, K_G = 1 and the enhancement has effectively vanished. A radius of 5 $\bar{b}$ ($\sim$ 20 $\mathring{A}$) is usually taken for the core radius, so it will be assumed that the attraction due to core energy

reduction disappears roughly 30 Å from the boundary. K_G = 24 at x = 30 Å and an average value for x = 0 - 30 Å would be around 70. Using a value of applied stress at which moderate dislocation generation from boundaries was observed in Cu (τ_{app} = 3 kg/mm^2 at ε_p = 3 x 10^{-4}), the energy available to move the dislocation to x = 30 Å can be calculated as roughly 10^{-4} ergs per cm of dislocation line (using K_G = 70, τ_{app} = 3 kg/mm^2, $\bar{b}$ = 3 x 10^{-7} mm and x = 30 x 10^{-7} mm). At the same time, a reasonable estimate of the core energy is 10 - 20% of the total self-energy (216), furnishing a value of 2 - 4 x 10^{-5} ergs/cm of dislocation (216). Therefore, if this core energy can be reduced 50% at the boundary, the attractive energy will be 1 - 2 x 10^{-5} ergs/cm or 10 - 20% of the available energy, indicating the attraction to be quite substantial. The above two tendencies for the dislocation to locate itself in the boundary region apply to all cases (these are the driving forces for dislocation annihilation at boundaries during annealing). In addition, the segregation to the ledges of solute atoms may hinder dislocation emission due to pinning or an increase in the local lattice friction stress.

It should be pointed out that the preference of triple points as active boundary source locations implies the presence of some extra stress concentration over other

locations along the boundary. Whatever the nature of this enhancement, it must account for the fact that little preference is shown between grain boundary triple points and twin boundary - grain boundary triple points. This additional enhancement may be connected with the large-scale enhanced strain contrast observed at some triple points, e.g. figure 68(c) (p.213). If this were the case, it could conceivably be related to a macroscopic K_G factor, such as is shown by the large ledges of figure 69, where the regions of enhanced strain contrast are far too large to be due to the microscopic stress concentration factors discussed previously. (Lack of dislocation emission from these ledges is now seen to be due to an insufficient stress concentration from these same microscopic factors, even though the ledges are of a very large height compared to most others.)

6.8 IMPLICATIONS OF THE MODEL

In view of the preceding model some comments can be made on the interconnected roles of solute and grain size. The relatively pure metals, such as the Cu and Ni used here, show signs of boundary source operation almost exclusively in fine grain size material (54). This would not be a result of the grain diameter per se, but of the defect structure of the grain boundaries associated with the production of such grain sizes. The mobility of this defect structure is high in high purity metals and the higher temperature anneals used to obtain the larger grain sizes would result in the annhilation of most of the boundary defect structure. The presence of substantial amounts of solute in alloys such as Fe-3Si would slow this annhilation process considerably. The result of this would

be a decrease in the total number of boundary defects, but the solute atmospheres at ledges might result in more large groupings of ledges, that is, more sources such as C in figure 77 and fewer like A, B and D. There would also be an increase in the average ledge height due to ledge combination. This does not appear to be a very large increase, as figure 19(b), p. 68 , shows that boundary sources in Fe-3Si of moderate grain size bear a remarkable resemblance to those in the Cu-1Sn, and the ledges are still not discernible. The net result of this process would then be an increase in the total number of dislocations generated in large-grained Fe-3Si, since the process would be more accentuated than in the finer grain sizes. This appears to be confirmed in acoustic emission work by Tangri and Tandon (217) which showed a definite increase, with an increase in grain diameter, for the total acoustic emissions up to 80% of the macroyield stress. (The stress relaxation achieved by each dislocation nucleation produces one acoustic pulse, thus GBD as well as lattice dislocation nucleation would be detected.) This process might be expected to maximize at some grain size and decrease thereafter, as even the large ledge groupings annhilated.

The boundary source model has implications for high temperature behavior, in that the sources could become partially regenerative. Through continued removal of the compensating GBD's (figure 79) by a combination of glide and climb, the ledge could continue nucleating dislocations until it vanished. This removal of ledges was postulated some time ago by Strutt and Gifkins (107) to account for the zone of intense shear observed

along boundaries in grain boundary sliding experiments and may now be feasibly explained.

The role of boundary generation in the yield process predicted by the model could also account for some aspects of ductile-brittle behavior. Thus the preferential location of sources on certain segments and in certain grains is due to the favorable local microscopic conditions, primarily a minimal root radius at the ledge corners, the distribution of which is governed by the mechanico-thermal treatment. For materials in which solute strongly pins both interior sources and all but the most favorable boundary sources, this preferential source location would be greatly accentuated. In the extreme, the bulk of the plastic strain must be provided by only a few grains, even near the macroyield point. A good example of such behavior might be in the deformation of ceramic materials, and this has been confirmed recently by etch-pitting work on polycrystalline MgO (105, 218). In other words, strong pinning of grown-in dislocations, relatively defect-free boundaries and a limited number of slip systems likely combine to produce boundary generation in this material in only a small fraction of grains, producing a high density of slip bands. This subsequently led to crack initiation in such grains, and fracture occurred after very little plastic strain. (It was also noted that the generated dislocations appeared to be of edge character.)

The major point from these examples is that better understanding of such phenomena can be obtained by examining the detailed behavior of grain boundaries during plastic deformation and applying the information

obtained to prediction of the macroscopic properties of interest.

In summary, the operation of grain boundary sources is at once simple and complex. Simple, in the physical operation of the model (one dislocation generated per ledge) and complex in the number of factors that produce the necessary stress, that govern whether or not the dislocation will be emitted into the grain interior, and that govern the characteristics of the source when it does generate dislocations into the interior. This complexity has been shown to account for the very individualistic character of boundary sources, particularly pertaining to their locations. Because of this complexity, only a very small fraction of the total number of boundary ledges available for activation actually become active, but this small fraction can have profound effects on major mechanical properties. It should be emphasized that an apparent reduction in the role of these sources as plastic deformation proceeds, is by no means the end of their role. Because of the large number of ledges remaining dormant, grain boundary sources could again be called upon to contribute plastic strain if they became energetically more attractive than alternate sources. This leads to perhaps the two most important points concerning this subject. All polycrystalline materials are ultimately capable of dislocation generation from grain boundaries, and the role of this generation must always be considered in the light of alternative sources of plastic strain.

7.0 CONCLUSIONS

These major points may be extracted from the preceeding text:

1) The hybrid technique of thin foil preparation resulted in foils relatively free of spurious defects due to foil handling,
2) The micro-mapping technique provided a means of obtaining comparative quantitative data as regards sparsely distributed thin foil phenomena (dislocation sources involved in yielding in this study),
3) Operation of grain boundary dislocation sources can occur in most metals with the right microstructural environment,
4) There was no concrete evidence for boundary dislocation sources of a regenerative nature. The majority of the sources observed possessed characteristics somewhat similar to the Li model of dislocation generation from grain boundaries (144),
5) The occasional emission of partial dislocations from grain boundaries resulted when the Burgers vector of the trailing partial of a dissociated perfect dislocation was normal to the applied stress (54) and was parallel to the dislocation line, i.e. of screw character,
6) The matrix value of stacking fault energy has an influence on the occurrence of this partial dislocation emission, i.e. substantial increases in SFE result in a reduced incidence of occurrence,
7) Solute or impurity atoms stabilize relatively high energy boundary defects, which can then become sources at low operating stresses. This preferential segregation at such sites may, however, make dislocation nucleation at these sites more difficult because of an

increased local shear modulus, or make dislocation emission more difficult due to solute pinning. These counteracting tendencies make the influence of solute or impurity atoms on boundary sources rather complex,

8) A high grain boundary defect density in the annealed state is initially favorable for boundary dislocation emission, but is likely to hinder such emission at higher strains,

9) The premacroyield region consists of two major strain regimes, with the first involving activation of those dislocation sources of very low operating stresses located in a small percentage of grains, and the second involving activation of many more sources of higher operating stresses located in most grains. The strain at which the transition occurs and the location of the dislocation sources vary from material to material,

10) A detailed model for grain boundary dislocation sources has been proposed which is based on groups of closely-spaced ledges of small height (a few hundred $\mathring{A}$ at most). The stress for dislocation nucleation at these ledges is achieved by concentration of the applied stress. The major component of this concentration arises from the individual ledge geometry and influence of adjacent ledges (K_G) and varies below a certain maximum value depending on the variation of ledge root radius. Other components may arise from elastic anisotropy (K_E) and modified GBD pileups (K_n). At triple points and kinks, an additional enhancement operates, and,

with the root radius variation, accounts for the non-homogeneous distribution of boundary sources. At low temperatures, only one dislocation can be nucleated per ledge and this requires the creation of a compensating GBD. Emission of this dislocation into the grain interior will be hindered by the reduction in self-energy the dislocation can achieve by remaining at the boundary. Emission may also be hindered by elastic anisotropy image forces and by pinning and increased lattice friction due to solute segregated to the boundary region,

11) The characteristics of the groups of ledges which comprise boundary sources (number, distribution of spacing and heights) are strongly influenced by the mechanico-thermal treatment which the material is given.

8.0 RECOMMENDATIONS FOR FUTURE WORK

This study, in its multi-faceted consideration of boundary sources and their operation, suggests a number of more specific studies on different aspects of the phenomenon.

1) It would be valuable to confirm or modify the source model presented here through more accurate direct observation, i.e. by high resolution electron microscopy of a material, such as the Cu-1Sn, which possesses well-delineated active sources. This observation would hopefully include the ledge numbers, heights and spacings, and the presence of any GBD's (compensating or in pileup form). The influence of grain misorientation on any of these could also be considered in such a study. The technique of weak-beam electron microscopy should prove helpful, since it furnishes very narrow dislocation contrast and could be used to study closely-spaced defects or dissociated GBD's. It must be kept in mind, however, that the grain boundary region is one of complex contrast behavior. Contrast components due to the different orientations of the two grains and the IGBD network will always be present. Also, the extension of the GBD core in the plane of the boundary reduces the GBD contrast (219) and the GBD strain field is shared by both grains, both of which add further complications to the study of individual boundary defects.

2) A relatively short project could clarify the utility of the Kikuchi line technique. This would involve more extensive measurements

of active boundary sources and different portions of non-active segments. It would be useful to determine the feasibility of relating the line broadening to the actual value of elastic strain, or to determine whether the strain is compressive or tensile. In situ thin foil tensile straining in the electron microscope could be used to test the ability of the technique for detecting potential sources before activation.

3) The influence of initial boundary defect density on the process of boundary dislocation generation could be determined in a number of ways. One would be a study of water-quenched versus slow-cooled high purity Cu, since fast cooling has been seen to greatly increase the boundary defect density, e.g. (81,82). Another way of changing only the GBD density might be to strain the Cu used in this study at a low strain rate, moderate temperature and low stress, such that grain boundary sliding would increase the GBD density while leaving the grain interiors relatively clean. The temperature would have to be below that where large boundary migration takes place, since this would drastically change other factors like ledge density. The material would then be room temperature tested as in this study.

4) It would be useful to ascertain the influence of varying levels of equilibrium solute segregation on boundary source operation in Cu, by premacroyield testing of material which had been given sufficiently long heat treatments at different temperatures. Slow and moderately

fast cooling from these temperatures would provide a comparison between boundary sources under the influence of full segregation and grain interior sources under varying degrees of pinning. At the same time, two different solute levels could be checked. One would be a hundred ppm or so of interstitial impurity, such as C or O, to first establish the effects of foreign atoms at the boundary. Then, tests could be conducted on an interstitial-free Cu-low Sn alloy to establish the additional effects of increased lattice friction stress. Auger electron spectroscopy would be useful to such a study in determining the level of segregation and its distribution on different boundaries.

5) The influence of strain rate and temperature on boundary source operation should be investigated by testing of a material such as the Cu-1Sn at strain rates around two orders of magnitude above and below that used here, then at a temperature well below room temperature (e.g. liquid nitrogen) and one above 0.3 of the melting point (where non-conservative GBD movement can occur). This would shed light on whether boundary sources are temperature sensitive, how the source characteristics change at higher temperatures, and how the rate of stress concentration influences these characteristics, if at all.

These are but a few of many conceivable studies, a fact occasioned by the relatively new nature of the field. Other studies could utilize a combination of direct and indirect techniques, such as

electron microscopy combined with acoustic emission and/or etch-pitting, or could include a larger variety of materials, such as BCC and HCP metals,or ceramics. Above all, there is a decided need for reliable quantitative data on the phenomenon of grain boundary source operation, both above and below the macroyield point. Such data is essential for future clarification of the various deformation theories for polycrystalline materials (micro-and macroyielding, work hardening, grain boundary sliding, etc.).

9 REFERENCES

1. Gleiter, H., phys. stat. sol., 45(b), 9 (1971).
2. Murr, L.E., Horylev, R.J. and Lin, W.N., Phil. Mag., 22, 515 (1970).
3. Chalmers, B., J. Less - Common Metals, 28, 277 (1972).
4. Gifkins, R.C., Interfaces Conference, Butterworths, Sydney (1969) p. 29.
5. Rosenhain, W. and Humphrey, J.C.W., J. Iron Steel Inst., 87, 219 (1913).
6. Rosenhain, W. and Ewen, D., J. Inst. Metals, 10, 125 (1913).
7. McLean, D., Met. Sci. J., 6, 109 (1972).
8. Aaron, H.B. and Bolling, G.F., Surface Science, 31, 27 (1972).
9. Bragg, W.L., Proc. Roy. Soc. (London), 52, 54 (1940).
10. Burgers, J.M., ibid, p. 52.
11. Read, W.T. and Shockley, W., Phys. Rev., 78, 275 (1950).
12. Mott, N.F., Proc. Roy. Soc. (London), 60, 391 (1948).
13. Gifkins, R.C., Mat. Sci. Eng., 2, 181 (1967).
14. Ryan, H.F. and Suiter, J.W., Phil. Mag., 10, 71 (1964).
15. Loberg, B., Norden, H. and Smith, D.A., Phil. Mag., 24, 897 (1971).
16. Ranganathan, S., Acta Cryst., 21, 197 (1966).
17. Bollmann, W., Phil. Mag., 16, 363, 383 (1967).
18. Balluffi, R.W. and Tan, T.Y., Scripta Met., 6, 1033 (1972).
19. Dimou, G. and Aust, K.T., Acta Met., 22, 27 (1974).
20. Kronberg, M.L. and Wilson, F.H., TMS - AIME, 185, 501 (1949).

21. Gleiter, H. and Chalmers, B., Prog. Mat. Sci., 16, High Angle Grain Boundaries, Pergammon Press, Oxford (1972) p. 43.
22. Brandon, D.G., Ralph, B., Ranganathan, S. and Wald, M.S., Acta Met., 12, 813 (1964).
23. Wagner, W.R., Tan, T.Y. and Balluffi, R.W., Phil. Mag., 29, 895 (1974).
24. Brandon, D.G., Acta Met., 14, 1479 (1966).
25. Pond, R.C. and Smith, D.A., to be published.
26. Schober, T. and Balluffi, R.W., phys. stat. sol., 44, 103, 115 (1971).
27. Schober, T. and Balluffi, R.W., Phil. Mag., 21, 109 (1970).
28. Levy, J., phys. stat. sol., 31, 193 (1969).
29. Fletcher, N.H., Interfaces Conference, Butterworths, Sydney (1969) p. 1.
30. Bishop, G.H. and Chalmers, B., Scripta Met., 2, 133 (1968).
31. Weins, M., Chalmers, B., Gleiter, H. and Ashby, M.F., Scripta Met., 3, 601 (1969).
32. Chalmers, B. and Gleiter, H., Phil. Mag., 23, 1541 (1971).
33. Baroux, B., Biscondi, M. and Goux, C., phys. stat. sol., 38, 415 (1970).
34. Hasson, G.C., Guillot, J.B., Baroux, B. and Goux, C., phys. stat. sol., 2(a), 551 (1970).
35. Bishop, G.H. and Chalmers, B., Phil. Mag., 24, 515 (1971).
36. Pumphrey, P.H., Scripta Met., 6, 107 (1972).

37. Ralph, B., Howell, P.R. and Page, T.F., phys. stat. sol., 55(b), 641 (1973).

38. Pumphrey, P.H., 7, 893 (1973).

39. Ishida, Y. and Smith, D.A., Scripta Met., 8, 293 (1974).

40. Balluffi, R.W. and Schober, T., Scripta Met., 6, 697 (1972).

41. Marcinkowski, M.J. and Das, E.S.P., Phil. Mag., 26, 1281 (1972).

42. Marcinkowski, M.J., Sadanada, K. and Tseng, W.F., phys. stat. sol., 17(a), 423 (1973).

43. Marcinkowski, M.J. and Sadanada, K., phys. stat. sol., 18(a), 361 (1973).

44. Marcinkowski, M.J. and Dwarakadasa, E.S., phys. stat. sol., 19(a), 597 (1973).

45. Marcinkowski, M.J., Tseng, W.F. and Dwarakadasa, E.S., J. Mat. Sci., 9, 29 (1974).

46. Tseng, W.F., Marcinkowski, M.J. and Dwarakadasa, E.S., ibid, p.41.

47. Balluffi, R.W., Komen, Y. and Schober, T., Surface Science, 31, 68 (1972).

48. Ishida, Y., Hasegawa, T. and Nagata, F., J. App. Phys., 40, 2182 (1969).

49. Ishida, Y. and Henderson-Brown, M., Acta Met., 15, 857 (1967).

50. Bell, R.L. and Langdon, T.G., Interfaces Conference, Butterworths, Sydney (1969) p. 115.

51. Ashby, M.F., Surface Science, 31, 498 (1972).

52. Gleiter, H., Baro, G. and Hornbogen, E., Acta Met., 16, 1053(1968)

53. Schober, T. and Balluffi, R.W., Phil. Mag., 24, 165 (1971).

54. Malis, T., Lloyd, D.J. and Tangri, K., phys. stat. sol., 11(a), 275 (1972).

55. Marcinkowski, M.J., Fundamental Aspects of Dislocation Theory, NBS Special Publication 317 (1970) p. 531.

56. Hirth, J.P. and Balluffi, R.W., Acta Met., 21, 929 (1973).

57. Das, E.S.P. and Marcinkowski, M.J., Acta Met., 20, 199 (1972).

58. Darinskii,B.M. and Fedorov, Yu.A., Sov. Phys.-Solid State, 13, 1008 (1971).

59. Gleiter, H., Acta Met., 17, 565 (1969).

60. McDonald, R.C. and Ardell, A.J., phys. stat. sol., 18(a), 407 (1973).

61. Ishida, Y. and McLean, D., Phil. Mag., 27, 1125 (1973).

62. Mikhailovskii, I.M., Sov. Phys-Solid State, 14, 2475 (1973).

63. Buzzichelli, G. and Mascanzoni, A., Phil. Mag., 24, 497 (1971).

64. Kegg, G.R., Horton, C.A.P. and Silcock, J.M., Phil. Mag., 27 1041 (1973).

65. Pumphrey, P.H. and Gleiter, H., Phil. Mag., 30, 593 (1974).

66. Westbrook, J.H., Met. Rev., 9, 415 (1964).

67. Westbrook, J.H., Interfaces Conference, Butterworths, Sydney (1969) p. 283.

68. Hondros, E.D. and Seah, M.P., Scripta Met., 6, 1007 (1972).

69. Papazian, J.M. and Beshers, D.N., Met. Trans., 2, 497 (1971).

70. Smith, D.A. and Smith, G.D.W., Met. Sci. J., 6, 111 (1972).

71. Seah, M.P. and Hondros, E.D., Proc. Roy. Soc. (London), 335A, 191 (1973).

72. Braunovic, M. and Haworth, C.W., J. Mat. Sci., 9, 809 (1974).

73. Westbrook, J.H. and Aust, K.T., Acta Met., 11, 1151 (1963).

74. Anthony, T.R., Acta Met., 19, 603 (1969).

75. Aust, K.T., Hanneman, R.E., Niessen, P. and Westbrook, J.H., Acta Met., 16, 291 (1968).

76. Aust, K.T. and Westbrook, J.H., Lattice Defects in Quenched Metals, Academic Press, New York (1965) p. 771.

77. Anthony, T.R. and Hanneman, R.E., Scr. Met., 2, 611 (1968).

78. Bercovici, S.J., Hunt, C.E.L. and Niessen, P., J. Mat. Sci., 5, 326 91970).

79. Bercovici, S.J., Niessen, P. and Byerly, J.J., Scr. Met., 3, 663 (1969).

80. Arkharov, V.I., Vangergeym, S.D., Krysova, S.K. and Plastovets, V.Kh., Phys. Metals and Metallography, 28, 304 (1969).

81. Hook, R.E., Met. Trans., 1, 85 (1970).

82. Bernstein, I.M. and Rath, B.B., Met. Trans., 4, 1545 (1973).

83. Kasen, M.B., Phil. Mag., 21, 1099 (1970).

84. Berghezan, A. and Fourdeux, A., J. App. Phys., 30, 1913 (1959).

85. Berghezan, A.,Fourdeux, A. and Amelinckx, S., Acta Met., 9, 464 (1961).

86. Hirsch, P.B.,Howie, R.W. and Whelan, M.J., Phil. Mag., 1, 677 (1956).

87. Kuhlmann-Wilsdorf, D., Structure and Properties of Thin Films, Wiley, New York (1959) p. 156.

88. Mascanzoni, A. and Buzzichelli, G., Phil. Mag., 22, 857 (1970).

89. Fujita, H. and Yamada, H., J. Phys. Soc. Jap., 29, 132 (1970).

90. Suits, J.C. and Chalmers, B., Acta Met., 9, 854 (1961).

91. Worthington, P.J. and Smith, E., Acta Met., 12, 1277 (1964).

92. Brentnall, W.D. and Rostoker, W., Acta Met., 13, 187 (1965).

93. Carrington, W.E., and McLean, D., Acta Met., 13, 493 (1965).

94. Johnston, T.L., Tetelman, A.S. and McEvily, Jr., A.J., IMRD, High Strength Materials, Wiley, New York (1964) p. 363.

95. Worthington, P.J., Acta Met., 15, 1795 (1967).

96. Carrington, W.E., Howard, J. and McLean, D., Scripta Met., 3, 517 (1969).

97. Moon, D.W. and Vreeland, Jr., T., J. App. Phys., 39, 1766 (1968).

98. Worthington, P.J., Quantitative Relation Between Properties and Microstructure, Israel University Press, Haifa (1969) p. 77.

99. Douthwaite, R.M. and Evans, J.T., Acta Met., 21, 525 (1973).

100. Hook, R.E. and Hirth, J.P., Acta Met., 15, 535 (1967).

101. Hook, R.E. and Hirth, J.P., Acta Met., 15, 1099 (1967).

102. Chuang, Y.-D. and Margolin, H., Met. Trans., 4 1905 (1973).

103. Evans, P.R.V., J. Less-Common Metals, 6, 253 (1964).

104. Vellaikal, G., Acta Met., 17, 1145 (1969).

105. Sinha, M.N., Lloyd, D.J. and Tangri, K., J. Mat. Sci., 8, 116 (1973).

106. Dudarev, Ye.F., Panin, V.Ye., Nikitina, N.V., Dikusar, L.D. and Sinigina, L.V., Phys. Metals and Metallography, 30, 133 (1970).

107. Strutt, P., Lewis, A.-M. and Gifkins, R.C., J. Inst. Metals, 93, 71 (1964).

108. Gifkins, R.C. and Langdon, T.G., J. Inst. Metals, 93, 347 (1964).

109. Odegard, B.C. and Thompson, A.W., Met. Trans., 5, 1207 (1974).

110. Thompson, A.W. and Odegard, B.C., Met. Trans., 4, 899 (1973).

111. Oblak, J.M. and Duvall, D.S., Proc. 29th Meeting of EMSA (1971) p. 114.

112. Davis, K.G., Teghtsoonian, E. and Lu, A., Acta Met., 1677 (1966).

113. Keh, A.S., Direct Observations of Imperfections in Crystals, Interscience, New York (1962) p 213.

114. Orlov, L.G., Soy. Phys. - Solid State, 9, 1828 (1968).

115. Bailon, J.-P. and Dorlot, J.-M., Acta Met., 19, 71 (1971).

116. Wilson, D.V., Acta Met., 16, 743 (1968).

117. Whelan, M.J., Hirsch, P.B., Horne, R.W. and Bollmann, W., Proc. Roy. Soc. (London), 240A, 524 (1957).

118. McGrath, J.T. and Bratina, W.J., Acta Met., 15, 329 (1967).

119. Price, C.W., Grain Boundary Dislocation Sources, M.Sc. Thesis, Ohio State University (1970).

120. Murr, L.E., App. Phys. Letters, 24, 533 (1974).

121. Hornbogen, E., Trans, ASM, 56, 16 (1963).

122. Hornbogen, E., Trans, ASM, 57, 469 (1964).

123. Calvayrae, Y. and Fayard, M., phys. stat. sol., 17(a), 407 (1973).

124. Usikov, M.P. and Utevskii, L.M., Phys Metals and Metallography, 11, 127 (1961).

125. Baro, G., Gleiter, H. and Hornbogen, E., Mat. Sci. Eng., 3, 92 (1968/69).

126. Baro, G. and Hornbogen, E., Quantitative Relations Between Properties and Microstructure, Israel University Press, Haifa (1969) p. 457.

127. Liu, C.T., Met. Trans., 4, 1743 (1973).

128. Warlimont, H., Iron Steel Inst. Spec. Report 93, London (1965) p. 73.

129. Douglas, D.L. and Barbee, T.W., J. Mat. Sci., 4, 138 (1969).

130. Kinsman, K.R., Aaronson, H.I. and Eichen, E., Met. Trans., 2, 1041 (1971).

131. Bonfield, W. and Li, C.H., Acta Met., 12, 577 (1964).

132. Bonfield, W., TMS-AIME, 233, 1719 (1965).

133. Van Towe, L.I. and Thomas, G., Acta Met., 11 881 (1963).

134. Thomas, G., J. Metals, 16, 365 (1964).

135. Conrad, H., Okaski, K., Gadgil, V. and Jon, M., Electron Microscopy and Structure of Materials, University of California Press, Berkeley (1972) p. 438.

136. Singh, R.N. and Tangri, K., Met. Trans., 1, 3151 (1970).

137. Tandon, K., private communication.

138. Ansell, G.S. and Weertman, J., TMS-AIME, 215, 838 (1959).

139. Codd, I. and Petch, N.J., Phil. Mag., 5, 30 (1960).

140. Leslie, W.C. and Keh, A.S., J. Iron Steel Inst., 200, 722 (1962).

141. Crussard, C., J. Austr. Inst. Metals, 8, 317 (1963).

142. Cottrell, A.H., NPL Symposium on Relation Between Structure and Strength of Metals and Alloys, HMSO, London (1963) p. 456.

143. Johannesson, T. and Tholen, A., Met. Sci. J., 6, 189 (1972).

144. Li, J.C.M., TMS-AIME, 227, 239 (1963).

145. Price, C.W. and Hirth, J.P., Mat. Sci. Eng., 3, 92 (1968/69).

146. Orlov, L.G., Sov. Phys.-Solid State, 9, 1836 (1968).

147. Gleiter, H., J. Less-Common Metals, 28, 297 (1972).

148. Saarinen, A.V.A. and Miekk-Oja, H.M., Met. Sci. J., 1, 145 (1967).

149. Harrison, E.A., Acta Met., 21, 1111 (1973).

150. Pumphrey, P.H. and Bowkett, K.M., Phil. Mag., 24, 225 (1971).

151. Malis, T., Lloyd, D.J. and Tangri, K., Phil. Mag., 26, 1081 (1972).

152. Gleiter, H. and Klein, H.P., Phil. Mag., 27, 1009 (1973).

153. Marcinkowski, M.J. and Tseng, W.F., Met. Trans., 1, 3397 (1970).

154. Das, E.S.P. and Marcinkowski, M.J., Mat. Sci. Eng., 8, 189 (1971).

155. Das, E.S.P. and Marcinkowski, M.J., Acta Met., 20, 199 (1972).

156. Frenkel, J., Z. Phys., 37, 572 (1926).

157. Mackenzie, J.K., Thesis, Bristol University (1949).

158. Hirth, J.P., Relation Between the Structure and Mechanical Properties of Materials, HMSO, London (1963) p. 218.

159. Frank, F.C., Growth and Perfection of Crystals, Wiley, New York (1958) p. 3.

160. Cabrera, N., Disc, Far-Soc., 28, 16 (1959).

161. Frank, F.C., Symposium on Plastic Deformation of Crystalline Solids, Carnegie Inst. of Technology and Office of Naval Research, Pittsburgh (1960) p. 89.

162. Nabarro, F.R.N., Adv. Phys., 1, 337 (1952).

163. Honeycombe, R.W.K., The Plastic Deformation of Metals, Arnold, London (1968) p. 239.

164. Langdon, T.G., Phil. Mag., 22, 689 (1970).

165. Gates, R.S., Acta Met., 21, 855 (1973).

166. Schober, T. and Balluffi, R.W., Phil. Mag., 24, 469 (1971).

167. Buzzichelli, G. and Mascanzoni, A., Mat. Sci. Eng., 5, 119 (1969/70).

168. Eshelby, J.D., Frank, F.C. and Nabarro, F.R.N., Phil. Mag., 42, 351 (1951).

169. Hirth, J.P., Met. Trans., 3, 3047 (1972).

170. Chung, D.H. and Buessem , W.R., Anisotropy in Single Crystal Refractory Compounds, Plenum, New York (1968) p. 217.

171. Hauser, J.J. and Chalmers, B., Acta Met., 9, 802 (1961).

172. Livingston, I.D. and Chalmers, B., Acta Met., 5, 322 (1957).

173. Hasselmann, D.P.H., Anisotropy in Single Crystal Refractory Compounds, Plenum, New York (1968) p. 217.

174. Abe, T., Bull. JSME, 12, 165 (1969).

175. Abe, T., Bull. JSME, 14, 1263 (1971).

176. Abe, T., Bull. JSME, 15, 917 (1972).

177. Abe, T., Bull. JSME, 16, 474 (1973).

178. Abe, T., Bull. JSME, 16, 1540 (1973).

179. Tangri, K., Lloyd, D. J. and Malis, T., Proc. Int. Symposium, Fifty Years of Metallurgy, Banaras, India (1973) in press.

180. Kelly, A., Strong Solids, Clarendon Press, Oxford (1973) p. 110.

181. Nabarro, F. R. N., Adv. Phys., 1, 269 (1952).

182. Tangri, K. and Tandon, K., Fourth Bolton Landing Conference on Grain Boundaries and Engineering Materials (1974) in press.

183. Marsh, D. M., Fracture of Solids, Wiley, New York (1973) p. 119.

184. Timoshenko, S. and Goodier, J. N., Theory of Elasticity, McGraw-Hill, London (1951) p. 84.

185. Paris, P. C. and Sih, G. C., Fracture Toughness Testing and Its Applications, ASTM, STP 381 (1964) p. 34.

186. Paris, P. C. and Sih, G. C., ibid., p. 35.

187. Gilman, J. J., J. App. Phys., 30, 1584 (1959).

188. Young, Jr., F. W. and Sherill, F.A., Can. J. Phys., 45, 757 (1967).

189. Lloyd, D. J., Worthington, P. J. and Embury, J. D., Phil. Mag., 22, 1147 (1970).

190. Thompson, A. W., Scripta Met., 8, 145 (1974).

191. Kasen, M. B., TMS-AIME, 245, 1660 (1969).

192. Malis, T. and Van Dorp, J., J. Phys. E: Sci. Instruments, 6, 424 (1973).

193. Brammar, I. S. and Dewey, M. A. P., Specimen Preparation for Electron Metallography, American Elsevier, New York (1965) p. 36.

194. Junkin, B., private communication.

195. Malis, T., Lloyd, D. J. and Tangri, K., Micron, 4, 333 (1973).

196. Hirsch, P. B., Howie, A., Nicholson, R. B., Pashley, D. W. and Whelan, M. J., Electron Microscopy of Thin Crystals, Butterworths, London (1965).

197. Booker, G. R., Joyce, B. A. and Bradley, R. R., Phil. Mag., 10, 1087 (1964).

198. Thomas, G., Techniques in Materials Science, American Elsevier, New York (1969) p. 159.

199. Loretto, M. H. and France, L. K., Phil. Mag., 19, 141 (1969).

200. Pumphrey, P. H. and Bowkett, K. M., Scripta Met., 5, 365 (1971).

201. Thomas, D. A. and Averbach, B. L., Acta Met., 7, 69 (1959).

202. Bilello, J. C. and Metzger, M., TMS-AIME, 245, 2279 (1969).

203. Holt, R. T., J. Inst. Metals, 100, 376 (1972).

204. Brown, N., Microplasticity, Interscience, New York (1968) p. 45

205. Rosenfield, A. R. and Averbach, B. L., Acta Met., 8, 624 (1960).

206. Tegart, W. J. M., Elements of Mechanical Metallurgy, MacMillan, New York (1966) p. 91.

207. Honeycombe, R. W. K., The Plastic Deformation of Metals, Arnold, London (1968) p. 332.

208. Reed, R. P. and Schramm, R. E., J. App. Phys., 45, 4705 (1974).

209. Cockayne, D. J. H., Jenkins, M. C. and Ray, I. L. F., Phil. Mag., 24, 1383 (1971).

210. Koster, W. and Spiedel, M. O., Z. Metallk., 56, 585 (1965).

211. Li, J. C. M. and Chou, Y. T., Met. Trans., 1, 1145 (1970).

212. Bell, W., Okamota, P. and Thomas, G., Acta Met., 13, 559 (1965).

213. Tegart, E. J. M., Elements of Mechanical Metallurgy, MacMillan, New York (1966) p. 197.

214. Tangri, K., private communication.

215. Nabarro, F. R. N., Theory of Cyrstal Dislocations, Clarendon Press, Oxford (1967) p. 118.

216. Weertman, J. and Weertman, J. R., Elementary Dislocation Theory, MacMillan, New York (1964) p. 47.

217. Tangri, K. and Tandon, K. N. T., Met. Trans., in press.

218. Sinha, M. N., Ph. D. Thesis, University of Manitoba (1974).

219. Tholen, A. R., Eighth International Congress on Electron Microscopy, Canberra (1974) p. 606.